ELUCIDATING THE REGULATORY ROLE OF *Arabidopsis thaliana* ARID-HMG PROTEIN ATHMGB15 IN POLLEN DEVELOPMENT

Thesis submitted for the Degree of Doctor of Philosophy (Science) of Jadavpur University

SONAL SACHDEV

Department of Biological Sciences

Bose Institute

2024

बसु विज्ञान मंदिर
BOSE INSTITUTE

(विज्ञान एवं प्रौद्योगिकी विभाग, भारत सरकार के एक स्वायत्त संस्था)
(An Autonomous Institute of Department of Science & Technology, Govt. of India)

मुख्य कैंपस / Main Campus :
93/1, आचार्य प्रफुल्ल चंद्र रोड़, कोलकाता - 700 009
93/1, Acharya Prafulla Chandra Road, Kolkata - 700 009
फोन/Phone: 2350-7073 (निदेशक/Director)
इपीएबीएक्स/EPABX : 2350-6619/6702/2402/2403, 2303-0000/1111
फैक्स/Fax : 91-33-2350-6790

शतवार्षिकी भवन / Centenary Building :
पी-1/12, सी.आई.टी. स्कीम-VII-एम, कोलकाता - 700 054
P-1 / 12, C.I.T. Scheme VII-M, Kolkata - 700 054
फोन/Phone: 2355-7434(निदेशक/Director), 2355-0595(रजिस्ट्रार/Registrar)
इपीएबीएक्स/EPABX : 2355-9416/9219/9544, 2569-3271, फैक्स/Fax : 91-33-2355-3886

समन्वित शैक्षिक परिसर / Unified Academic Campus :
ब्लॉक-ईएन, प्लॉट नं-80, सेक्टर-V, सॉल्ट लेक सिटी, कोलकाता - 700 091
Block-EN, Plot No.-80, Sector-V, Salt Lake City, kolkata - 700 091
फोन/Phone: 2569-3131(निदेशक/Director)
इपीएबीएक्स/EPABX : 2569-3123/28, फैक्स/Fax : 91-33-2569-3127

संदर्भ सं. / Ref. No. _____ दिनांक / Date :

TO WHOM IT MAY CONCERN

This is to certify that the thesis entitled "ELUCIDATING THE REGULATORY ROLE OF *Arabidopsis thaliana* ARID-HMG PROTEIN ATHMGB15 IN POLLEN DEVELOPMENT" submitted by Ms. Sonal Sachdev who her name registered on 16th September 2019 for the award of Ph.D. (Science) degree of the Jadavpur University, is absolutely based upon her own work under the supervision of Prof. Shubho Chaudhuri and that neither this thesis nor any part of it has been submitted for either any degree / diploma or any other academic award anywhere before. (Registration number SLSBT1109419 and Index. Number 94/19/Life Sc./26.)

Shubho Chaudhuri
14/11/2024

Signature of Supervisor

डॉ. शुभो चौधुरी / Dr. Shubho Chaudhuri
प्रोफेसर / Professor
जैविक विज्ञान विभाग / Department of Biological Sciences
बसु विज्ञान मंदिर / BOSE INSTITUTE
ईएन 80, सेक्टर V, बिधाननगर/EN 80, Sector V, Bidhannagar
कोलकाता / Kolkata-700 091 (भारत/India)

DECLARATION

I hereby declare that the research work presented in this thesis, titled "ELUCIDATING THE REGULATORY ROLE OF *Arabidopsis thaliana* ARID-HMG PROTEIN ATHMGB15 IN POLLEN DEVELOPMENT" is entirely based on the experiments I conducted during my Ph.D. research at the Department of Biological Sciences, Bose Institute, Kolkata, India, under the supervision of Prof. Shubho Chaudhuri. This thesis is submitted for the award of the Ph.D. (Science) degree from Jadavpur University, Kolkata, India. The research is original and has not been submitted, either in part or in full, for any degree or diploma at any other university.

Sonal Sachdev

14 November 2024

Sonal Sachdev

Index. Number 94/19/Life Sc./26

Registration number SLSBT1109419

Dedication

To my niece Shanaya

For inspiring me to exemplify the accomplishments women can attain despite societal norms.

To my Family and Friends

For their unwavering love and support that served as a constant source of motivation, guiding me through every moment.

To my Mentors

For their tireless encouragement and consistent belief in my potential, pushing me to thrive and succeed.

To Myself

For persevering through all obstacles while embracing an authentic life.

Acknowledgment

I express my deepest gratitude to my supervisor, Prof. Shubho Chaudhuri. His unwavering support, encouragement, and passion for science have been a constant inspiration throughout this journey. His kindness and carefree demeanor have always created a positive and welcoming environment, making even the most challenging moments feel manageable. Sir's sense of responsibility and commitment to excellence in research has pushed me to grow both as a scientist and a person. I am incredibly fortunate to have had the opportunity to learn from Prof. Chaudhuri, and his mentorship has shaped not only my academic growth but also my personal development. His positive outlook has inspired me to navigate challenges with utmost confidence.

I vividly recall my first day in Sir's lab as if it were just yesterday. Over the years, he generously shared his expertise, teaching me hands-on techniques and passing down invaluable tips and insights. These small but significant lessons will always hold a special place in my heart, and I will forever be grateful to him for his kindness and unwavering support.

Thank you, Sir, for believing in me and for always encouraging me to aim higher. Thank you for always pushing me to think critically and aim for excellence. Without your support, my first-author publication in the esteemed Plant Physiology would have remained nothing more than a distant dream. This thesis would not have been possible without your guidance, and for that, I am deeply grateful.

My heartfelt gratitude to Dr. Ronita Nag Chaudhuri, a powerful and inspiring force in my academic journey. Her unwavering strength and clarity of vision have not only shaped my approach to research but also encouraged me to find and trust my own voice. She has shown me the importance of standing firm in one's convictions and navigating the challenges of science with resilience and integrity. Her mentorship has been a guiding light, and I am profoundly thankful for her wisdom, support, and the example she sets as a brilliant and fearless scientist.

I am grateful to my research advisor, Prof. Kaushik Biswas, for his invaluable guidance, expertise, and constant encouragement throughout my journey. His unwavering support has profoundly shaped my research outcome.

Occasionally, we encounter remarkable individuals, Prof. Sujoy K. Dasgupta and Prof. Maitrayee Dasgupta are two such exceptional scientists who have greatly contributed to my development of a scientific mindset, through brief interactions.

My mentors from my undergraduate curriculum, Dr. Kashi Nath Ghosh and Dr. Illora Sen were the foundational figures who ignited my passion for plant biology. Their significant influence played a crucial role in my academic success, helping me achieve top honor and secure a gold medal at the university examinations.

Prof. Rita Kundu, my primary mentor during my master's course, instilled in me a strong work ethic and a rigorous laboratory discipline. Her constant encouragement to strive for excellence enabled me to excel and achieve the highest marks in the master's examination, earning me a second gold medal during the university examinations.

Dr. Soumitra Paul was the first mentor to emphasize the significance of publishing in reputable journals to validate my research efforts.

I sincerely thank the Director of Bose Institute for allowing me to work at this esteemed institute and for granting me access to its excellent research facilities. I am also grateful for the six-month extension of my fellowship beyond the stipulated tenure.

My heartfelt thanks to the technical, non-technical, and administrative staff at Bose Institute for their support and assistance in resolving both technical and non-academic matters.

I extend appreciation to the Madhyamgram Experimental Farm (MEF) for supporting my transgenic research, particularly during the challenging pandemic period. I am especially grateful to Dr. Sambit Dutta and Bapi da for their invaluable assistance during that time.

I extend my gratitude to the University Grants Commission (UGC), India, for the financial support, which made the pursuit of my academic goals possible.

The three-year research grant from the Science, Engineering and Research Board (SERB) played a crucial role in enabling significant progress and accomplishments in my Ph.D. research.

The research experience would have been significantly less engaging without the presence of the best lab mates one could wish for. They turned what could have been a mundane journey into an exciting and enjoyable adventure, filled with countless memorable moments. I am deeply appreciative of my seniors, Dr. Adrita Roy, Dr. Dipan Roy, Dr. Amit Paul, Dr. Rwitie Malik, Dr. Pratiti Dasgupta and Dr. Jinia Chakrabarty for warmly welcoming me and teaching me essential experimental skills. I am grateful to my peers for their support during challenging times and for assisting me with my research and analysis. My heartfelt thanks go to my juniors, Ms. Ruby Biswas, Mr. Vishal Roy, Ms. Sabini Basu, with a special mention for Ms. Ayantika Nandi and Ms. Rukshar Parveen, whose playful nature kept the lab vibrant and cheerful. am grateful to Ms. Asmita Chakrabarty, Ms. Mouli Naskar, and Ms. Paroma Mitra for their invaluable contributions as mentees, which provided me with the opportunity to learn and develop my skills in scientific mentoring. I also extend sincere gratitude to laboratory attendants especially to Nadiram da, Uttam da and Binod da for their unwavering support and familial care.

To JC, VSL, OBONTICKA RUKSHAA —without you, the final chapter of my Ph.D. would have been a boring grind instead of a hilarious series finale; Every joke and giggle kept me sane (mostly).

I thank my 93-year-old grandfather, who proves that a long life requires a steadfast commitment to health and that living each moment to the fullest involves passionately pursuing what you love.

I want to extend my heartfelt gratitude to my childhood friend Nick, who guided me through my darkest moments. He inspired me to see the greater good in every situation and reminded me that abandoning one's dreams is never an option. His belief that there is always light at the end of the tunnel gave me hope and strength, helping me become the best version of myself.

It would not be enough to thank my elder sister, Tasheena, who has been like a second mother, has consistently supported my dreams and encouraged me to pursue excellence. Her untiring support convinces me that siblings are truly angels in disguise.

It feels impossible to adequately express the depth of my gratitude to Mamma and Papa in mere words. They have always offered unconditional love and support. I am forever thankful for their undying belief in me, despite my flaws.

I extend my heartfelt thanks to my entire family, each of whom has played an invaluable role in countless ways, providing me with a constant place of comfort and support throughout my life.

I humbly thank The Almighty for blessing me with the strength and resilience to overcome challenges throughout this journey. His guidance and grace have helped me achieve my goals and accomplish this thesis.

Finally, I am deeply thankful to myself for persevering, for having the courage to choose this path, and for trusting that my passion for science has the power to make a meaningful difference.

Truly

Sonal

Table of Contents

Abbreviations

ARID	*AT Rich Interaction Domain*
CDS	*Coding Sequence*
ChIP	*Chromatin Immunoprecipitation*
DEGs	*Differentially Expressed Genes*
DEPC	*Diethyl pyrocarbonate*
DMSO	*Dimethyl sulfoxide*
DNA	*Deoxyribonucleic acid*
DNaseI	*DeoxyribonucleaseI*
DTT	*Dithiothreitol*
EDTA	*Ethylene diamine tetra acetic acid*
EMSA	*Electrophoretic mobility shift assay*
EtBr	*Ethidium bromide*
FPKM	*Fragments Per Kilobase Million*
GFP	*Green Fluorescent Protein*
GO	*Gene Ontology*
GUS	*β-glucuronidase*
HMG	*High Mobility Group*
JA	*Jasmonic Acid*
JA-Ile	*Jasmonic acid Isoleucine*
MeJA	*Methyl-Jasmonate*
MOPS	*3-[N-Morpholino] propane sulfonic acid*
MS	*Murashige & Skoog*
PAGE	*Polyacrylamide gel electrophoresis*
PGM	*Pollen germination medium*
PMSF	*Phenyl methane sulphonyl fluoride*
RNA	*Ribonucleic acid*
SDS	*Sodium dodecyl sulfate*
TAE	*Tris-acetate EDTA*
TBE	*Tris-borate EDTA*
TE	*Tris-EDTA*
TEMED	*N N N'N'-Tetramethylene diamine*
TFs	*Transcription Factors*
TSS	*Transcription Start Site*
YFP	*Yellow fluorescent protein*
β-Me	*β-Mercaptoethanol*

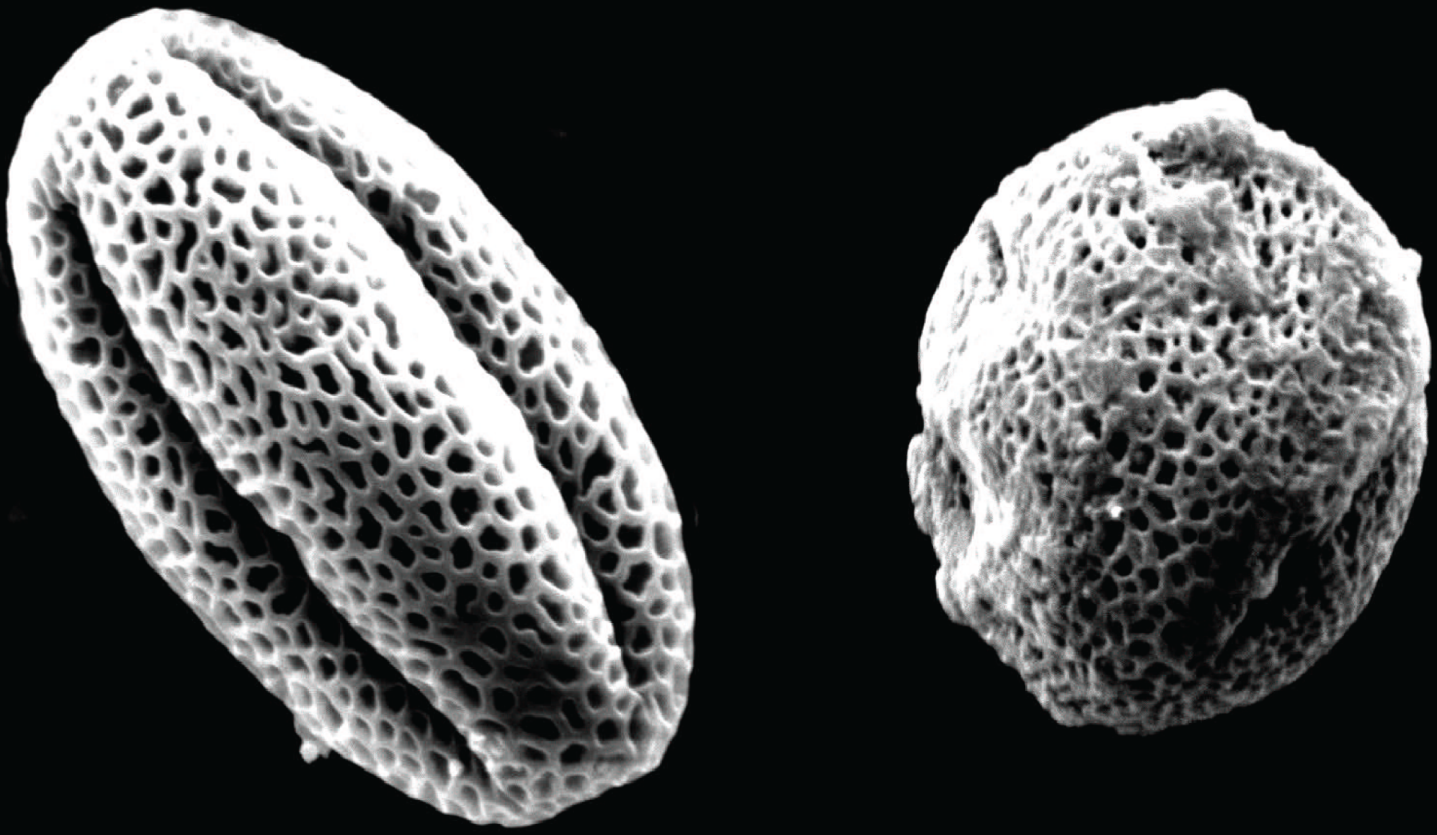

Abstract

The development of male gametophytes in angiosperms is a highly intricate and synchronized process, governed by a sophisticated interplay between various hormonal signaling pathways that ensure the successful progression of fertilization. This process encompasses multiple critical events, including pollen maturation, anther dehiscence, pollen release, and the germination of pollen tubes. Central to these regulatory mechanisms are phytohormones, which act as master integrators of both internal developmental signals and external environmental cues, thereby orchestrating the fine-tuning of plant growth, reproduction, and adaptive responses. Jasmonic acid (JA) and its derivatives are critical, modulating processes like pathogen resistance, root growth, and senescence, while playing a vital role in male reproductive development, including stamen differentiation, pollen viability, and essential transcriptional networks for pollen maturation.

The *Arabidopsis thaliana* genome features a family of High Mobility Group (HMG) chromatin remodelers known to act as transcriptional activators, pivotal for the regulation of numerous genes. AtHMGB15 stands out as an ARID-HMG protein characterized by an AT-rich interaction domain alongside the canonical HMG-Box DNA-binding domain, with its expression predominantly elevated in flowers and pollen grains. This research delves into the molecular and biological mechanisms by which AtHMGB15 regulates pollen development, focusing on its integration with the JA hormone pathway. Detailed phenotypic analysis of the *athmgb15-4* mutant uncovered notable reproductive defects, including delayed flowering, shorter siliques, reduced seed set, and compromised pollen viability. Mutant pollen grains exhibited abnormal morphology, delayed germination, and impaired tube growth. Molecular profiling and *in silico* analysis revealed a significant down-regulation of genes involved in JA biosynthesis and signaling in *athmgb15-4* plants, accompanied by a roughly tenfold reduction in jasmonic acid and its derivatives in floral tissues. Remarkably, exogenous application of methyl jasmonate rescued pollen morphology and germination, reinstating the expression of JA signaling genes, which underscores the essential role of AtHMGB15 in JA-mediated developmental processes. Furthermore, biochemical assays suggest a direct physical interaction between AtHMGB15 and the MYC2 protein (a MYC2 transcription factor crucial in the JA pathway), forming a transcriptional activation complex that upregulates critical JA-responsive genes, including *MYB21* and *MYB24*, integral to stamen and pollen development.

These findings highlight AtHMGB15 as a crucial positive regulator of JA signaling, orchestrating the precise spatial and temporal expression of developmental regulators. Our work provides compelling insights into the interplay between chromatin architecture and hormone signaling in plant reproductive biology, positioning AtHMGB15 as a key player in ensuring successful male gametophyte development. By shedding light on how JA coordinates developmental and environmental signals, this study not only advances our understanding of plant reproductive biology but also presents promising implications for improving crop fertility and resilience in changing environmental conditions.

Introduction

In the living kingdom, organisms encounter diverse endogenous signals and environmental stimuli, prompting evolutionary adaptations to sophisticated mechanisms for perception and response. Cellular physiology, protein modification, gene regulation, and genome remodeling are orchestrated responses to internal and external stimuli. Regulation of gene expression, which is pivotal for DNA-dependent processes, occurs within the chromatin. Alterations in chromatin are crucial for the proper functioning of these processes. Despite considerable knowledge about specific plant responses to developmental or environmental cues at the level of individual proteins and genes, their impact on the entire genome remains less explored.

Plant development encompasses both embryonic and postembryonic phases, with the former involving the establishment of the apical-basal axis, shoot apical meristem (SAM), and root apical meristem (RAM). The subsequent postembryonic phase involves the formation of leaf, stem, and flower meristems. Previous studies highlight the role of chromatin remodelers in crucial plant growth and development processes, such as the establishment and maintenance of meristem, differentiation of cell and tissue, initiation of organs, flower morphogenesis, and the regulation of flowering time along with involvement of plant chromatin remodelers responses to major phytohormone signals (Ojolo et al., 2018).

Stem cells in the root apical meristem (RAM) and shoot apical meristem (SAM) located at the root and shoot tips, respectively, have been extensively investigated in plants. SWI/SNF chromatin remodeling ATPases play a crucial role in maintaining the homeostasis and identity of stem cells in both plants and mammals (Shen et al., 2000). Arabidopsis SWI/SNF subfamily chromatin remodelers, including SPLAYED (SYD), BRAHMA (BRM), Chromatin Remodelling Proteins (CHR12 and CHR23)are implicated in the regulation of various developmental processes in plants (Farrona et al., 2004, Wu et al., 2012). Disruptions in the Polycomb group (PcG) repressive complex, chromatin assembly or histone acetylation may result in aberrant development of RAM or SAM (Xu and Shen, 2008).

Cellular differentiation arises from widespread shifts in gene expression patterns, driven by numerous transcriptional regulators and epigenetically mediated through chromatin remodeling. (Taylor-Teeples et al., 2015).

Vegetative phase to flowering transition holds critical importance for reproductive success of plants and involves the transformation of the shoot apical meristem (SAM) into an inflorescence

meristem (IM) and the subsequent floral meristems (FMs) initiation (Sablowski, 2007, Kaufmann et al., 2010). While the SAM ensures continuous growth, FMs' determinate nature is key for reproduction and crop yield (Liu et al., 2011). Complex regulatory networks integrate internal signals (e.g., hormones) and external cues (e.g., photoperiod, vernalization) to control flowering (Wils and Kaufmann, 2017). In *Arabidopsis*, a MADS-box repressor complex involving MADS AFFECTING FLOWERING 4/5 (MAF4/5), FLOWERING LOCUS C (FLC) and SHORT VEGETATIVE PHASE (SVP) represses flowering by inhibiting FLOWERING LOCUS T (FT) and SUPPRESSOR OF OVEREXPRESSION OF CONSTANS 1 (SOC1), with vernalization overriding this repression (Ojolo et al., 2018). CONSTANS (CO) activates FT during long days, forming a complex with FD at the SAM to floral meristem (FM) identity genes *LEAFY (LFY)* and *APETALA1 (API*), initiating floral development (Takagi et al., 2023) (Yamaguchi, 2021). LFY then recruits chromatin remodelers to activate AGAMOUS, facilitating organ formation (Wu et al., 2012).

Most of these factors are tightly regulated at the transcription level through chromatin remodeling to controls tissue and stage specific expression during developmental processes/events. The present study is to understand the role of plant nuclear architectural protein, ARID-HMG, during pollen development, we will focus the literature survey on different aspects of flower development and the present knowledge on architectural protein.

Flower development

A flower is the most complex and crucial structure of plants. Flowering plants i.e., the Angiosperms are most recently diverged branch of plants. The molecular genetics of the flower was critically studies in the late 1980s thereby giving us one of the classic developmental models of flowers namely the ABC model. Stages of flower development as described in earlier studies constitutes about 20 stages from the initiation of floral primordia to the dehiscence of anther locules enabling seed dispersal (Alvarez-Buylla et al., 2010). Stages 1-4 represent the development from floral primordia to sepal and pedicel elongation. The four sepals are the first floral organ to appear at stage 3 of pollen development. Petal, stamen and carpel primordia initiation takes place almost simultaneous around stage 5 and 6 respectively, followed by differentiation and elongation within the closed buds from stages 5-9. Stages 6-13 marks the initiation and development of the gynoecium alongside elongation of petals and stamen filaments. At the 13th stage the gynoecium is completely receptive to pollination. Stage 14 marks the beginning of

silique formation thereby representing the Xero hours after pollination (0 HAP). The seeds begin to develop at stage 15, mature and ready for dispersal through the stages 16-20 *(Figure In_1*).

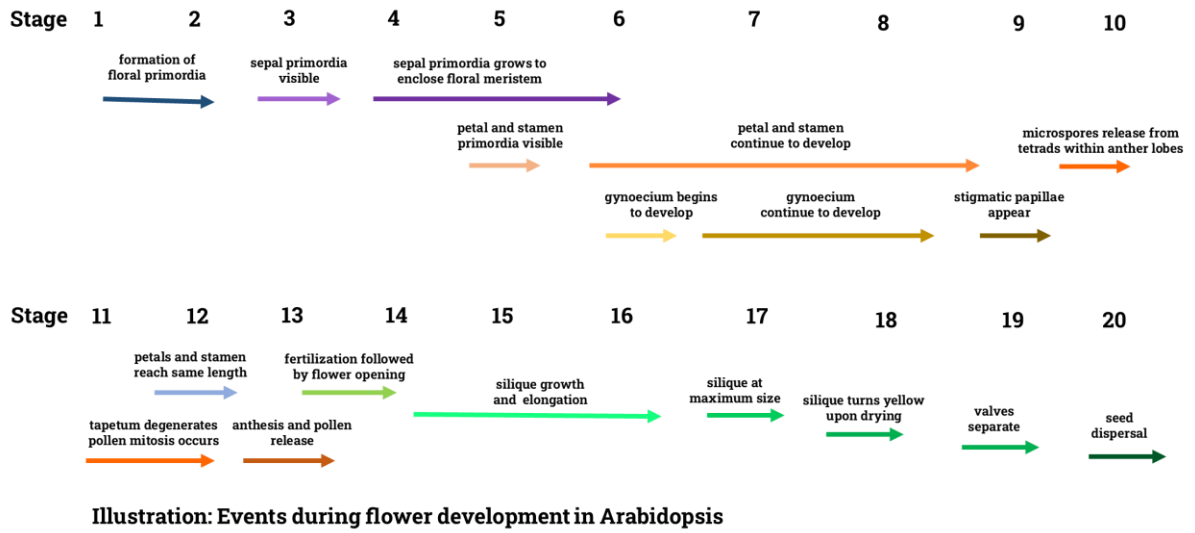

Figure In_1: Diagram depicting the developmental stages of Arabidopsis flowers.

Genes directing flower development in Arabidopsis

Research on flower development in *Arabidopsis thaliana* has provided a detailed understanding of the gene networks governing each floral organ's formation. The homeodomain transcription factor WUSCHEL (WUS) maintains stem cell identity in the shoot apical meristem, while *CLAVATA (CLV)* genes restrict WUS activity, forming a regulatory loop that controls meristem size (Alvarez-Buylla et al., 2010, Liu et al., 2011). SHOOT MERISTEMLESS (STM) promotes stem cell proliferation until a critical size is reached, countered by ULTRAPETALA1 (ULT1), which limits meristem growth. Floral meristem (FM) specification involves dynamic gene expression changes, with *LEAFY (LFY)* and *AINTEGUMENTA (ANT*) playing pivotal roles. LFY is essential for FM identity, as mutations in *lfy* result in leaf production instead of flowers, while overexpression leads to floral transformation of leaves and shoots. Flowering onset requires repressing *TERMINAL FLOWER 1 (TFL1) and EMBRYONIC FLOWER (EMF1, 2)* genes, while FMI genes *like LFY, APETALA 1 (AP1), APETALA 2 (AP2), and CAULIFLOWER (CAL)* are upregulated, forming a complex gene regulatory network responsive to internal and external cues (Wils and Kaufmann, 2017, Taylor-Teeples et al., 2015). Vernalization epigenetically downregulates the floral repressor FLOWERING LOCUS C (FLC), with SHORT VEGETATIVE PHASE (SVP) modulating flowering in response to temperature. LFY and AP1 collaborate to maintain FM identity,

repressing genes like *AGAMOUS-LIKE 24 (AGL24) and SUPPRESSOR OF OVEREXPRESSION OF CO 1 (SOC1)* (Sheldon et al., 2000, Liu et al., 2008). Mutations in *lfy* and *ag* suggest their roles in ensuring floral meristem determinacy, with CAL acting redundantly to AP1 (Liu et al., 2009). Additionally, microRNAs, including miR156, miR319, and miR172, are crucial in regulating the floral transition, while MADS-box genes integrate various signaling pathways to coordinate floral organ development and meristem identity (Waheed and Zeng, 2020, Spanudakis and Jackson, 2014).

The ABC and extended model

The conceptualization of the ABC model by Merowitz and his group is a pioneer in the study of flower development. The study described four homeotic mutations namely *agamous (ag), apetala1 (ap1), apetala 3 (ap3)* and *pistillata (pi)* in *Arabidopsis thaliana*, affecting fundamental processes in floral development (Bowman et al., 1989). The FM is divided into four regions eventually giving rise to the floral whorls: sepals, petals, stamens and carpel. LFY protein through cofactors governs the spatio-temporal expression of AG, AP3 and PI. The ag flowers possess only sepals and petals with complete absence of stamens and carpels (Coen and Meyerowitz, 1991, Coen, 1991). MADS-box proteins act as master regulators of floral identity (Yan et al., 2016). ap2 mutants are temperature sensitive exhibiting different phenotype at different temperatures mostly affecting the two outer whorls. On the contrary, *ap3* mutation affects the first and third whorls, whereas in the *pi* mutants, all whorls except the first are gravely affected. Expanding upon earlier genetic investigations in *Antirrhinum majus* (snapdragon) and *Arabidopsis thaliana*, Coen and Meyerowitz suggested that specific organ identities are determined by a distinctive interplay of homeotic 'A,' 'B,' and 'C' gene functions within each floral whorl (Coen and Meyerowitz, 1991). The A function specifies sepals, A and B functions make the petals, B and C define the stamens and C is responsible for carpel development. The extended ABCE model suggests *SEPALLATA (SEP)* genes represented as E behave as crucial co-factors necessary for laying floral meristem identity and organ specification in all whorls shown in *Figure In_2* (Krizek and Fletcher, 2005, Ditta et al., 2004, Ó'Maoiléidigh et al., 2014, Turczyn, 2011).

Over the past decades great advancements have been made on the ABCE model suggesting the ABCE genes are mandatory but insufficient to define floral identity. Target genes of the ABCE genes associate the floral organ specification-Gene regulatory network (FOS-GRN) to processes in the establishment of organ primordia, initiation and development. Presently a substantial

network exists with more than thousands of genes responsible for developing each of the floral organs.

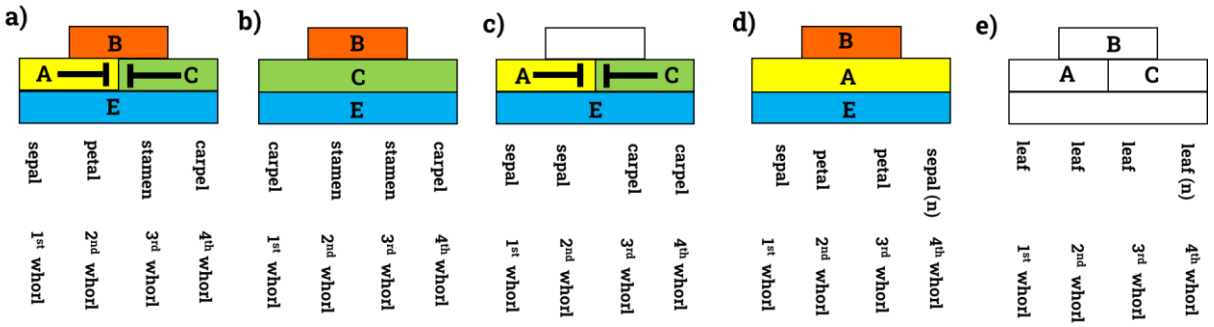

Illustration: ABCE model showing floral-organ patterning

FigureIn_ 2: Diagram depicting the ABCE model describing organ patterning Arabidopsis flowers. a) Diagram portraying wild-type Arabidopsis thaliana flower has four organ whorls: sepals (class A activity) in the first, petals (class A and B activity) in the second, stamens (class B and C activity) in the third, and carpels (class C activity) in the fourth, with class E activity needed for all organ types. b) Diagram showing an apetala 2 (ap2) mutant shows carpels in the first whorl and stamens in the second and third, with class C activity expanded due to a loss of class A activity. c) Diagram featuring pistillata mutant sepals in the first two whorls and carpels in the last two, lacking class B activity. d) Diagram displaying an agamous (ag) mutant repeated whorls of sepals and petals, lacking class C activity, which leads to expanded class A activity and loss of determinacy. e) Diagram depicting sepallata (sep1 sep2 sep3 sep4) quadruple mutant having repeating leaf-like structures, losing class E activity and disrupting class A, B, and C functions along with floral determinacy.

Development of the third whorl

The stamen comprises two morphologically evident components: the anther and the filament. The filament, a vascular tube, functions to secure the stamen to the flower and facilitates the transportation of water and nutrients. The anther houses both reproductive (microgametophyte) and nonreproductive tissues, playing a pivotal role in the production and release of pollen grains. This process is essential for the occurrence of pollination and fertilization within the flower. Immediately after the establishment of stamen primordia, the anther and filament begin differentiate (Goldberg et al., 1993).

Stamens occupy the third whorl in the flower and its specification of this organ depends primarily on the overlying activity of the B, C and E genes of the ABCE model (Ó'Maoiléidigh et al., 2014, Turczyn, 2011). The floral meristem, similar to the shoot apical meristem, is organized into three distinct cell layers, with stamen primordia generally arising from periclinal cell divisions within the L2 layer. (Jenik and Irish, 2000). The number of stamens is conversed in

families and the location of stamen primordia is predetermined in the floral meristem (Coen and Meyerowitz, 1991, Goldberg et al., 1993, Coen, 1991). The specification of stamen primordia occurs independent of other floral organ primordia (Hicks and Sussex, 1971). Genetic and molecular investigations have revealed that the specification of stamen primordia is influenced by the interaction of various homeotic genes, such as *APETALA3 (APS), PISTILLATA (PI), and AGAMOUS (AG)* in *Arabidopsis*, and their equivalents in snapdragon, *DEFICIENS (DEF), GLOBOSA (GLO), and PLENA (PLE)* (Sommer et al., 1990, Coen, 1991). Mutations in these genes lead to the loss of stamen primordia and the transformation of third-whorl primordia into a different floral organ type. Similar homeotic genes with analogous functions have been identified in other plant species, including tobacco, petunia, tomato, and corn, highlighting their conserved role in stamen primordia specification across diverse plants (Goldberg et al., 1993, Hansen et al., 1993, Angenent et al., 1992, Van Der Krol and Chua, 1993, Pnueli et al., 1994, Schmidt et al., 1993, Veit et al., 1993) .

Genes involved in organogenesis and polarity during stamen development

The size, number and boundaries of floral organ primordia is under tight regulation and interplay between a plethora of genes. Repression of WUS leads to a decline in the number of cells involved in the floral primordia thereby compromising the floral organ architecture (Weiss et al., 2005). *CLAVATA (CLV)* mutation increases meristem size resulting in more number of floral whorls with altered phyllotaxis (Clark et al., 1993, Fletcher et al., 1999). *ULT* controls cell proliferation thus disruption in its activity results in larger SAM and primordia. *PERIANTHIA (PAN),* encoding a bZIP class of transcriptional regulator, is under positive regulation of *WUS*, and plays a role in initiating the program that commits cells of floral organ primordia to undergo organ initiation (Fletcher et al., 1999, Running and Meyerowitz, 1996, Chuang et al., 1999). *ANT* gene encoding a transcription factor of the AP2 family regulates the organ size during organogenesis (Krizek, 1999).

ANT and FILAMENTOUS FLOWER/YABBY1 (FIL/YAB1) play key roles in organ polarity and growth by defining abaxial/adaxial organ identity, while NAC transcription factors like CUP SHAPED COTYLEDON 1 (CUC1), CUC2, and CUC3 establish boundaries and lateral organ separation through growth repression. *CUC* genes are epigenetically regulated, and mutations can lead to fewer petals, fused whorls, and reduced fertility. Organ polarity is critical for morphogenesis, with hormone gradients contributing to this process. *YABBY and KANADI* genes determine abaxial fate, while *PHAB* family genes *REVOLUTA (REV), PHABULOSA (PHB) and*

PHAVOLUTA (PHV) along with *JAGGED (JAG) and NUBBIN (NUB),* guide adaxial fate, particularly in the two inner whorls (Alvarez-Buylla et al., 2010).

Anther Development

Within the stamen head, the anther compartment comprises diploid cells undergoing meiosis to generate haploid microspores, which then differentiate into pollen grains or male gametophytes(Schmitz, 1977). In contrast, sporogenous cells within the ovary ultimately produce the female gametophyte, or embryo sac, containing the haploid egg cell. The phenomenon of pollination is necessary to transfer pollen grains to the stigma of the pistil. The compatible pollen grains successfully grow the pollen tube that carries the sperm cells to the egg cell for fertilization within the embryo sac (Goldberg et al., 1993)

Extensive studies on the expression of genes in stamen have been conducted in several model and crop species as early as in the 1980s around the same time as ABC model was established. A plethora of studies have been conducted since owing to the importance of stamen in crop development with respect to hybrid vigour.

Structurally, anthers are four lobed structures with a paddle like shape as depicted in *Figure In_3* (Goldberg et al., 1993). They exhibit bilateral symmetry, composed of two theca, each comprising an abaxial (lower) and adaxial (upper) lobe. Each lobe functions as a microsporangium, providing support to the developing germinal cells. Typically, most angiosperm anthers consist of four distinct somatic cell layers surrounding the germinal cells at the onset of meiosis: the epidermis, the endothecium, then the middle layer, and finally the tapetum, arranged from outermost to innermost. Regions known as intermicrosporangial stripes (IMS) 1 and 2 contain epidermal and endothecial cells, which undergo structural reorganization before anthesis to facilitate pollen dispersal (Cheng et al., 1979). The connective tissue, joining the four lobes, encloses the central vascular tissue, while extending along the Y-axis of the anther into the filament, which connects the anther to the flower base. Collectively, the filament and anther constitute the stamen (Marchant and Walbot, 2022).

SPOROCYTELESS (SPL) a downstream target of *AG* is necessary for sporogenesis during both stamen and carpel development. It is found to be ubiquitously expressing throughout the early phase of anther development. *AG* induces and upregulates *SPL* but is not crucial for the maintenance of *SPL* expression and its sporogenous activity in the microspore cells. Somatic

differentiation of the sporogenous tissue through division of archesporial cells and subsequent periclinal division is carried out by *BARELY ANY MERISTEM 1 &2 (BAM1 & 2).* Another crucial role of the *JAG and NUB* genes apart from determination of the adaxial fate, is the formation of four-lobed microsporangia. EXCESS MICROSPOROCYTES1 (EMS1) and EXTRA SPOROGENOUS (EXS), putative LRR receptor kinase, are involved in establishment of proper number microsporangial initials followed by production of tapetal cell and middle cell layer identities.

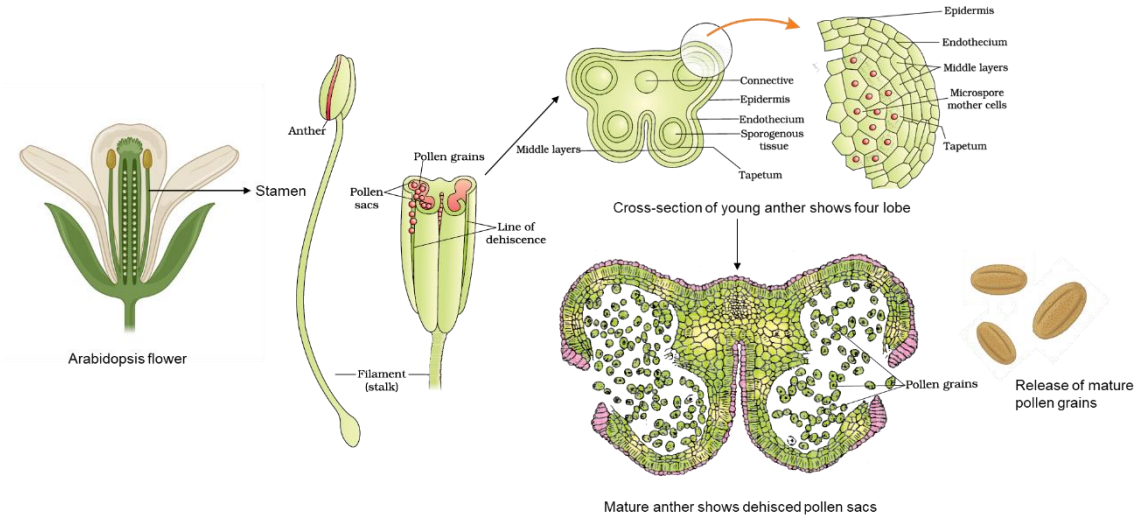

Illustration: Cross-section of an Anther

Figure In_3: Illustration showing the different layers in the four-lobed anthers of Arabidopsis flower.

Research in *Datura* has shown that the floral meristem is structured into three distinct layers—L1, L2, and L3—which contribute to the formation of various anther tissues after the initiation of stamen primordia. (Satina and Blakeslee, 1941).

Similar to the shoot apical meristem in *Arabidopsis*, the floral meristem is organized into three histogenic cell layers with distinct lineages: L1 (epidermal layer), L2 (subepidermal layer), and L3 (inner core). Stamen primordia originate primarily from the L2 layer undergoing periclinal division (Scott et al., 2004, Jenik and Irish, 2000).

In most plants, specific tissues and cell types originate from a singular germ layer. For instance, the L1 layer produces the epidermis and stomium, the L2 layer gives rise to archesporial cells, microspore mother cells, endothecium, and middle-wall layers situated between the epidermis and outer tapetum, while the L3 layer produces the connective, inner tapetum and vascular bundle(Schmitz, 1977).

Goldberg described anther development in tobacco begins with the initiation of primordia to its culmination post-fertilisation from stages -7 to stage 12 (Goldberg et al., 1993). Anther development in Arabidopsis was characterised into 14 stages on the basis of distinctive cellular events(Sanders et al., 1999). In both the studies these stages could be broadly classified into two phases.

The first phase (stages 1-8) in Arabidopsis depicted development of anther primordia to microspore tetrad formation and release. The bilateral symmetry was established along with formation of anther locules and walls, connective and vascular tissue through stages 1 to 4. Periclinal division in the archesporial cells give rise to parietal and sporogenous cell lineages further giving rise to the endothecium, the middle layer, tapetum and microspore mother cells (MMC). The MMC in each of the four locules undergo meiosis to generate tetrad of haploid microspores through stages 5 to 7. Tapetum becomes vacuolated around stage 6. At stage 8, the callose layer surrounding the tetrad undergoes degeneration and the microspores are eventually released from the tetrads. The second phase (stages 9-14) begins at the onset of stage 9 and continues till the process of fertilisation is complete. Stages 9 to 12 the microspores undergo differentiation into three-celled pollen grains, starting with microspores developing an exine wall and forming vacuoles alongside pollen mitosis and initiation of tapetum degeneration. Anther dehiscence begins during stage 12 and by stage 14 where it dehisces through ruptures along the stomium releasing the mature tricellular pollen grains and finally the process culminates by withering off of the stamens, petals and sepals, only the fertilised carpel bearing the developing seeds stand (Sanders et al., 1999, Marchant and Walbot, 2022, Goldberg et al., 1993). *Table In_1* below outlines the events related to each of the 14 stages of anther development alongside the corresponding stages of flower development (Smyth et al., 1990, Sanders et al., 1999, Bowman et al., 1989).

Table 1: Events occurring during anther development in Arabidopsis

Anther Development Stages	Description of Events and Corresponding Flower Development Stages
Stage 1	Emergence of rounded stamen primordia. (Flower Stage 5)
Stage 2	Archesporial cells form in four corners of the L2 layer. Primordia become oval.
Stage 3	Four mitotic regions form, creating primary parietal and sporogenous layers. (Flower Stage 7)

Stage 4	Four-lobed anther forms with stomium regions and vascular initiation. (Flower Stage 8)
Stage 5	Locules and microspore mother cells (MMCs) wereclearly defined and established. (Flower Stage 9)
Stage 6	MMCs enter meiosis; middle layer degenerates; tapetum vacuolates.
Stage 7	Meiosis completes, forming tetrads of microspores.
Stage 8	Callose degenerates surrounding the tetrads, releasing individual microspores. (Flower Stages 10)
Stage 9	Anther expands; microspores develop exine walls; septum cells visible.
Stage 10	Degeneration of Tapetum begins. (Flower Stages 11-12)
Stage 11	Pollen mitosis; tapetum degenerated; endothecium expands; fibrous bands and stomium differentiation begin.
Stage 12	Tricellular pollen grains present within anther locules; septum breaks, forming bilocular anther.
Stage 13	Anther dehiscence and pollen release. (Flower Stages 13-14)
Stage 14	Stamen senescence; cells shrink and degrade. (Flower Stages 15-16)
Stage 15	Stamen falls off from the flower. (Flower Stage 17)

Over the past few years, a plethora of genes have been identified for the specific roles during anther development. Comparisons between mRNA and nuclear RNA populations in the tobacco organ system revealed that approximately 10,000 mRNAs are specific to anthers and are not detectable in the cytoplasm and nucleus of cells, neither in other vegetative nor floral organ systems (Kamalay and Goldberg, 1984, Kamalay and Goldberg, 1980). These results imply that the transcriptional activation of specific gene sets is essential for establishing and maintaining distinguished cell types and roles during anther development. Within the anther lobe development of pollen grains is yet another aspect of study. The proper and timely development of Male gametogenesis within these anther lobes is crucial to bring about successful fertilisation. The process of development of Pollen grains are briefly described in the following subsection.

Pollen Development

Pollen grains are the highly reduced haploid male gametophytes in flowering plants, typically composed of two or three cells. Their primary function is to deliver two sperm cells to the embryo sac for fusion with the egg and central cell. Both these sperm cells are functionally identical and competent. This double fertilization process, along with the specialized function of the male gametophyte, is regarded as a crucial innovation in the evolutionary accomplishment of flowering plants(Gómez et al., 2015, Hackenberg and Twell, 2019). Pollen development requires a variety of genes expressing during different phases of anther development which govern the specification of anther cell types supporting pollen growth and maturation (Koltunow et al., 1990).

The regulatory mechanisms of male gametogenesis encompass several critical processes, including the influence of asymmetric cell division and cell cycle control in developmental patterning, the role and regulation of the various transcription factors in cell specification, as well as chromatin remodeling (Borg and Berger, 2015, Russell and Jones, 2015, Hackenberg and Twell, 2019). Additionally, effective interaction between germline and non-germline cells plays a pivotal role in development of male gametophyte (Berger and Twell, 2011). During the development process establishment of Germ cell fate requires unequal compartmentalisation of daughter nuclei. Also, the timely mitosis and proper orientation of spindle fibre is crucial for asymmetric microspore determination and subsequent cell fate determination (Oh et al., 2010).

In higher plants, development of male gametophyte involves a sophisticated process that relies on the synchronized involvement of various cell and tissue types, each exhibiting specific patterns in gene expression. Both the gametophytic (pollen) and sporophytic (anther, tapetum) tissues play quintessential roles in this process. The male gametophytic life cycle consists of two distinct phases, the first phase is a developmental phase occurring within the developing anther locules and concludes with the formation of mature pollen grains. The latter or functional phase, begins when the grains adhere to the stigma surface, continues with pollen tube growth, and culminates with double fertilization (Honys et al., 2006). In *Arabidopsis*, the development of the male gametophyte (*Figure In_4*) is a tightly orchestrated process that unfolds within the anthers. It begins with the differentiation of diploid microspore mother cells from archesporial cells. These microspore mother cells go through meiosis, giving rise to tetrads of haploid microspores enclosed in a callose wall. Once the callose degrades, the microspores are released and expand, each preparing for the first mitotic division namely pollen mitosis I. This division results in a

bicellular pollen grain, comprising a large vegetative cell and a smaller generative cell nestled within the vegetative cell's cytoplasm. The generative cell subsequently divides once more, undergoing pollen mitosis II producing two sperm cells. Ultimately, this sequence culminates in the formation of mature, tricellular pollen, consisting of a vegetative cell and two sperm cells, primed for double fertilization (Twell, 2011, Scott et al., 2004, Honys et al., 2006).

Studying pollen development provides a window into understanding cell fate, patterning, polarity, and signaling. The process leading to pollen grain formation and release commences with meiosis and entails precise structural and molecular alterations, necessitating gene expression in the gametophytic and sporophytic tissues of the anther (McCormick, 1993). Flowering plants maintain the stem cell niche in the meristematic tissue which is capable of forming reproductive organs with diploid sporogenous cells (Pandian, 2022).

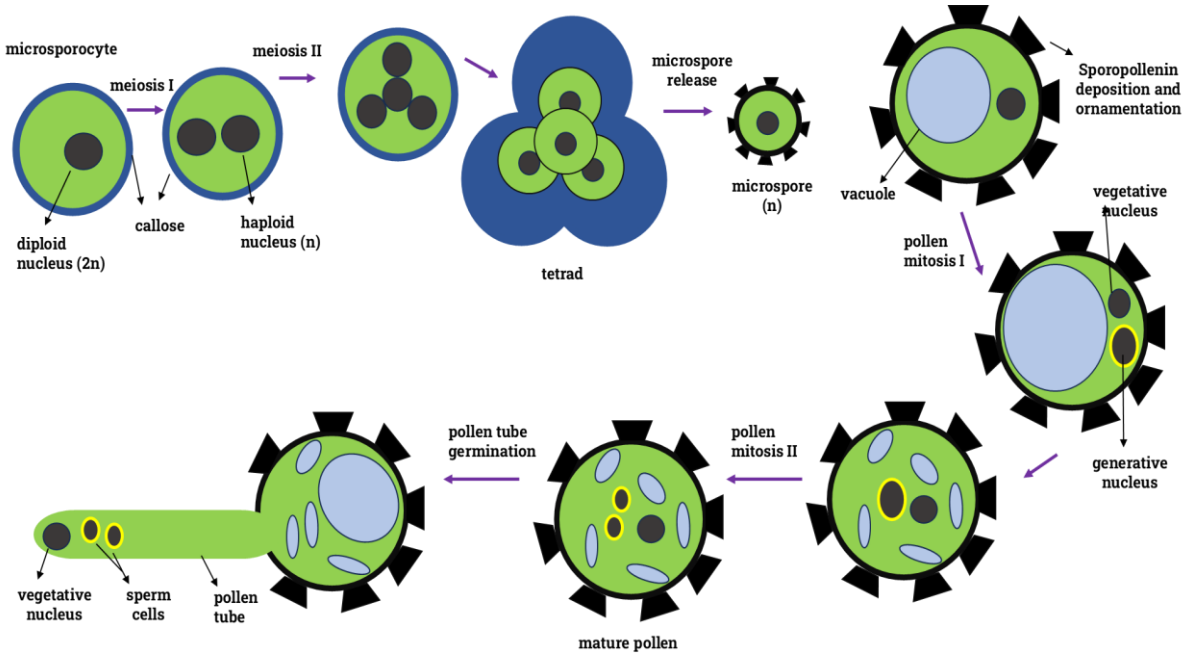

Figure In_4: Diagram depicting the events occurring during Pollen development in Arabidopsis

Pollen development begins around stage 7 of anther development where the microspore mother cell (2n) undergoes meiosis forming tetrads of haploid microspores (n) protected by callose layer (Alvarez-Buylla et al., 2010). Pollen wall synthesis is believed to begin during meiosis when tapetum-secreted callases degrade callose surrounding the microspores (Hearn, 2002, Zhang et

al., 2024b). As tapetal cells undergo programmed cell death (PCD), young microspores form primexine, a cellulose-based matrix that guides sporopollenin deposition (Jiang et al., 2013, Shi et al., 2015, Zhang and Li, 2014, Lallemand et al., 2013). By pollen maturation, despite species-specific variations, mature pollen generally consists of three layers: the outermost exine, inner intine, and tryphine. The exine, with its three sub-layers (reticulate, sexine, and nexine), features taxon-specific sculpting, crucial for species identification. Composed largely of sporopollenin, a highly stable and mostly non-degradable biopolymer, the exine's structure varies among species (Brooks and Shaw, 1968). For example, Arabidopsis pollen has a reticulate surface filled with tryphine, while wind-pollinated species like rice and maize have smoother surfaces with less tryphine, reflecting species-specific adaptations(Gong et al., 2015, Wilson and Zhang, 2009, Shi et al., 2015).

The tapetum plays a crucial role in pollen development, acting as the source of various nutrients, sugars, and enzymes necessary for the developing microspores (Parish and Li, 2010). The mutants compromised in properly developed tapetum exhibit defective pollen phenotype and male sterility. *EXCESS MICROSPOROCYTES1* (*EMS1*) associated with tapetum specification when mutated shows an absence of a tapetal layer thereby producing innumerable microspores (Zhao et al., 2002). Whereas mutation in the *TAPETUM DETERMINANT1* (*TPD1*) leads to an ill-formed tapetum that is indistinguishable from nearby cell layers (Yang et al., 2005). Hence the specification of the tapetum during early anther development is primarily governed by the TPD1-EMS1-SERK1/2 signaling pathway, where TPD1 serves as the ligand recognized by EMS1, with SERK1/2 acting as potential coreceptors (Li et al., 2017, Jia et al., 2008, Chen et al., 2019, Wei and Ma, 2023). The callose wall, primarily composed of β-1,3-glucan, must be degraded appropriately to ensure proper pollen development (Dong et al., 2005). Evidence advocates development of tapetum and its function are controlled by numerous critical transcription factors, including DYSFUNCTIONAL TAPETUM1 (DYT1), DEFECTIVE IN TAPETAL DEVELOPMENT AND FUNCTION1 (TDF1), MALE STERILITY1 (MS1), ABORTED MICROSPORES (AMS), FAT TAPETUM and AtMYB103 (Zhang et al., 2006a, Yang et al., 2007, Xu et al., 2014, Zhang et al., 2007, Zhu et al., 2008, Sanders et al., 1999, Li et al., 2006).

In nature, there may be two instances where the plant develops male sterility. Either the pollen formed is defective and hence non-viable or the healthy pollen grains are trapped within a defective anther where improper or delayed dehiscence doesn't allow timely pollination and subsequent fertilization (Sanders et al., 1999). The POLLENLESS, SIDECAR POLLEN (SCR), and GEMINI POLLEN1/2/3 produce defective pollen grains primarily due to disruption in the meiotic division during pollen development. Whereas, male sterile mutants such as the *non-dehiscent 1,*

defective in anther dehiscence 1 (dad1), delayed dehiscence 1/2/3/4/5 (dd1/2/3/4/5) and male sterile 35 (ms35) may form viable pollen but defective anther dehiscence machinery makes these plants infertile (Scott et al., 2004, Sanders et al., 1999, Goldberg et al., 1993).

Once pollen grains are formed, the subsequent event of proper pollen tube growth becomes a critical factor for effective fertilization and many genes are accountable for the same. Mutation in AtbZIP34 retards the pollen tube elongation (Gibalová et al., 2009). Double mutants *agl66agl164-2* produced aberrant pollen tubes suggesting the crucial role of MIKC* transcription factors (AGAMOUS-LIKE 30, AGL65, AGL66, AGL94 and AGL104) in pollen maturation and tube growth (Adamczyk and Fernandez, 2009, Zobell et al., 2010, Verelst et al., 2007, Liu et al., 2013, Qiu et al., 2024). AtMIKC*-type MADS transcription factors, including Agamous like 30 (AGL30), AGL65, AGL66, AGL94, and AGL104, regulate JINGUBANG transcription and expression, thereby influencing the level of pollen dormancy in Arabidopsis (Zhang et al., 2024a). The deficit of Pollen-Expressed Transcription Factor 2 (PTF2) and AtTFIIB1 significantly disrupts germination of pollen grains and its tube growth, highlighting the crucial roles that TFIIB-related transcription factors p lay in these processes (Niu et al., 2013, Zhou et al., 2013). The triple mutation in MYB97, MYB101, and MYB120 results in excessive pollen tube growth within the embryo sacs, consequently hindering proper sperm release (Liang et al., 2013). It was confirmed in a study conducted in 2014 that a significant role in this process of pollen tube growth is played by the ARID-HMG DNA-binding protein AtHMGB15 where its predominant expression is observed in the vegetative nuclei of tricellular pollen grains and pollen tubes (Xia et al., 2014).

Phytohormone Influence during Anther and Pollen Development

Flower development hinges on a delicate balance between meristem size regulation and organ initiation, influenced by hormones like cytokinin, gibberellin, and auxin. While auxin is vital for organ initiation and organogenesis, stamen development relies on almost all phytohormones specifically gibberellins and jasmonic acid (Song et al., 2013). Petal formation is particularly affected by gibberellins (GA), auxin, and jasmonic acid (JA), while gynoecium development is predominantly regulated by auxin (Chandler, 2011).

The development of male gametophytes in angiosperms is an intricately orchestrated process, seamlessly integrating various plant hormones (auxin, GA, cytokinin, JA, brassinosteroids, abscisic acid) and signaling pathways to ensure precise coordination (Marciniak and Przedniczek, 2019, Wilson and Zhang, 2009, Mascarenhas, 1990). The precise timing and spatial

regulation of crucial hormone signaling factors control pollen maturation, the dehiscence of anthers, the release of pollen grains onto the stigma, and the subsequent germination of pollen tubes, all essential for successful fertilization (Tosun and Koyuncu, 2007, Radovic et al., 2016, Sotomayor et al., 2012). The increase of auxin in the pistil post-pollination indicates its function during pollen tube growth and elongation (Wu et al., 2008, Aloni et al., 2006, Radovic et al., 2016).

When studied extensively an interplay between three hormones in the late stages of anther development (stages 9-13) was observed. During flower development (stage 10), auxin (IAA) climaxes in the stamens, driving filament elongation and preventing early dehiscence. Auxin also triggers jasmonic acid (JA) production via the ARF6/8, which surges at stages 11 and 12, coordinating filament growth, maturation of pollen grains, anther dehiscence, and flower opening (Nagpal et al., 2005, Ishiguro et al., 2001). Research has shown that disrupting auxin biosynthesis or transport can significantly impact initiation of stamen and late-stage development of stamen (Cecchetti et al., 2008). Specifically, the double mutants *yuc2 yuc6* and *mdr1 pgp1* exhibit defects in filament elongation, anther dehiscence, and maturation of pollen (Cheng et al., 2006, Geisler et al., 2005). In contrast, the *pin1*, *pin3 pin7*, and *yuc1 yuc4* mutants display severe phenotypes, including the absence or reduced number of stamens (Paponov et al., 2005, Cheng et al., 2006, Cecchetti et al., 2008).

Gibberellins (GA) support filament elongation and microsporogenesis, with mutants deficient in GA showing halted pollen development before microspore mitosis(Cheng et al., 2004). Gibberellins (GAs) are minimally involved in the initiation of stamen development but become crucial during later stages, especially for tapetum function and pollen (microgametophyte) formation (Plackett et al., 2011, Marciniak and Przedniczek, 2019).

The GA pathway influences tapetum function by regulating *OsGAMYB* in rice or *AtMYB33 and AtMYB65* in *Arabidopsis thaliana*, with evidence linking tapetum PCD through GAMYB-mediated upregulation of *OsC6*, a gene essential for rice tapetum secretory functions, suggesting that GAMYB orchestrates various aspects of stamen development (Aya et al., 2009, Zhang et al., 2010, Plackett et al., 2011).

Research on GA signaling mutants in *Arabidopsis thaliana* and rice underscores their importance (Chhun et al., 2007). Mutations in the GA receptors GA-INSENSITIVE DWARF1a and b (AtGID1a, b) disrupt stamen elongation, highlighting their precise roles in stamen development (Iuchi et al., 2007). In rice, the *osgid1-4* mutant, which lacks the GID1 receptor, exhibits halted anther development before or during meiosis, blocking tetrad formation and suggesting that GID1-dependent signaling is vital for meiotic progression, either directly or through effects on

pollen mother cells (Aya et al., 2009, Griffiths et al., 2006). Transcriptional studies confirm active GA signaling genes during the premeiotic stage (Liu et al., 2017).

The *ga1-3* mutant, which is deficient in gibberellin (GA) due to a mutation in *ent-copalyl diphosphate synthase* (CPS), an enzyme liable for the conversion of geranylgeranyl diphosphate (GGDP) to *ent-copalyl diphosphate*, exhibits male sterility (Sun and Kamiya, 1994). This sterility is characterized by the failure of filament elongation and the arrest of anther development at stage 10 of floral development (Cheng et al., 2004). Impaired filament elongation and disrupted anther development at floral stages 11 or 12 are a result of mutations in genes that encode the GA-biosynthetic enzymes, GA 20-oxidase (GA20ox) and GA 3-oxidase (GA3ox) (Rieu et al., 2008, Plackett et al., 2012, Hu et al., 2008).

GA signaling promotes the ubiquitin-mediated degradation of the DELLA protein RGA, with 38% of RGA-suppressed genes active in the male gametophyte across various microsporogenesis stages (Hou et al., 2008). Efficient fertilization relies on the precise timing of elongation in filamnts, pollen maturation, and anther dehiscence. The overlap in expression of RGA-regulated and jasmonate-responsive genes suggests a critical interplay between GA and JA pathways during stamen development (Hou et al., 2008).

Role of Jasmonic Acid in pollen development

Phytohormone JA and its derivatives are essential for two major stamen developmental processes (elongation of filament and dehiscence of anther) along with the maturation of the male gametophyte (Huang et al., 2017b, Mandaokar et al., 2006).

Jasmonic acid (JA) biosynthesis initiates with the action of the phospholipase A gene, Defective in Anther Dehiscence (DAD1), which converts lipids from anther plastids and membrane sources into α-linolenic acid, the primary precursor for JA as depicted in *Figure In_5* (Ishiguro et al., 2001). Lipoxygenases subsequently transform this α-linolenic acid, yielding a substrate for Allene Oxide Synthase (AOS), which produces epoxylinolinate (Park et al., 2002, Caldelari et al., 2011). Following this, Allene Oxide Cyclase (AOC3) catalyzes the conversion of epoxylinolinate into phytodienoic acid (OPDA), with all these reactions occurring within the plastids of the cells (Stintzi and Browse, 2000). Oxophytodienoate Reductase (OPR3) then acts on OPDA to generate 12-oxophytodienoic acid (OPC8), which undergoes a series of beta-oxidation processes via the ACX1 enzyme in the peroxisome to produce jasmonic acid (JA) (Avanci et al., 2010). This JA must then be converted

into its biologically active form, JA-Isoleucine (JA-Ile), within the cytoplasm, allowing it to migrate into the nucleus and participate in downstream signaling pathways essential for various physiological responses (Wasternack et al., 2013).

Several male sterile mutants have been detected as being impaired in the biosynthesis of JA (Sanders et al., 2000, McConn and Browse, 1996). These include the *fad* triple mutant (*fad3–2 fad7–2 fad8*), which is deficient in the fatty acid precursors necessary for JA synthesis (McConn and Browse, 1996). Another mutant, *defective in anther dehiscence 1* (*dad1*), encodes a phospholipase A1 enzyme responsible for catalyzing the initial step in the JA biosynthesis pathway (Ishiguro et al., 2001). Furthermore, research has revealed that the DAD1 gene is a direct transcriptional target of AG, providing insight into the regulatory networks that link JA biosynthesis with developmental gene expression (Ito et al., 2007).

Notably, these sterile conditions can be effectively reversed through the exogenous application of JA, demonstrating the hormone's pivotal role in precisely timing anther dehiscence. Among the four genes that encode the 13-LOX enzymes, only the *lox3lox4* double mutant displayed a male sterile phenotype highlighting the importance of LOX3 and/or LOX4 during stamen development (Caldelari et al., 2011). The *delayed dehiscence2-2* (*dde2-2*) mutant displays defects in filament elongation and anther dehiscence is triggered by a disruption in the gene encoding ALLENE OXIDE SYNTHASE (AOS) (von Malek et al., 2002).The *aos* mutant exhibited severe male sterility where the flowers fail to make silques, caused by defects in anther development, highlighting the critical role of AOS in the biogenesis of all biologically active jasmonates (Park et al., 2002). Additionally, the *dd1* and *opr3* mutants belongs to the *12-OXOPHYTODIENOATE REDUCTASE (OPR3)* gene family, which plays a vital role in JA production (Stintzi and Browse, 2000, Ishiguro et al., 2001). The *OPR3/DD1* gene is expressed specifically in the stomium and septum cells of the anther, which are essential structures for facilitating pollen release (Stintzi and Browse, 2000). The sterility phenotypes examined in these mutants bring emphasis to the significance of JA in anther development.

Additional studies revealed that ARF6 and ARF8 regulate the expression of JA-biosynthetic genes such as *DAD1*, *LOX2*, *AOS*, and *OPR3*, thereby controlling jasmonic acid production in flower buds, which is crucial for processes like dehiscence of anther and pollen maturation indispensable for proper anther development (Nagpal et al., 2005, Tabata et al., 2010, Reeves et al., 2012).

The signaling process initiates when JA-Ile binds to the Jas domain of the JAZ (Jasmonate ZIM domain) proteins, leading to the displacement of the entire repression complex, which includes

TOPLESS, NINJA, and JAZ proteins, from MYELOCYTOMATOSIS ONCOGENES 2 (MYC2), a bHLH transcription factor as illustrated in *Figure In_6* (Thines et al., 2007, Browse, 2009, Dombrecht et al., 2007, Chini et al., 2007).

This repressor complex is subsequently marked by the E3 ubiquitin ligase SCF-COI1 for degradation via the proteasome (Zhai et al., 2015, Xu et al., 2002, Xie et al., 1998). As a result, MYC2 is released to activate the transcription of downstream target genes (Thines et al., 2007, Browse, 2009, Dombrecht et al., 2007, Devoto et al., 2002, Wasternack and Song, 2017).

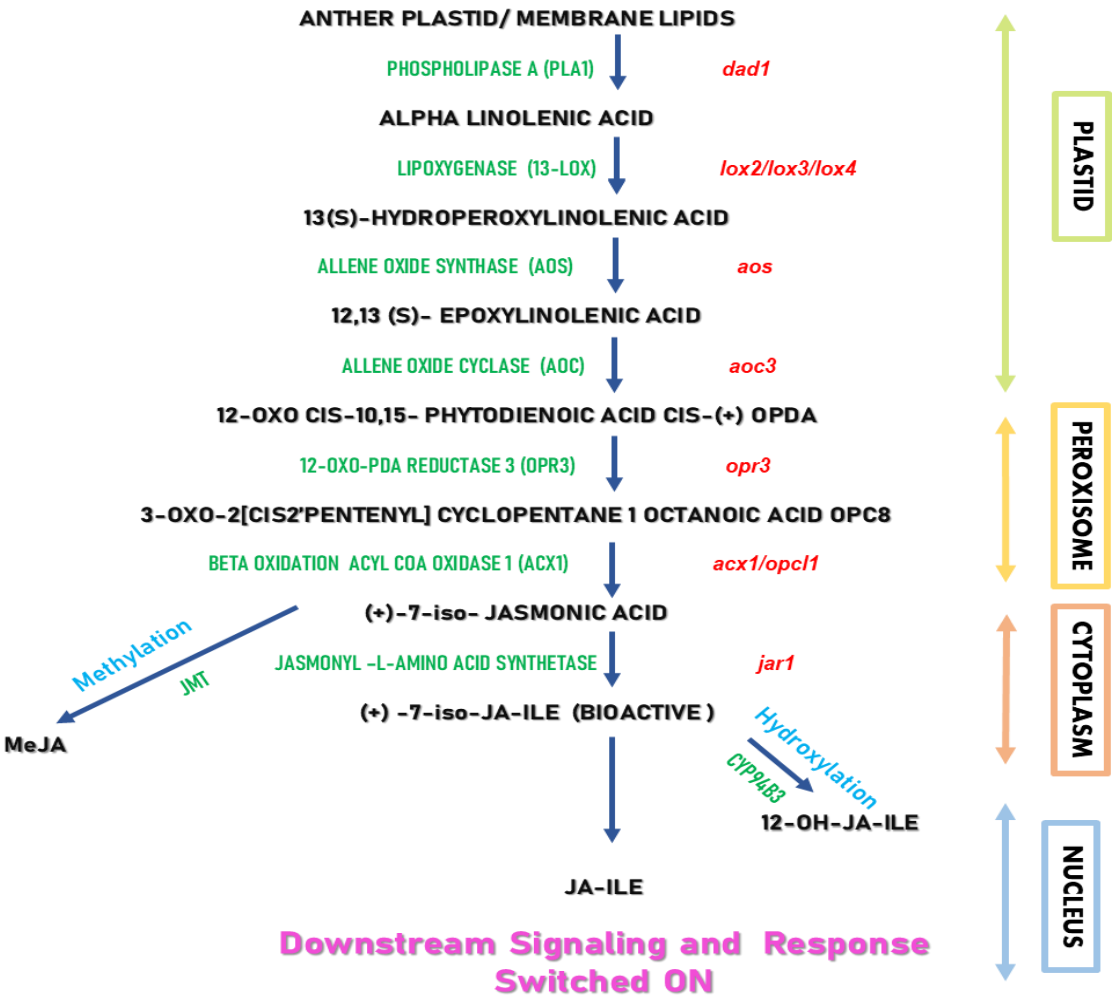

Figure In_5: Schematic of the JA Biosynthesis pathway showing important genes and the products formed at each step. The compartment of the cell where the conversion takes place is mentioned on the right. The text in red shows the mutants associated with the genes at each step of the biosynthetic pathway.

Male sterility is also detected in the *coronatine insensitive 1* (*coi1*) mutant, which serves as a JA receptor and exhibits severe defects in pollen development and anther dehiscence (Xie et al.,

1998). In *coi1* flowers, the stamens have short filaments compared to wild-type flowers, and the anthers remain irreversibly indehiscent even upon exogenous Methyl JA application, having pollen grains with prominent vacuoles (Xu et al., 2002, Xie et al., 1998, Feys et al., 1994). Jasmonic acid (JA) gathers in the cytosol, where it is conjugated to various amino acids by the JA-amido synthetase JASMONATE RESISTANT1 (JAR1) (Staswick and Tiryaki, 2004). While the *jar1* mutant remains fully fertile, it exhibits a more than 70% reduction in JA-Ile concentrations in flowers (Suza and Staswick, 2008).

The MYC2 transcription factor (TF), belonging to the basic helix-loop-helix (bHLH) family, plays a pivotal role in mediating the plant's response to JA. It exerts its influence by binding to G-box motifs located in the promoter regions of JA-responsive genes, thereby activating their transcription (Dombrecht et al., 2007, Pozo et al., 2008, Kazan and Manners, 2013, Figueroa and Browse, 2012). Research has demonstrated that MYC2, in conjunction with MYC3, MYC4, and MYC5, functions redundantly to regulate critical processes such as development of stamen and production of seeds (Qi et al., 2015, Gao et al., 2016).

While individual and double mutants for these genes do not display noticeable defects in stamen development but triple mutants *myc2myc3myc4*, *myc2myc4myc5*, and *myc3myc4myc5* exhibit significantly delayed stamen development (Schweizer et al., 2013, Dombrecht et al., 2007). In particular, their anthers fail to undergo dehiscence at floral stage 13, leading to a failure of pollen grains to germinate in vitro. Nonetheless, it is important to note that dehiscence of anther and pollen maturation can still occur at later stages of flower development.

When examining quadruple mutants, a significantly severe phenotype is observed compared to their triple mutant counterparts. These quadruple mutants display pronounced deficiencies in stamen development, exemplified by notably shorter filaments, indehiscent anthers, and the production of nonviable pollen grains (Qi et al., 2015). This illustrates the complex interplay and redundancy among the MYC transcription factors in the intricate control of stamen development and reproductive success in plants (Kazan and Manners, 2013).

The MYC2 TF plays a crucial role in coordinating JA signaling, particularly through its interaction with R2R3-type MYB transcription factors, specifically MYB21 and MYB24, during the maturation of stamens (Song et al., 2011). This interaction leads to the formation of a MYC–MYB complex, which not only activates transcription but also interacts with JAZ proteins to inhibit their repressive effects (Yang et al., 2020, Zhang et al., 2021). Additionally, GA is known to influence the expression of *MYB21 and MYB24*, thereby promoting stamen growth (Cheng et al., 2009).

Research has demonstrated that DELLA proteins, which are key regulators of GA signaling, inhibit JA biosynthesis by downregulating the expression of genes such as *DAD1* and *LOX1*. In the absence of GA, DELLA can also form complexes with MYB21 and MYB24, repressing their transcriptional activities (Cheng et al., 2009). However, the presence of GA triggers the ubiquitination of DELLA, leading to the upregulation of JA biosynthesis genes, including *DAD1 and LOX1* (Huang et al., 2020). Consequently, the elevated levels of JA promote the expression of *MYB21 and MYB24* (Huang et al., 2020).

This intricate interplay illustrates how GA and JA signaling pathways synergistically regulate stamen elongation by controlling MYC–MYB signaling networks (Song et al., 2014, Chini et al., 2016). Mutant analyses further elucidate the functional roles of these *MYB* genes; for instance, myb21 mutants exhibit shortened filament lengths that prevent them from reaching the stigma, resultant in complete male sterility, although their pollen grains remain viable (Mandaokar et al., 2006). In contrast, myb24 mutants are completely fertile, underscoring that MYB21 is needed for filament elongation, while *MYB24* contributes to pollen viability and anther dehiscence. The myb21/myb24 double mutants, however, demonstrate compromised stamen development and complete sterility, highlighting the critical importance of *MYB21 and MYB24* in the regulation of reproductive success in plants (Mandaokar and Browse, 2009, Huang et al., 2017a, Song et al., 2011, Mandaokar et al., 2006, Huang et al., 2017b).

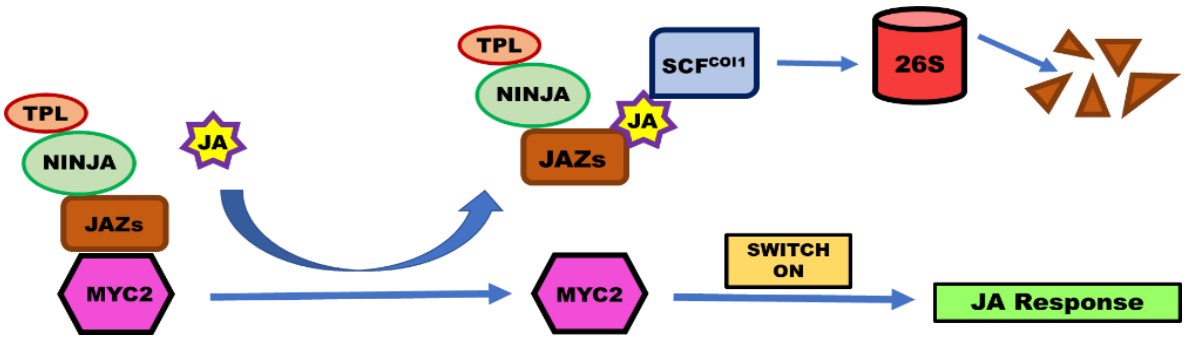

Figure In_6: Schematic of the JA Response pathway highlighting the important genes at each step. TOPLESS (TPL), NINJA and JAZ form a repression complex repressing the activity of MYC2 under low JA levels. Once JA-Ile concentration increases in the cell, it binds to the Jas domain of JAZ targeting them for proteasomal degradation via SCF^{COI1} E3 ubiquitin ligase. Once the repression is lifted the MYC2 switches on the transcription of crucial genes.

Transcriptional regulation: role of non-histone protein

In eukaryotic cells, chromatin serves as the foundation for nuclear processes like replication, recombination, repair, and transcription. The dynamic nature and versatile conformations of chromatin act as control mechanisms for DNA targeting processes.

The ease of access in eukaryotic DNA is contingent on the hierarchical organization of chromatin, involving intra- and inter-nucleosome interactions, and the effect of non-histone chromatin architectural proteins. Interplay exists among these levels, wherein one level may supersede another or multiple levels may act synergistically. (McBryant et al., 2006)

Nucleosomes are fundamental units of chromatin. At the first level, nucleosome stability relies on the quantity and type of interactions between core histones and the surrounding DNA, along with interactions among proteins within the core histone octamer. They consist of a nucleoprotein core wrapping 147 base pairs of DNA around a core histone octamer, namely, H2A, H2B, H3, and H4. Factors such as core histone variants, post-translational histone modifications, and linker histone binding to DNA collectively affect nucleosome organization and stability.

These nucleosome core particles assemble into an array of oligonucleosomes, forming a progressively compact structural hierarchy of chromatin. Upon linear arrangement of nucleosomes in chromatin arrays, a level two of organization emerges. Amino terminal tails of histone proteins establish connections with adjoining and distant nucleosomes, within and across discrete fibers.

The level three of organization is superimposed on these 'intrinsic' constraints and is influenced by chromatin-binding proteins that modify the architecture of the underlying fiber. The compact structure of oligo-nucleosomes hinders the interaction of DNA-binding protein factors with DNA. Certain chromatin architectural proteins can circumvent intrinsic constraints, introducing topological effects and resulting in distinctive supramolecular assemblies that significantly affect DNA accessibility (McBryant et al., 2006).

Cells have evolved specialized proteins to manipulate complex chromatin structures during nuclear processes. The modulation of chromatin structure is essential for gene transcription. This modification of the chromatin landscape is carried out through the coordinated actions of histone modifiers, chromatin remodelers, and architectural proteins. These activities are necessary across the entire locus, including the promoter, upstream regulatory regions, and the gene body, to successfully initiate and sustain transcription. Histone modifiers are enzymes that add or remove chemical groups (like methyl, acetyl, or phosphate) from histone proteins, altering

chromatin structure and influencing gene expression. Chromatin remodelers are protein complexes that use energy from ATP to reposition, eject, or restructure nucleosomes, making DNA accessible for transcription. Architectural proteins organize and stabilize chromatin structure, shaping the three-dimensional genome landscape and facilitating or restricting interactions between regulatory elements and gene promoters.

Architectural proteins

Architectural proteins are a class of proteins that shape and organize chromatin structure, influencing how DNA is folded within the cell nucleus. They play a crucial role in forming higher-order chromatin organization and ensuring proper spatial arrangement of the genome, which impacts gene regulation and overall genome stability. Examples of architectural proteins include: CCCTC-binding factor (CTCF), Cohesin and Condensin Complexes, High Mobility Group (HMG) Proteins and Linker Histones (such as H1). By controlling chromatin organization, architectural proteins are essential for gene accessibility, expression regulation, and the overall functional organization of the genome.

Proteins exhibiting strong binding affinity to the four-way (Holliday) junction DNA encompass recombination enzymes, along with a remarkably diverse array of ostensibly unrelated proteins. These embrace HMG1 box proteins, members of the HMGI-Y family, winged helix proteins (including linker histones), the SWI/SNF complex, and some prokaryotic proteins with no apparent connection (Bustin, 1996). These proteins have a unified tendency to bind to bent DNA, induce DNA bending upon binding, and/or preferentially interact with DNA crossings. Consequently, they primarily function as architectural proteins, although some, such as the SWI/SNF complex, have definite functional roles. Because of their ability to bind to or facilitate the formation of specific DNA structures, these proteins are often interchangeable in cellular processes. Moreover, because multiple protein motifs can recognize a particular DNA structure, it is not astonishing that seemingly unrelated proteins fall into the same functional category (Zlatanova and van Holde, 1998). High-mobility group (HMG) proteins in eukaryotes are one of many families of architectural proteins that play a crucial role in stabilizing alternative DNA structures and modulating chromatin dynamics by influencing the twisting and untwisting of linker DNA (Roy, 2016, Mallik et al., 2018).

HMG Proteins

Over five decades ago, studies on the second utmost abundant chromosomal proteins after histones were published (Bianchi and Agresti, 2005). High Mobility Group (HMG) proteins have emerged as a distinct class based on their extractability from calf thymus chromatin and unique biochemical properties (Goodwin, 1973). The term was coined based on its rapid mobility during gel electrophoresis owing to its small size and high solubility (Zhang, 2008). Mammalian HMG proteins, divided into three families (HMGA, HMGB, HMGN), exhibit characteristic primary structures. In plants, the HMGA and HMGB families have been extensively studied, but no evidence of HMGN proteins has been found, suggesting their exclusivity to vertebrates (Bustin, 2001a, Bustin, 2001b).

HMGB Proteins

Amid the several HMG proteins, the role of high-mobility-group B (HMGB) chromosomal proteins in disrupting nucleosome structure, a key aspect of regulating DNA accessibility in chromatin, has been meticulously discussed in previous studies. HMG-box proteins play architectural roles in nucleoprotein complex assembly and participate in processes, such as transcription and recombination. The HMGB proteins are characterized by the HMG-box DNA-binding domain (Grasser, 2003, Grasser, 2006). The HMG-box is a conserved nearly 75-amino acid protein domain recognized as a characteristic feature of chromosomal high-mobility group (HMG) proteins, particularly the HMGB type (Antosch et al., 2012, Štros et al., 2007). Its L-shaped fold, formed by three alpha-helices, exhibits conservation beyond the amino acid sequence similarity. Functionally, the HMG-box domain primarily mediates DNA binding through the minor groove, inducing DNA bending by widening the minor groove and compressing the major groove. Functionally, the HMG -box domain primarily mediates DNA binding through the minor groove, inducing DNA bending by widening the minor groove and compressing the major groove, thereby facilitating nucleoprotein complex assembly, recombination, and transcription (Agresti, 2003). These findings proposed a model in which HMGB proteins, along with histone H1, modulate the equilibrium between alternative nucleosome conformations, impacting chromatin compaction, mobility, and accessibility. Thus, highlighting the potential of HMGB proteins in orchestrating crucial cellular processes related to gene regulation and chromatin dynamics (Cato, 2008, Mallik et al., 2018).

Plant HMGB proteins

Plant genomes encode HMG-box proteins, with small chromosomal HMGB proteins representing the extremely diversified subgroup. Plant HMGB proteins, typically around 30 kDa, possess a central HMG-box DNA-binding domain verged by basic N-terminal and acidic C-terminal domains. In various proteins interacting with DNA, HMG-box domains often occur in combination with different functional protein domains, contributing to diverse nuclear functions. The HMGB family in plants exhibits considerable structural variability, with Arabidopsis HMGB proteins ranging from 14.2 to 26.9 kDa due to differences in N- and C-terminal domain sizes. Despite the mild conservation of amino acid sequences, these terminal domains modulate various properties, such as DNA interactions, chromatin association, and protein interactions. HMGB gene expression varies widely but is generally considered ubiquitous across different plant species.

Database analyses indicate the presence of HMGB-type proteins in all plants and algae. Studies have highlighted the dynamic nature of plant HMGB proteins within the cell nucleus, where they transiently bind to chromatin, thereby influencing chromatin structure and accessibility to regulatory factors.

Plant HMGB proteins show greater structural diversity than their animal counterparts do. For example, the Arabidopsis genome encodes eight HMGB proteins based on amino acid sequences. Experimental analyses revealed differences in functionality, emphasizing the need for experimental validation, particularly in domains with lower sequence conservation.

Previous findings have highlighted the complexity of HMGB proteins with potential redundancy among family members. Their expression levels are critical for proper plant performance, and further research is needed to unravel the specific interactions and regulatory roles of HMGB variants under different growth conditions. Understanding these aspects is crucial for comprehending the contribution of HMGB proteins to plant stress responses (Pedersen and Grasser, 2010).

Plant HMGB proteins play crucial roles as specific cofactors in cellular pathways. The observed redundancy and specificity among HMGB variants highlights their intricate contributions to plant development and stress responses.

Phylogenetic analysis encompassing all HMG-box proteins found in terrestrial plants and primitive species such as *Selaginella moellendorfii* (pteridophyte), *Physcomitrella patens (moss)*,

and *Chlamydomonas reinhardtii* and *Volvox carteri*, (green algae) classifies them into four discrete families based on their structure and their similarity in amino acid sequence: chromosomal HMGB proteins, AT-rich interaction domain (ARID)-HMG proteins, 3xHMG-box proteins, and Structure-Specific Recognition Protein1 (SSRP1). An overview of the structural and functional characteristics of the distinct families, highlighting their roles in various cellular functions, is presented below *(Figure In_7).*

Chromosomal HMGB Proteins: Plant chromosomal HMGB proteins have structural differences from their mammalian counterparts, featuring a single HMG-box flanked by basic and acidic regions, and are known to interact with transcription factors like DOF, though their role in enhanceosome formation remains unclear.

3xHMG-Box Proteins: Unique to plants, 3xHMG-box proteins contain an N-terminal basic domain and three HMG-box domains at the C-terminal, are expressed in a proliferation-dependent manner, and may play roles in chromosome condensation and segregation during cell division.

SSRP1 (Structure-Specific Recognition Protein1): As a component of the FACT complex, SSRP1 functions as a histone chaperone facilitating RNA polymerase II transcription, is crucial for plant development, and influences flowering time, leaf growth, and genomic imprinting in Arabidopsis.

ARID-HMG Proteins: Characterized by the presence of ARID (AT-Rich Interaction Domain) and HMG-box domains, ARID-HMG proteins are plant-specific, bind AT-rich DNA sequences, and are found across both higher and lower plant species, though their precise functions in plants remain to be determined. The proteins harbouring an ARID and an HMG-box domain seem to be explicit for plants (Riechmann et al., 2000, Štros et al., 2007). A related protein was identified in the *Selaginella moellendorfii* and *Physcomitrella patens*, indicating the occurrence of ARID-HMG proteins in both higher and lower plant species (Antosch et al., 2012, Hansen et al., 2008, Štros et al., 2007).

In summary, the structural and functional diversity of HMG-box proteins, including ARID-HMG, 3xHMG-box, and SSRP1, underscores their significance in various cellular processes, with specific implications for plant development and genomic imprinting (Antosch et al., 2012, Roy, 2016). Ongoing research is aimed at uncovering the precise roles and mechanisms associated with these proteins in plants.

ARID-HMG proteins in Arabidopsis

Previous studies searched the *Arabidopsis* database and the Plant Chromatin Database to identify plant proteins harbouring both ARID and HMG-box domains. The analysis revealed four such sequences in *Arabidopsis* and two in rice, with no similar sequences found in other organisms through GenBank search. The structural characteristics of ARID-HMG proteins, including size and domain arrangement, are conserved among different species. The proteins, typically ranging from ~35 to 52 kDa (except for the larger *Physcomitrella* protein), exhibit a consistent structural arrangement. The N-terminal section houses the ARID, whereas the C-terminal part accommodates the HMG box, as illustrated. To further elucidate the relationships among ARID-HMG proteins, a neighbor-joining tree was created using amino acid sequences from *Arabidopsis*, poplar, rice, maize, and *Physcomitrella*. Phylogenetic analysis grouped these proteins into subfamilies showing both monocot- and dicot-specific branches. The amino acid sequences of the ARID and HMG-box domains, along with a short-conserved region between them, displayed significant conservation among ARID-HMG proteins from various plant species (Hansen et al., 2008).

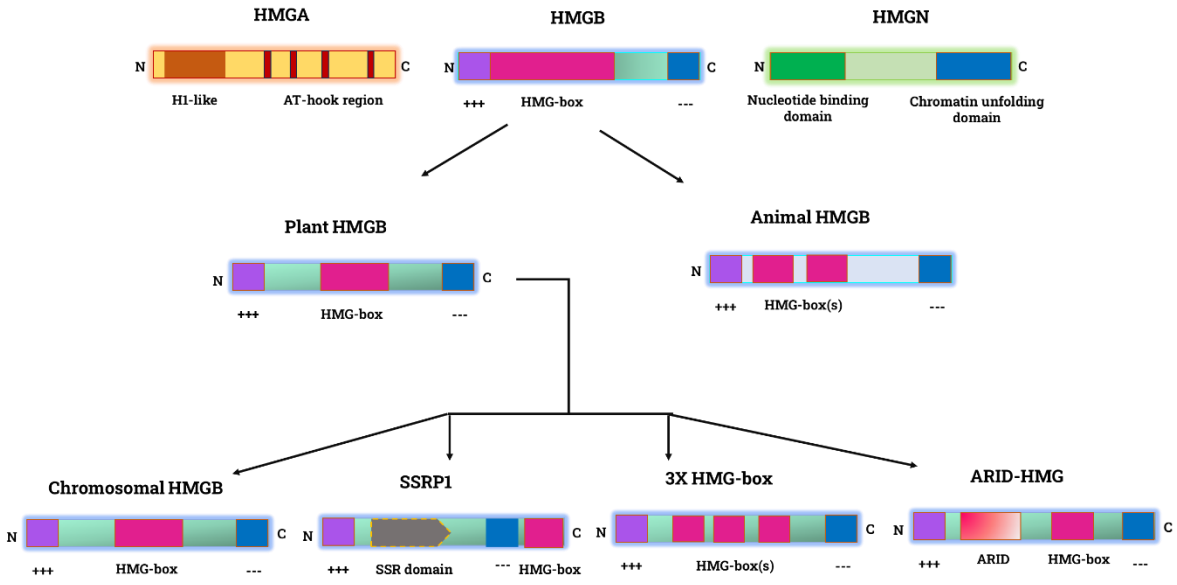

Illustration: HMG family of proteins

Figure In_7: Diagram illustrating the High Mobility Group (HMG) superfamily members, including HMGA, HMGB, and HMGN proteins. The HMG-box family is primarily divided into plant and animal HMG-box proteins. Plant HMGBs are further categorized into Chromosomal HMGB, SSRP1, 3X HMG-box, and ARID-HMG protein subgroups.

In *Arabidopsis thaliana*, 15 members of the HMG-box family have been identified that contain at least one HMG-box domain, a well conserved DNA-binding domain, four of which belong to the novel ARID-HMG group (Hansen et al., 2008, Mallik et al., 2018, Roy, 2016). They are AtHMGB9, AtHMGB10, AtHMGB11 and AtHMGB15 of which the first two were characterised by Hansen *et al* in 2008 and the latter two in our laboratory by Roy *et al* in 2016. Multiple sequence alignment of the concerned protein sequences from different members of the Brassicaceae family revealed that AtHMGB10 and AtHMGB11 were closely related and diverged from the tree earlier than the other two members. All four proteins were predominantly localized in the nucleus, although in AtHMGB9, AtHMGB10, and AtHMGB15, fluorescence was noticed in the cytosol, which was greatly weaker than that in the nucleus but was clearly detectable (Roy, 2016).

Tissue-specific expression of all four ARID-HMGs revealed that *AtHMGB11 and AtHMGB15* showed much weaker expression than *AtHMGB9 and AtHMGB10*. *AtHMGB10* was expressed throughout with a spike in imbibed seeds, whereas *AtHMGB9* expression peaked in leaves and siliques compared to other tissues. *AtHMGB11* expression spiked in the young and mature siliques. Studies revealed *AtHMGB15* expressed majorly in the seedlings, young and mature flowers and young pods.

AtHMGB15 in plant development and stress response

Previous studies from our lab have highlighted the binding bias of ARID-HMGs to AT-rich regions as observed through the DNA binding assay. AtHMGB15 also possesses the property of DNA circularisation like those of other ARID-HMG proteins (Roy, 2016).

A study performed in our lab by Mallik *et al* in 2020, provided an insight to the AtHMGB15 occupancy in the euchromatin region with the highest enrichment in the gene bodies. They focussed on the involvement of the ARID or HMG-box domain of AtHMGB15 in DNA binding events. DNA binding research conducted with the protein, full-length and its truncated forms revealed that the DNA binding activity of full-length AtHMGB15 is predominantly facilitated by the ARID domain, as no DNA-protein complexes were detected in the case of the HMG domain. This study simultaneously revealed the DNA recognition sequence of AtHMGB15 through both in-vitro and in-vivo analysis from the DNA binding assay. It was found that AtHMGB15 has a preference to bind to an AT rich sequence with a motif *A(A/C)−ATA−(A/T)(A/T)* (Mallik et al., 2020).

Another crucial aspect of this study revealed the involvement of AtHMGB15 during cold stress response in *Arabidopsis* seedlings. Initially they investigated for the involvement of environmental cues dictating expression of AtHMGB15 which revealed expression for Cold stress spiked among the other environmental cues namely, salinity, drought, ABA, UV and heat stress. In silico sequence analysis from the Chip-chip results showed presence of stress responsive elements in the 500bp upstream region of AtHMGB15 start site. Genome wide DNA binding studies indicated a significant enrichment of about 4689 loci during cold stress whereas about 6128 loci were enriched in the control dataset. Analysis of 1855 overlapping loci was crucial as it accounted for the regions that have the strong binding sites for ATHMGB15. The outcomes of the enrichment in Gene Ontology (GO) molecular function (MF) categories related to pollen development and its germination, as well as transcriptional regulation, are noteworthy. Key genes within these categories include MICK_MADS transcription factors, proteins involved in cell wall biosynthesis in pollen tissue, actin-binding proteins, calcium transporters, calcium-dependent protein kinases, helicases, and chromatin remodelers like SWI/SNF. The reinforcement of chromatin modifications, helicase activity, and actin filament categories further supports the anticipated associations, given that chromatin remodeling complexes, such as SWI/SNF or RSC, typically incorporate helicases and Actin-related proteins in their functional components. Notably, the enrichment in categories related to the response to stress and abiotic stimuli sheds light on the previously unrecognized role of AtHMGB15. Network analysis of cold-induced genes enriched for AtHMGB15 binding sites revealed three highly connected clusters, prominently associated with hormone signaling, stress response, and ion transport pathways.

By integrating ChIP-chip data with pre-existing gene expression profiles under cold stress, we identified Gene Ontology (GO) categories enriched in MAPK signaling, cold response, abscisic acid response, transcription regulation, abiotic stress response, and hormone-mediated signaling pathways. AtHMGB15 was found to bind to transcription factors from DREB, MYB, bHLH, WRKY, and NAC families, along with Ca2+-binding signaling proteins—all of which are upregulated early in response to cold. Additionally, AtHMGB15 binding was detected at 2 hours on genes like osmoprotectants (AtGolS, AtP5CS, AtRafS1), LEA family proteins (ERD10, RD17), KIN proteins, hydrophilic proteins (RD29A, RD29B), cellular metabolism proteins, and other cold-induced genes (such as COR47), although their peak expression occurred at later stages. Despite the peak expression of AtHMGB15 occurring at 12 hours, conducting ChIP-chip at the 2-hour mark allows for the identification of AtHMGB15 binding loci that undergo rapid expression or repression during the early stages of cold stress response. In cases where gene expression peaks or declines at later time points, it could be postulated that AtHMGB15 is involved in priming these loci for subsequent transcriptional changes, contributing to a delayed response. These results fortified

the involvement of AtHMGB15 throughout cold stress response in *Arabidopsis* seedlings (Mallik et al., 2020).

Another study led by Xia et al in 2014, revealed the substantial role of AtHMGB15 in pollen tube growth. It exhibits preferential expression in pollen grains and its tubes, localizing specifically to the vegetative nuclei of tricelled pollen grains and its tubes. AtHMGB15 expression when knocked down through Ds insertion resulted in impaired pollen tube growth, causing a substantial decrease in seed set. Mutation in the *athmgb15-1* impacted the expression of 1686 genes in mature pollen, particularly those associated with the formation of cell wall and its modification, cellular signaling and transport during pollen tube growth. Furthermore, in vitro studies indicated that AtHMGB15 not only binds to DNA but also interacts with transcription factors AGL66 and AGL104, essential for pollen maturation and tube growth (Xia et al., 2014).

Proper stamen development is necessary for the reproductive success and continuity of plant species, as any abnormalities in this process can lead to male sterility. This intricate developmental pathway is governed by precise genetic controls that ensure the correct anatomical and morphological formation of stamens, as well as the production of viable pollen grains, which are crucial for successful pollination and fertilization. Plant hormones act as key endogenous mediators of genetic information, playing a significant role in this process. Research on the developing stamen of Arabidopsis has provided constructive perceptions into the critical components of jasmonate signaling involved in stamen maturation. Strong genetic evidence supports the involvement of various jasmonate-related factors, including key enzymes responsible for jasmonate synthesis, hormone perception co-receptors, and transcription factors that facilitate the translation of jasmonate signaling into gene expression changes.

Recent findings reveal AtHMGB15 emerging as a vital transcriptional regulator within the vegetative cells of male gametophytes, playing a significant role in growth of pollen tube. This research focuses on investigating the involvement of the ARID-HMG DNA-binding protein AtHMGB15 in the processes underlying pollen development. However, the mechanistic role of AtHMGB15 regulation in pollen development is not well studied. This study aims to explore the possible intersection between AtHMGB15 and the jasmonate pathway, focusing on how their combined actions regulate the spatiotemporal expression of critical factors necessary for stamen and pollen development in *Arabidopsis thaliana*.

Objectives

- *Phenotypic characterizing of athmgb15-4 mutant focusing on pollen properties (morphology study of whole plant, root, silique, seeds, pollen structure, viability and pollen tube germination).*

- *To identify the principle pathway(s) regulated ATHMGB15 during pollen development using RNA seq approach (pathways that are responsible for this phenotypic defect elucidate the role of the architectural protein AtHMGB15 in the pollen developmental pathway by comparing the transcriptome of wild type and athmgb15-4 mutant flowers.)*

- *Generation of complementation line: Complementation of mutant athmgb15-4 with full length AtHMGB15 CDS, to study the rescue of morphological, physiological, and phenotypic defects characterized in the mutant.*

- *Identifying the player(s) of the principle pathways responsible for the mutant phenotype.*

Chapter One

Section 1

Phenotypic analysis of athmgb15 mutants to understand the role of AtHMGB15 in pollen development.

Section 2

Comparative transcriptome analysis to decode the pathways affected by AtHMGB15 deletion.

Section 3

Complementation of ATHMGB15 in the mutant background to confirm the Rescue of defects in complementation lines, reinforcing the validity of our study.

Material and Method

Section 1

Plant Material and Growth Conditions

For the current study, the *Arabidopsis thaliana* ecotype Columbia-0 (Col-0) and *athmgb15-4* (T-DNA insertion line of AtHMGB15 (GABI_351D08) previously obtained from Eurasian Arabidopsis Stock Centre (NASC), and the T-DNA insertion line of AtHMGB15 (SALK057612C) was obtained from the Arabidopsis Biological Resource Centre (ABRC) were used. Both the T-DNA insertional lines were previously screened in our lab.

Seeds were sterilized and sown on Murashige & Skoog (MS) agar plates. After being stratified at 4°C, the seeds were germinated under a light cycle of 16 hours of light (approximately 150±10 µmol m^{-2} s^{-1}) and 8 hours of darkness at 22°C in the plant growth chamber.

For phenotypic observation and comparative studies, the seedlings were transferred to a soil-rite mix and grown until maturation. The 14-day-old seedlings were used to compare the rosette pattern and root length simultaneously. Inflorescence bolting pattern was studied during 25 to 40-day-old plants. Freshly opened mature flowers were harvested around 9 am to 11 am (IST) during the flowering stage 13 for various flower and pollen grain-related studies. Siliques were harvested from 45-60 days old plants.

For seed propagation, the seeds were collected from mature siliques, dehydrated via airdrying or in vials with silica gel and stored for months at a stretch at 4°C.

Sterilization of Seeds and Seed Plating

Preparation of Murashige & Skoog Media:

- 34.08gms (One sachet) of MS media (Himedia PT010) with vitamins and sucrose was dissolved in 800 ml of Millipore water to prepare one litre of MS media.
- To the solution, 0.44 g of $CaCl_2$ was added.
- The pH was then adjusted to 5.6-5.8 using a 10 (N) KOH solution.
- The media was divided into 5 parts and to each conical about 0.8% wt/vol Himedia PT pure agar was added.

- To maintain sterility the MS media was autoclaved at 15 psi and 121°C for 15 minutes.
- In a laminar airflow hood, the media was allowed to cool, and approximately 25 ml was poured per tissue culture plate. For the *athmgb15-4* plants to the plates, Sulfadiazine was mixed to a final concentration of 5µg/ml.

Solutions Required for Seed Sterilization:

- 70% (v/v) Ethanol Solution: 35 ml of stock 100% (v/v) ethanol was mixed with autoclaved Millipore water to make up a final volume of 50 ml.
- 50% (v/v) Bleach Solution: 25 ml from 4% (v/v) stock solution of sodium hypochlorite was added to autoclaved Millipore water to make up a final volume of 50 ml
- 0.05% (v/v) Tween-20 Solution: 25µl of Tween-20 was added to prepare a 50ml of solution.

The solutions were filter-sterilized in a laminar airflow and stored at 4°C.

Sterilization and Plating of Seeds:

- In a sterile laminar airflow hood, Arabidopsis seeds were suspended in 200 µl of 70% ethanol solution and vortexed gently for 5 to 7 minutes.
- The ethanol solution was eliminated, and the seeds were washed nine times with 600 µl of filter-sterilized water, with occasional vortexing.
- The seeds were then soaked in 600 µl of 50% bleach solution (sodium hypochlorite) for no more than 5 minutes, followed by complete rinsing with water as in the previous step.
- The seeds were treated with 600 µl of 0.05% Tween-20 solution for 10 minutes and rinsed thoroughly with water twelve times or more, with repeated vortexing until all traces of Tween-20 were removed.
- The seeds were suspended in sterile water, and approximately 20-25 seeds were carefully placed on MS agar plates.

RNA isolation, Synthesis of cDNA and Real-time PCR

Materials Required Before Starting RNA Isolation:

- TRIzol® (Takara) reagent.
- Liquid nitrogen to enable uniform homogenization of tissue.
- DEPC water: 0.1% DEPC (Sigma) in water, stirred for ~3 hours in the dark.
- Mortar and pestle treated with DEPC water overnight and baked for the next 48 hours at 200°C in a dry heat oven.
- 70% and 75% ethanol made in DEPC water.

- DNase I (Thermo Scientific) enzyme and 10X DNase I buffer for DNase treatment.
- Centrifuge was set to cold settings to ensure proper isolation of RNA.

RNA Isolation by TRIzol Method:

Tissue Homogenization:

- 100 mg of flower sample was homogenized in liquid nitrogen to a fine powder and suspended in 1 ml of TRIzol reagent (Invitrogen) per 100 mg of tissue.
- The homogenate was incubated at room temperature for 10 minutes.

Centrifugation and Phase Separation:

- The homogenate was centrifuged at 12,000g for 10 minutes at 4°C, and the supernatant was transferred to a new autoclaved tube.
- To the supernatant, 200 µl of chloroform per 1 ml of TRIzol reagent was added, mixed gently, and centrifuged at 12,000g for 15 minutes.

RNA Precipitation:

- The aqueous phase (supernatant) was collected and total RNA was precipitated by adding 0.5 ml of isopropyl alcohol per 1 ml of TRIzol reagent.
- The samples were centrifuged at 12,000g for 10 minutes at 4°C.

RNA Washing:

- The RNA pellet was washed with 75% ethanol prepared in DEPC water.
- The RNA pellet was air-dried, dissolved in 50 µl of RNase-free water, and subjected to DNase I treatment mentioned below.

DNase I Treatment:

- The isolated RNA was treated with DNase I (Thermo Scientific) for 2 hours at 37°C to ensure removal of any DNA contamination.
- The DNase I digestion reaction was set up as follows:

Component	Amount (µl)
RNA	50
10X DNase I buffer with $MgCl_2$	10
DNase I (1U/µl)	4
H_2O	136
Total volume	200

Extraction with TRIzol and Chloroform:

- The reaction mix was extracted with equal volumes of TRIzol (100 µl) and chloroform (100 µl), mixed properly, and centrifuged at 12,000 rpm for 10 minutes at 4°C.

RNA Precipitation:

- The upper aqueous phase (~200 µl) was moved to a fresh microcentrifuge tube, and 100% ethanol (2.5X of sample volume) and 3M Na-Acetate pH 5.2 (0.1X of sample volume) were added, mixed properly, and incubated to precipitate RNA, either at -20°C overnight or at -80°C for at least 1 hour, respectively.
- The samples were then centrifuged at 13,000 rpm for 30 minutes at 4°C to pellet the RNA.

Final RNA Washing and Dissolution:

- The supernatant was carefully removed, and the RNA pellet obtained, was rinsed using 1 ml of 75% ethanol, followed by centrifugation at 13,000 rpm for 10 minutes at 4°C.
- After centrifugation, the supernatant was discarded, and the RNA pellet was dried and dissolved in 30 µl of RNase-free water.

RNA Quality Check:

- The RNA concentrations were determined using a Nanodrop spectrophotometer.
- The quality of RNA was checked by denaturing MOPS-formaldehyde agarose gel electrophoresis.

Denaturing MOPS-Formaldehyde Gel Electrophoresis:

Preparation of 10X MOPS Buffer (1 Litre):

Components	Final concentration (mM)	Amount
3-[N-Morpholino] propane sulfonic acid (MOPS)	200	41.8g of MOPS
Sodium Acetate.3H2O	20	2.72g of Sodium Acetate
EDTA	10	20ml from 0.5M stock

The pH of the buffer was set to 7.0 using 10N NaOH and filtered using a 0.2uM filter syringe in a sterile autoclaved container.

Gel Casting and Running:

- 1.5 g of agarose was added to 10 ml of 10X MOPS buffer and 72 ml of DEPC-treated water, heated to dissolve the agarose completely.
- After cooling to ~65°C, 18 ml of formaldehyde was added, and the gel was immediately poured into a gel casting tray and solidified at room temperature.

- The gel was equilibrated by running it in 1X MOPS running buffer in a gel running tank for 30 minutes at 80V before use.

Sample Preparation and Electrophoresis:

- Each 10 µl sample was mixed with 3 µl of ethidium bromide (1 mg/ml), incubated at 65°C for 15 minutes in a dry heat bath, and snap chilled on ice for 5 minutes.
- 6 µl of 5X RNA loading dye was added to each sample, and the samples were run on the denaturing MOPS gel.
- The samples were electrophoresed in 1X MOPS at 80V for 2 hours.
- The quality of RNA was confirmed by observing high-quality 18S and 28S bands of RNA. Total RNA was measured using a NanoDrop spectrophotometer and then subjected to cDNA synthesis.

Reagent	Volume (ul)
Saturated aqueous Bromophenol Blue solution	3.2
600mM EDTA	1.60.4
37% (12.3M) Formaldehyde	1.5
100% Glycerol	0.4
Formamide	616.8
10X MOPS Buffer	0.8
RNase free water	376

cDNA Synthesis from RNA:

To synthesize the first strand cDNA, reverse transcription was conducted using 5 µg of RNA and an oligo dT (18) primer. The process was carried out in two steps:

Step I-Preparation of Reaction Mix A:

A reaction mix was prepared with the following components:

Component	Amount
Total RNA	5 µg
Oligo dT(18) primer (0.5 µg/µl)	1 µl
RNase-free water	Volume made up to 13 µl

Incubation in Thermocycler: The mix was incubated at 65°C for 5 minutes in a thermal cycler and then quickly snap-chilled on ice for 2 minutes.

Step II- Preparation of Reaction Mix B:

A second reaction mix was prepared with the following components:

Component	Amount
5X First strand buffer	4 µl
dNTP mixture (10 mM of each dNTP made in RNase-free water)	2 µl
Reverse transcriptase (200 U/µl, RevertAid, Thermo scientific)	1 µl

Combination of Mixes and Incubation: The contents of mix B were added to mix A, resulting in a total reaction volume of 20 µl, which was then incubated at 42°C for 1 hour.

Termination: The reaction was terminated by heating up at 70°C for 15 minutes.

Quantitative PCR (qPCR) for gene expression analysis

The qPCR analysis was conducted using the PowerUp SYBR Green PCR Master Mix (Applied Biosystems, #A25742), with gene-specific primers for the reactions performed on an Applied Biosystems 7500 FAST machine.

To check the *AtHMGB15* transcript level, RNA was isolated from six independent sets of flower samples. A total of 5 µg of RNA was utilized for cDNA synthesis using RevertAid RT (Thermo Scientific) as described above. The relative fold change of the gene of interest was calculated using the 2-ΔΔCt method, with normalization against the AtαEF 1α transcript (At1g07920). The fold change was denoted with regard to the wild type. The primers for this study are listed in Annexure 1.

Morphological differences between wild-type and *athmgb15-4* mutant plants

Comparison of Seedlings tissue

- The 25-day seedlings were observed to check the growth pattern of the rosettes of wildtype and *athmgb15-4* plants.
- The roots of these rosettes were detangled and placed on a black surface to measure using a mm unit scale.
- The study was conducted using 5 batches grown from independent harvests throughout one year. Each batch consisted of 20 plants each of wild type and *athmgb15-4* mutant plants.
- Images were clicked using a DSLR camera against a dark background.

Comparison of Flowering time

- The wild type and *athmgb15-4* plants were grown meticulously in individual pots containing soil mix.
- The appearance of the first bolt was noted in each of the plants.
- The number of leaves at the period of bolting was also noted.
- The percentage of plants flowering at 30 days post germination (dpg) and 40 dpg was noted.
- In a population of 5 batches grown from independent harvests throughout one year. Every batch consisted of 100 plants each of wild type and *athmgb15-4* plants.
- Images were clicked using a DSLR camera against a dark background.

Comparison of Siliques

- The mature but green siliques were harvested from wild type and *athmb15-4* plants
- They were placed on a dark background to measure using a mm unit scale.
- The images were clicked using a DSLR camera against a dark background.

Visualization of Seeds by Decolorization of Siliques:

- The mature green and dry siliques were collected from wild-type and mutant plants.
- These usually exhibit a greenish tint due to the presence of various pigments in the cells, such as chlorophyll and the drier ones were opaque.
- To remove these pigments and make the seeds within the silique visible, the siliques were boiled in 80% ethanol for over an hour in a water bath. This process effectively caused the chlorophyll pigments to disappear.
- After the boiling process, the siliques were rinsed thoroughly with lukewarm water to remove any residual ethanol.
- Subsequently, the siliques were dried in a petri dish, preparing them for further analysis or experimentation.
- The dried siliques were then placed on a slide and observed under a stereo-zoom microscope to examine and count the number of seeds present per silique.

Comparison of Pollen Grains

Scanning Electron Microscopy

- Extraction of Pollen Grains: Pollen grains were meticulously extracted from the anthers of dried flowers. The flowers were obtained from wild-type plants and the *athmgb15-4* mutant.
- Refinement Process: To ensure purity and uniformity, the extracted pollen grains underwent a refining process. The pollen was passed through a series of fine meshes with decreasing pore sizes. This sieving process helped separate the pollen grains based on size and removed any debris or contaminants.
- Mounting on Brass Stubs: The refined pollen grains were carefully transferred and mounted onto brass stubs. A layer of carbon tape was used to securely adhere the pollen grains to the brass stubs. This step was crucial to prevent the samples from dislodging during subsequent procedures.
- Gold Coating: Once the pollen grains were mounted, they were coated with a thin layer of gold.

  This coating was applied using an Edwards gold sputter coater, which deposited a uniform gold layer on the samples. The gold coating served to increase the electrical conductivity of the pollen grains, which is essential for imaging under a scanning electron microscope (SEM).
- Visualization under SEM: The samples were visualized using a Scanning Electron Microscope SEM FEI 200 model.

  Imaging was performed at different accelerating voltages: 5 kV, 10 kV, and 20 kV, at various magnifications to understand the topology of the Exine surface and its ornamentation pattern. These varying voltages allowed for the optimization of image resolution and contrast, enabling detailed observation of the pollen grain surface morphology.

Pollen Tube Germination Assay

Pollen germination assay was performed as described previously (Li et al., 1999) with modifications.

- Harvesting of Pollen: Pollen grains were collected from mature flowers of wild-type and *athmgb15-4* mutant plants.
- Pollen Collection: Freshly opened flowers were carefully plucked, with 20 to 50 flowers being collected in a 1.5 ml microcentrifuge tube. The flowers were then allowed to dry at for 30 minutes, at room temperature with the tube cap kept open.

- Preparation of Pollen Germination Medium: Freshly prepared pollen germination medium comprised several key components due to their properties mentioned below:
  - Sucrose: Serves as an energy source and osmotic stabilizer.
  - Boric acid: Maintains cell wall integrity.
  - $CaCl_2$, $MgSO_4$, KCl: Provides calcium ions, essential for pollen tube growth.
  - mM Tris–MES: Acts as a buffer to maintain pH stability.
  - PEG 4000: Controls the water potential of the medium and protects the newly germinated pollen tubes.
  - The pH of the medium was meticulously adjusted to 5.8 with tris base to optimize conditions for pollen germination.

Components	Stock Conc.	Final Conc.
MES-Tris (pH 5.8)	200 mM	5 mM
KCl	1 M	1 mM
$MgSO_4$	1 M	0.8 mM
Boric acid	100 mM	1.5 mM
$CaCl_2$	1 M	10 mM
Sucrose		5% w/v
PEG 4000		15% w/v

- Pollen Submersion: 1 ml of germination medium was added to the tubes, submerging the flowers completely. The tube was vortexed at maximum speed for 1 minute to dislodge the pollen grains. The tube was then centrifuged at 3000 rpm for 5 minutes at room temperature to concentrate the pollen.
- Supernatant Removal and Pollen Resuspension: The supernatant, containing floating flower residues, was carefully removed, leaving behind the pollen pellet.

  The pollen pellet was resuspended in 1 ml of germination medium using a vortex, and the suspension was incubated in a plant growth chamber maintained at 22-25°C.
- Observation and Examination of Pollen Germination: Pollen germination was observed at various time intervals: 2 hours, 4 hours, 6 hours, and 24 hours after incubation in the germination medium. 10 µl of the pollen suspension was taken and placed on a clean glass slide. Pollen germination and pollen tube length were visualized under a Nikon ECLIPSE Ni microscope capturing detailed images of the emerging pollen tubes and the overall germination dynamics. The Pollen germination rate was assessed by examining random fields independently selected across the slide surface at various time points.

Pollen Viability Assay by Trypan Blue Staining

- Preparation of Pollen Samples: Pollen samples were collected from flowers of wild type and *athmgb15-4* mutant. The collected pollen grains were suspended in water to create a uniform pollen suspension.
- Dilution with Trypan Blue Solution: The pollen suspension was then diluted at a 1:1 ratio using a 0.4% Trypan Blue solution. This dilution ensured an optimal concentration of Trypan Blue for effective staining.
- Principle of Trypan Blue Staining: Trypan Blue staining is a well-established method used to distinguish dead cells from live cells. The principle behind this method is based on cell membrane integrity. Cells with intact membranes can effectively exclude the dye, remaining unstained. Whereas, cells with compromised or damaged membranes cannot exclude the dye, allowing it to penetrate and stain the cells blue.
- Incubation: The diluted pollen samples were incubated with the Trypan Blue solution for a specified period to allow adequate staining. This incubation time ensures that dead cells are thoroughly stained while live cells remain unstained.
- Microscopy and Imaging: After incubation, the stained pollen samples were observed under a microscope. The microscope allowed for the differentiation between live and dead pollen grains based on their staining:
    - Stained (Blue) Pollen Grains: Indicate dead cells with compromised membranes.
    - Unstained (Transparent) Pollen Grains: Indicate live cells with intact membranes.

  The proportion of stained versus unstained pollen grains was analyzed to assess pollen viability. This analysis provided a clear distinction between viable and non-viable pollen, allowing for the evaluation of pollen health and viability in both wild-type and mutant samples.

Quantification and Statistical Analysis

Statistical analyses were performed utilizing GraphPad Prism 8 (GraphPad Software) and IBM SPSS Statistics (v29.0.2.0). The data presented in the figures reflect either the means of three or more experimental replicates or the means of three or more independent experiments, as detailed in each figure caption. A combination of Student's t-tests, one-way Analysis of Variance (ANOVA) and two-way ANOVA was employed to assess statistical significance, depending on the nature of the data. These analyses were carried out in both GraphPad Prism and IBM SPSS Statistics. Specific details regarding the statistical tests used, including the conditions under which they were applied, are provided in the corresponding figure legends to ensure clarity and transparency.

Section 2

RNA isolation and Illumina Sequencing

Isolation of RNA:

- Total RNA was isolated utilizing the RNASure® Mini Kit (Nucleopore-Genetix) According to the Manufacturer's protocol.
- About 200 mg of young flowers (flowering stages 12 to 13) from wild-type and *athmgb15-4* mutant plants.
- The RNA isolated from three independent replicates was pooled to ensure sufficient quantity and consistency before being used for sequencing.

RNA sequencing:

- The pooled RNA samples were outsourced for and sequenced using the Illumina NextSeq 500 platform at Eurofins Genomics India Pvt. Ltd., utilizing 2×75 bp chemistry to generate approximately 30 million paired-end reads per sample.
- The quality and quantity of the RNA samples were checked on 1% denaturing RNA agarose gel and NanoDrop/Qubit Fluorometer, respectively.
- The RNA-Seq paired-end sequencing libraries were prepared from the QC-passed RNA samples using the Illumina TruSeq Stranded mRNA sample Prep kit.
- Quantity and quality of the PCR enriched (QC) of the library were analyzed on Agilent 4200 Tape Station (Agilent Technologies) using high sensitivity D1000 Screen tape as per manufacturer instructions.
- After obtaining the Qubit concentration for the libraries and the mean peak sizes from the Agilent Tape Station profile, the PE Illumina libraries were loaded onto NextSeq 500 for cluster generation and sequencing. The Bioinformatic workflow applied for the study has been mentioned above in the workflow (*Figure Ch1_1)*.
- The raw sequencing reads were processed, beginning with the removal of adaptors using Trimmomatic v0.35.
- Subsequently, the cleaned reads were mapped to the Arabidopsis genome (TAIR10) using TopHat v2.1.1.
- Differential gene expression analysis was performed using Cufflink v1.3.0.

- In this analysis, genes with a fold change (FC) value greater than 0 and a P-value threshold of 0.05 and those with a fold change greater than ±1 and a P-value cutoff filter of 0.05 were identified as differentially expressed genes.

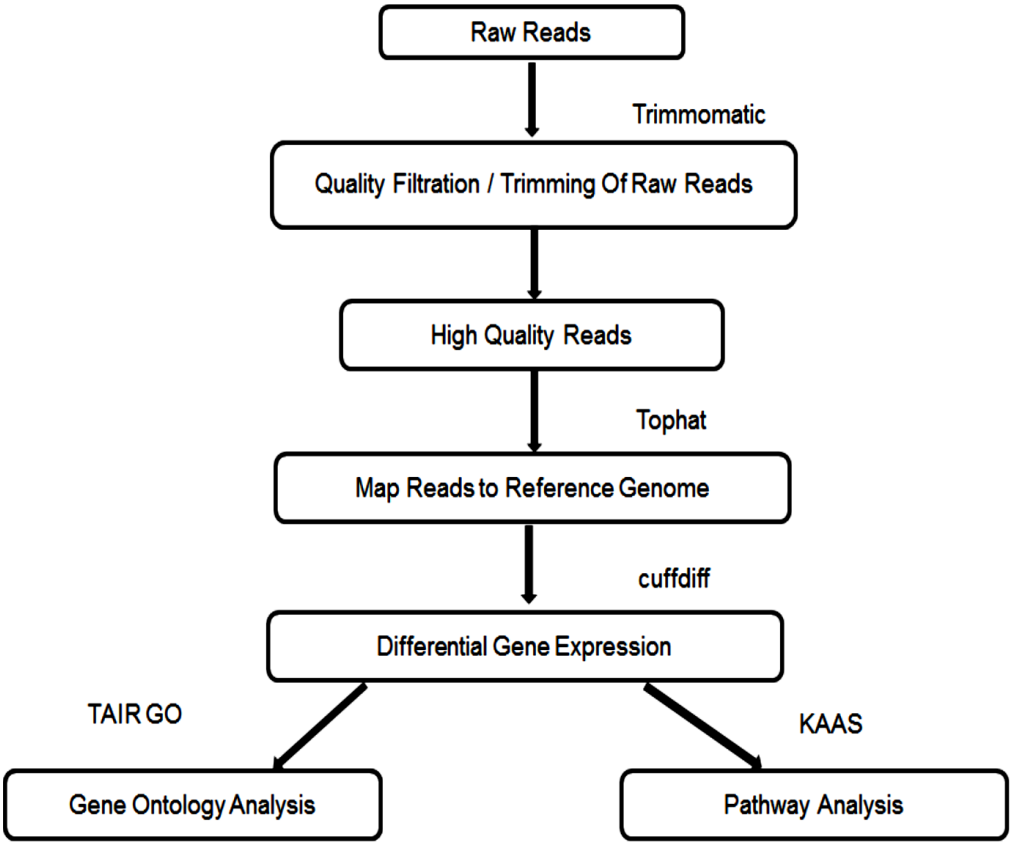

FigureCh1_1: Schematic bioinformatic workflow adopted for the study

RNA Sequencing for Replicates:

- For each replicate, total RNA was isolated from young flowers (200 mg) as previously described.
- The RNA quality was assessed using an Agilent TapeStation, ensuring that the RNA Integrity Number (RIN) was greater than 7. This quality check was performed by Theomics International Pvt. Ltd.
- To further confirm RNA integrity, samples were analyzed using an Agilent Bioanalyzer 2100, and only those samples displaying clean rRNA peaks were selected for subsequent analyses.

- The libraries for RNA sequencing were prepared using the KAPA Stranded RNA-Seq Kit with RiboErase (KAPA Biosystems, Wilmington, MA, USA).
- The quality and quantity of the final libraries were meticulously examined using the Agilent Bioanalyzer 2100 and the Life Technologies Qubit 3.0 Fluorometer, respectively.
- The libraries were then size-selected to obtain fragments of approximately 140 bp ±10%. Sequencing was conducted on the Illumina NovaSeq 6000 platform, achieving an average depth of 20 million reads per sample using 2×150 bp chemistry.
- The reads obtained were mapped to the Arabidopsis genome (TAIR10) as outlined previously.

Submission and availability of Sequencing Datasets

The sequencing datasets have been submitted to the NCBI platform to ensure availability in the public domain. The RNA-seq data is available in the NCBI Sequence Read Archive (SRA) repository under the following accession numbers: PRJNA874885 and PRJNA974968.

Validation of the Transcriptome Data by RT q-PCR

The qPCR analysis was conducted using using cDNA obtained from Wildtype and *athmgb15-4* mutant flowers with the PowerUp SYBR Green PCR Master Mix (Applied Biosystems, #A25742), with gene-specific primers for the reactions performed on an Applied Biosystems 7500 FAST machine. The genes were selected from the FDR-corrected pool showing significant differential gene expression. The relative fold change of the gene of interest was calculated using the 2-ΔΔCt method, with normalization against the AtαEF 1α transcript (At1g07920). The fold change was presented with respect to the wild type. The primers for this study are listed in Annexure.

Functional Annotation and Bioinformatic Analysis

The bioinformatics analysis was conducted using several specialized tools and programs. Gene ontology analysis for the differentially expressed genes (DEGs) was achieved using The ShinyGO v0.77 program. This analysis encompassed the ontologies of Biological Processes, Molecular Functions, and Cellular Components, providing insights into the roles of the DEGs within these categories. Additionally, ShinyGO v0.77 was utilized to identify significantly enriched KEGG

pathways associated with the DEGs, offering a deeper understanding of the biological pathways that are affected.

The significantly downregulated genes from the enriched pool were filtered preferentially and validated for downstream analysis.

Comparative Analyses of Various Datasets with the RNA-Seq data of Wildtype vs *athmgb15-4* flower tissue

The RNA-Seq data from the flower tissue of Wildtype vs *athmg15-4* was compared with the previously available dataset from the pollen tissue of Wildtype vs athmg15-1 published by the group Xia et al in 2014. This dataset would give us an idea of the common transcription factors from the datasets.

The RNA-Seq data from the flower tissue of Wildtype vs *athmg15-4* was then compared to the previously available ChIP on chip dataset from the seedling tissue of Wildtype. This dataset with AtHMGB15 binding occupancy under control conditions was generated in our lab and published in 2020 by Malik et al. The common pool gave us an idea of the differentially regulated transcription factors and targets that have an AtHMGB15 binding occupancy.

For the comparison between various datasets, Venn diagrams were generated using the Venny v2.0 tool. This allowed for the visualization of overlaps and differences between the gene sets under investigation.

Hormone Estimation

The estimation of the content of Jasmonic Acid (JA) and derivatives was conducted using electron spray ionization coupled with mass spectrometry (ESI-MS), following the method previously described (Liu et al., 2010).

- About 500 mg of fresh flower tissue was collected from wild-type and *athmgb15-4* plants in triplicates.
- The flower tissue was homogenized in liquid nitrogen and extracted overnight in methanol (HPLC grade) at 4°C.
- On the following day post-extraction, the homogenates were centrifuged, and the supernatants were diluted 5 times with HPLC-grade water.

- The diluted samples were then processed using a Sep-Pak C18 cartridge (Pierce #89870) for solid-phase extraction (SPE).
- The SPE cartridge was sequentially washed with 20% (v/v) and 30% (v/v) methanol.
- The bound compounds of interest were eluted using 100% (v/v) methanol.
- The eluates were further diluted tenfold with methanol and loaded onto the ESI-MS for detection.
- The infusion rate was set at 5µl/min and the spectrum list for detected compounds with a mass of up to 1500g/mol was recorded for subsequent analysis.

Analytical standards of Methyl Jasmonate (MeJA, Sigma #392707), Jasmonic Acid (JA, Sigma #J2500), and JA-isoleucine (JA-Ile, Cayman Chemical #10740) were used to detect the exact peak for each compound.

The relative abundance of these derivatives in the wild-type and *athmgb15-4* flowers samples was quantified and expressed as a fold change relative to the wild-type samples.

Hormone Treatment

Treatment:

The wild-type and *athmgb15-4* plants were grown individually in pots with soil mix.

- At the onset of flowering, Methyl jasmonate (MeJA) treatment was administered to the inflorescence consisting of buds and unopened flowers, at two different concentrations of 0.5 mM and 2 mM (Sigma #392707).
- Unsprayed wild-type and mutant flowers were used as experimental controls.

Rate of Pollen Germination:

- To quantify the rate of Pollen Tube germination MeJA treatment was applied to the early buds twice daily for two consecutive days as described (Park et al., 2002).
- Following the final treatment, the flowers were immediately harvested for further analysis.
- The harvested flowers were utilized to perform a pollen germination assay at various time points following the methodology described previously.

Expression analysis:

Additionally, to check the expression of Jasmonate pathway-related genes an experimental design was laid out as follows:

- For this experiment, unopened flowers were treated with 0.5 mM MeJA early in the morning.
- flowers (just opened) were harvested about four hours after the final MeJA treatment.
- Total RNA was isolated from wild-type and mutant flowers (Control and treated) and subsequent cDNA synthesis was performed as described previously.
- Reverse transcription-quantitative PCR (RT-qPCR) was performed as described previously, to assess gene expression levels in response to the exogenous hormone treatment.
- The relative fold change of the gene of interest was calculated using the 2-ΔΔCt method, with normalization against the AtαEF 1α transcript (At1g07920).
- The fold change was represented with respect to the wild type. The primers for this study are listed in Annexure.

Section 3

Transformation of Arabidopsis Using the Floral Dip Method

The transformation of Arabidopsis through the floral dip method as described by (Zhang et al., 2006b) requires several key components:

Component Descriptions:

- MS Media: Prepared as outlined in Section 1.
- MS Selection Media: MS media with 25 µg/ml Hygromycin for selection purposes.
- Liquid LB Medium: Prepared using 10 g tryptone, 5 g yeast extract, and 10 g NaCl per liter.
- Sucrose Solution: Freshly prepared at 5% (wt/vol).
- Silwet L-77: Surfactant used in the transformation process.
- Ethanol 70% (vol/vol): Used for sterilization.
- Agrobacterium Clone: Full-length AtHMGB15 clone in LBA4404 strain.
- Arabidopsis Plants: Wild-type (WT) Arabidopsis plants.

Preparation of Arabidopsis Plants for Floral Dip:

- Arabidopsis seeds were sterilized and plated as described in Section 1.
- After germination, seedlings were grown under long-day conditions (16 h light/8 h dark at 20°C) for two weeks before being transferred to moist soil (approximately 6 seedlings per pot).
- Plants were grown in a growth chamber under short-day conditions for 3–4 weeks, before being moved to long-day conditions to induce flowering.
- To encourage the growth of immature flower clusters, the first flower bolts were removed, allowing secondary inflorescences to proliferate from axillary buds. Agrobacterium treatment was performed 6–8 days after clipping the first bolts.
- To increase transformation efficiency and reduce contamination, siliques were removed from the plants before transformation, thereby enhancing nutrient supply to newly transformed cells and decreasing the number of wild-type seeds.

Floral Dip Transformation Procedure:

- A single colony of Agrobacterium containing the gene of interest in a binary vector was inoculated into 5 ml of liquid LB medium with necessary combination of antibiotics and incubated at 28°C for 48 hours.
- This feeder culture was used to inoculate 500 ml of liquid LB with appropriate antibiotics, which was then incubated at 28°C for 16–24 hours until the cells reached the stationary phase (OD ~1.5–2.0).
- Agrobacterium cells were harvested by centrifugation at 4,000g for 10 minutes at room temperature and resuspended in freshly prepared 5% sucrose solution.
- Silwet L-77 was mixed to a concentration of 0.02% (vol/vol), and the suspension was moved to a 500 ml beaker for dipping. Plants were dipped twice, with a 7-day interval, to increase transformation frequency.
- The aerial parts of the plants were inverted and dipped in the Agrobacterium suspension for 10 seconds with gentle agitation, ensuring that both inflorescences and the rosette were submerged.
- After dipping, the plants were allowed to drain for 3–5 seconds and were then covered with plastic to maintain high humidity for 16–24 hours, avoiding exposure to high temperatures or excessive light.
- The following day, the cover was removed, and the plants were returned to the greenhouse or growth chamber for normal growth over the next month. Once the siliques turned brown, watering was withheld, and the drying plants were wrapped with wax paper to collect dry seeds.

Screening of Primary Transformants:

- MS selection media plates containing hygromycin were prepared.
- Harvested seeds were sterilized and plated, with approximately 100 seeds per plate.
- Seeds were vernalized at 4°C for 3 days and then moved to a growth chamber under long-day conditions.
- After 7–10 days, transformants were identified as seedlings with healthy green cotyledons, true leaves, and roots extending into the selective medium.

- Potentially positive transformants were transferred to fresh selection plates once true leaves emerged and were allowed to grow for an additional 1–2 weeks to confirm their transgenic nature.
- Transformed plantlets were transplanted into soil rite, covered with plastic film to maintain high humidity for 2 days, and grown under proper light for seed collection.

DNA Isolation and Confirmation of Transgenic Lines

DNA was harvested from the leaves of T2 generation plants to confirm transgenic lines using the Plant DNAzol method, which relies on a guanidine-detergent lysing solution for RNA hydrolysis and selective DNA precipitation. PCR was then performed using gene-specific primers to verify the presence of the transgene.

Validation of Transgenic Lines Using PCR

Following genomic DNA isolation, PCR was conducted utilizing gene-specific primers as detailed in Annexure 1. The components for the 20 µl PCR reaction were assembled as follows:

PCR Component	Volume (in µl)
Reaction buffer (10X)	2.0
dNTPs (10 mM)	0.5
$MgCl_2$ (25 mM)	0.6
Forward Primer (10 µM)	0.3
Reverse Primer (10 µM)	0.3
DNA Polymerase (5 U/µl, Abcam)	0.3
Template (1/10th diluted gDNA)	5.0
DMSO	1.0
Nuclease-free water	Volume made up to 20.0

The PCR cycling conditions were set as follows:

PCR Step	Temperature	Time	Cycles
Initial Denaturation	95°C	5 mins	1
Denaturation	95°C	45 secs	
Annealing	50°C	45 secs	35

Extension	72°C	2 mins	
Final Extension	72°C	7 mins	1
Hold	4°C		

The PCR products were subsequently visualized on a 1.2% agarose gel, and positive clones were identified and selected based on the results.

RNA Isolation, cDNA Synthesis and Quantitative PCR (qPCR) for Gene Expression Analysis

RNA was isolated from wild-type, *athmgb15-4*mutant, and AtHMGB15 overexpression in mutant background (*athmgb15-4*-OE_{A4}) transgenic plants. This was achieved using the Nucleopore plant RNA isolation kit, following the manufacturer's protocol. To synthesize the first strand of cDNA, reverse transcription was performed using 5 µg of RNA and an oligo dT(18) primer, as described in Section 1. The RT-qPCR analysis was conducted as described in Section 1.

Morphological differences between wild-type, *athmgb15-4* and *athmgb15-4*-OE_{A4} plants

Phenotypic analysis and comparison of *athmgb15-4*-OE_{A4} with wild-type and *athmgb15-4* mutant plants was performed as described in Section 1.

Hormone Estimation

The estimation of the content of Jasmonic Acid (JA) and derivatives was conducted using electron spray ionization coupled with mass spectrometry (ESI-MS), following the method previously described in Section 1.

Observation and Inference

Section 1

Confirmation of *AtHGMB15* expression in *athmgb15* mutants

The mutant lines were previously screened in our lab for homozygous lines. Southern blot and northern blot analysis were also performed for the *athmgb15-4*. To re-confirm the expression of AtHMGB15 specifically in the mutant flowers RNA was isolated (*Figure Ch1_2A)*, the RT-qPCR was performed using flower tissue of *athmgb15-4*, SALK057612C_9 and SALK057612C_15. The expression analysis revealed a 10-fold decrease in AtHMGB15 expression in *athmgb15-4* flowers and about a 5-fold reduction in Salk lines when compared to the levels in wild-type flowers (*Figure Ch1_2B*). This difference in expression was possibly due to the difference in the site of T-DNA insertion in the mutant lines. In the *athmgb15-4* mutants the AtHGMB15 gene was disrupted with a T-DNA insertion in the 1st exon whereas, in the SALK057612C_9 and SALK057612C_15 lines, the insertion is at the 1kb promoter region of the AtHMGB15 gene. Therefore, we selected and proceeded with *athmgb15-4* for most of our phenotypic studies due to its lowered expression of *athmgb15-4* in comparison to the other two mutant lines.

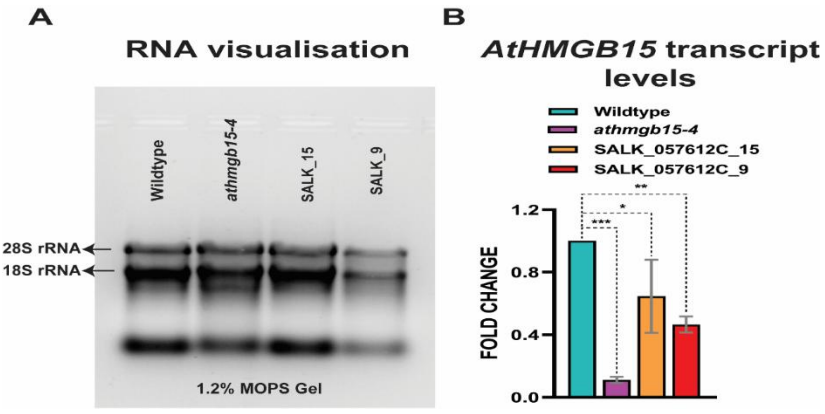

Figure Ch1_2: Expression of AtHMGB15 transcripts in mutant flowers. A) Visualization of RNA isolated from flowers of wild type vs mutants. B) RT-qPCR showing significant reduction of AtHMGB15 transcript in mutant lines. The fold change was represented with respect to the wild type. Error bars represent mean±SD (n=6). The significance of the results was assessed through a one-way ANOVA with Tukey's post hoc test (denotes P ≤ 0.05, ** denotes P ≤ 0.001, *** denotes P ≤ 0.0001).*

Morphological differences in the seedling stage between wildtype and *athmgb15-4* mutants

The seedlings of wild type and *athmgb15-4* were compared from the day of germination to 25 days. The rosette of both plants was healthy with no observable difference in the leaf numbers

and size (*Figure Ch1_3A)*. However, when we observed the length of the roots at the same stage there was a difference between the two (*Figure Ch1_3B)*. The roots of mutant seedlings were slightly shorter in comparison to those of the wild type. The study was conducted over one year in five batches to rule out the possibility of season variation (*Figure Ch1_3C)*.

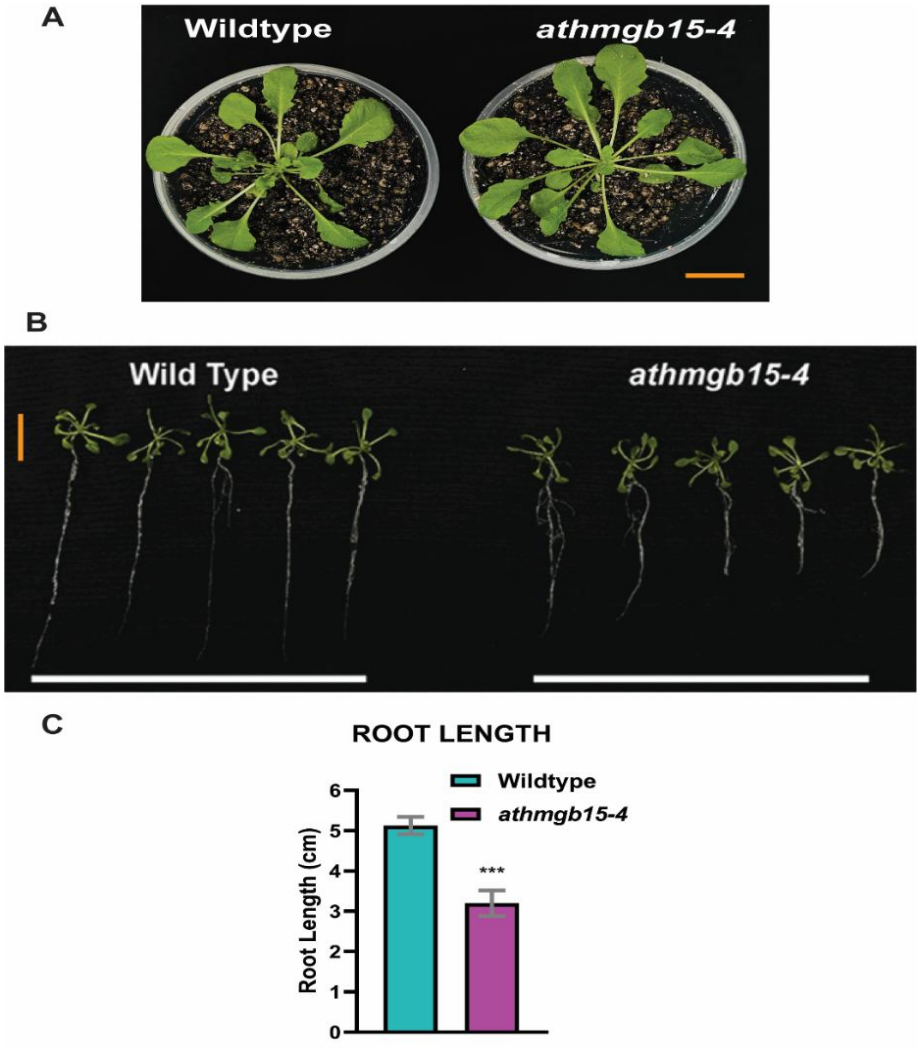

*Figure Ch1_3: Morphological analysis at the Seedling stage. A) Rosettes of wild type and athmgb15-4 showing no visible difference in size. Scale bar=2 cm. B) Roots of wild type are slightly longer than athmgb15-4. The experiments were repeated with 100 plants for each and 5 seedlings from wildtype and athmgb15-4 were used for pictorial representation. The scale bar (orange) is 1cm. C) Quantification of root length. Measurement was done using 100 seedlings for each observation. Error bars represent mean ± SD (n=100) The significance was calculated by paired two-tailed student's t-test Asterisks represent significant differences between Wildtype and athmgb15-4, ***P< 0.001.*

The root length was measured in over 100 plants and represented through a bar graph. Thus, it is undeniable that ATHMGB15 plays a crucial role during Root development in Arabidopsis. Although it is beyond the scope of this study, it could be investigated further.

AtHMGB15 influences Flowering time in Arabidopsis

The wildtype and *athmgb15-4* plants were potted in a soil mix and grown under regular growth conditions (long days) to study the flowering time. Notably, wild-type plants bolted around 27-30 days from the time of germination. But, to our surprise, the *athmgb15-4* plants did not bolt until

35 to 37 days on average (*Figure Ch1_4A)*. This observation motivated us to study the time of flowering in a larger population of plants for one year to negate the effects of seasonal variation. During the study of around 300 plants, we saw a high percentage of *athmgb15-4* mutants exhibiting delayed bolting (*Figure Ch1_4B-E)*.

The number of leaves at the time of bolting was calculated (*Figure Ch1_4F)*. Wild-type plants bolted when the rosette comprised about 12-15 leaves. Whereas, the rosettes of *athmgb15-4* mutant plants consisted of 17-21 leaves at the time of first bolt emergence. This indicated a delay in the time of conversion from the vegetative phase to the inflorescence stage of the mutant plants. A plausible explanation could be that the chromatin remodeller AtHMGB15 is involved in the flowering time which could be another topic of investigation in the future.

The siliques were shorter in the *athmgb15-4* mutants

Another interesting observation while studying the morphology of the aerial portion of the plants was that the siliques were visibly shorted in the mutants. Siliques are elongated, capsule-shaped fruits of the Arabidopsis plants bearing the seeds. A silique splits at maturity into two segments, known as valves, which remain attached at the top. These valves separate to reveal a central partition that retains the seeds. Upon closer analysis under a stereo-zoom microscope, it was revealed that the mutant siliques had a lower number of fertilized seeds within each pod (*Figure Ch1_5A-C)*. The fresh weight of the mature siliques of the wild type was higher than that of *athmgb15-4* mutants (*Figure Ch1_5D)*. The overall shorted siliques and reduced seeds per silique culminated in a lower seed yield in our mutants (*Figure Ch1_5E)*.

The lowered seeds produced per plant in mutants could be due to a poor rate of fertilization. In dicot plants, the seeds are healthy when a proper and timely double fertilization occurs. The abortive seeds are an alibi for poor or unfertilized ovules and directly hint at a defective male gametophyte. This is when the current research took an eventful turn to delve deep into the study of Pollen properties in the *athmgb15-4* mutants.

The Pollen grains of athmgb15-4 mutants were defective in morphology

The mature pollen grains were carefully isolated from the wild type and *athmgb15-4* flowers and subjected to visualization under a scanning electron microscope (SEM) (*Figure Ch1_6)*. The pollen grains of typical Arabidopsis wild-type plants are ellipsoidal. They are about 35-40um long

and the diameter at the center is about 20um. There is the presence of three equally spaced longitudinal slits representing each of the pollen apertures. The apertures are the regions in the pollen where the exine layer is absent, i.e., the sporopollenin deposition is absent. These apertures are specialized openings where the intine extends into the pollen tube at the time of pollen tube germination during fertilization.

The wild-type pollen grains in Arabidopsis display a uniform layer of sporopollenin. The ornamentation pattern is honeycomb-like, exhibiting a reticulate pattern of exine wall formation. The SEM analysis revealed more than 30% of mutant pollen grains were spheroidal and irregularly shaped, while the rest of the pollen grains were morphologically identical to wild-type pollen. The defective pollen grains were smaller in size than the wildtype pollen measuring only 20um in diameter. The exine wall in these spheroidal pollen grains was somewhat undulating without a clear reticulate pattern of ornamentation. The non-uniform sporopollenin deposition masked the pollen apertures as observed under the SEM (*Figure Ch1_7)*.

The SEM analysis revealed more than 30% of mutant pollen grains were spheroidal and irregularly shaped, while the rest of the pollen grains were morphologically identical to wild-type pollen. The defective pollen grains were smaller in size than the wildtype pollen measuring only 20um in diameter. The exine wall in these spheroidal pollen grains was somewhat undulating without a clear reticulate pattern of ornamentation. The non-uniform sporopollenin deposition masked the pollen apertures as observed under the SEM (*Figure Ch1_7)*. The apertures are crucial for the pollen tube germination that is prompted on the stigmatic surface at the time of fertilization. Conclusively, the SEM imaging analysis confirmed defects in pollen morphology owing to pollen grain shape, size, aperture and ornamentation pattern of the exine wall layer.

Pollen tube germination was retarded in *athmgb15-4* mutants

Upon morphological analysis of the pollen grains, we were interested in studying the physiological activity in both the wild-type and mutant pollen grains. We isolated freshly opened flowers and subjected them to the Pollen germination media (PGM) to monitor the rate of pollen tube germination under the light microscope (*Figure Ch1_8A)*. The PGM mimics the environment on the stigmatic surface of the female gametophyte at the time of onset of fertilization.

A time-dependent in-vitro pollen tube germination assay was conducted where the number of germinated pollen grains was noted at 2 hours after adding the mature pollen grains to PGM followed by observation at 4 hours and 6 hours.

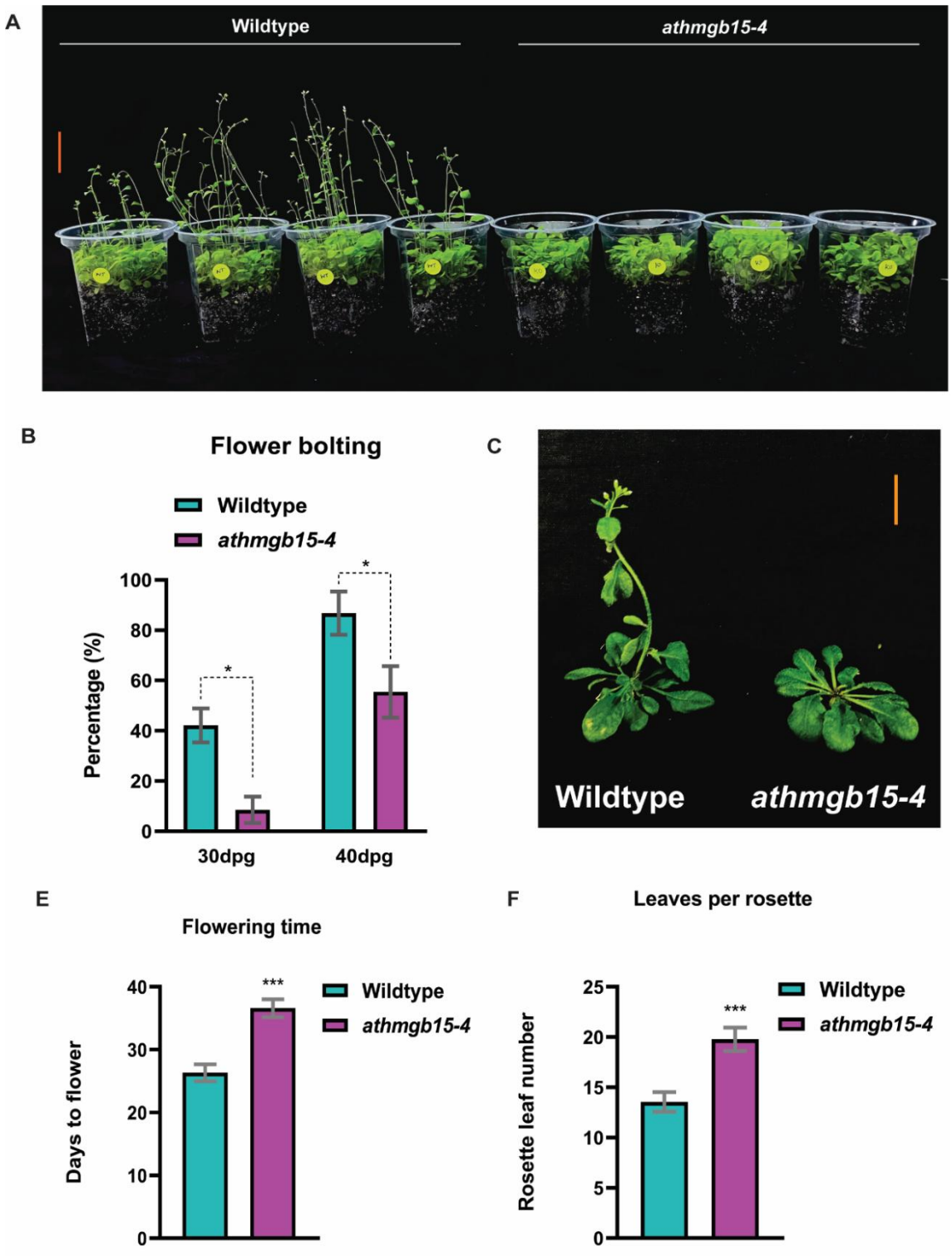

*Figure Ch1_4: Delayed flower bolting in athmgb15-4 mutant. A) Wild type and athmgb15-4 mutant plants to monitor the flower bolting phenomenon. The experiments were repeated with 120 pots for each and 5 pots from wildtype and athmgb15-4 were used for pictorial representation. Scale bar (orange) is 2.5cm. B) Quantitative analysis of flower bolting between athmgb15-4 and wild type. The experiments were done from seeds of 4 to 5 independent harvests. Data were collected from 100 plants of each batch. Error bars represent mean±SD (n=400), and significance was calculated by paired two-tailed Student's t-test. Asterisks represent significant differences between wild type and athmgb15-4, *P<0.05. dpg, days post-germination. C) Delayed flowering of athmgb15-4 compared to wild type. Scale bar=2 cm. E) Days from germination to flowering. Error bars represent mean±SD (n=27), and significance was calculated by paired two-tailed Student's t-test. Asterisks represent significant differences between wild type and athmgb15-4, ***P<0.001. F) Number of*

*rosette leaves at bolting. Error bars represent mean±SD (n=27), and significance was calculated by paired two-tailed Student's t-test. Asterisks represent significant differences between wild type and athmgb15-4, ***P<0.001.*

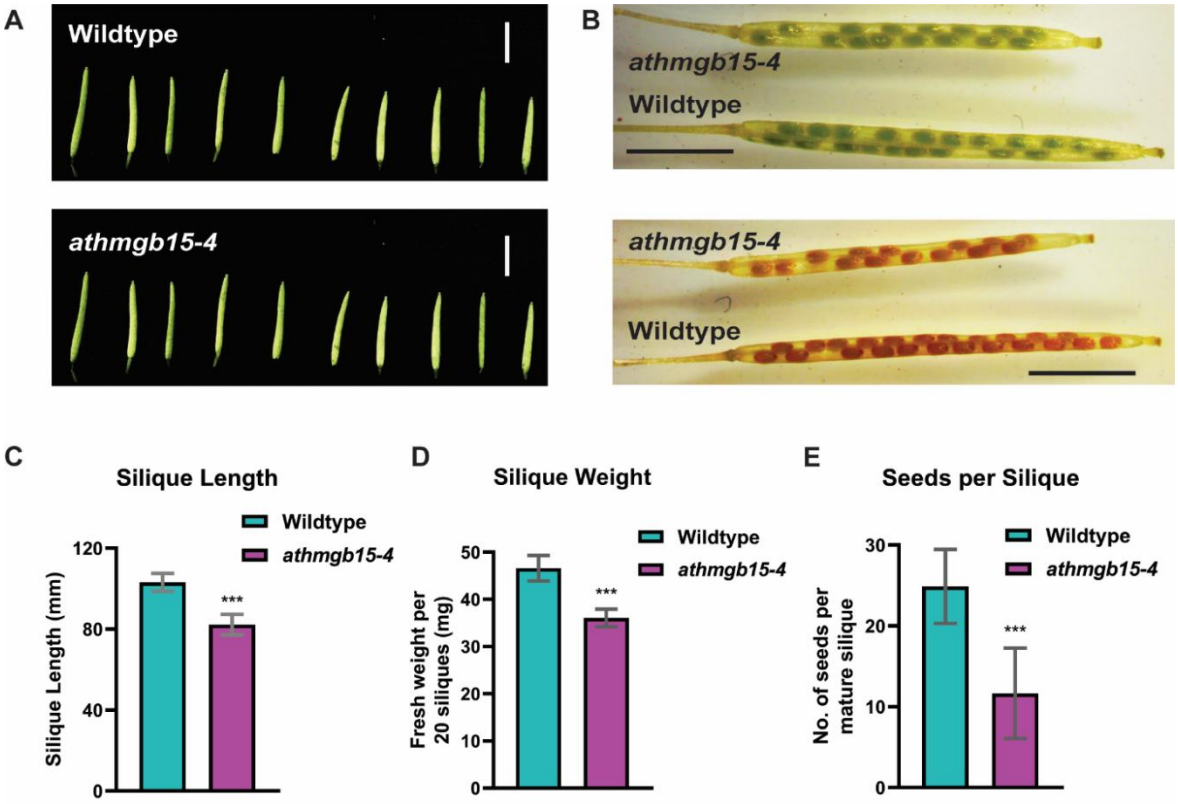

*Figure Ch1_5: Shorter Siliques and reduced seed set observed in athmgb15-4 mutant. A) Comparative silique length of wild type and athmgb15-4. Scale bar=5 mm. B) Comparitive seed set between wild type and athmgb15-4. Scale bar=2.5 mm. C) Quantitative analysis of silique length between wild type and athmgb15-4. 20 siliques were measured for each observation. Error bars represent mean±SD (n=20). D) Quantitative silique fresh weight between wild type and athmgb15-4. Measurement was taken using 20 siliques for each observation. Error bars represent mean±SD (n=20). E) Number of seeds per pod was counted from mature siliques of wild type and athmgb15-4. Error bar represents mean±SD (n=30). The significance of all these results was analyzed by paired two-tailed Student's t-test Asterisks represent significant differences between wild type and athmgb15-4, ***P<0.001.*

Imaging under a light microscope revealed a steady increase in the number of germinated pollen grains in wildtype was observed. From 50% germinated pollen grains at 4 hours to almost >95% of pollen grains germinated by the 6-hour window. Except that was not the situation with the *athmgb15-4* mutant pollen grains. The mutant pollen grains were extremely retarded in their rate of germination as revealed in the time-kinetics analysis. Initially, at 2 hours, less than 5% of the pollen grains germinated and at 6h hours about 40% of pollen grains germinated (*Figure Ch1_8B)*.

The poor rate of germination was alarming but the underlying reason is connected to the masked pollen apertures. The previously reported morphological defect and an inappropriate layer of sporopollenin at the regions of the aperture hindered the proper exudence of the pollen tube at the time of pollen tube germination.

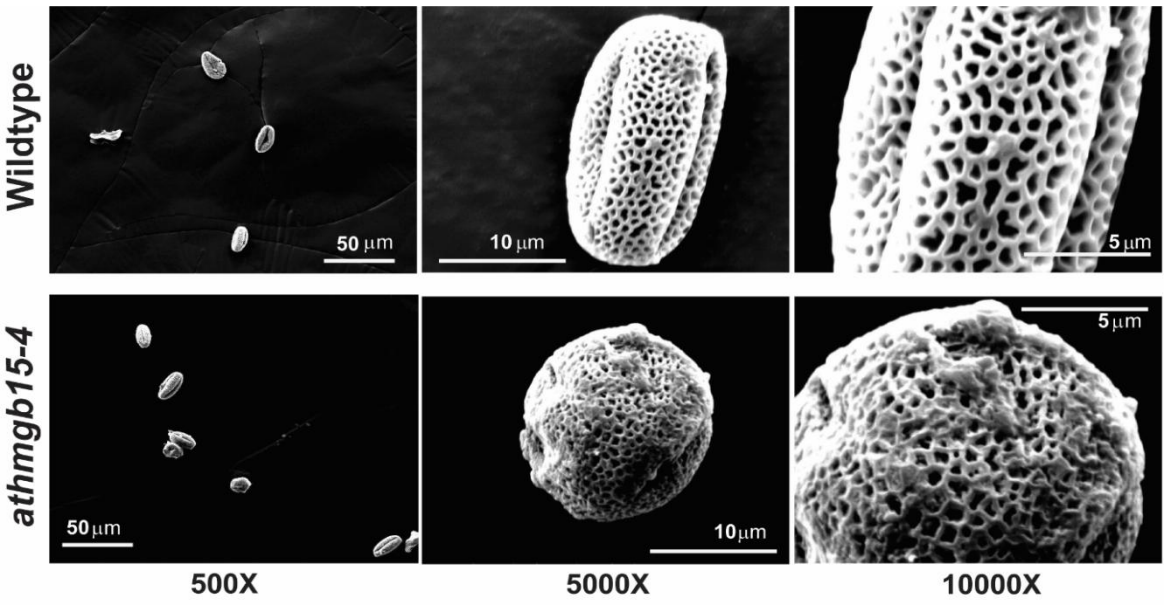

Figure Ch1_6: Morphological differences between wild type and athmgb15-4 pollen grains. Upper panel showing SEM of pollen grains isolated from wild type showing ellipsoidal shape with reticulate ornamentations. Lower panel represents the defective pollen morphology of athmgb15-4 mutant having a spheroidal shape with irregular ornamentation. The experiment was repeated at least 10 times with pollen grains isolated from different batches of wild type and athmgb15-4.

Pollen viability is compromised in the mutants

Pollen viability is crucial to ensure successful fertilization of the egg cells to produce the seeds. To ensure the vitality and reproductive vigor of the plants the pollen cells must be viable. To check the viability, pollen grains of both wildtype and *athmgb15-4* were isolated and stained with Trypan blue solution. Trypan blue is an acid azo-dye a negatively charged dye, which stains the dead, non-viable cells. It labels the dead cells by entering the cytoplasm through the leaky channels and porous cell membranes of the dead cells. The non-viable cells take up a stain bright blue and are easily distinguishable from the healthy cells which do not take up any stain. The number of viable wild-type pollen grains was significantly higher than those of mutants. The fields observed under the microscope showed a higher percentage of blue cells in *athmgb15-4* corresponding to a higher number of dead non-viable cells (*Figure Ch1_9A-B)*.

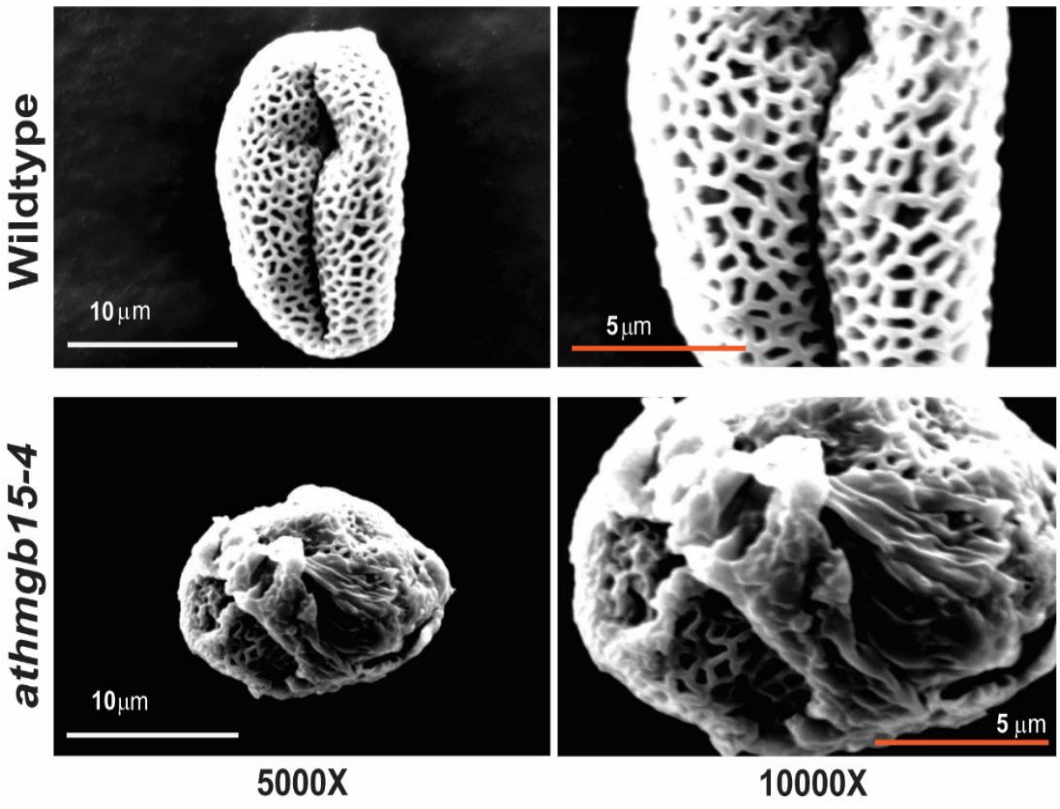

Figure Ch1_7: Morphological differences between wild type and athmgb15-4 pollen grains. Upper panel showing SEM of pollen grains isolated from wild type showing fully developed pollen aperture. The lower panel represents the defective pollen morphology of the athmgb15-4 mutant having an underdeveloped pollen aperture. The experiment was repeated at least 10 times with pollen grains isolated from different batches of wild type and athmgb15-4.

Therefore, we could conclude that almost half the population of pollen grains was nonviable in the *athmgb15-4* mutant. this number is similar to the percentage of non-germinated pollen tubes in the mutant, hinting at a correlation between the two. Also, the number of morphologically challenged pollen grains was almost similar to this numerical.

Hence conclusively it can be stated that the poor rate of germination, defective morphology of pollen grains and the overall reduced viability in the mutants are directly associated with the absence of ATHMBG15 in the mutants thereby highlighting the importance of AtHMGB15 in the development of Male gametophyte in Arabidopsis thaliana.

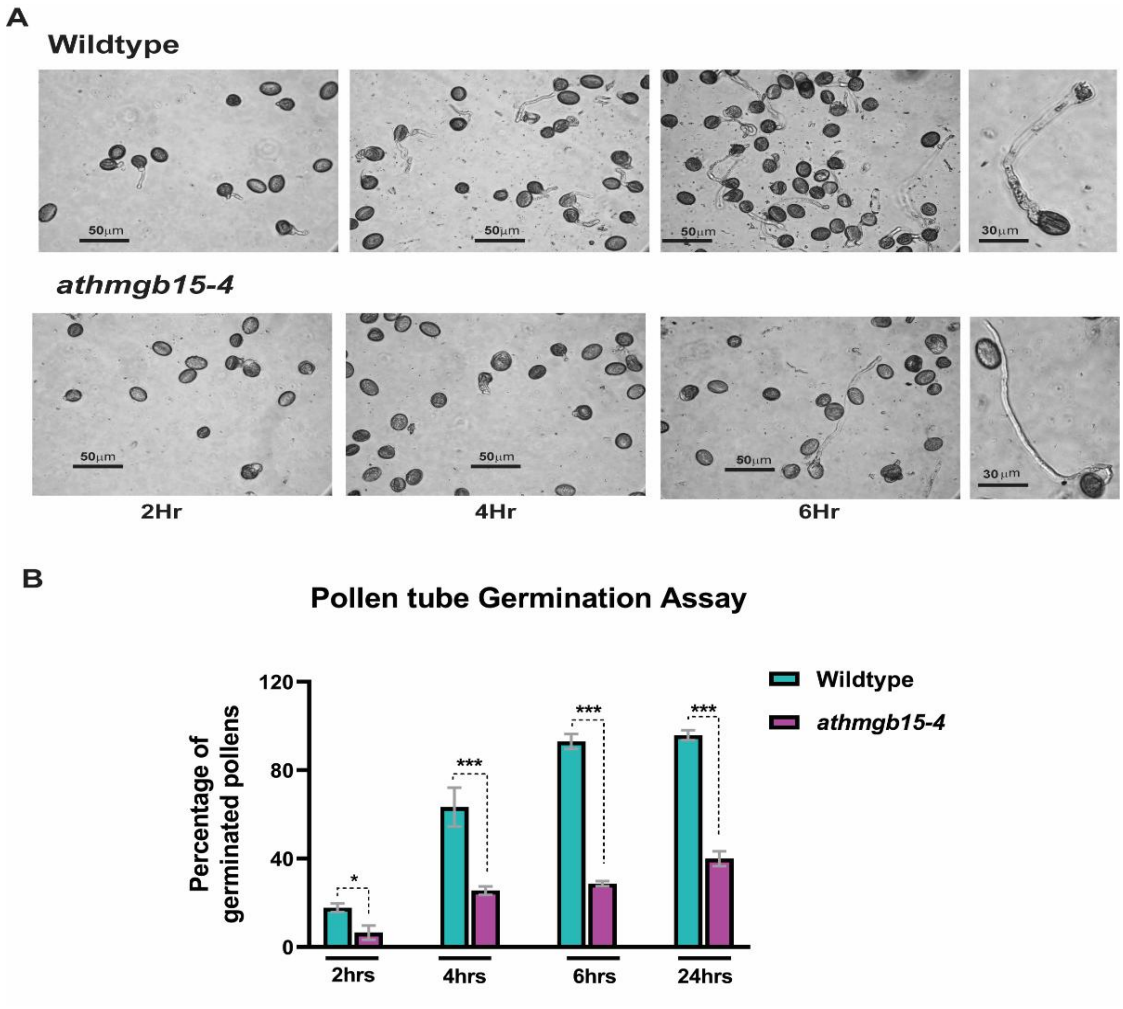

*Figure Ch1_8: Pollen germination rate is retarded in athmgb15-4. A) Freshly isolated pollen grains from wild type and athmgb15-4 were subjected to time depedent in-vitro germination assay. B) Graphical representation of the rate of pollen germination of wild type and athmgb15-4 at the given time points. Error bars represent mean±SD (n=10). The significance was analyzed by paired two-tailed Student's t-test. Asterisks represent significant differences between wild type and athmgb15-4, *P<0.05, ***P<0.001.*

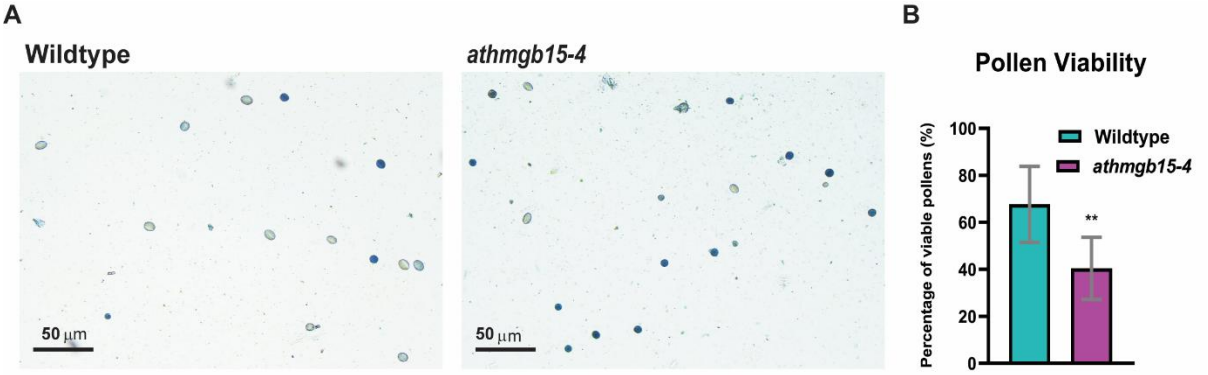

*Figure Ch1_9: athmgb15-4 reveals a higher number of non-viable pollen grains. A) The Tryan blue stain colors the dead cells bright blue. Wild type shows a lower number of blue-stained cells in comparison to athmgb15-4 pollen grains. B) Graphical representation of the number of viable pollen grains in wild type vs athmgb15-4 mutants. The significance was analyzed by paired two-tailed Student's t-test. Asterisks represent significant differences as indicated **P<0.01.*

Section 2

Analysis of the Transcriptome Data

To investigate how AtHMGB15 regulates the gene expression during pollen development transcriptome profiling was carried out using flowers from wild type and *athmgb15-4* plants. High-quality data was generated for Wildtype samples were in the range of 5.51 Gb and Mutant in the range of 4.41 Gb. A detailed summary of the report obtained is mentioned below.

- Library Preparation

The QC-passed RNA samples were then processed for library preparation. The PE libraries were prepared from total RNA using TruSeq stranded mRNA Library Prep Kit as per the kit protocol. The mean of the libraries fragment sizes are 359bp and 371bp for samples Wild type and *athmgb15-4* mutant, respectively. The libraries were sequenced on NextSeq 500 using 2 x 75 bp chemistry.

- High Quality Read Statistics

Adapter removal and quality trimming were carried out on raw sequencing data using Trimmomatic v0.35, eliminating adapter sequences, ambiguous reads (with over 5% unknown nucleotides “N”), and low-quality sequences (with more than 10% of bases below a 20 Phred score). Reads shorter than 50 nucleotides were also discarded, resulting in high-quality, paired-end reads suitable for reference-based mapping. These processed reads were then mapped to the reference genome using TopHat under default parameters, achieving approximately 96.5% alignment for both Wildtype and *athmgb15-4* mutant samples.

- Differential Gene Expression (DGE) Analysis

The reference genome of Arabidopsis thaliana, with a genome size of 116.846 MB was used for analysis. The GFF (Gene Feature Format) files used for analysis were used from TAIR database. There is total of 37,891 genes present in Arabidopsis thaliana GFF file. The differential gene expression analysis was carried out using Cufflink v1.3.0 along with the GFF file. Genes with Fold Change (FC) values above zero and a P-value threshold of 0.05 were classified as up-regulated, while those with FC values below zero were marked as down-regulated. Further categorization of these genes was based on their statistical significance (which can be either "yes" or "no"), determined by an FDR (False Discovery Rate) of 0.05 following Benjamini-Hochberg correction for multiple testing.

Differential gene expression analysis was carried out using cuffdiff between Wildtype vs Mutant, total commonly expressed genes were 23,888, which includes 1,863 significantly upregulated genes and 1,933 significantly downregulated genes.

Graphical Representation of Differentially Expressed Genes via Volcano Plot

The R script was used to depict the graphical representation and distribution of differentially expressed genes which were found in wildtype as well as *athmbg15-4* samples. The 'volcano plot' arranges expressed genes along dimensions of biological as well as statistical significance (*Figure Ch1_10)*.

The red block to the right of zero indicates upregulated genes, while the blue block to the left represents significantly downregulated genes. The Y-axis shows the negative log of the p-value ($p \leq 0.05$) from the statistical test, where data points with lower p-values (indicating high significance) appear higher on the plot. Non-differentially expressed genes are represented by the black block.

Graphical Representation of Gene Ontology Analysis

Geno Ontology Analysis was initially performed using TAIR GO database and ShinyGO for genes expressed in Wildtype and Mutant samples.

A detailed GO analysis of differentially enriched genes is shown as a histogram (*Figure Ch1_11)*. The results are reviewed under GO categories: biological process, molecular function, and cellular component.

The bubble plot representing gene ontology (GO) term enrichment analysis of differentially expressed genes (DEGs) highlights significant enrichment in biological processes such as pollen tube development, cell growth and regulation, cell wall development, biogenesis and organization, hormone-mediated signaling and response pathways, response to jasmonic acid (JA), as well as various biosynthetic and metabolic processes (*Figure Ch1_12)*.

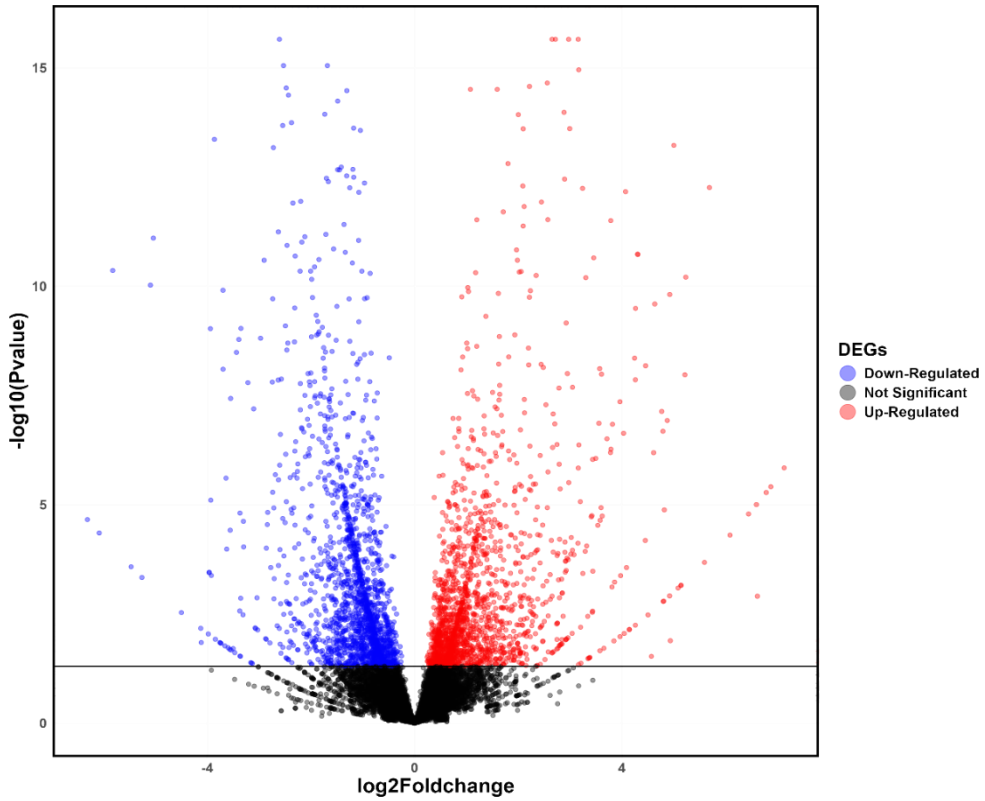

Figure Ch1_10: Volcano plot representing the distribution of differentially regulated genes. Blue dots represent the significantly downregulated genes, the red dots represent the significantly upregulated genes of the dataset and the black dots represent genes below the p-value 0.05 cutoff, hence not significant.

Graphical Representation of Functional Annotation of Pathways

Functional annotation of pathways was carried out using KAAS online server for genes expressed in Wildtype and Mutant samples.

All the sample genes were mostly categorized into different functional KAAS pathway categories. The majority of the genes were annotated for Signal transduction, Translation and Carbohydrate metabolism (*Figure Ch1_13)*.

The Kyoto Encyclopedia of Genes and Genomes (KEGG) analysis further revealed significant enrichment in pathways such as α-linolenic acid metabolism, carotenoid biosynthesis, and secondary metabolite biosynthesis within our dataset, as outlined below.

Heatmap showing Differentially Expressed Genes

An average linkage hierarchical cluster analysis was performed on selective differentially expressed genes using R version R4.4.1. Differentially expressed genes were subjected to hierarchical clustering analysis. To visualize the expression patterns, heatmaps were generated using log-transformed and normalized gene expression values. The clustering was performed based on Pearson's uncentered distance metric and the average linkage method (*Figure Ch1_14)*.

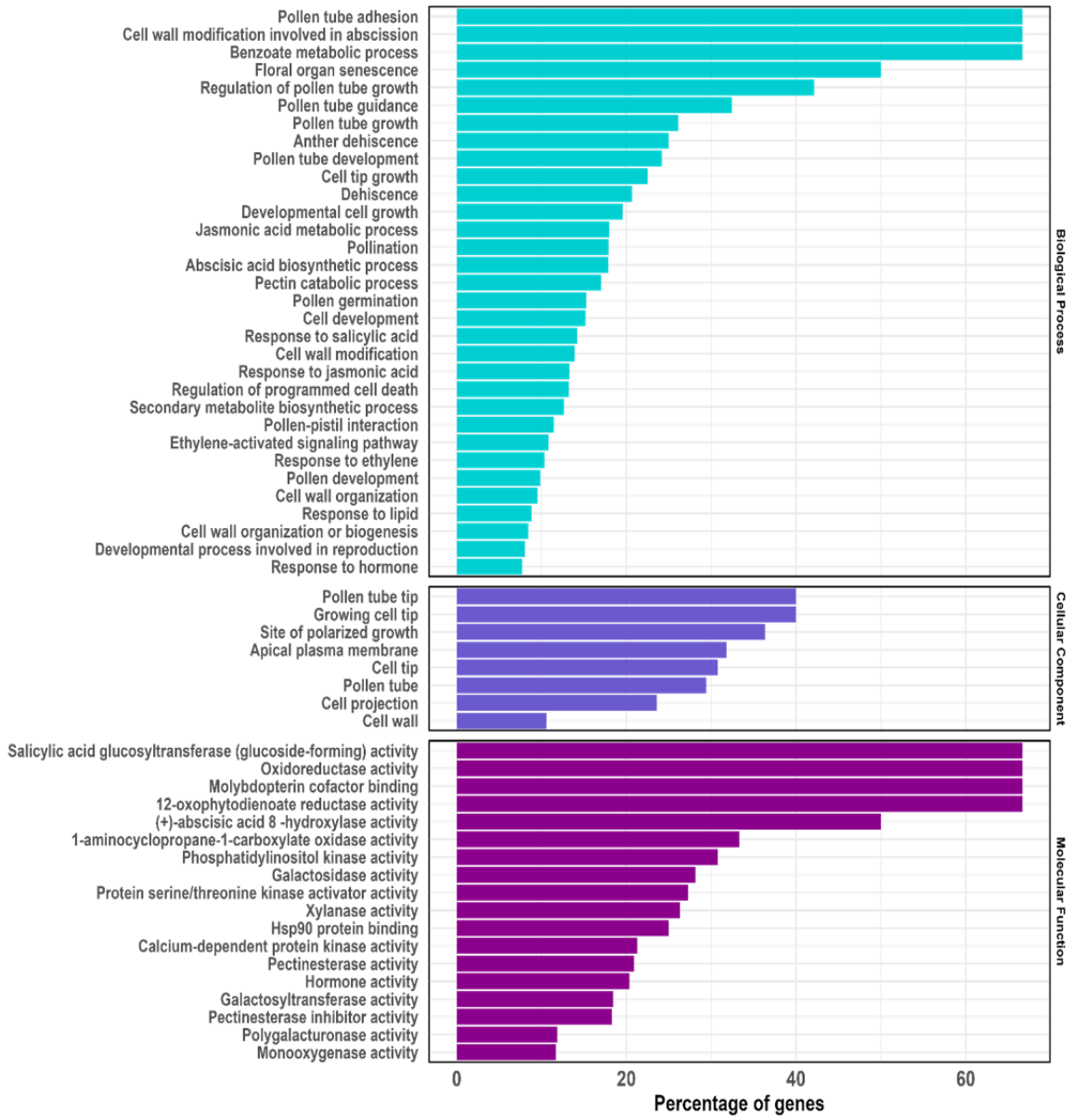

Figure Ch1_11: Gene ontology analysis of differentially expressed genes represented as a histogram. The results are categorized under the GO classifications: Biological Process, Molecular Function, and Cellular Component.

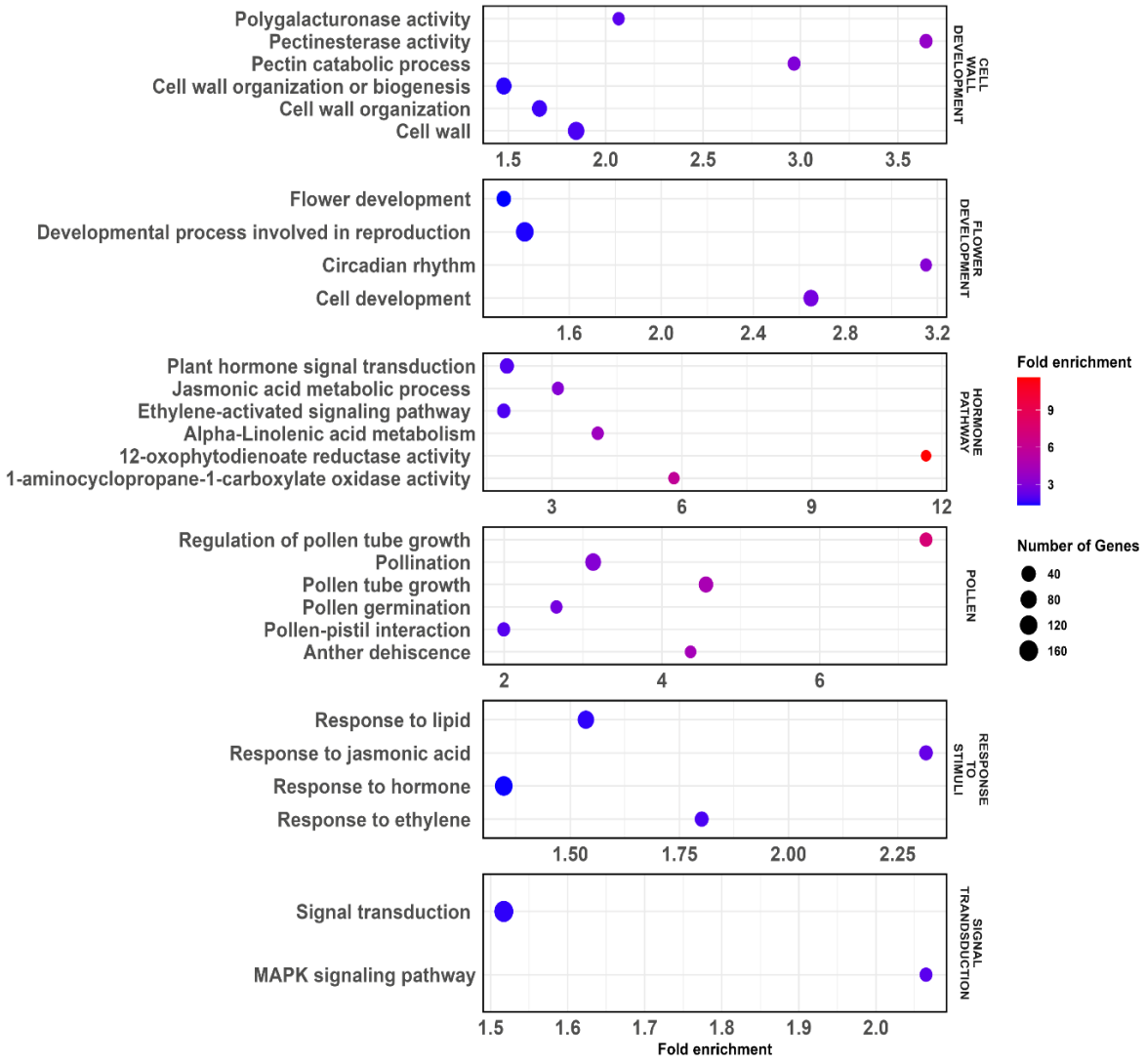

Figure Ch1_12: Bubble plot representing the gene ontology enrichment. The data was distributed into six major subcategories namely Cell development, Flower Development, Hormone Pathway, Pollen, Response to Stimuli and Signal Transduction. The size of the bubble represents the gene size and the Colour scale represents fold enrichment.

In the heatmap, each horizontal row corresponds to an individual gene, identified by its gene ID. The color gradient reflects the logarithmic scale of gene expression levels, with high expression values represented in red and low expression levels in blue.

Expression Profile of Pollen-Related Genes

The Differentially regulated genes from the enriched gene pool were analyzed. The GO analysis highlighted the enrichment of the genes involved in Cell wall Organisation and Biogenesis,

Pollen development-related genes, Protein Kinases, and Phosphatases involved in Pollen development, Biosynthesis, and Response to Hormones along with a few more clusters.

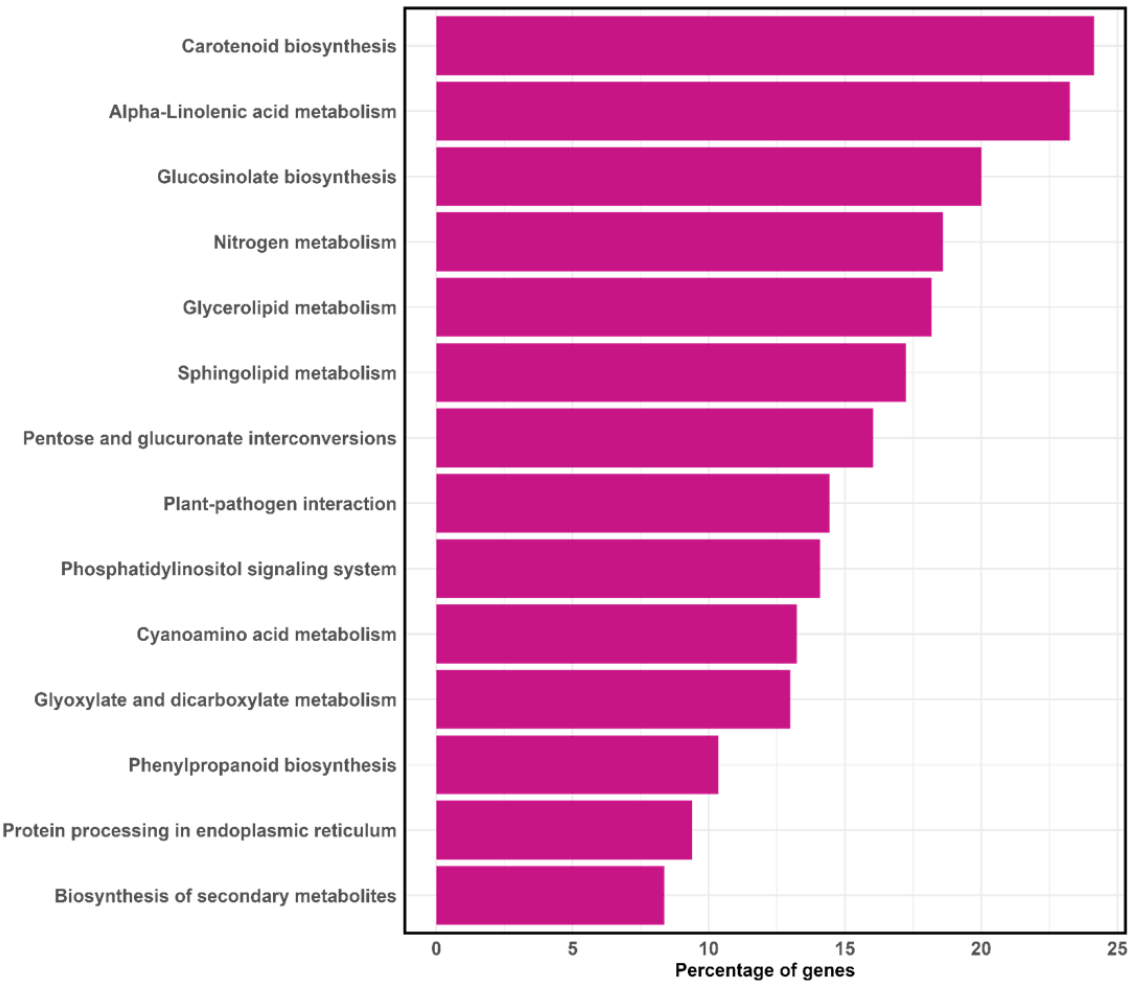

Figure Ch1_13: Histogram showing the KEGG ontology of Differentially Enriched Genes.

These genes were then selected and categorized into two groups and heatmaps showing the hierarchical clustering were plotted for each group (*Figure Ch1_15)*. The first group consisted of genes involved in overall Pollen Development (*Figure Ch1_15A)* Related genes and the second consisted of Cell Wall Biogenesis (*Figure Ch1_15B)*.

Validation of Differentially Expressed Genes

While delving deep into the transcriptome data we identified many subgroups that were significantly enriched in our dataset. We were concerned with the genes involved in Pollen development and Pollen related processes.

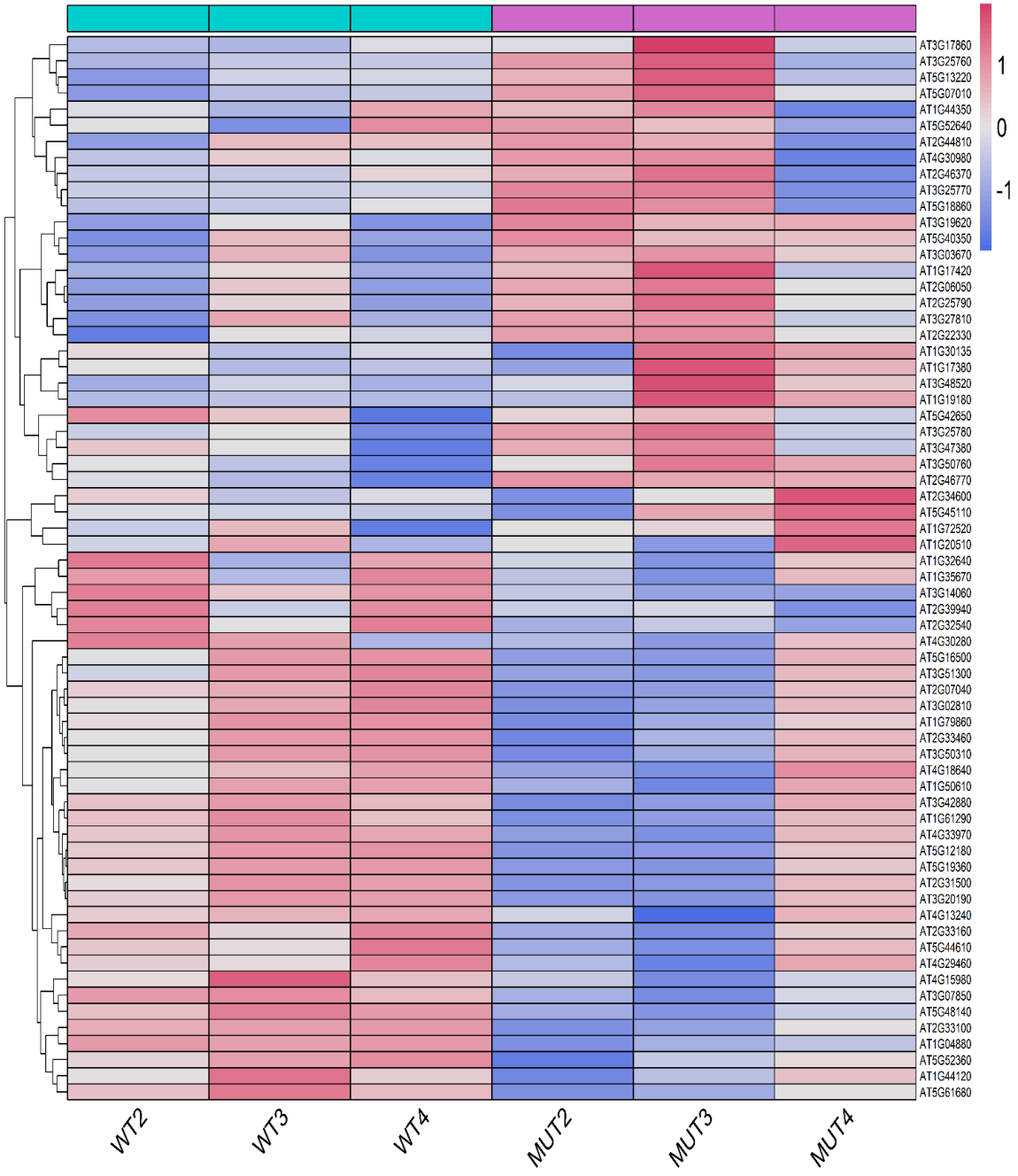

Figure Ch1_14: A composite heatmap showing the level of gene abundance in wildtype (WT2/3/4) and athmgb15-4 (MUT2/3/4) flowers. The scale represents the log2FC ratio of gene abundance between samples.

We were particularly interested in the down-regulated dataset and hence took help from the literature made available over the last few years that highlighted the importance of the genes involved in Pollen Development.

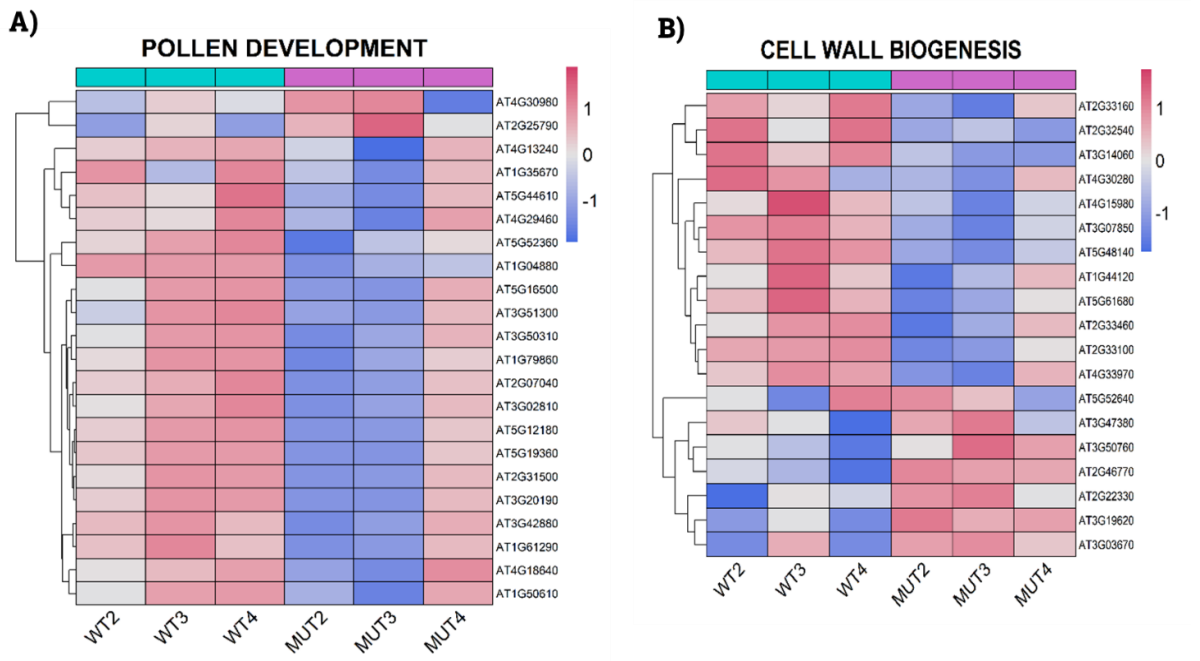

Figure Ch1_15: Heatmap showing the relative expression of major gene pool belonging to the Pollen Development and Cell wall Biogenesis and Organisation. The heatmaps show the level of gene abundance wildtype (WT2/3/4) and athmgb15-4 (MUT2/3/4) flowers. The scale represents the log2FC ratio of gene abundance between samples.

Table Ch1_1: List of top 10 significant differentially expressed genes involved in Pollen Development and Related Processes:

Gene ID	*Gene Name*	*log2 FC*	*P-value*	*Gene Description*
AT5G50260	*CEP1*	*2.65204*	*2.22E-16*	*Cysteine proteinases superfamily protein*
AT1G72520	*LOX4*	*-2.6074*	*2.22E-16*	*PLAT/LH2 domain-containing lipoxygenase family protein*
AT2G33100	*CSLD1*	*-2.529*	*8.88E-16*	*cellulose synthase-like D1*
AT4G17615	*CBL1*	*-1.6824*	*8.88E-16*	*calcineurin B-like protein 1*
AT3G20190	*PRK4*	*-1.3076*	*3.33E-15*	*Leucine-rich repeat protein kinase family protein*
AT3G48360	*BT2*	*2.88277*	*1.04E-14*	*BTB and TAZ domain protein 2*
AT3G48520	*CYP94B3*	*-2.3747*	*1.80E-14*	*cytochrome P450, family 94, subfamily B, polypeptide 3*
AT1G47270	*TLP6*	*-0.9663*	*4.34E-13*	*tubby like protein 6*
AT1G17420	*LOX3*	*-2.3125*	*3.14E-10*	*lipoxygenase 3*
AT2G39800	*P5CS1*	*1.3749*	*4.88E-10*	*delta1-pyrroline-5-carboxylate synthase 1*

Upon analysis, we selected a few targets that showed significant downregulation in the mutant (as shown in *Table Ch1_1 and Annexure_3*) and proceeded with their validation via the RT-qPCR.

Pollen-related Protein kinases and phosphatases were enriched in our dataset. Few critical kinases identified as necessary genes involved in ensuring proper and timely pollen development were downregulated (*Figure Ch1_16).* The MAP Kinases such as the *MPK3, MK6,*

and MKK9 were significantly downregulated in the dataset. Pollen-related Kinases, i.e., *PRK2A, PRK3, PRK4, PRK5, PRK6. The calcium-depenedent protein kinases like CPK16, CPK17, CPK24, CPK34* were downregulated. As observed earlier the pollen grains of the mutant exhibited defective pollen cell wall and hence to gain further insights, we analyzed the transcriptome data for genes associated with cell wall biosynthesis. Our RNA-seq analysis uncovered a notable reduction in the expression of genes associated with cell wall biosynthesis in *athmgb15-4* flowers. This includes genes like pectin lyase, cellulose synthase, pectin methylesterase, and extensin, all of which are essential for proper pollen wall formation. (*Figure Ch1_17)*. We then selected genes from the Hormone biosynthesis, response and signaling and validated them. There was a significant downregulation of the genes belonging to the ethylene pathway, Gibberellic Acid, Jasmonic Acid and Auxin response pathway in the *athmgb15-4* mutant flower (*Figure Ch1_18)*.

Comparative Analysis of DEGs between *athmgb15-4* and *athmgb15-1*

Our transcriptome data had a good spread of DEGs as represented through the GO and KEGG enrichment and hence we considered comparing it to pre-existing datasets. Previously published work on *athmgb15-1* mutants by *Xia et al 2014* carried out a microarray analysis from the pollen tissue showing 1986 differentially expressed genes in the mutant (Xia et al., 2014). We compared 757 genes of the FDR-corrected upregulated from our dataset with 1101 upregulated genes from the microarray dataset and extrapolated 60 genes that were common to both the mutants as listed in the *Table Ch1_2 and Annexure_4*. Whereas about 111 genes (*Table Ch1_3 & Annexure_5*) were common in the downregulated pool of 905 and 585 genes in the *athmgb15-4* and *athmgb15-1* data sets, respectively.

The common genes listed in the tables were represented as venn diagrams (*Figure Ch1_19A-B)* and then subjected to GO enrichment to get a fair idea of the processes they were involved (*Figure Ch1_19C)*. Though the pollen microarray did not consist of many genes from the early pollen development pathway, instead exhibited genes enriched during Pollen tube growth, pollen tube cell tip elongation, pollination and regulation of pollen tube growth. Cell tip elongation and its guidance through the style of the female gametophyte to reach the ovary is a crucial step in the process of fertilization. The protein kinases and the serine-threonine kinases involved in pollen tube compatibility and recognition were enriched.

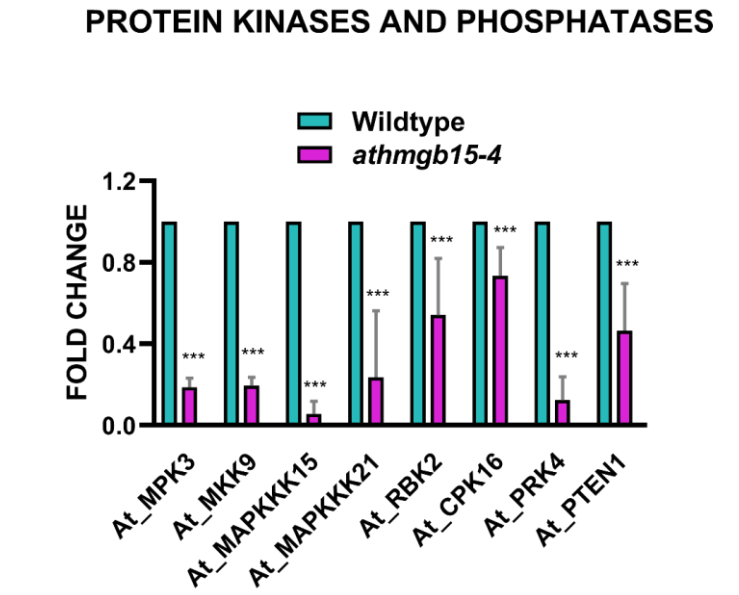

*Figure Ch1_16: Expression of differentially regulated genes was analyzed between wildtype and athmgb15-4 using RT-qPCR. The fold change was represented with respect to wildtype. Error bars represent mean ± SD (n=5). The significance for each gene was analyzed by paired two-tailed Student's t-test. Asterisks represent significant differences between Wildtype and athmgb15-4, ***P< 0.001.*

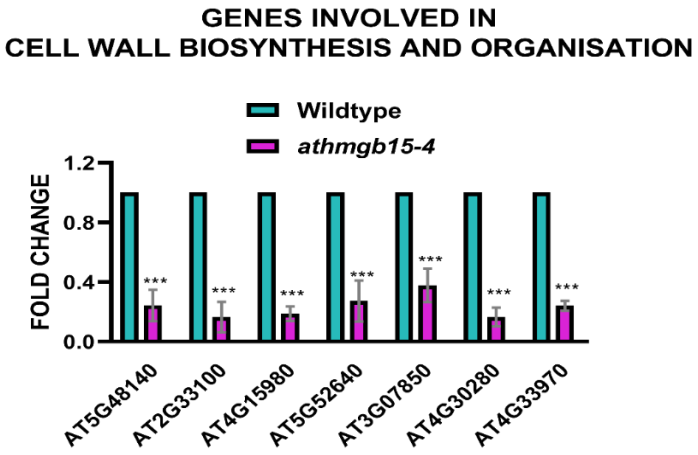

*Figure Ch1_17: Expression of differentially regulated genes was analyzed between wildtype and athmgb15-4 using RT-qPCR. The fold change was represented with respect to wildtype. Error bars represent mean ± SD (n=5). The significance for each gene was analyzed by paired two-tailed Student's t-test. Asterisks represent significant differences between Wildtype and athmgb15-4, ***P< 0.001.*

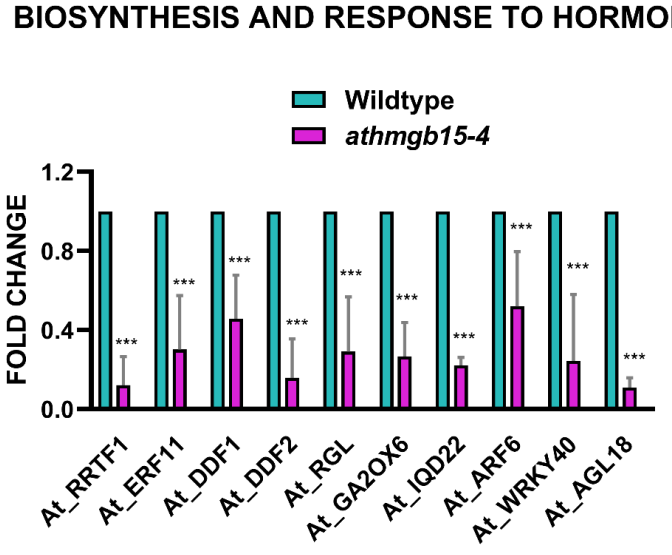

*Figure Ch1_18: Expression of differentially regulated genes was analyzed between wildtype and athmgb15-4 using RT-qPCR. The fold change was represented with respect to wildtype. Error bars represent mean ± SD (n=5). The significance for each gene was analyzed by paired two-tailed Student's t-test. Asterisks represent significant differences between Wildtype and athmgb15-4, ***P< 0.001.*

Table Ch1_2: Summary of top 10 from the 60 upregulated genes common to athmgb15-1 and athmgb15-4 mutants:

Gene ID	Gene Name	log2 FC	P-value	Gene Description
AT1G28327	F3H9.2	6.08527	4.98E-05	E3 ubiquitin-protein ligase
AT1G18860	WRKY61	5.23186	6.19E-11	WRKY DNA-binding protein 61
AT5G19560	ROPGEF10	4.76675	7.35E-08	ROP uanine nucleotide exchange factor 10
AT4G32375	AT4G32375	4.26237	3.21E-10	Pectin lyase-like superfamily protein
AT3G09240	BSK9	4.24345	4.43E-09	kinase with tetratricopeptide repeat domain-containing protein
AT3G01900	CYP94B2	3.53445	2.97E-05	cytochrome P450, family 94, subfamily B, polypeptide 2
AT2G30240	ATCHX13	3.40899	1.90E-05	Cation/hydrogen exchanger family protein
AT3G09520	EXO70H4	3.19734	8.54E-06	exocyst subunit exo70 family protein H4
AT1G02580	MEA	2.80852	4.36E-06	SET domain-containing protein
AT4G00955	AT4G00955	2.70456	1.42E-07	wall-associated receptor kinase-like protein

Table Ch1_3: Summary of top ten from the 111 down-regulated genes common to athmgb15-1 and athmgb15-4 mutants:

Gene ID	Gene Name	log2 FC	P-value	Gene Description
AT5G55980	MDA7.2	-5.8234	4.36E-11	serine-rich protein-like protein
AT1G67623	F12A21.25	-5.4693	0.00026	F-box family protein
AT1G24110	F3I6.3	-5.0964	9.42E-11	Peroxidase superfamily protein
AT3G05140	RBK2	-4.4381	0	ROP binding protein kinases 2
AT2G03840	TET13	-3.9394	9.35E-10	tetraspanin13
AT5G25430	F18G18.170	-3.8626	4.33E-14	HCO3- transporter family
AT3G21570	AT3G21570	-3.8023	0	proline-rich nuclear receptor coactivator
AT1G19090	RKF2	-3.6964	1.24E-10	receptor-like serine/threonine kinase 2
AT1G04880	F13M7.13	-3.5488	3.71E-08	HMG (high mobility group) box protein with ARID/BRIGHT DNA-binding domain-containing protein
AT5G48140	MIF21.3	-3.5101	0	Pectin lyase-like superfamily protein

Also, to our surprise apart from the pollen-related processes, Linolenic acid metabolism-related genes were enriched. α-linolenic acid is the precursor of the JA and hence we believe that the JA pathway could be a point of study. JA is widely known to contribute to the proper development of the male gametophyte. So, we were confident that this plant hormone and its pathway may be an important aspect of this study.

Comparative analysis of DEG in *athgmb15-4* flower vs CHIP-chip AtHMGB15 binding in wildtype seedlings

We then considered comparing the DEGs of *athgmb15-4* flower RNAseq data with previously published CHIP-chip AtHMGB15 binding in wild-type seedlings from our lab (*Figure Ch1_20A-B)*. This common pool obtained from this comparison sheds light on the genes that are differentially regulated in the *athgmb15-4* mutant flowers and also have the AtHMGB15 binding occupancy (*Figure Ch1_20C)*. This tells us about the binding pattern of AtHMGB15 involved in various pathways that may be crucial to pollen development. There were about 583 and 520 genes common to the CHIP-chip AtHMGB15 control binding in wildtype with the FDR-corrected downregulated and upregulated DEGs of *athmgb15-4* flower tissue, respectively.

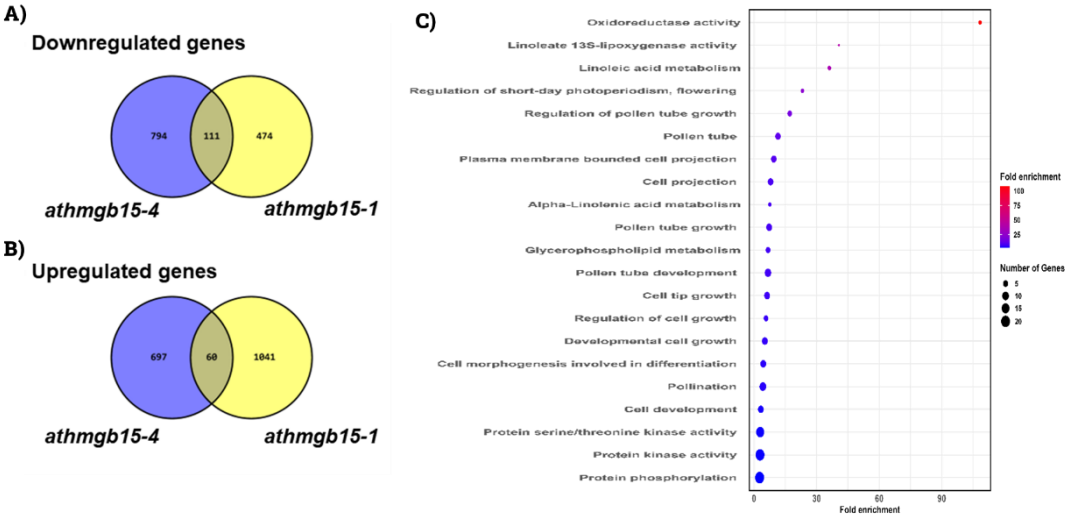

Figure Ch1_19: Comparative analysis of DEGs (flower tissue) with Xia et al 2014 (pollen tissue) datasets: A&B) Venn diagrams representing 111 downregulated genes and 60 upregulated genes in comparison with Xia et al 2014 (pollen tissue) dataset, respectively. C) Bubble plot showing GO term enrichment of a common set of genes between athmgb15-4 and Xia et al 2014 (pollen tissue) dataset.

We analyzed the GO enrichment for the 1103 genes (*Annexure 6&7*) from the common pool and observed a high number of genes involved in Reproductive processes including pollen cell wall, pollen tube and cell tip growth, anther dehiscence, and circadian rhythm along with Lipid metabolic processes and Cell wall development. A few of the pollen cell wall components like the galacturonases, polysaccharides, pectins and cellulose synthases were also affected.

Hormone metabolic processes, and plant hormone-mediated signal transduction pathway-related genes were also gravely enriched. Kinase activity was also enriched especially The MAP Kinase signaling. We observed that overall, many signaling pathways associated with plant

hormones such as Ethylene, Salicylic acid and JA were enriched. Genes related to the JA precursor metabolism, biosynthesis and response pathways were all enriched.

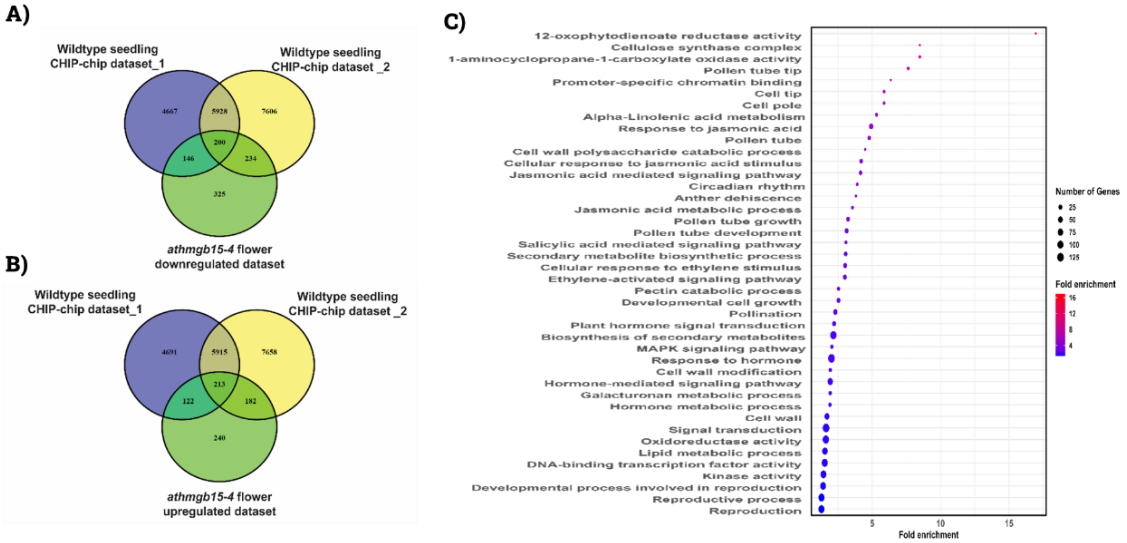

Figure Ch1_20: Comparative analysis of DEGs (flower tissue) with CHIP-chip AtHMGB15 control binding in wildtype Mallik et al 2020 (seedling tissue) datasets. A&B) Venn diagrams representing a total of 580 downregulated genes and 518 upregulated genes in comparison with wildtype ChIP-chip dataset_1 and 2 from Mallik et al 2020 (seedling tissue), respectively. C) Bubble plot showing GO term enrichment common between athmgb15-4 (flower tissue) and ChIP-chip dataset from Mallik et al 2020 (seedling tissue).

AtHMGB15 affects the Jasmonic Acid pathway

The above comparisons and analyses revealed a promising direction to our study hinting at the involvement of AtHMGB15 in regulating the JA during pollen development. We then analyzed the JA-related genes and saw a significant number of biosynthesis and response-related genes were differentially regulated (*Table Ch1_4 and Annexure_8*).

Table Ch1_4: List of top 10 significant differentially expressed genes involved in JA Biosynthesis, Response and Signaling:

Gene ID	*Gene Name*	*log2 FC*	*P-value*	*Gene Description*
AT2G06050	*OPR3*	*-2.0484*	*0*	*oxophytodienoate-reductase 3*
AT1G17380	*JAZ5*	*-1.8745*	*0*	*jasmonate-zim-domain protein 5*
AT1G20510	*OPCL1*	*-1.9844*	*0*	*OPC-8:0 CoA ligase1*
AT4G35770	*SEN1*	*3.99227*	*0*	*Rhodanese/Cell cycle control phosphatase superfamily protein*
AT5G13220	*JAZ10*	*-1.5969*	*0*	*jasmonate-zim-domain protein 10*
AT1G72520	*LOX4*	*-2.6074*	*2.22E-16*	*PLAT/LH2 domain-containing lipoxygenase family protein*
AT4G16740	*TPS03*	*1.07668*	*3.11E-15*	*terpene synthase 03*
AT3G48360	*BT2*	*2.88277*	*1.04E-14*	*BTB and TAZ domain protein 2*

AT3G48520	*CYP94B3*	*-2.3747*	*1.80E-14*	*cytochrome P450, family 94, subfamily B, polypeptide 3*
AT2G46370	*JAR1*	*-1.4501*	*2.17E-13*	*Auxin-responsive GH3 family protein*
AT2G06050	*OPR3*	*-2.0484*	*0*	*oxophytodienoate-reductase 3*

The table of the JA pathway genes revealed that major JA biosynthesis genes were downregulated in the mutant flowers. Also, the JA response and signaling-related genes were lowered in expression. The JA biosynthesis begins when the Phospholipase A encoding gene, *Defective in in Anther Dehiscence (DAD1)* converts the available anther plastids and membrane lipid into the a-Linolenic Acid, the widely known major precursor of the JA (*Figure 5)*.

This α-linolenic acid is then acted upon by the lipoxygenases 3/4 to give the subsequent substrate for *Allene Oxide Synthase (AOS)* to give epoxylinolinate. The *Allen Oxide Cyclase (AOC3)* converts the previous product to phytodieonic acid or OPDA. These steps occur in the plastid of the cells. The *Oxophytodieonic Reductase (OPR3)* produces OPC8 where a series of beta-oxidation takes place via the *ACX1* giving the JA occurring in the Peroxisome. This JA has to be converted into the bioactive JA-Isoleucine within the cytoplasm which migrates into the nucleus to carry out the downstream signaling process.

The signaling begins at the onset of JA-Ile binding to the Jas domain of the JA ZIM domain protein (JAZs) and migrating the whole repression complex consisting of TOPLESS-NINJA-JAZ away from the MYC2, a bHLH Transcription factor. This repressor complex is then tagged with E3 ubiquitin ligase SCF-COI1 for the proteasome degradation pathway. This renders the MYC2 free to carry out the transcription of the downstream pathway genes (*Figure 6)*.

After the in-silico analyses, from the JA pathway genes as shown in the heatmap (*Figure Ch1_21A),* we selected a handful of genes involved in the JA pathway, that were significantly downregulated, to validate our transcriptome data by RT-qPCR. It resulted in low expression of all the candidate genes, proving the role of AtHMGB15 in governing the JA biosynthesis and Response.

The JA biosynthesis and signaling genes were significantly downregulated in the *athmgb15-4* mutant flowers (*Figure Ch1_21B-C)*. To confirm the role of AtHMGB15 in manipulating the JA pathway we intended to reconfirm the theory in other lines of *athmgb15* mutants, namely SALK_057612C_15 and SALK_057612C_9. These mutants have a T-DNA insertion at the promoter region of the gene as shown in the schematic (*Figure Ch1_22A)*. The lines were checked for homozygosity and were used for subsequent analyses (*Figure Ch1_22B)*. The wildtype and Salk line mutant flowers were collected and the RNA isolated was converted to cDNA to check the

expression of JA genes via RT-qPCR. As anticipated, there was significant downregulation of all the candidate JA pathway genes as observed in the flowers of *atmhgb15-4* mutants (*Figure Ch1_22C).* This experiment confirmed that in the absence of AtHMGB15, the plants exhibited lowered expression of JA pathway-related genes. This led to the avenue to inspect the levels of JA and its derivatives in the mutant flowers.

Estimation of hormones in *athmgb15-4* flowers

The transcriptome data analysis revealed a lowered expression of the genes involved in the biosynthesis of JA. We were curious to check whether this downregulation reflects the JA levels in the flower tissue. We took the approach of measuring the hormone content by Electron Spray Ionization coupled Mass Spectroscopy. To carry out the hormone estimation experiment, we procured three different JA and their derivatives namely Methyl Jasmonate (MeJA) and Jasmonic Acid Isoleucine (JA-Ile).

We identified the peaks of the standards based on their molecular weight and noted them (*Figure Ch1_23A)*. We then proceeded with the flower tissue of wildtype and *athmgb15-4* mutants for estimation.

As predicted, there was a sharp reduction in the amount of all the derivates (*Figure Ch1_23A)*. There was about a 10-fold decline with the least for Ja-Ile which is the bioactive form of JA within the plant cell (*Figure Ch1_23B)*. It is JA-Ile that migrates from the cytoplasm to the nucleus and binds to the JA-responsive repressor complex. This sets the MYC2 free to transcribe and further allows the transcription of other JA-responsive genes to carry out the necessary cellular functions associated with the development of male gametophytes.

Methyl jasmonate application restores normal pollen development and expression of JA pathway genes in *athmgb15-4* mutants

Given the observed reduction in JA levels in the flowers of the *athmgb15-4* mutant, it was crucial to explore the potential of exogenous MeJA (methyl jasmonate) treatment to compensate for this deficiency. The effect of applying MeJA externally to the flowers after a 48-hour treatment was investigated by evaluating pollen tube germination (*Figure Ch1_24A)*. The results were compelling, as they revealed that exogenous MeJA application on buds and young flowers of the *athmgb15-4* mutant effectively restored pollen tube germination (*Figure Ch1_24B)*. Remarkably,

the germination rate of these treated mutant pollen grains reached levels comparable to those observed in wild-type pollen grains, suggesting a significant recovery.

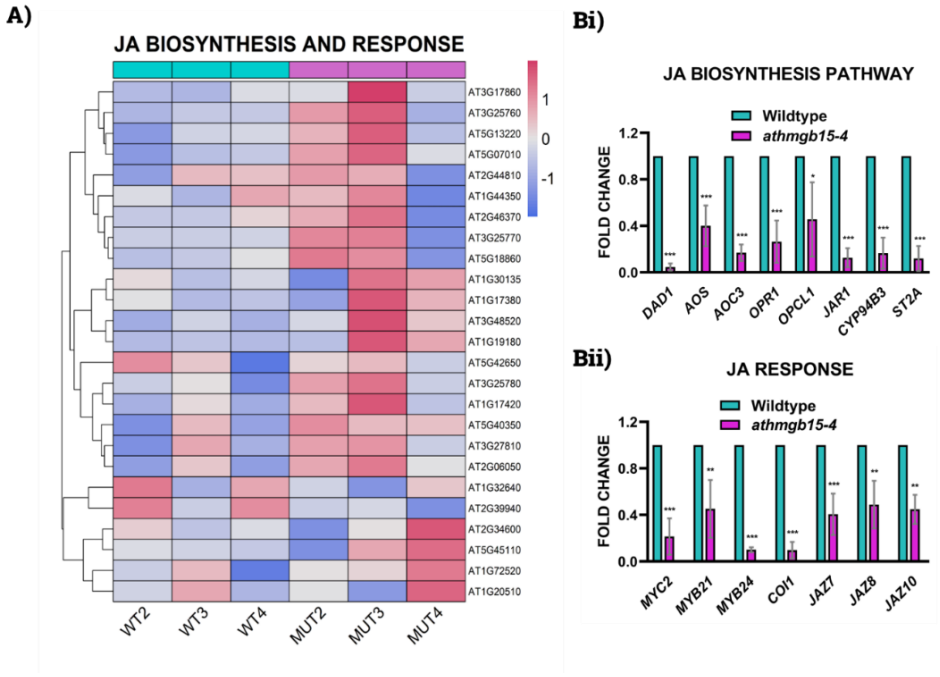

*Figure Ch1_21: A) Heatmap showing the differential expression of genes in three biological replicates of each of the wildtype (WT2/3/4) and athmgb15-4 (MUT2/3/4) flowers involved in JA biosynthesis and response. Heatmap generated using log2FC values. Bi) JA biosynthesis and Bii) JA response pathway show Expression of differentially regulated JA biosynthesis and signaling genes was analyzed between wild type and athmgb15-4 using RT-qPCR. The fold change was represented with respect to wild type. Error bars represent mean±SD (n=6). The significance for each gene was analyzed by paired two-tailed Student's t-test. Asterisks represent significant differences between wild type and athmgb15-4, *P<0.05, **P<0.01, ***P<0.001.*

In addition to observing the phenotypic changes, we also conducted a thorough analysis of the expression levels of key JA biosynthesis and signaling genes following the MeJA treatment. The results indicated a pronounced upregulation in the expression of genes such *as AOS, OPR3, MYC2, JAZ1*, and *JAZ10* in wild-type and *athmgb15-4* flowers post-treatment (*Figure Ch1_25)*.

This upregulation points to a direct response to the exogenous application of MeJA, suggesting that the treatment successfully reactivated the JA signaling pathway. The combined observations from the restoration of pollen tube germination and the induction of JA signaling genes strongly suggest that the reduced endogenous JA levels in *athmgb15-4* plants are indeed responsible for the diminished expression of JA-responsive genes during pollen development. These findings provide valuable insights into the critical role of JA in pollen development.

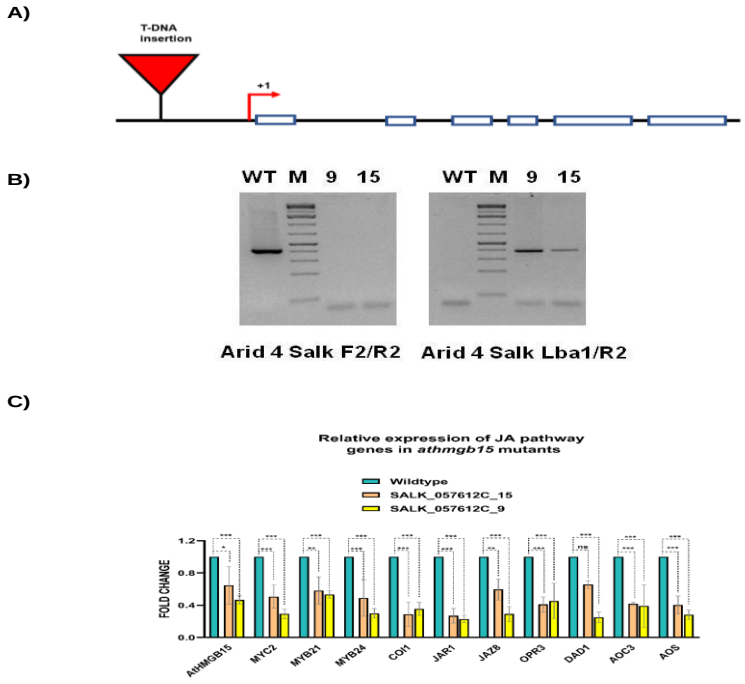

*Figure Ch1_22: A) Schematic diagram showing the T-DNA (red triangle) insertion in the AtHMGB15 promoter region in SALK_057612C. White rectangles represent the exon regions. Red arrow denotes the Transcription start site. B) PCR screening of homozygous lines of SALK_057612C. We have identified two homozygous lines name SALK_057612C_15 & SALK_057612C_9. C) RT-qPCR analysis revealed low expression of JA genes in the athmgb15 mutants SALK_057612C_15 & SALK_057612C_9 in comparison to the wildtype. The fold change was represented with respect to wildtype. Error bars represent mean ± SD (n=5). The significance for each gene was analyzed by one-way analysis of variance (ANOVA) with Tukey's post-hoc test. Asterisks represent significant differences as indicated (*P< 0.05, **P< 0.01, ***P< 0.001, ns, not significant).*

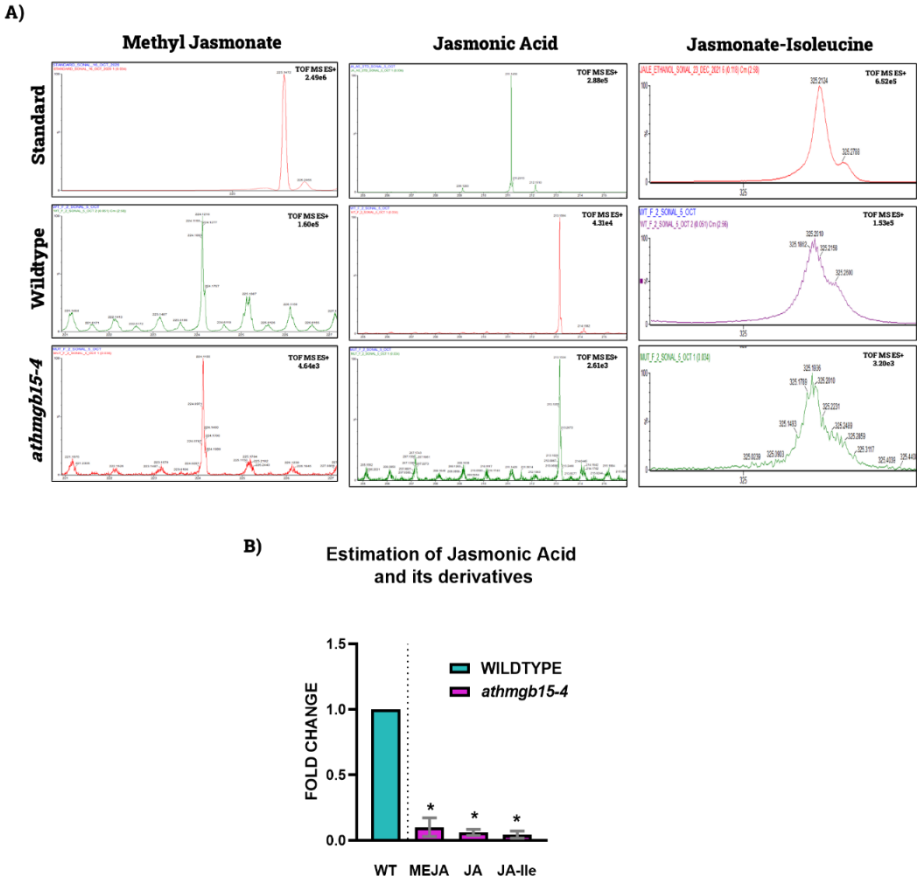

*Figure Ch1_23: A) Mass spectra of standard, wildtype and athmgb15-4 flower samples showing reduced levels of Methyl Jasmonate, Jasmonic Acid and Jasmonate-Isoleucine in flowers of athmgb15-4 mutant. B) JA and its derivatives were measured from the flowers of wild type and athmgb15-4 and represented as fold change with respect to wild type. Error bars represent mean±SD (n=3). The significance was analyzed by one-way ANOVA with Fisher's LSD post hoc test. Asterisks represent significant differences as indicated (*P<0.05) JA, jasmonic acid; MeJA, methyl jasmonate; JA-Ile, jasmonic acid isoleucine.*

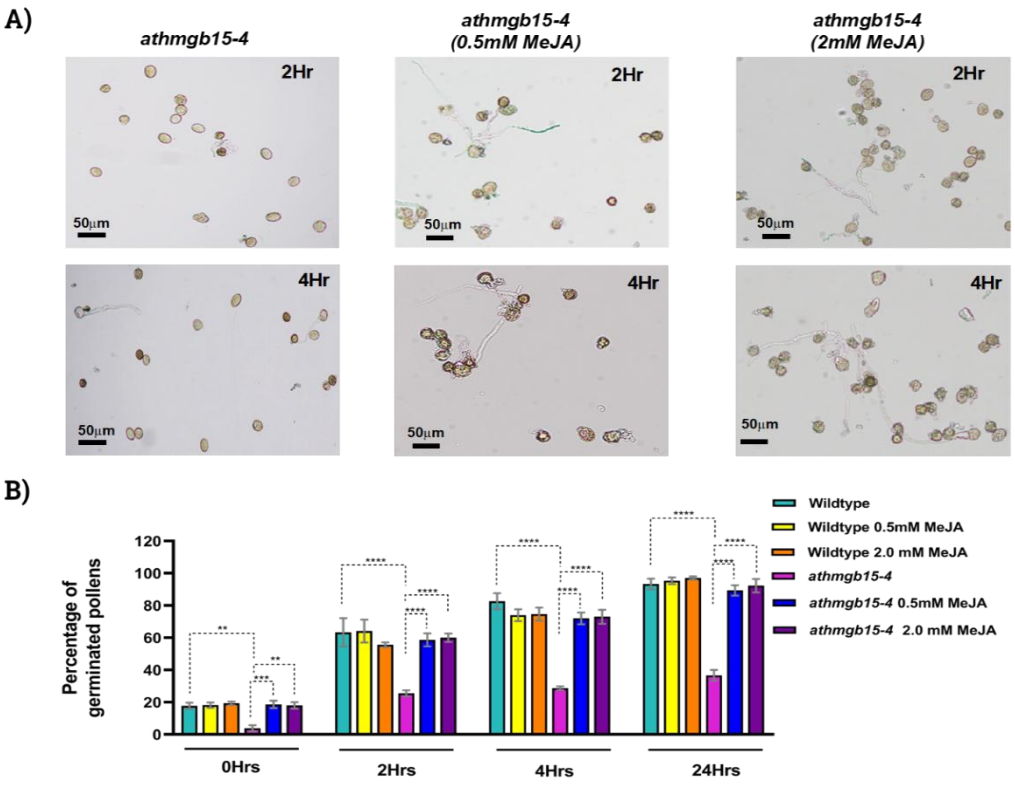

*Figure Ch1_24: A) Restoration of in vitro pollen germination of athmgb15-4 on treatment with exogenous MeJA (0.5 and 2 mM). B) Quantification of the rate of pollen tube germination in the presence of different concentrations of methyl jasmonate. Error bars represent mean±SD (n=3). The significance was analyzed by two-way ANOVA with Tukey's post hoc test. Asterisks represent significant differences as indicated (**P<0.01, ***P<0.001, and ****P<0.0001).*

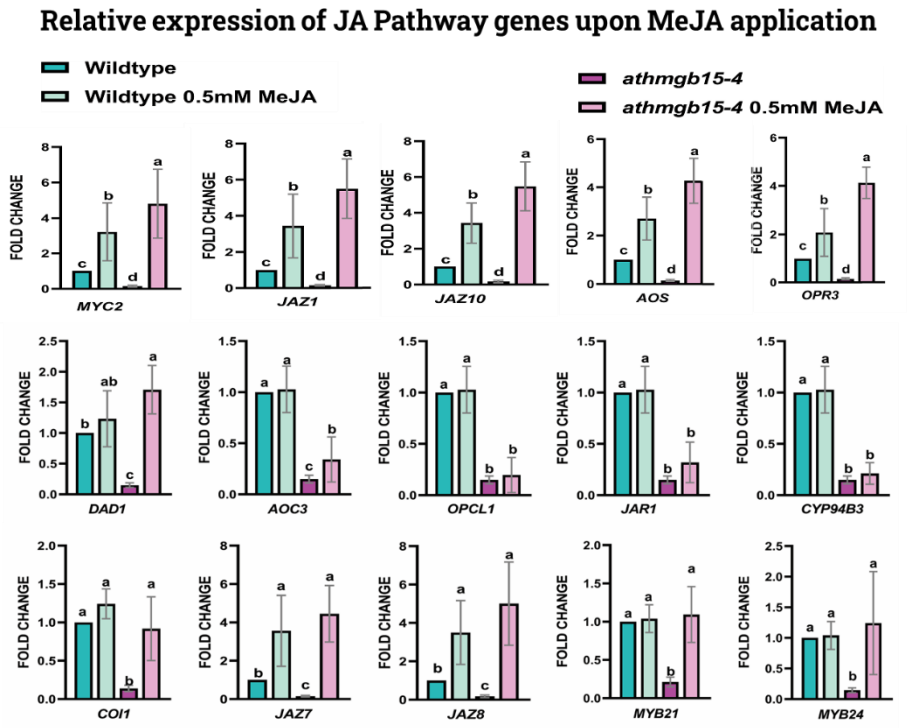

Figure Ch1_25: Expression of genes strongly induced by exogenous MeJA (0.5 mM) in flowers of wild type and athmgb15-4. The fold change was represented with respect to wildtype. Error bars represent mean±SD (n=6). Letters indicate significant differences according to a one-way ANOVA with Tukey's post hoc test (P<0.05).

Section 3

Transformation of Arabidopsis Using the Floral Dip Method and Screening of Positive Transformants

The *AtHMGB15* full-length CDS were previously cloned into gateway vector pMDC84 and transformed into agrobacterium cells for downstream transformation into Arabidopsis plants. The floral dip method was applied to generate the *athmgb15-4*-OE_{A4} plants. The seeds from the T0 phase were collected and dried before plating onto Hygromycin selection MS plates. The positive transformants would ideally grow true leaves in the presence of hygromycin due to its resistance whereas wildtype seedlings would only germinate and form cotyledonary leaves. The non-transformants would not progress to the formation of true leaves and eventually decolorize and die off. We observed true transformants which were healthily growing in the presence of hygromycin (*Figure Ch1_26A)*. A single leaf from these plants was plucked from the 12-leaved stage and subjected to genomic DNA isolation. This PCR confirmed the presence of CDS in true transformants. Upon rigorous screening, we were able to generate the *athmgb15-4*-OE_{A4} plants (*Figure Ch1_26B-C)*.

The next experiment was to confirm the expression of *AtHGMB15* in the *athmgb15-4*-OE_{A4} plants confirming the complementation of *AtHGMB15* in *athmgb15-4* mutant background. We isolated the RNA and converted to cDNA from the *athmgb15-4*-OE_{A4} along with wild-type and *athmgb15-4* mutant plants to check the expression (*Figure Ch1_27A)*. Realtime analysis revealed a 6-fold increase of *AtHGMB15* expression in *athmgb15-4*-OE_{A4} in comparison to wild-type and about a 10-fold increase in comparison to *athmgb15-4* mutants confirming the complementation (*Figure Ch1_27B)*.

Phenotypic differences between wild-type, *athmgb15-4* and *athmgb15-4*-OE_{A4} plants

The complementation lines were overexpressing the AtHMGB15 and hence we proceeded with its phenotypic characterization. The *athmgb15-4* was delayed in bolting whereas the *athmgb15-4*-OE_{A4} recovered the delayed phenomenon and followed the bolting pattern similar to wildtype plants (*Figure Ch1_28A)*.

The siliques were shorter with more abortive seeds in comparison to wildtype. Similarly, the complementation lines were longer with almost no abortive seeds hinting at the positive role of AtHMGB15 in seed development (*Figure Ch1_28B)*.

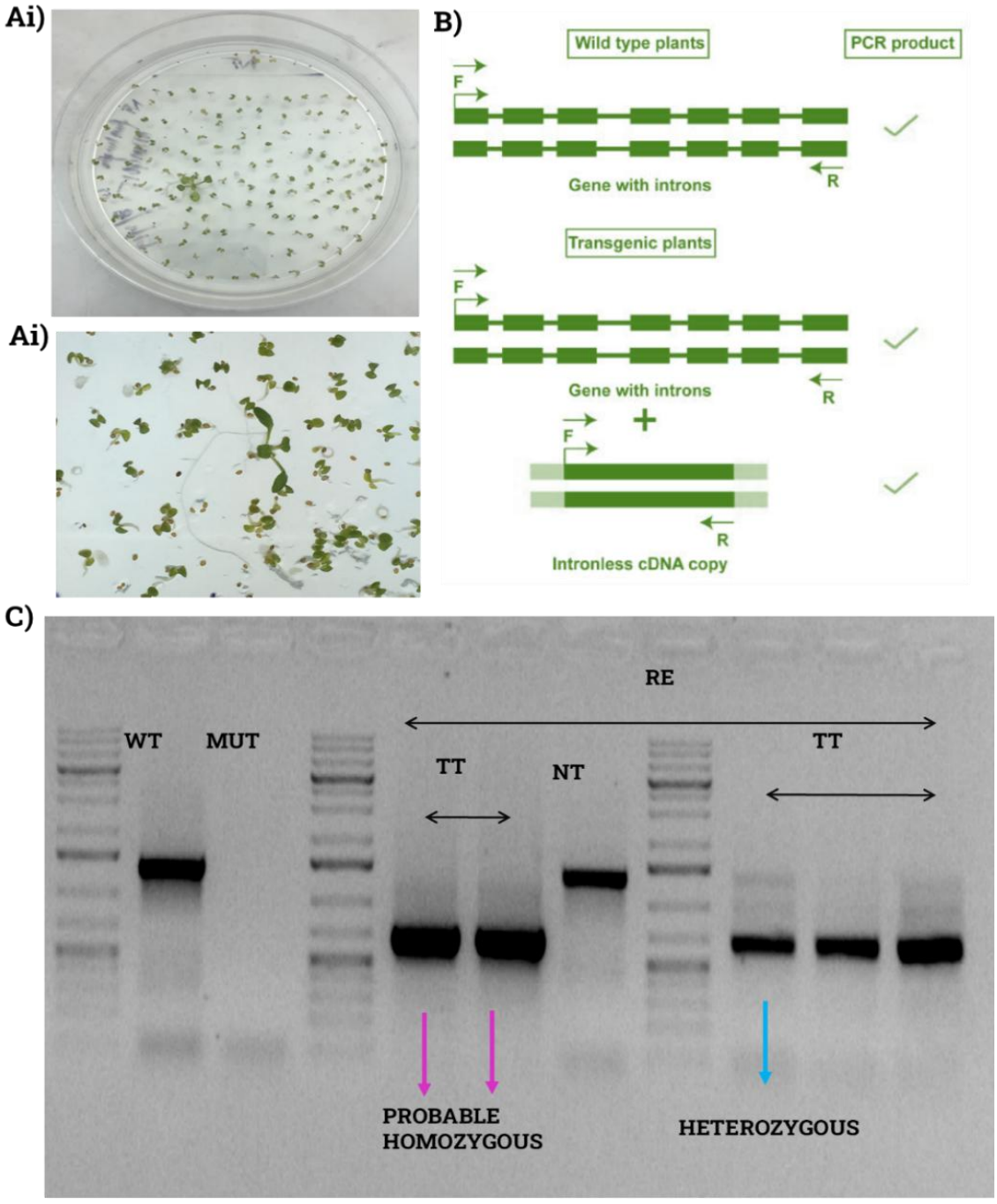

Figure Ch1_26: Ai&ii) Selection plates show the positive transformants with four leaves. B) Schematic showing the possible PCR outcome to confirm the transgenic lines. C) Gel image showing the genomic copy of AtHMGB15 in wildtype (WT) and absence of it in the mutant (MUT). True transformants (TT) have a copy of the intronless gene whereas non-transformants (NT) do not as observed during screening of the athmgb15-4-OE_{A4} plants (RE).

Defective Pollen Properties were rescued in the complementation line *athmgb15-4*-OE$_{A4}$

As observed in Section 1, the pollen properties were compromised in the *athmgb15-4*. Hence, we decided to compare the pollen germination pattern of *athmgb15-4*-OE$_{A4}$ to wild-type pollen grains *(Figure Ch1_29Ai)*.To our satisfaction, the complementation lines rescued the lowered rate of pollen germination of mutants (*Figure Ch1_29Aii)*. They were healthy and had a very high rate of pollen tube germination similar to that of wildtype pollen grains. The pollen morphology was studied which revealed ellipsoidal pollen grains with proper reticulate pattern of sporopollenin deposition in the pollen grains of the complementation lines. The defects associated with improper shape and poor pattern of wall deposition in *athmgb15-4* pollen grains were completely recovered such that they resembled the pollen grains of wildtype plants (*Figure Ch1_29B)*. The defects owing to the pollen properties of the mutants were thereby shown to recover in the complementation lines corroborating the role of AtHMGB15 in guiding proper pollen development in Arabidopsis plants.

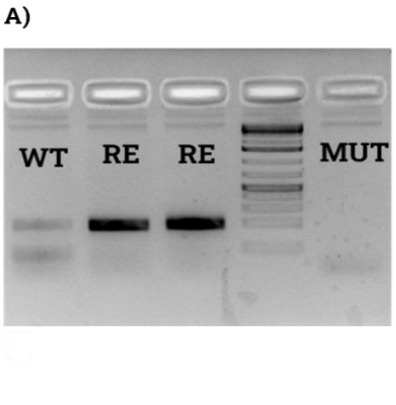

*Figure Ch1_27: A) Gel image showing high expression of AtHMGB15 in the complementation lines. (WT-wildtype, RE- athmgb15-4-*OE$_{A4}$ *and MUT-athmgb15-4). B) RT-qPCR to check AtHMGB15 transcript level in wild type, athmgb15-4, and athmgb15-4-OEA4. The fold change was represented with respect to the wild type. Error bars represent mean±SD (n=6). Letters indicate significant differences according to a one-way ANOVA with Tukey's post hoc test (P< 0.05).*

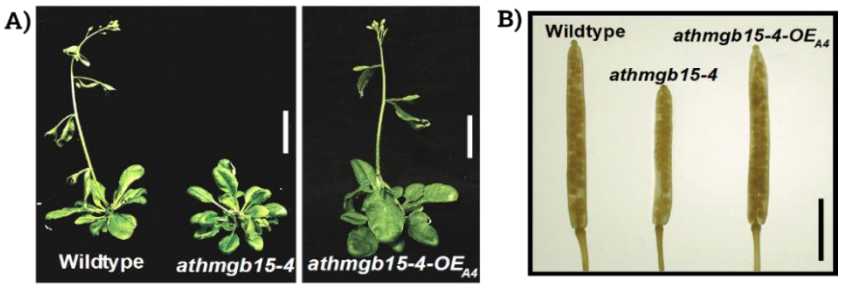

*Figure Ch1_28: (A) Comparative flower bolting pattern between wild type, athmgb15-4, and athmgb15-4-*OE$_{A4}$*. Scale bar=2 cm. (B) measurement of silique length of wild type, athmgb15-4, and athmgb15-4-*OE$_{A4}$*. Scale bar=4 mm.*

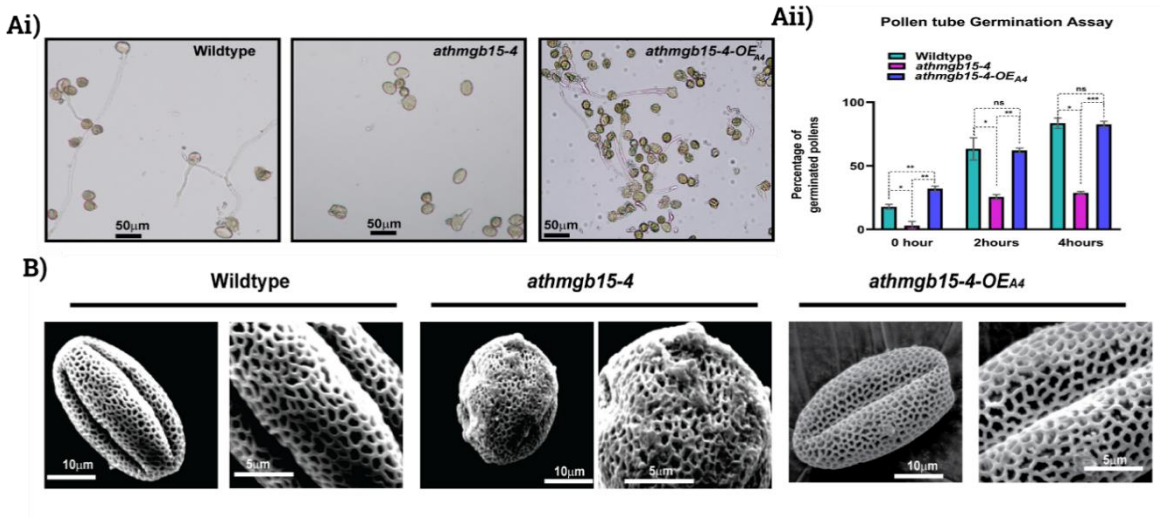

*Figure Ch1_29: Ai) Comparative in vitro pollen germination analysis was conducted between wild type, athmgb15-4, and athmgb15-4-OE$_{A4}$. (Aii) Quantification of pollen germination rates is shown, with error bars representing the mean ± SD (n=6). Statistical significance at each time point was determined using one-way ANOVA followed by Fisher's LSD post hoc test. Asterisks indicate significant differences as follows: *P<0.05, **P<0.01, ***P<0.001, with "ns" denoting no significant difference. (B) SEM analysis was performed to examine pollen morphology.*

Jasmonic Acid Pathway rescued in the complementation lines

The defects owing to pollen grain morphology and germination pattern were recovered in the complementation lines and hence we proceeded to examine the expression of genes involved in the JA which were gravely downregulated in our mutants. The JA biosynthesis and response-related genes were induced in expression in comparison to the mutants thereby showing expression higher than that of wild-type flowers (*Figure Ch1_30A-B)*. This was a major recovery of defect where the whole JA pathway was repressed due to the absence of AtHHMGB15 in the system. This confirmed the active role of AtHMGB15 in regulating JA pathway during flower development.

With the induction of JA biosynthesis genes, we were confident that the JA content in the system had also been replenished. The biosynthesis genes showed significantly higher expression compared to wild-type flowers, making it evident that the end products would also be present at higher levels than in the mutants. Thus, we measured the JA(s) content and the results were favorable. The levels of JA, JA-Isoleucine and MeJA were rescued and significantly higher than the levels in mutants and wildtype flowers (*Figure Ch1_30C)*. Hence, we can conclude that the *athmgb15-4*-OE$_{A4}$ successfully rescued all the defects owing to the *AtHMGB15* deletion, thereby. confirming its role in governing the pollen development and the JA pathway.

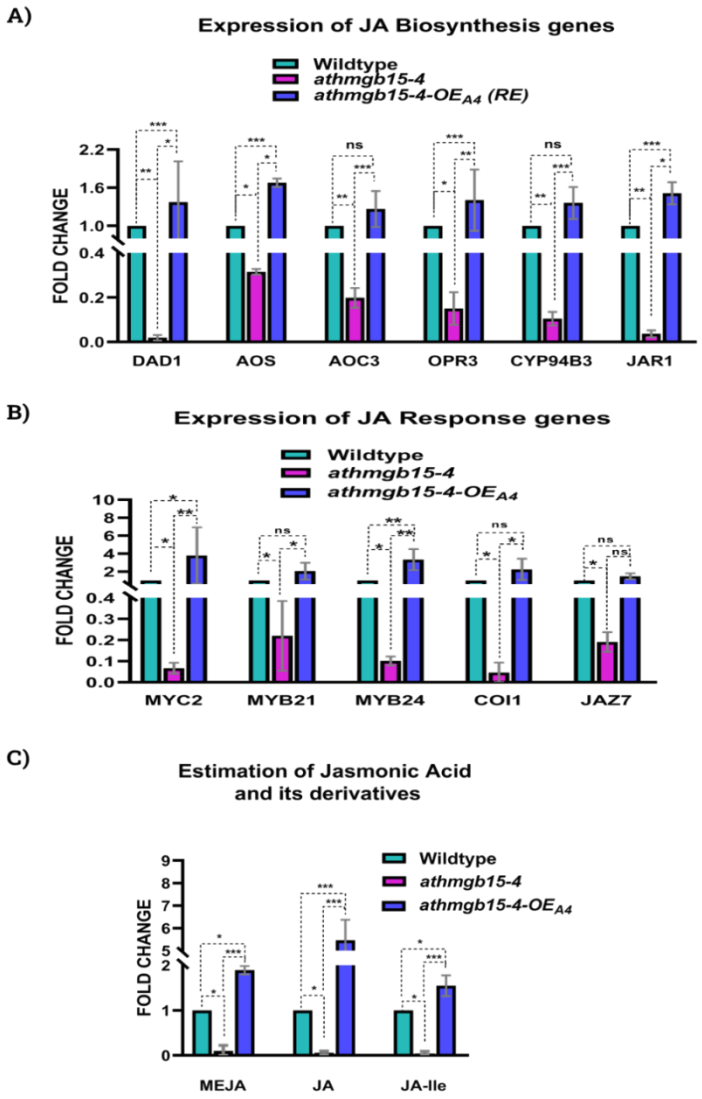

*Figure Ch1_30: Expression of A) JA biosynthesis and B) signaling genes in wild-type, athmgb15-4, and athmgb15-4-OE$_{A4}$ flowers. The fold change for each gene is presented relative to the wild type, with error bars indicating the mean ± SD (n=8). Statistical significance for each gene was evaluated using one-way ANOVA followed by Tukey's post hoc test. Asterisks denote significant differences as follows: *P<0.05, **P<0.01, ***P<0.001, with "ns" indicating no significant difference. C) Jasmonic acid (JA) and its derivatives were quantified from the wild type flowers, athmgb15-4, and athmgb15-4-OE$_{A4}$ lines, with the results expressed as fold change relative to the wild type. The data are presented as mean ± SD (n=3), with error bars indicating variability. Statistical significance was assessed using one-way ANOVA followed by Fisher's LSD post hoc test, where asterisks denote significant differences (*P<0.05, ***P<0.001). The compounds measured include JA (jasmonic acid), MeJA (methyl jasmonate), and JA-Ile (jasmonic acid isoleucine).*

Discussion

Optimal pollen development and fully functional floral organs are essential for successful pollination and maintaining genetic diversity. These intricate processes are tightly controlled by endogenous signals. In this study, we investigated the role of the Arabidopsis ARID/HMG group transcriptional regulator, AtHMGB15, in pollen development. A previous study by Xia et al. (2014), utilizing a Ds insertion line, along with our research employing a different T-DNA mutant allele of *AtHMGB15*, both demonstrated similar defects in pollen morphology and delayed pollen growth in mutant plants. These allelic mutants of *athmgb15* exhibit a marked reduction in seed set, further highlighting the critical role of AtHMGB15 in pollen viability.

Given the observed defects in pollen morphology and viability in the absence of functional AtHMGB15, we aimed to investigate its role in pollen formation and maturation throughout Arabidopsis floral development. Pollen development initiates following the meiosis of sporogenous cells at stage 10 of flower development and progresses through stages 12 to 13, culminating in the formation of the pollen cell wall (Sanders et al., 1999). This developmental process is followed by filament elongation and anther dehiscence, which facilitates the release of mature pollen grains capable of germination (Goldberg et al., 1993; Scott et al., 2004). In our study, we focused on comparing the gene expression profiles of wild-type and *athmgb15-4* mutant flowers during the early stages of floral development. This comparison was aimed at identifying AtHMGB15-regulated genes crucial for pollen development, to further understand its regulatory role in this process.

Our findings indicated a significant downregulation of genes involved in the formation of the pollen cell wall in the *athmgb15* mutant. Specifically, the reduced expression of key genes associated with cell wall biosynthesis and modification is likely responsible for the abnormal morphology and altered structural integrity of the pollen grains observed in these mutants. The disruption of normal cell wall formation appears to impair the mechanical properties and proper development of the pollen, leading to its defective morphology. Therefore, it can be concluded that the insertion of the AtHMGB15 mutation leads to defective pollen morphology, highlighting the essential role of AtHMGB15 in regulating pollen cell wall formation and ensuring proper pollen development.

A significant finding of the study was the differential expression of genes involved in α-linolenic acid metabolism and JA response pathways. α-linolenic acid is recognized as a precursor for the synthesis of the plant phytohormone jasmonic acid (JA). It was observed through RT-qPCR

analysis that genes responsible for JA biosynthesis and signaling were markedly downregulated in the flowers of the *athmgb15-4* mutant. This downregulation resulted in a substantial decrease in jasmonate levels within the *athmgb15-4* mutant plants.

Interestingly, the impaired JA signaling and abnormal pollen morphology observed in *athmgb15-4* were completely restored through the exogenous application of methyl jasmonate. These results indicate that the defects in pollen development are a direct result of the downregulation of JA biosynthesis, highlighting the pivotal role of AtHMGB15 in this pathway.

revious research has firmly established jasmonic acid (JA) as a critical phytohormone involved in multiple stages of flower development. JA plays an essential role in regulating various processes, including anther development, stamen elongation, anther dehiscence, flower opening, and pollen maturation (McConn and Browse 1996; Ishiguro et al. 2001; Mandaokar et al. 2006; Mandaokar and Browse 2009; Qi et al. 2015; Huang et al. 2017a, 2017b; Huang et al. 2020). Moreover, studies have shown that mutants impaired in JA biosynthesis or signaling pathways exhibit significant fertility defects, including reduced seed set or complete male sterility (Feys et al. 1994; Xie et al. 1998; Ishiguro et al. 2001; Park et al. 2002; Cheng et al. 2009). These findings highlight the indispensable role of JA in flower and pollen development, with its absence leading to severe reproductive failures.

Collectively, the low jasmonate levels observed in *athmgb15-4* plants underline the essential role of AtHMGB15 in regulating the JA pathway, which is critical for the development of viable pollen grains in Arabidopsis. This regulation ensures the proper expression of JA-responsive genes during pollen development, thereby maintaining hormonal balance and supporting reproductive success. The findings from this study not only enhance the understanding of the role of JA in plant fertility but also highlight AtHMGB15 as a key regulator in maintaining the hormonal pathways necessary for robust pollen development.

This chapter establishes that AtHMGB15 is a critical regulator of pollen development in Arabidopsis, functioning through the JA signaling pathway. The complementation of the *athmgb15-4* mutant with a *35S::AtHMGB15* construct successfully restored both the morphological and functional aspects of pollen, as well as the expression of JA-related genes. The recovery of normal pollen tube germination rates and pollen morphology in these complementation lines, along with the restoration of delayed bolting and silique size, strongly indicates that the defects observed in the *athmgb15-4* mutant are directly related to disruptions in the JA pathway. Furthermore, the overexpression of JA signaling genes in the

complementation lines, even beyond wild-type levels, suggests that AtHMGB15 not only supports JA biosynthesis but also enhances JA signaling during critical stages of pollen development.

In conclusion, our study provides compelling evidence that AtHMGB15 is a pivotal regulator of the JA pathway, ensuring proper pollen development and fertility in Arabidopsis. The ability of AtHMGB15 to modulate both the biosynthesis and signaling of the JA pathway encouraged us to explore the potential interactor(s) of AtHMGB15 that are involved in regulating pollen development via the JA pathway.

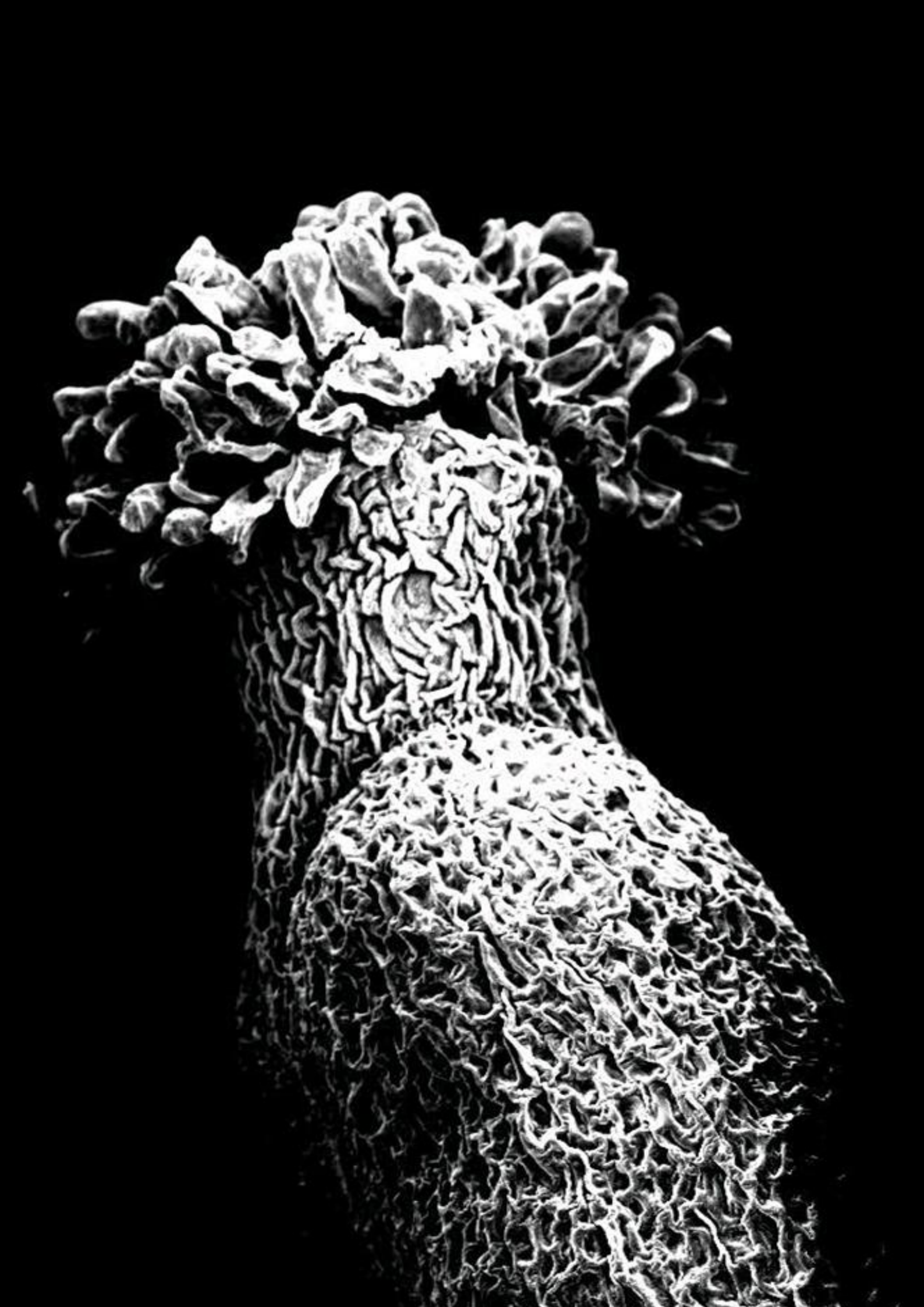

Chapter Two

Investigating key interactors of AtHMGB15, responsible for mutant phenotypes, elucidating its functional network.

Material and Method

Chromatin Immunoprecipitation (ChIP)

According to the manufacturer's instructions, the nuclei were isolated from crosslinked tissue (control and cold-stressed) using the Plant Nuclei Isolation Kit (Sigma, #CELLYTPN 1) as described previously by (Mallik et al., 2020).

The following buffers were used throughout the experiment:

Solution Name	Composition
Nuclear Lysis Buffer	50 mM Tris-Cl (pH 8.0), 10 mM EDTA, 1% SDS, 1 mM PMSF
ChIP Dilution Buffer	16.7 mM Tris-Cl (pH 8.0), 1.2 mM EDTA, 167 mM NaCl, 1.1% Triton-X100
Low Salt Wash Buffer	150 mM NaCl, 0.1% SDS, 1% Triton-X100, 2 mM EDTA, 20 mM Tris-Cl (pH 8.0)
High Salt Wash Buffer	500 mM NaCl, 0.1% SDS, 1% Triton-X100, 2 mM EDTA, 20 mM Tris-Cl (pH 8.0)
LiCl Wash Buffer	0.25 M LiCl, 1% NP-40, 1% Sodium deoxycholate, 1 mM EDTA, 10 mM Tris-Cl (pH 8.0)
TE Buffer	1 mM EDTA, 10 mM Tris-Cl (pH 8.0)
Elution Buffer	1% SDS, 100 mM $NaHCO_3$
PMSF (Freshly added)	250mM

All subsequent steps were performed at 4-8°C using pre-cooled buffers and rotors.

Cell Lysis

Preparation of 1X Nuclear Isolation Buffer (NIB): 1X NIB was prepared from 4X NIB by diluting it with deionized water. Before the extraction procedure, 1 mM DTT was added to the 1X NIB.

Tissue homogenization: The flower tissue was ground into a fine powder using liquid nitrogen in an autoclaved mortar and pestle.

The powder was transferred into a new 15 mL Falcon tube containing 3 mL of 1X NIB with 1 mM DTT. The mixture was gently mixed without vortexing.

Filtration: The slurry was passed through an autoclaved 100-mesh filter. The filtrate was collected in a fresh 15 mL Falcon tube.

Centrifugation: The tube was centrifuged at 1260g for 10 minutes at 4°C. The supernatant was discarded by inverting the tube, and the pellet was resuspended in 500 µL of 1X NIBA (1X NIB + 1 mM DTT + 1 mM PMSF).

Cell Membrane Lysis: Triton X-100 was added to a final concentration of 0.3% for cell membrane lysis.

Isolation of Nuclei

Nuclei Preparation: The lysate from the previous step was gently layered on top of 800 µL of 1.5M sucrose in a 1.5 mL centrifuge tube.

Centrifugation: The tube was centrifuged at 12,000g for 10 minutes at 4°C. The upper green phase and sucrose cushion were discarded by inverting the tube without disturbing the nuclei pellet.

Washing: The pellet was washed twice with 750 µL of NIBA buffer and then resuspended in 300 µL of Nuclei Storage Buffer. The sample was kept on ice and resuspended carefully using a cut pipette tip.

Crosslinking

Formaldehyde Addition: 8.1 µL of 37% formaldehyde was added to 300 µL of the lysate and incubated on a rocker at room temperature for 15 minutes.

Quenching: 22.5 µL of 2M glycine was added to quench the excess formaldehyde, followed by rocking for 10 minutes.

Centrifugation: The tubes were centrifuged at 13,000 rpm for 5 minutes at 4°C. The supernatant was discarded, and the pellet was dissolved in 600 µL of freshly prepared Nuclear Lysis Buffer.

Sonication and DNA Shearing

Un-sonicated Sample: 50 µL of the suspension was set aside.

Sonication: The remaining suspension was sonicated at 40Hz with a 0.4 duty cycle for 7 cycles of 10-second pulses.

Post-Sonication: 50 µL of the sonicated cell lysate was taken.

Reverse Crosslinking: 10 µL of 5M NaCl was added to both the sonicated and unsonicated lysates, and the samples were boiled at 65°C for 15 minutes to reverse the crosslinks between DNA and proteins.

Phenol-Chloroform Extraction: 60 µL of phenol-chloroform isoamyl mix was added and gently mixed. The tubes were centrifuged at 13,000 rpm for 5 minutes at room temperature. The aqueous phase was collected, and 50% glycerol was added before running the samples on a 1.2% agarose gel.

Dilution of Nuclear Lysate

Centrifugation: The nuclear lysate after sonication was centrifuged at 13,000 rpm for 5 minutes at 4°C, and the supernatant was transferred to a fresh 2 mL tube.

Dilution: The nuclear lysate was diluted 4 times (final dilution of 1:4).

Aliquoting: The diluted lysate was divided into two Eppendorf tubes (1.5 mL), with 1/10th of the lysate labeled as "input" for immunoprecipitation.

Immunoprecipitation

10 µL of the AtHMGB15 antibody (4.6 mg/mL) was added to each tube (1 mL) and incubated at 4°C overnight.

Bead Addition

30 µL of Magna Beads was added to the nuclear lysate-antibody suspension and left on a cyclo-rotor for 3 hours at 4°C.

Washing of Magna Beads

Washing: The tubes were placed on a magnetic rack, and the supernatant was discarded. 1 mL of low salt wash buffer was added, followed by rotation for 5 minutes, and the supernatant was discarded.

Further Washes: High salt wash buffer, LiCl wash buffer, and two TE washes were performed sequentially.

Elution: After the final TE wash, 250 µL of pre-warmed elution buffer (65°C) was added to the beads, vortexed, and incubated for 15 minutes at 65°C.

The supernatant (IP) was collected, and the step was repeated twice.

The Input sample volume was adjusted to 500 µL using an elution buffer.

Reverse Crosslinking

20 µL of 5M NaCl was added to both the Input and IP tubes, and the tubes were incubated overnight in a 65°C water bath.

DNA Precipitation and Cleanup

Spin Down: The tubes were pulse-spuned to remove the solution from the lids.

Preparation of Enzyme Cocktail: EDTA, Tris-Cl, and proteinase K were added to each tube as per the following:

- 10 µL of 0.5 M EDTA (pH 8)
- 20 µL of 1 M Tris-Cl (pH 6.5)
- 2 µL of proteinase K

Incubation: The reaction was incubated at 45°C for 2-3 hours before proceeding to phenol-chloroform extraction.

Phenol-Chloroform Extraction: 550 µL of phenol-chloroform isoamyl mix was added and gently mixed. The tubes were centrifuged at 13,000 rpm for 15 minutes at room temperature.

Precipitation: The top aqueous layer was transferred to a fresh tube. 1/10th volume of 3M Na-acetate (pH 5.2), 3 volumes of 100% ethanol, and 3 µL of glycogen (20 mg/mL) were added to the solution. The tubes were stored at -20°C overnight.

DNA Solubilization

Centrifugation: The tubes were centrifuged at 13,000 rpm for 15 minutes at 4°C. The supernatant was discarded by decanting.

Ethanol Wash: The pellet was washed with 1 mL of 70% ethanol and centrifuged again at 13,000 rpm for 15 minutes at room temperature.

Air Drying and Dissolution: The DNA pellet was air-dried, dissolved in 30 µL of TE buffer, and stored at 4°C overnight before proceeding to qRT-PCR.

Presence of AtHMGB15 binding motif

ATHMGB15 binding motif A(A/C)--ATA---(A/T)(A/T) was confirmed in our lab in the study by *Malik et al 2020.* This motif was searched for in the 1kb upstream region of the JA pathway-related genes and primers were designed flanking those motifs. This search was also confirmed on the PlantPan 3.0 and followed by ChIP RT-qPCR.

Quantitative ChIP-RT-qPCR (qPCR)

ChIP-qPCR was conducted to validate the targets of interest. qPCR was performed using PowerUp SYBR Green PCR Master Mix (Applied Biosystems, #A25742) along with gene-specific primers in an Applied Biosystems 7500 FAST machine.

For the control dataset, immunoprecipitated (IP) DNA from the control samples was normalized to the input DNA, and the fold change was determined relative to a negative control region (with a p-value >0.05 and minimal normalized signal ratio) using the 2^-ΔΔCt method. Three independent replicates of samples were used for the qPCR analysis, with each sample containing at least 60 seedlings. Statistical significance was assessed using one-way ANOVA with Tukey's post hoc test (P<0.05). The primers used for ChIP analysis are listed in Annexure 1.

Electrophoretic Mobility Shift Assay (EMSA)

EMSA was performed using the protocol described previously (Roy, 2016, Mallik et al., 2020). The components required for EMSA are as follows:

Solution Name	Composition
EMSA Buffer	100mM Tris-Cl (pH 7.5), 50mM NaCl, 5mM $MgCl_2$, 1mM EDTA, 50% Glycerol, 1mM DTT
Native PAGE Gel	5%-7% Acrylamide, 0.5X TBE, 0.1% APS, 0.1% TEMED, 5% Glycerol (optional)
Acrylamide Gel Elution Buffer	0.5M Ammonium acetate, 10mM Magnesium acetate, 1mM EDTA (pH 8.0)

Generation of AtHMGB15 Target Loci DNA Substrates for EMSA

Primers for target genes of *MYC2, MYB21,* and *MYB24* having the AtHMGB15 binding motif in 1kb upstream region from genomic DNA (isolated using Plant DNAzol®) were used to PCR amplify the desired fragment. The amplified fragments were resolved on a native PAGE gel in 0.5X TBE buffer. The target DNA fragment was excised from the gel, chopped into small pieces, and soaked overnight in 2-3 volumes of acrylamide gel elution buffer on a rotating wheel. DNA was then purified via phenol: chloroform extraction followed by ethanol precipitation. The resulting DNA pellet was dissolved in 50µl of TE buffer, and its concentration was measured using a Nanodrop spectrophotometer.

End Labeling of DNA by Forward Reaction

In the forward reaction, T4 Polynucleotide Kinase (T4 PNK) transfers the γ-phosphate from P^{32}ATP to the 5′-hydroxyl group of the DNA molecule. The steps are as follows:

Labeling Components:

Component	Volume
25bp DNA (A/T or G/C rich)	5.0 µl
10X Reaction Buffer A	2.0 µl
γ P^{32}ATP (3000 Ci/mmol)	5.0 µl
T4 PNK (10U/µl, Fermentas)	1.0 µl
Nuclease-free H_2O	Up to 20 µl

Purification of End-Labeled DNA Fragments

- The labeled DNA fragments were purified using the QIAquick Nucleotide Removal Kit (QIAGEN) according to the manufacturer's instructions.
- Labeling and Binding Assay: The DNA fragments from AtHMGB15 target loci were end-labeled with γP^{32} ATP (3500 Ci/mmol) using T4 Polynucleotide Kinase (Thermo Scientific) and purified using QIAquick Nucleotide Removal Kit (QIAGEN) according to the manufacturer's instructions.
- The amount of radiolabel incorporated was quantified using a Beckman Coulter LS 6500 Liquid Scintillation Counter. For measurement, 1 µl of the sample was added to 3 ml of Scintillation Cocktail-O, and the radioactive count was recorded.
- Approximately 5 × 10^4 cpm of γP^{32} labeled DNA (~7 fmol) was mixed with varying concentrations of full-length AtHMGB15 protein (ranging from 0.6 µM to 9 µM) in the presence of 1X EMSA buffer. The DNA-protein mixture was incubated on ice for 1 hour and analyzed using 5% native PAGE in 0.5X TBE at 4°C.
- Before sample loading, the gel was pre-equilibrated by electrophoresis at 150V for an hour at 4°C. The gel was dried and analyzed by phosphoimaging in a phosphor imager typhoon Trio+ system.

Site-Directed Mutagenesis (SDM)

Site-directed mutagenesis was performed following the protocol (Roy, 2016).The procedure involves the following steps:

Isolation of DNA containing the insert of interest, used as the DNA template (pGEM T-easy vector harboring the AtHMGB15 binding motif in 1kb upstream region of *MYC2. MYB21* and *MYB24*).

Two synthetic partially overlapping primers, each containing the desired mutation, were used. These primers were complementary to opposite strands of the vector and extended using Pfu turbo during temperature cycling, generating a mutated plasmid containing the specific mutation.

The list of mismatch primers for is provided in Annexure_1. The reaction setup was as follows:

Reaction Components	Volume
Template DNA (50 ng/µl)	1.0 µl
10X Pfu Buffer	5.0 µl
Forward Primer (10 µM)	1.0 µl
Reverse Primer (10 µM)	1.0 µl
dNTPs (10 mM)	1.0 µl
Pfu Turbo (2.5 U/µl, Agilent)	1.0 µl
Nuclease-free H_2O	Up to 50 µl

PCR program for site-directed mutagenesis:

Steps	Temperature	Time	Cycles
Initial denaturation	95°C	1 min	1 cycle
Denaturation	95°C	50 sec	17 cycles
Annealing	56°C	50 sec	
Extension	68°C	1 min/kb	
Final Extension	68°C	1 hour	1 cycle
Hold	4°C	Indefinite	

Post-PCR, the products were treated with 1 µl of DpnI endonuclease (10 U/µl, Agilent) at 37°C for 1-2 hours to digest the parental (methylated and hemimethylated) DNA template, selectively leaving the mutation-containing plasmids intact.

The DpnI-treated PCR products (10 µl) were transformed into competent DH5α cells.

Positive mutant clones having mutated AtHMGB15 binding motifs were verified through sequencing and subject to EMSA as described previously.

Bimolecular Fluorescence Complementation (BiFC) Assay

- For the BiFC assay, the coding sequences (full-length) of *AtHMGB15* and *MYC2* were cloned using the Gateway cloning system (Invitrogen) into the binary vectors pSITE-cEYFP-N1 (CD3-1651) and pSITE-nEYFP-C1 (CD3-1648), respectively.
- These constructs allowed for the expression of fusion proteins with complementary fragments of YFP (yellow fluorescent protein) attached to each protein of interest.
- Agrobacterium strain EHA105, harboring the cloned vectors, was used for transient expression. As a control, empty vectors were also transformed into the same strain.
- The transformed Agrobacterium was infiltrated into onion epidermal cells, as previously described by(Roy et al., 2019).

Infiltration buffer composition:

Component	Stock	Working
MES-KOH (pH 5.6)	0.5 M	10mM
$MgCl_2$	1 M	10mM
Acetosynringone	500mM	100mM

Volume made in sterile H_2O.

- This method allows the expression of the proteins in plant cells and enables the study of protein-protein interactions *in vivo.*
- After infiltration, the onion epidermal peels were carefully excised, rinsed with 1× PBS, and incubated for 16 hours.
- After washing, the samples were mounted on microscope slides and observed for interaction using confocal microscopy (Stellaris 5, Leica).
- For fluorescence detection, a laser with an excitation wavelength of 488 nm was used, and the emitted fluorescence was captured in the 513 to 560 nm range.
- The gain was set at 86 with an intensity of 2%, ensuring optimal imaging conditions for the detection of YFP fluorescence, which indicates the interaction between AtHMGB15 and MYC2 in plant cells.

Coimmunoprecipitation assay

Co-immunoprecipitation was performed as previously described (Nie et al., 2021) with experimental modifications as follows:

Cloning and Transformation

- The full-length coding sequence of MYC2 was cloned into the pGWB618 vector, which contains a Myc tag for subsequent detection.
- Following successful cloning, the positive recombinant plasmid was transformed into Agrobacterium tumefaciens strain EHA105.

Bacterial Preparation for Leaf Infiltration

- The transformed *A. tumefaciens* cells were cultured, and the bacterial suspension was centrifuged to pellet the cells.
- The pelleted cells were resuspended in infiltration buffer, to a final optical density (OD_{600}) of 0.3.

Infiltration buffer composition:

Component	Stock	Working
MES-KOH (pH 5.6)	0.5 M	10mM
$MgCl_2$	1 M	10mM
Acetosynringone	500mM	100mM

Volume made in sterile H_2O.

- The bacterial suspension was incubated in the dark for 3 hours at room temperature before infiltration into plant leaves.

Plant Infiltration and Sample Collection

- The prepared A. tumefaciens suspension was infiltrated into the leaves of *athmgb15-4* control plants and *athmgb15-4-OEA4-FLAG* transgenic lines.
- After 48 hours of infiltration, the infected leaves were harvested and immediately frozen in liquid nitrogen for preservation.

Protein Extraction

- Total protein was extracted from the harvested leaves using 3 mL extraction buffer per gram of leaf tissue.

The composition is as follows:

Component	Final Concentration
Tris-HCl (pH 7.4)	50mM
EDTA	1 mM
NaCl	150 mM
Glycerol	5% (v/v)
Triton X-100	0.5% (v/v)
PMSF	1 mM
Protease Inhibitor Cocktail Tablets (Roche)	1X

- The leaf tissue was homogenized in the extraction buffer, and the homogenate was centrifuged at 20,000 g for 30 minutes to collect the supernatant.

Preclearing and Immunoprecipitation

- The collected supernatant was precleared with protein Aplus agarose beads (BB#-PA001PD) to reduce nonspecific protein interactions.
- Following pre-clearing, an input sample was collected from the extract for control purposes.
- Immunoprecipitation was then carried out by incubating the extract with Anti-Myc antibody (Abcam #9E10) overnight at 4°C.
- The antibody-protein complexes were pulled down using Magna ChIP Protein A+G Magnetic beads (Millipore #16-663) as described previously.

SDS-PAGE and Western Blotting

The composition of reagents required are listed below:

Name of Solution	Composition
30% Acrylamide Mix	Acrylamide 29.2% (w/v); N,N-Methylene Bis-acrylamide 0.8% (w/v). Filter sterilized and stored in the dark at 4°C. No autoclaving.
10% Resolving Gel (5 mL)	30% acrylamide mix – 1.6 mL, 1.5 M Tris-Cl (pH 8.8) – 1.3 mL, 10% SDS – 50 µL, 10% APS – 50 µL, TEMED – 2 µL. Volume made up with water to 5 mL.
5% Stacking Gel (2 mL)	30% acrylamide mix – 330 µL, 1.0 M Tris-Cl (pH 6.8) – 250 µL, 10% SDS – 50 µL, 10% APS – 50 µL, TEMED – 2 µL. Volume made up with water to 2 mL.
SDS-PAGE Running Buffer	Glycine – 14 g, Tris – 3 g, SDS – 1 g. Volume made up with water to 1000 mL.
4X SDS-PAGE Loading Buffer	50 mM Tris-HCl (pH 6.8), 2% SDS, 10% glycerol, 12.5 mM Na-EDTA, 0.02% Bromophenol Blue. 1% β-mercaptoethanol is added before use.
Destaining Solution	50% Methanol, 10% Glacial Acetic Acid.
Staining Solution	2% Coomassie Blue R 250 in destaining solution, filtered before use.

- The co-immunoprecipitated protein samples were extracted from the magnetic beads by boiling in 2× SDS sample buffer.
- The samples were then separated on a 10% (v/v) SDS-PAGE gel and transferred to a PVDF membrane.
- The co-immunoprecipitated proteins were detected using anti-FLAG M2 antibody (Sigma-Aldrich #F1804) and anti-Myc antibody (Abcam #9E10).
- Detection was performed using an Enhanced Chemiluminescence (ECL) substrate (Bio-Rad), and signals were visualized by chemiluminescence.

- Each co-immunoprecipitation experiment was repeated at least three times to ensure reproducibility and consistency of results.

Co-Immunoprecipitation in Arabidopsis Overexpressing MYC2-GFP

- In a parallel experiment, the leaves of *athmgb15-4-OEA4-FLAG* were infiltrated with Myc-MYC2 and the empty pGWB618 vector (control).
- The same procedure as described above was followed. However, in this case, the protein complex was pulled down using Anti-FLAG Affinity beads (Abcam #270704), and subsequent detection was carried out with both anti-Myc and anti-FLAG M2 antibodies.
- For co-immunoprecipitation in Arabidopsis plants, protein extracts were obtained from Arabidopsis thaliana lines overexpressing MYC2-GFP and Col-0 control plants.
- Protein extraction was performed as described previously, and immunoprecipitation was carried out using anti-GFP nanobody magnetic beads (Antibodies.com #A310039).
- The presence of AtHMGB15 was detected using a custom-made affinity-purified anti-AtHMGB15 antibody (Thermo Scientific).
- The MYC2-GFP fusion protein was detected with anti-GFP (Plant specific) antibody (Antibodies.com #A50024).
- Western blot analysis using preimmune sera served as an experimental control.
- Detection was performed using an Enhanced Chemiluminescence (ECL) substrate (Bio-Rad), and signals were visualized by chemiluminescence.
- Each co-immunoprecipitation experiment was repeated at least three times to ensure reproducibility and consistency of results.

Promoter assay

Agrobacterium-mediated transient assay and fluorometric GUS assay were performed as described previously (Bedi and Nag Chaudhuri, 2018).

- 2-kb promoter regions of *MYC2*, *MYB21*, and *MYB24* were cloned into the pKGWFS7 vector, containing GUS as the reporter gene, by Gateway cloning (Invitrogen).
- Similarly, the full-length coding sequence of *AtHMGB15* and *MYC2* was cloned in pMDC84 and pCambia1304, respectively.

- The Agrobacterium tumefaciens strain EHA105 harboring the vectors were grown overnight at 28°C in LB medium with rifampicin (50 µg/mL) and spectinomycin (100 µg/mL) / Kanamycin (100 µg/mL) depending on the vector resistance.
- The overnight cultures of the transformed Agrobacterium were centrifuged at 5000 rpm for 10 minutes at room temperature.
- The resulting pellet was washed twice with 5 mL of infiltration buffer and resuspended in 2 mL of the same buffer.

GUS Infiltration Buffer Composition is mentioned as follows:

Reagent	Stock concentration	Working concentration
MgCl2	1 M	10 mM
MES (pH 5.6)	1 M	10 mM
Acetosyringone	0.5 M	100 µM

Volume made up with Water

- The optical density (OD) was measured and adjusted to 0.8.
- The Agrobacterium tumefaciens strain EHA105, harboring *pMYC2, pMYB21, and pMYB24,* was cultured overnight. This was then mixed separately with different combinations of Agrobacterium strains containing *35S::AtHMGB15 and 35S::MYC2.*
- The co-infiltration mixtures were prepared in a 1:1 ratio and incubated at 28°C for 3 hours before infiltration into 6-week-old Nicotiana tabacum (tobacco) leaves.
- The tissue was harvested after 48 hours. The harvested tissue was homogenized using liquid nitrogen, and 500 µL of GUS extraction buffer was added.

GUS Extraction Buffer Composition:

Reagent	Working concentration	Stock concentration
$NaHPO_4$ (pH 7)	50 mM	1 M
β-mercaptoethanol	10 mM	14.4 M
Na_2EDTA	10 mM	0.5 M
Sarcosyl	0.1%	30%
Triton X-100	0.1%	10%

Volume made up of Water

- The suspension was centrifuged at 13,000 rpm for 15 minutes at 4°C.
- The supernatant was collected and kept on ice.
- To estimate the fluorescence from MU, 1 mM of GUS extraction buffer was added to 50 µL of the protein extract and incubated at 37°C for 60 minutes.

- The reaction was stopped by adding 100 µL of 0.2 M Na_2CO3.
- Fluorometric analysis: GUS activity was quantified using 1 mM 4-Methylumbelliferyl-β-D-glucuronide (MUG) substrate, and fluorescence was measured at 455 nm with an excitation wavelength of 365 nm, using a Thermo Scientific Varioskan Flash fluorimeter.
- Protein concentration measurement: The total protein content in leaf extracts was determined using the Bradford assay, with absorbance measured at 595 nm.
- GUS activity quantification: GUS activity was expressed as nanomoles of 4-Methylumbelliferone (4-MU) produced per milligram of protein. Data were collected from 15 biological replicates to ensure statistical robustness.

Preparation of Standard Curve

MU Standard Curve: A 100 mM MU (β-umbelliferone) stock was prepared by dissolving 17.62 mg of MU in 1 mL of DMSO, yielding a concentration of 100 nmol/µL (10^5 picomoles/µL). Two standard curves were prepared, one in the µM range and another in the nM range.

BSA Standard Curve: The BSA standard curve was prepared using the Bradford reagent, following the standard protocol.

Study of *myc2* mutants

SALK_083483 (*atmyc2-2*) and SALK_061267 (*atjin1-2*) were also procured for the study. As mentioned in the previous chapter, they were grown and subjected to phenotypic studies. The JA pathway expression and JA(s) content were analyzed as described in Chapter 1.

Routine Cloning

List of clones prepared for each of the study are listed in Annexure_2.

The cDNA or genomic DNA obtained was used for the amplification of sequences encoding full-length coding and promoter region respectively, using gene-specific primers listed in Annexures. The products were subsequently inserted into a cloning vector.

The following components were added for the PCR setup:

PCR Components	Volume
Template DNA (cDNA or genomic DNA)	2.0 µl
10X Standard Taq Reaction Buffer	3.0 µl

dNTPs (10 mM)	1.0 µl
Forward Primer (10 µM)	1.0 µl
Reverse Primer (10 µM)	1.0 µl
Taq DNA Polymerase (5 U/µl, Fermentas)	0.5 µl
Nuclease-free H_2O (up to)	30 µl

PCR Program:

PCR Steps	Temperature	Time	Cycles
Initial Denaturation	94°C	5 min	1
Denaturation	94°C	30 sec	30
Annealing	55°C	30 sec	
Extension	72°C	2 min	
Final Extension	72°C	10 min	1
Hold	4°C	∞	

Gel extraction of the DNA fragment of interest

The PCR amplicons and a molecular weight ladder (GeneRuler 1kb plus DNA ladder, Thermo Scientific) were run on a 1.8% agarose gel until the ladder was fully resolved. The gel was visualized under a UV transilluminator and the amplicons were excised from the gel using a sharp scalpel. The amplicons were extracted from the gel using a gel extraction kit (GeneJET Gel Extraction Kit, Thermo Scientific) according to the manufacturer's protocol.

Cloning the gene of interest into pGEM®-T Easy Vector to construct a recombinant plasmid

TA Cloning of the gene fragment obtained from PCR amplification
The gel-eluted fragments containing the coding region were ligated into the pGEM®-T Easy Vector (Promega).

Ligation Reaction Components	Volume
2X Rapid Ligation Buffer	5.0 µl
T4 DNA Ligase (3 Weiss Units/µl)	1.0 µl
pGEMR-T Easy Vector (50 ng)	1.0 µl
PCR product(s) (150 ng)	1.0 µl
Nuclease-free H_2O (up to)	10 µl

Transformation of the ligation product(s) into *Escherichia coli* DH5α

The ligation products were transformed into *E. coli* DH5α cells. Positive clones selected by restriction digestion and sequencing were subsequently transformed into an expression vector, for subsequent study.

For Luria-Bertani (LB) Medium Preparation (pH 7.5) the following ingredients were added to 800 ml of Millipore water, mixed, and sterilized by autoclaving:

Ingredient	Amount
Yeast extract	5 g
Tryptone (Casein hydrolysate)	10 g
NaCl	10 g
Adjust pH to 7.5 with 1N NaOH	
Make up to 1000 ml with H_2O	

For LB agar, 1.5% agar was added to the LB broth and autoclaved.

Preparation of Competent *E. coli* DH5α Cells

A colony of *E. coli* DH5α was grown overnight in 10 ml of LB medium at 37°C with shaking. A 1 ml aliquot of the overnight culture was inoculated into 300 ml of LB medium in a 1-liter flask and grown at 37°C with shaking until the OD600 reached 0.6 (~2-3 hours). The culture was cooled on ice for ~1 hour with occasional swirling. The cells were harvested by centrifugation at 5000 rpm for 15 minutes at 4°C, and the supernatant was discarded.

Solutions for Competent Bacterial Cell Preparation

- Solution I: 80 mM $MgCl_2$, 20 mM $CaCl_2$
- Solution II: 0.1 M $CaCl_2$, 15% Glycerol

The pellet was resuspended in 30 ml of ice-cold Solution I and gently vortexed. Cells were combined into two tubes and centrifuged as described in step d. After discarding the supernatant, the pellet was resuspended in 30 ml of ice-cold Solution II and incubated on ice for 20 minutes. The cell suspension was centrifuged again, and the supernatant was removed. The final pellet was resuspended in 3 ml of Solution II and aliquoted (100 µl per tube). The competent cells were snap-frozen in liquid nitrogen and stored at -80°C.

Transformation of Competent Cells with Ligated Product

Competent DH5α cells were thawed on ice, and 10 µl of the ligation mix was added. The mixture was incubated on ice for 30 minutes, followed by a 90-second heat shock at 42°C. The tubes were immediately placed on ice for 5 minutes, after which 1 ml of LB broth (without antibiotics) was added, and the cells were allowed to recover for 1 hour at 37°C with shaking. The cells were pelleted and spread on LB agar plates containing antibiotics. For blue-white selection, 4 µl of IPTG (1 M) and 20 µl of X-Gal (40 mg/ml) were added to each plate before spreading. The plates were incubated overnight at 37°C.

Selection of the transformed colonies

The positive colonies were further selected and confirmed by restriction digestion and DNA sequencing.

Isolation of Plasmid DNA from Transformed Cells via the Alkaline Lysis Method

Single, well-isolated white colonies were inoculated into 2 ml of LB broth containing necessary antibiotics. The cultures were incubated overnight at 37°C with shaking. After incubation, the cells were pelleted by centrifugation at 13,000 rpm for 2 minutes, and plasmid DNA was extracted using the alkaline lysis method, as outlined as follows. The solutions required are listed below:

Solution	Composition	Preparation & Storage
Solution I	50 mM glucose, 25 mM Tris-Cl (pH 8.0), 1 mM EDTA (pH 8.0)	Autoclaved and stored at 4°C. Before use, RNase A is added to a final concentration of 100 µg/ml.
Solution II	0.2 N NaOH, 1% (w/v) SDS	Freshly prepared and used at room temperature.
Solution III	3 M potassium acetate (pH adjusted to 5.5 with glacial acetic acid)	Autoclaved and stored at 4°C.

- The bacterial pellet was resuspended in 200 µl of Solution I containing RNase A. Lysis was carried out by adding 400 µl of Solution II, incubating at room temperature for 2-3 minutes, with gentle inversion of the tubes. Neutralization was achieved by adding 300 µl of Solution III, followed by incubation on ice for 15 minutes.
- The samples were centrifuged at 13,000 rpm for 10 minutes. The supernatant was carefully transferred to a new microcentrifuge tube, avoiding any white precipitate, and plasmid DNA was precipitated using 0.7 volumes (~630 µl) of isopropanol.
- The samples were centrifuged again at 13,000 rpm for 10 minutes, after which the DNA pellet was washed with 1 ml of 70% ethanol, air-dried, and resuspended in 20 µl of TE buffer.

- The isolated plasmid DNA was subjected to restriction enzyme digestion (double digestion) to cleave both the vector backbone and the DNA insert, allowing for separation and analysis via agarose gel electrophoresis. Successful ligations were indicated by the presence of bands corresponding to the released insert.
- A 20 µl reaction mixture was prepared for the restriction digestion of the plasmid DNA and incubated at 37°C for 3-4 hours. After incubation, 5 µl of 6X gel loading dye was added to each sample, which was then loaded onto an agarose gel for electrophoresis.

Restriction Digestion

Component	Volume
Plasmid DNA	5.0 µl
10X Reaction Buffer	2.0 µl
Restriction Enzyme 1 (10 U/µl)	0.5 µl
Restriction Enzyme 2 (10 U/µl)	0.5 µl
Nuclease-Free H_2O	Up to 20 µl

Sequencing of Plasmid DNA for Clone Confirmation

Positive clones identified through restriction digestion were further analyzed using DNA sequencing. Plasmid DNA was isolated according to the manufacturer's instructions, with the Miniprep plasmid isolation kit (Thermo Scientific). The isolated DNA was sequenced using the Big Dye Terminator Automated Sequencer (Applied Biosystems). A 10 µl reaction mixture for sequencing PCR was prepared as follows:

Sequencing Components

Component	Volume
Ready Reaction Mix	1.0 µl
5X Buffer	2.0 µl
Plasmid DNA (100-150 ng)	1.0 µl
Primer (M13F/M13R) (3 pmole)	1.0 µl
Nuclease-Free H_2O	Up to 10 µl

PCR Program

Step	Temperature	Time	Cycles

Initial Denaturation	96°C	2 mins	1
Denaturation	96°C	30 secs	25
Annealing	55°C	15 secs	
Extension	60°C	4 mins	
Hold	4°C		

Purification of Sequencing Products

- Add 10 µl of nuclease-free water to the PCR products to make a final volume of 20 µl. Transfer to 0.5 ml microcentrifuge tubes.
- Add 1 µl of 125 mM EDTA and 2 µl of 3M Na-Acetate (pH 5.2) to each sample and mix thoroughly.
- Add 50 µl of 100% ethanol and incubate in the dark at room temperature for 20 minutes.
- Centrifuge at 13,000 rpm for 30 minutes, then wash the pellet with 200 µl of 70% ethanol at 13,000 rpm for 5 minutes.
- Air dry the DNA pellet and dissolve in 12 µl of Hi-Di Formamide.
- Heat the samples at 95°C for 5 minutes, snap chill on ice for 5 minutes, and load 10 µl of each sample into the automated sequencer for sequencing.

The sequenced clones that were properly ligated were selected for further cloning procedures.

Gateway Cloning

Cloning the Gene of Interest into the Entry Vector pENTR/D-TOPO

The TOPO cloning method was used for the directional cloning of the gene of interest into the pENTR/D-TOPO vector, allowing entry into various vector systems within the Gateway System. The clone prepared are listed in *Annexure _2* and the process are outlined below:

Generation of Blunt-End PCR Product: The gene of interest was amplified using a thermostable, proofreading DNA polymerase. The PCR primers included a 4-base pair sequence (CACC) at the 5' end of the forward primer, enabling directional cloning and producing a blunt-ended PCR product.

PCR Components for 50 µl Reaction Volume:

Component	Volume
Template DNA (<200ng)	1.0 µl
2X PCR Buffer	25 µl
dNTPs (2 mM)	10 µl
Forward Primer (10pmol/µl)	1.5 µl
Reverse Primer (10pmol/µl)	1.5 µl
KODFx NEO DNA Polymerase (1.0U/µL) (Toyobo)	1.0 µl
Nuclease-free H_2O	Up to 50 µl

PCR Amplification: The gene of interest was amplified following a specific PCR program, and the resulting PCR products were run on an agarose gel.

Step	Temperature	Time	Cycles
Initial Denaturation	94°C	2 mins	1
Denaturation	98°C	10 secs	35
Annealing	55°C	30 secs	
Extension (1min/kbp)	68°C	2 mins	
Final Extension	68°C	7 mins	
Hold	4°C		

Gel Extraction: The amplified PCR products were gel-extracted using a Qiagen Gel Extraction Kit to purify the desired gene fragment for further cloning.

TOPO Cloning Reaction Using pENTR/D-TOPO Cloning Kit (Invitrogen)

The TOPO cloning reaction was performed as follows:

Reaction Components:

Component	Volume
PCR product (150ng)	0.5-2 µl
Salt solution	1 µl
TOPO vector (150ng)	1 µl
Nuclease-free H_2O	Up to 6 µl

- The reaction mix was gently mixed and incubated at room temperature for 5-30 minutes (PCR product: TOPO vector ratio of 0.5:1 to 2:1).
- The reaction mixture was then used to transform competent *E. coli* DH5α cells following the standard transformation protocol.
- Transformed cells were plated on LB agar plates supplemented with Kanamycin (50 µg/ml).
- Positive clones were checked by restriction digestion and sequencing before the LR clonase reaction.

Mlu I Digestion: After confirming the clones through restriction enzyme digestion and sequencing, the plasmid DNA was further subjected to Mlu I digestion. This step removes a portion of the vector containing the kanamycin resistance cassette (smaller fragment), allowing further selection of clones in the destination vector that also contains the kanamycin resistance cassette. Additionally, linearizing the entry clone enhances cloning efficiency by up to two-fold.

Mlu I Digestion Setup:

Restriction Digestion Components	Volume
Plasmid DNA (~5 µg)	5.0 µl
10X Reaction buffer	2.0 µl
Mlu I (10 U/µl) (Thermo Scientific)	0.5 µl
Nuclease-free H_2O	Up to 20 µl

After Mlu I digestion, the products were analyzed on a 1% agarose gel, and the larger DNA fragment containing the gene of interest was extracted using a gel extraction kit (Qiagen). The concentration of the eluted DNA was determined using a nanodrop spectrophotometer.

Cloning the Gene of Interest into Destination Vector

The LR reaction was performed to transfer the gene of interest from the Gateway entry clone pENTR/D-TOPO (Mlu I digested) into the destination vector using LR Clonase II.

LR Clonase Reaction Setup:

Reaction Components	Volume
Entry clone (50–150 ng)	1–7 µl
Destination vector (300 ng)	1 µl
LR Clonase II enzyme	2 µl

- The reaction mixture was thoroughly mixed and incubated at 25°C for 1 hour.
- The reaction was terminated by adding 1 µl of Proteinase K (10 mg/ml) and incubating at 37°C for 10 minutes.
- 6 µl of the LR Clonase reaction mixture was used to transform *E. coli* DH5α cells following the standard transformation protocol.
- Both restriction digestion and sequencing confirmed positive clones.

Observation and Inference

Presence of AtHMGB15 binding motif

In the previous chapter, we compared the DEGs of flower tissue to the AtHMGB15 control binding in seedling tissue and found the presence of AtHMGB15 binding in over 1100 genes. We analyzed the 3kb upstream region of the JA biosynthesis and response-related genes to look for the presence of ATHMGB15 binding motif *A(A/C)--ATA---(A/T)(A/T)* as deciphered by Malik *et al* in 2020 from our lab. We used PlantPan3.0 to conduct this search and found the presence of the binding motif within the 1kb promoter region of *AOS, LOX4 CYP94B3, ST2A, COI1, MYC2, MYB21* and *MYB24 (Figure Ch2_1A).* We designed primers to give an amplicon of about 200bp flaking the motif.

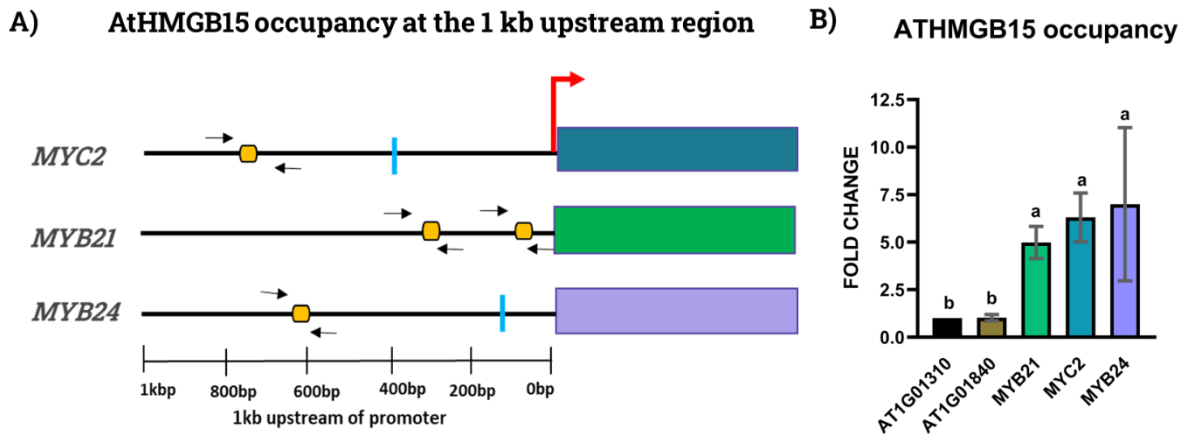

Figure Ch2_1: A) AtHMGB15 binding motif was present at 1kb upstream promoter region of MYC2, MYB21, and MYB24. B) ChIP analysis demonstrates AtHMGB15 occupancy at the promoter/upstream regions of MYC2, MYB21, and MYB24. The data were normalized against non-binding regions corresponding to At1g01310. Error bars represent the mean ± SD (n=5). Significant differences were identified using one-way ANOVA followed by Tukey's post hoc test (P<0.05), as indicated by different letters.

We took 1gm wildtype flower tissue and performed the ChIP assay with the custom-made affinity-purified native anti-AtHMGB15 antibody. ChIP-qPCR was carried out using the primers designed as mentioned in Annexure 1. At1G01840 and At1G01310 were used as negative controls as they did not possess an AtHMGB15 binding motif. As predicted the list of genes mentioned above did show an increase in fold change concluding the presence of AtHMGB15 binding motif *(Figure Ch2_1B).*

A literature study suggests that the basic-helix-loop-helix (BHLH) transcription factor *MYC2* is the master regulator of JA-signalling (Kazan and Manners, 2013). Also, *MYB21* and *MYB24,* the

R2R3-MYB transcription factors are considered the regulators of JA signaling during stamen development (Huang et al., 2017a, Huang et al., 2020, Yang et al., 2020). We were trying to narrow our search for the important players in the JA signaling cascade that influence the entire JA pathway and pollen development. For subsequent experiments, we proceeded with the analysis of *MYC2, MYB21* and *MYB24.*

Confirmation of AtHMGB15 DNA binding

The DNA binding assay was carried out to confirm the *in-vivo* binding of AtHMGB15 protein to the binding motif present in the 1kb upstream region of *MYC2, MYB21* and *MYB24.* AtHMGB15 protein was previously isolated and incubated with radiolabelled DNA fragments of *MYC2, MYB21* and *MYB24.*

Upon increasing the concentration of AtHMGB15 protein there was a significant shift in the DNA-protein complex when observed on a 5% native PAGE *(Figure Ch2_2)*.

The electrophoretic shift was absent when the protein was incubated with the fragment of At1G01310 (negative control) even at higher concentrations. This provided validation to our study, confirming the presence of an AtHMGB15 binding site on the gene of interest enables the DNA protein interaction.

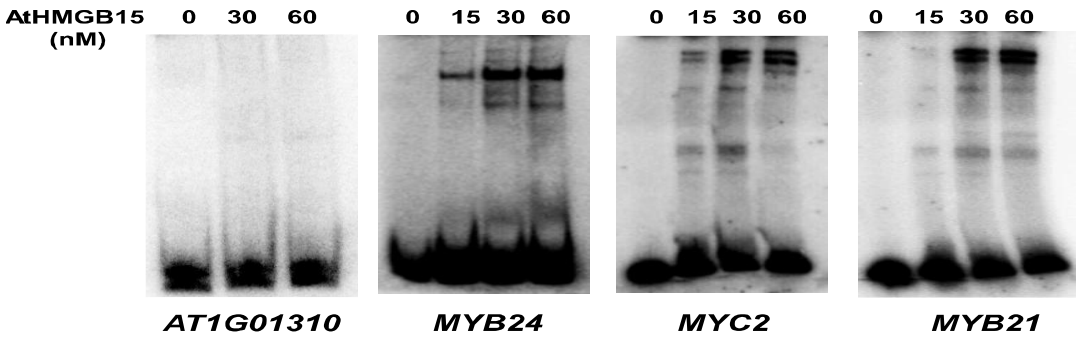

Figure Ch2_2: EMSA was conducted using 32P-labeled DNA fragments of At1g01310 (Negative control), MYB24, MYC2, and MYB21, with increasing concentrations of recombinant AtHMGB15 ranging from 15 to 60 nM.

To reconfirm this DNA-protein interaction we took the approach of introducing a site-direct mutagenesis at the AtHMGB15 binding motif as indicated in the subsequent figures *(Figure Ch2_3/4/5 A)*. Ideally, even a single bp mutation must affect the interaction lowering the ability of the protein to bind the DNA at the binding motif. These mutated fragments were radiolabelled

and incubated with increasing concentrations of AtHMGB15 protein. After incubation, they were run on a 5% native page and observed under the typhoon scanner. It was observed that there was no binding at lower concentrations of the protein *(Figure Ch2_3/4/5 C)*. DNA-protein interaction was visible only at higher concentrations of AtHMGB15. Therefore, there was a sharp decline in the binding pattern due to the introduction of the mutation in the AT-rich binding motif. This highlights the importance of each of the bases in the binding motif enabling proper DNA-Protein interaction *in vivo*.

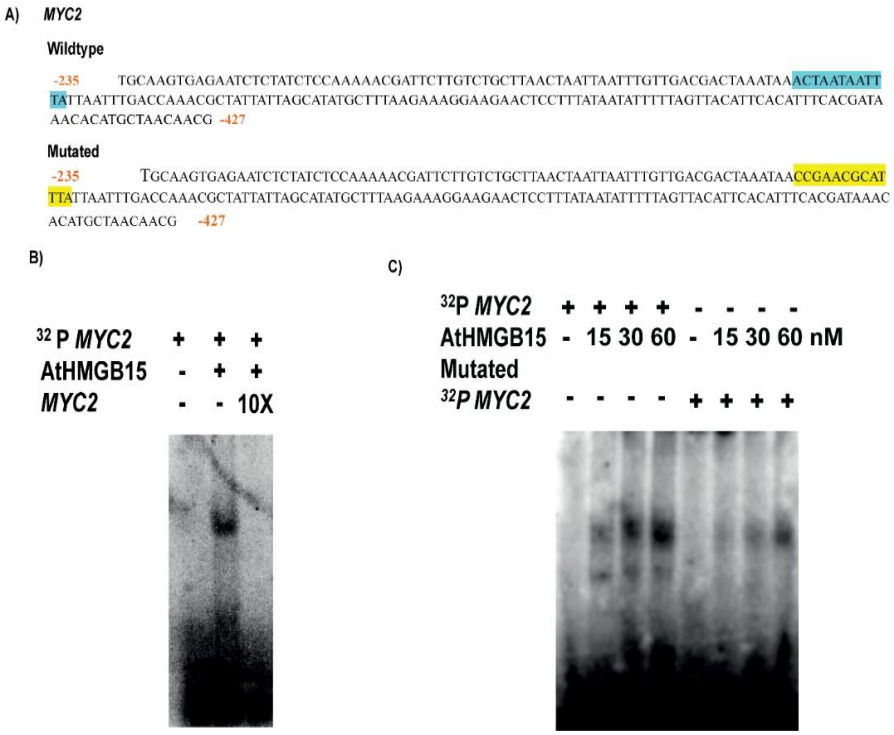

Figure Ch2_3: DNA Binding Analysis of MYC2 using Recombinant AtHMGB15 A) The AtHMGB15 binding site in MYC2 is highlighted in cyan, while the corresponding mutated motif is marked in yellow. B) For the DNA binding assay, 32P-labelled DNA fragments (~7 fmol) of MYC2 were incubated with 60 nM of AtHMGB15. Self-competition was performed using a 10X excess of unlabeled DNA fragments. C) Mutated AtHMGB15 binding motifs from ~150 bp MYC2 fragments were used in an EMSA assay. 32P-labelled DNA fragments (~7 fmol) were tested for binding in the presence of increasing concentrations of AtHMGB15 (0–60 nM).

AtHMGB15 activates the transcription of *MYC2*

The binding of AtHMGB15 to the promoter and upstream region of *MYC2* led us to explore its potential role in regulating *MYC2* transcription. To investigate this, approximately 2 kb of the *MYC2* promoter and upstream region was cloned into the pCambia1304 vector, replacing the 35S promoter, to create the *pMYC2::GUS* reporter construct. This construct was then introduced into *Nicotiana benthamiana* plants to assess the activity of the *MYC2* promoter (*pMYC2*) by measuring GUS activity, both in the absence and presence of AtHMGB15. Although *AtHMGB15* is not a transcription factor (TF), it can modulate transcription when interacting with a TF. Furthermore, prior research identified a *MYC2*-binding site within the promoter region of the *MYC2* gene (Zander et al., 2020).

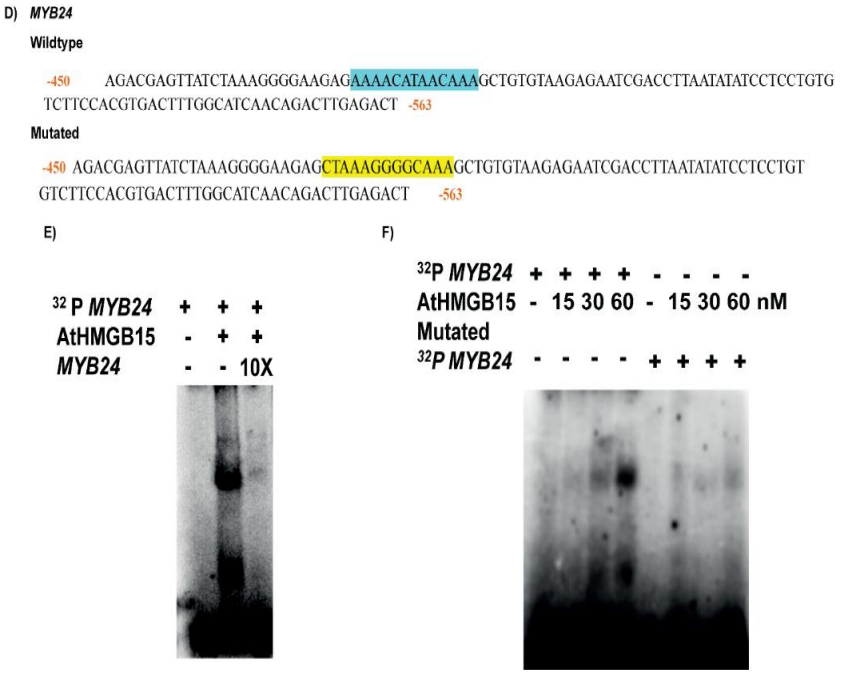

Figure Ch2_4: DNA Binding Analysis of MYB24 using Recombinant AtHMGB15. D) The AtHMGB15 binding site in MYB24 is highlighted in cyan, while the corresponding mutated motif is shown in yellow. E) 32P-labelled DNA fragments (~7 fmol) of MYB24 were used for DNA binding in the presence of 60 nM AtHMGB15. Self-competition was conducted with a 10X excess of unlabelled DNA fragments. F) The AtHMGB15 binding motifs in ~150 bp fragments of MYB24 were mutated and tested using an EMSA assay. 32P-labelled DNA fragments (~7 fmol) were incubated with increasing concentrations of AtHMGB15 (0–60 nM) to assess binding.

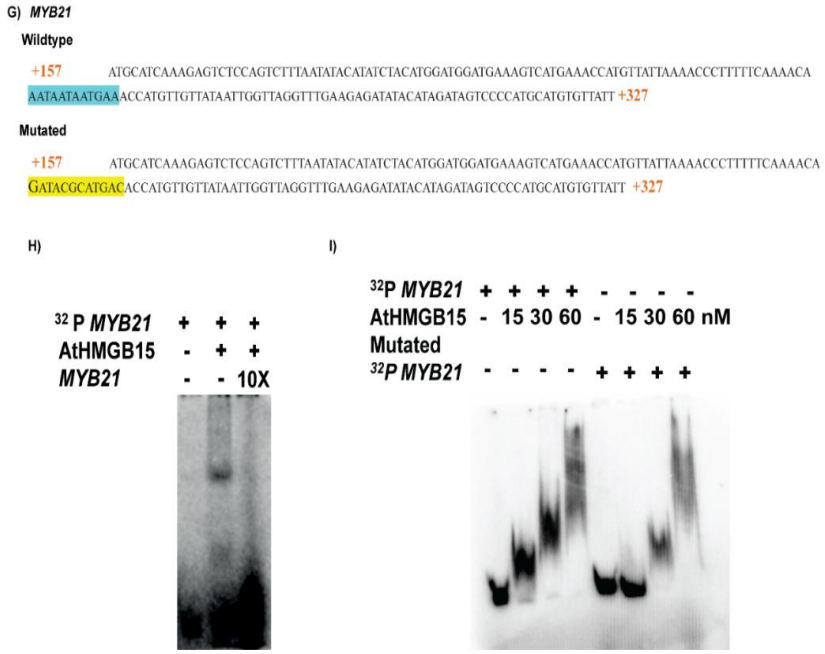

Figure Ch2_5: DNA Binding Analysis of MYB21 using Recombinant AtHMGB15. G) The AtHMGB15 binding site in MYB21 is highlighted in cyan, with the corresponding mutated motif shown in yellow. H) 32P-labelled DNA fragments (~7 fmol) of MYB21 were used for DNA binding in the presence of 60 nM AtHMGB15. Self-competition was carried out using a 10X excess of unlabelled DNA fragments.I) The AtHMGB15 binding motifs in ~150 bp fragments of MYB21 were mutated and tested using an EMSA assay. 32P-labelled DNA fragments (~7 fmol) were incubated with increasing concentrations of AtHMGB15 (0–60 nM) to evaluate binding.

Based on this, we hypothesized that AtHMGB15 functions as a coactivator in conjunction with the MYC2 transcription factor to regulate *MYC2* transcription. To test this hypothesis, we measured *MYC2* promoter activity in the presence of both AtHMGB15 and MYC2 proteins.

As depicted in *Figure Ch2_6A*, the promoter activity of *MYC2* increased in the presence of AtHMGB15 (*pMYC2* + AtHMGB15) compared to the control (*pMYC2* alone). Similarly, we observed an elevated promoter activity when MYC2 alone was present *(pMYC2* + MYC2), confirming earlier findings that MYC2 regulates its self-transcription. Notably, promoter activity was significantly

higher when both MYC2 and AtHMGB15 were present *(pMYC2* + MYC2 + AtHMGB15) compared to the activity observed with either protein alone. This substantial increase in promoter activity in the presence of both AtHMGB15 and MYC2 suggests that AtHMGB15 acts in concert with the MYC2 transcription factor to positively enhance the transcription of MYC2 *(Figure Ch2_6B)*.

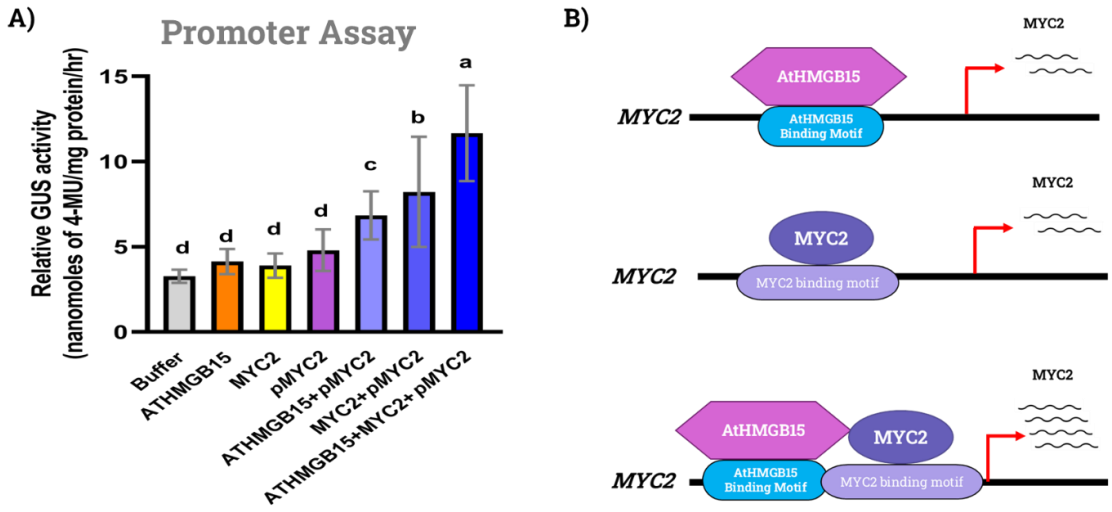

Figure Ch2_6: A) 2 kb promoter region of MYC2 (pMYC2) cloned into a GUS reporter construct, and Agrobacterium-mediated infiltration was performed in Nicotiana tabacum using 35S::AtHMGB15 and 35S::MYC2 constructs. After 48 hours, a GUS reporter gene assay was conducted using MUG as the substrate. Error bars represent the mean ± SD (n = 15). Significant differences between the datasets are indicated by different letters, as determined by a one-way ANOVA followed by Tukey's post hoc test (P < 0.05). B) Schematic showing the probable interaction of AtHMGB15 and MYC2 in enhancing the transcription of MYC2.

Interaction between Chromatin Remodellor AtHMGB15 and bHLH Transcription Factor MYC2

To gain deeper insights into the physical interaction between AtHMGB15 and MYC2, a Bimolecular Fluorescence Complementation (BiFC) assay was employed. This technique allowed for the visualization of protein-protein interactions in living, onion epidermal cells by reconstituting a functional fluorescent protein when two proteins of interest come into proximity. In this study, constructs encoding the N-terminal half of Yellow Fluorescent Protein (nYFP) fused to MYC2 and the C-terminal half of YFP (cYFP) fused to AtHMGB15 were generated. These constructs were introduced into *Agrobacterium tumefaciens* strains for subsequent co-infiltration into onion epidermal cells, which serve as a convenient and established model for transient expression studies in plant research.

Once infiltrated, the fusion proteins—MYC2-nYFP and AtHMGB15-cYFP—were expressed within the onion epidermal cells. If the two proteins physically interact, the two halves of YFP come together, restoring its fluorescence *(Figure Ch2_7)*. As anticipated, the BiFC assay revealed the

reconstitution of a Yellow Fluorescent Protein (YFP) signal, particularly in the nucleus and nucleolus. This indicates that AtHMGB15 and MYC2 form a complex within these subcellular compartments, highlighting their potential role in nuclear processes, such as transcriptional regulation.

The specific localization of the YFP signal to the nucleolus is particularly intriguing, as the nucleolus is often associated with ribosomal biogenesis but is also increasingly recognized for its involvement in broader cellular functions, including stress responses and the regulation of gene expression.

Importantly, no YFP fluorescence was observed in the control samples, which were infiltrated with constructs that did not enable interaction between MYC2 and AtHMGB15. The absence of fluorescence in these control treatments provides strong evidence that the interaction between MYC2 and AtHMGB15 is specific and necessary for YFP reconstitution. This specificity further validates the physical interaction between the two proteins in planta, suggesting their collaborative role in regulating downstream transcriptional processes.

To further validate the interaction between AtHMGB15 and MYC2, we conducted a transient co-immunoprecipitation (co-IP) assay. This involved using Arabidopsis plants that were engineered to overexpress AtHMGB15-Flag, in the *athmgb15-4* mutant background. The purpose of these plants was to provide a source of AtHMGB15-Flag for interaction studies.

We then infiltrated these transgenic plants with Agrobacterium carrying a construct for Myc-tagged MYC2. In parallel, we used *athmgb15-4* mutant plants, which do not express AtHMGB15-Flag, as controls to assess the specificity of the interaction.

Following infiltration, we performed the co-IP assay to isolate the MYC2-Flag complex. This was achieved by using an anti-Myc antibody, which selectively binds to Myc-tagged MYC2, pulling it down from the cell extracts. To detect whether AtHMGB15-Flag was present in the immunoprecipitated complex, we used the anti-Flag antibody.

The results of the Western blot analysis revealed that Myc-tagged MYC2 was able to co-immunoprecipitate with AtHMGB15-Flag, demonstrating a physical interaction between these two proteins *(Figure Ch2_8)*. This finding supports the hypothesis that AtHMGB15 and MYC2 interact in planta, further confirming their role in transcriptional regulation.

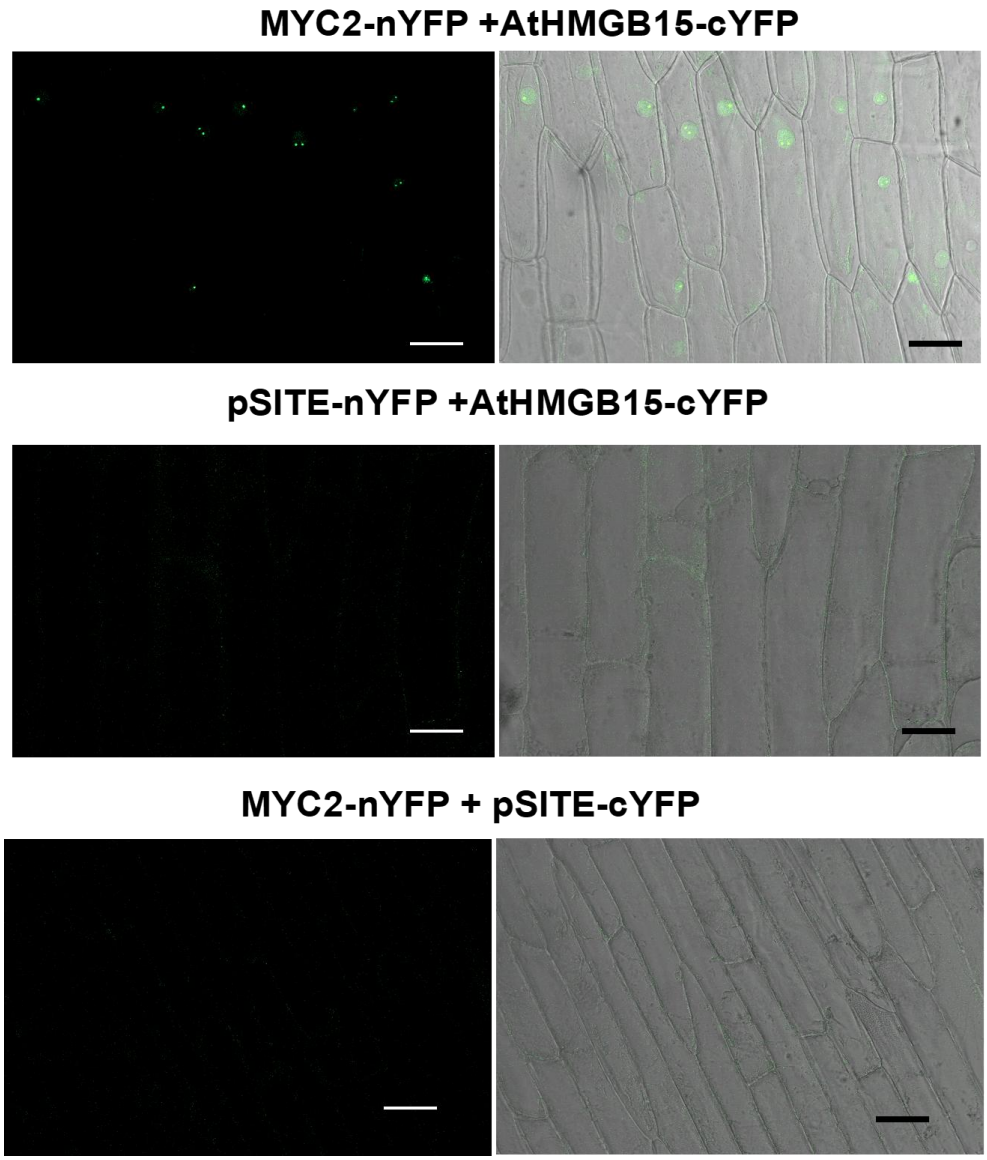

Figure Ch2_7: The Bimolecular Fluorescence Complementation (BiFC) assay was employed to confirm the interaction between AtHMGB15 and MYC2 in onion epidermal cells using split Yellow Fluorescent Protein (YFP). In this assay, AtHMGB15-cYFP was co-expressed with MYC2-nYFP. Control experiments were conducted with AtHMGB15-cYFP+pSITE-nYFP-C1 and MYC2-nYFP+pSITE-cYFP-N1. The scale bar in the images is 50 µm.

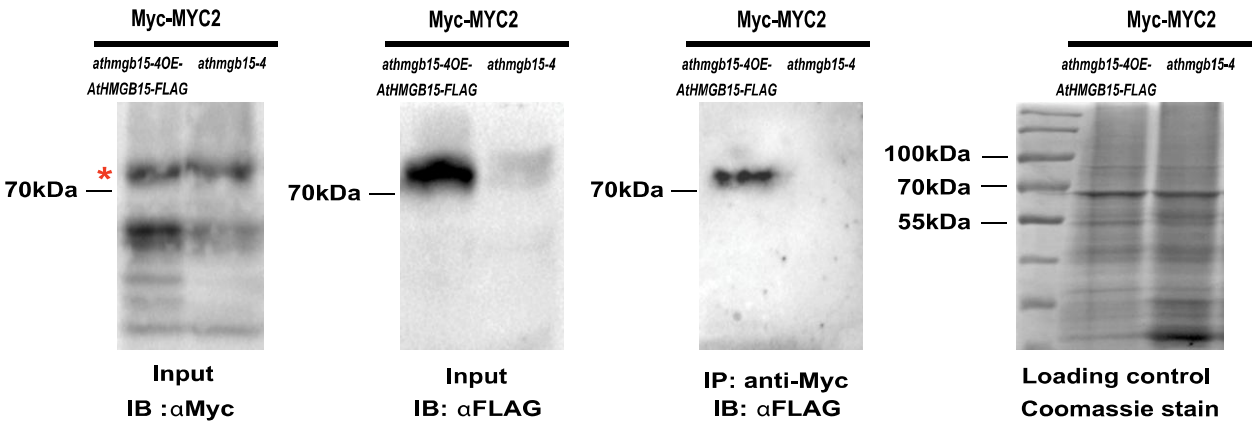

Figure Ch2_8: Transient co-immunoprecipitation (co-IP) assay was used to confirm the interaction between AtHMGB15 and MYC2. Protein extracts were prepared from the leaves of athmgb15-4OEA4-FLAG plants and athmgb15-4 plants transiently expressing Myc-MYC2. These extracts were subjected to immunoprecipitation using an anti-Myc antibody. The immunoprecipitated complexes were then analyzed by immunoblotting with anti-FLAG antibodies (IB: αFLAG) to detect AtHMGB15-Flag and anti-Myc antibodies (IB: αMyc) to detect Myc-MYC2. Extracts from athmgb15-4 plants

expressing only Myc-MYC2 served as a control. Coomassie blue staining for Rubisco was used to ensure equal protein loading across the lanes. band of interest marked by an asterisk (*).

Alternatively, we performed another transient co-immunoprecipitation (co-IP) assay using a different experimental setup. We first infiltrated Myc-tagged MYC2 (Myc-MYC2) into the leaves of Arabidopsis plants that overexpress AtHMGB15 with a C-terminal Flag tag (AtHMGB15-Flag). After infiltration, the leaf tissue was used for immunoprecipitation with anti-FLAG affinity beads, which specifically bind to the Flag-tagged protein (AtHMGB15-Flag). This allowed us to pull down the protein complex containing AtHMGB15-Flag and any associated proteins.To identify the interacting proteins within this complex, we used an anti-Myc antibody to detect the presence of Myc-tagged MYC2 *(Figure Ch2_9)*. For comparison, we also conducted a control experiment by infiltrating leaves of AtHMGB15-Flag plants with an empty vector (pGWB618), which served as a negative control. This control helped to ensure that any detected interactions were specifically due to the presence of Myc-MYC2 and not due to non-specific binding or background noise.

To conclusively verify the interaction between MYC2 and AtHMGB15 *in vivo*, a detailed co-immunoprecipitation (co-IP) assay was performed using transgenic Arabidopsis plants expressing MYC2-GFP. In this assay, proteins from these plants were extracted and subjected to immunoprecipitation using anti-GFP magnetic beads, which specifically pull down the MYC2-GFP fusion protein along with any interacting partners.

Following immunoprecipitation, the presence of AtHMGB15 in the precipitated complex was detected using a specific AtHMGB15 antibody, as outlined in *Mallik et al. (2020).* Arabidopsis Col-0 plants, which do not express the MYC2-GFP construct, were used as a control to ensure that any observed interaction was specific to the MYC2-GFP and AtHMGB15 complex.

The results from this experiment confirmed a positive interaction between MYC2 and AtHMGB15 *in vivo*, as evidenced by the presence of AtHMGB15 in the immunoprecipitated fraction from the MYC2-GFP expressing plants, but not in the control. This result strongly supports the conclusion that MYC2 and AtHMGB15 interact within the living plant cells *(Figure Ch2_10)*.

These experimental results provide strong evidence for a direct physical interaction between AtHMGB15 and the MYC2 protein. This interaction facilitates the formation of an activator complex that enhances the transcriptional activity of MYC2. Specifically, the data suggest that AtHMGB15 acts in conjunction with MYC2 to boost its ability to regulate gene expression. By forming this activator complex, AtHMGB15 effectively supports MYC2 in its role as a transcription factor, leading to increased transcriptional activation of genes under downstream control of MYC2.

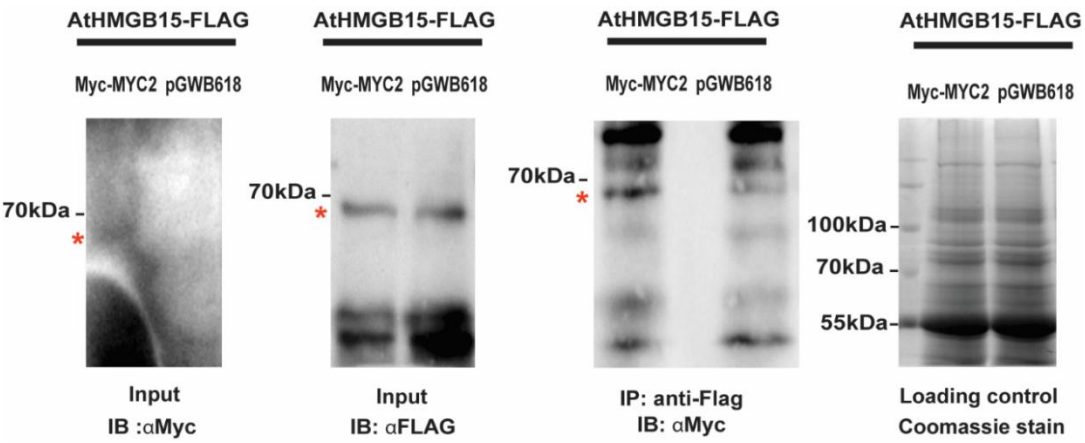

Figure Ch2_9: Total protein was extracted from leaves of athmgb15-4OEA4-FLAG plants transiently expressing Myc-MYC2 and from control plants infiltrated with empty pGWB618. The proteins were then subjected to immunoprecipitation using Anti-Flag affinity beads. Subsequent immunoblot analysis was performed with anti-Myc (IB: αMyc) and anti-Flag (IB: αFlag) antibodies. Coomassie blue staining for Rubisco was used to ensure uniform protein loading across the lanes, with the band of interest marked by an asterisk (*).

AtHMGB15-MYC2 Activation complex regulates the expression of *MYB21/MYB24*

Previous studies and experimental results suggest that MYC2 interacts with R2R3-MYB transcription factors, MYB21 and MYB24, which play crucial roles in regulating anther and pollen development in response to jasmonic acid (JA) (Goossens et al., 2017). Our RT-qPCR analysis conducted in in *athmgb15* mutants indicated that the expression levels of *MYB21* and *MYB24* are significantly reduced. Additionally, *in silico* analysis identified MYC2-binding sites in the promoter region of *MYB24*, suggesting a direct regulatory relationship.

Given that AtHMGB15 and MYC2 form a transcriptional activator complex, we hypothesized that this complex could influence the transcription of R2R3-MYB TFs. To test this, we examined *MYB21* and *MYB24* expression in flowers of two MYC2 knockout lines, *myc2-2* and *jin1-2*, which have been well-characterized previously (Boter et al., 2004; Lorenzo et al., 2004).

Our findings showed a marked downregulation of many JA pathway genes, especially in both *MYB21* and *MYB24* in these *myc2* mutant lines *(Figure Ch2_11A)*. Consistent with this, we observed a significant decrease in jasmonate levels in the *myc2* mutant lines, further confirming the role of MYC2 and the AtHMGB15-MYC2 complex in regulating JA-dependent gene expression *(Figure Ch2_11B)*. The *myc2* mutant line was subjected to pollen tube germination assay. We observed a similar low success of tube germination in the *myc2* mutants as well but they were not as severe as in the *athmgb15-4.* All the above results hinted at the role of the AtHMGB15-MYC2

activation complex in governing JA pathway and pollen development via the regulation of the MYBs *(Figure Ch2_11C)*.

We presumed that AtHMGB15 is a co-activator paired with the transcription factor MYC2 involved in the regulation of transcription of *MYB21* and *MYB24 (Figure Ch2_12A)*. To examine this hypothesis, we assessed the promoter activity of *MYC2* in the presence of both the proteins, MYC2 and AtHMGB15.

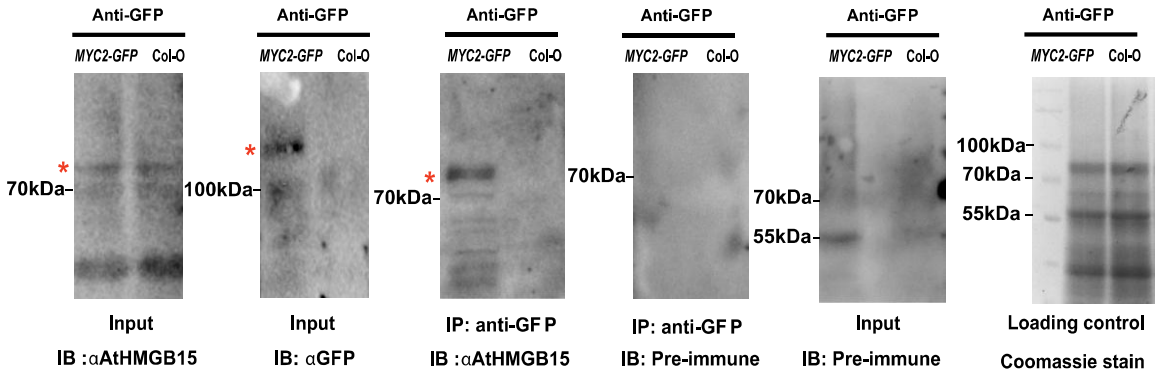

Figure Ch2_10: Co-immunoprecipitation (co-IP) assay was performed in planta to confirm the in vivo interaction between AtHMGB15 and MYC2. Total protein was extracted from MYC2-GFP seedlings and subjected to immunoprecipitation using anti-GFP magnetic beads. The immunoprecipitated complexes were then analyzed by immunoblotting with anti-AtHMGB15 (IB: αAtHMGB15) and anti-GFP (IB: αGFP) antibodies, as well as preimmune sera. Wild-type seedlings served as the control. Coomassie blue staining for Rubisco was used to verify equal protein loading across the lanes, with the band of interest marked by an asterisk (*).

To further investigate the regulatory role of AtHMGB15 and MYC2 in transcriptional activation, we analyzed the promoter activities of *MYB21* and *MYB24* in the presence of these transcription factors *(Figure Ch2_12B)*. The promoter activity of *pMYB24* was substantially enhanced by the independent presence of AtHMGB15 and MYC2, but no additional increase in activity was observed when both proteins were present together.

In contrast, for *pMYB21*, promoter activity was notably increased only when MYC2 was present. While AtHMGB15 showed strong DNA-binding affinity to the *MYB21* promoter region, it did not independently increase promoter activity. Interestingly, the combined presence of both AtHMGB15 and MYC2 led to a substantial increase in *pMYB21* activity, suggesting that these two proteins form an activation complex to regulate *MYB21* transcription *(Figure Ch2_12B)*.

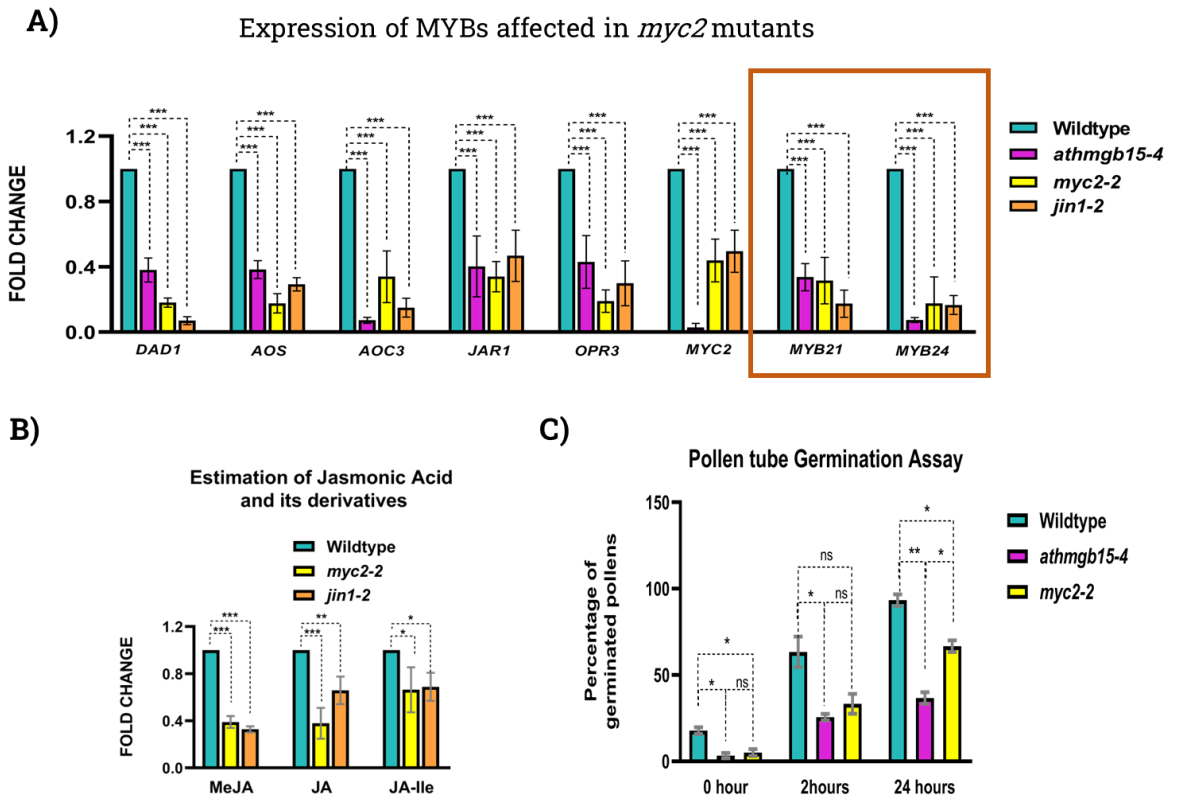

*Figure Ch2_11: A) RT-qPCR analysis of JA gene expression in MYC2 knockout mutants (myc2-2 and jin1-2) and athmgb15-4 mutants, with fold changes normalized to wild type. Error bars represent the mean ± SD (n=4). Statistical significance for each gene was determined using one-way ANOVA followed by Tukey's post hoc test. Significant differences are indicated by asterisks (***P<0.001). B) Comparative analysis of JA and its derivatives in the flowers of wild type and MYC2 knockout mutants (myc2-2 and jin1-2). Error bars represent the mean ± SD (n=3). Fold changes for each compound were normalized to wild type. Statistical significance was assessed using one-way ANOVA with Tukey's post hoc test, with asterisks indicating significance (*P<0.05, **P<0.01, ***P<0.001). C) Pollen germination assay showing time-dependent germination profile of wildtype, athmgb15-4 and myc2-2. Error bars represent mean±SD (n=3). The significance was analyzed by two-way ANOVA with Tukey's post hoc test. Asterisks represent significant differences as indicated (*P<0.01, **P<0.001, ***P<0.0001 and ns stands for not significant).*

These findings suggest that AtHMGB15 plays a critical role in regulating the transcription of R2R3-MYB TFs during flower development, particularly influencing the growth and development of stamens and pollen grains.

In conclusion, the AtHMGB15-MYC2 activator complex plays a pivotal role in regulating stamen development by modulating the transcription of key R2R3-MYB transcription factors, particularly MYB21 and MYB24. Through both independent and cooperative mechanisms, this complex ensures the precise expression of these MYBs, which are essential for the proper elongation of stamens and the development of pollen grains in a JA-dependent manner.

Our findings reveal that AtHMGB15, although not a transcription factor itself, enhances the transcriptional activity of *MYC2*, forming a functional complex that promotes stamen

development. This regulation is crucial for fertility, as defects in this pathway lead to shorter stamens and reduced seed yield, as observed in *athmgb15* mutants. Thus, AtHMGB15 is a critical co-regulator in the MYC2 signaling network, contributing to reproductive success in Arabidopsis through its impact on floral development.

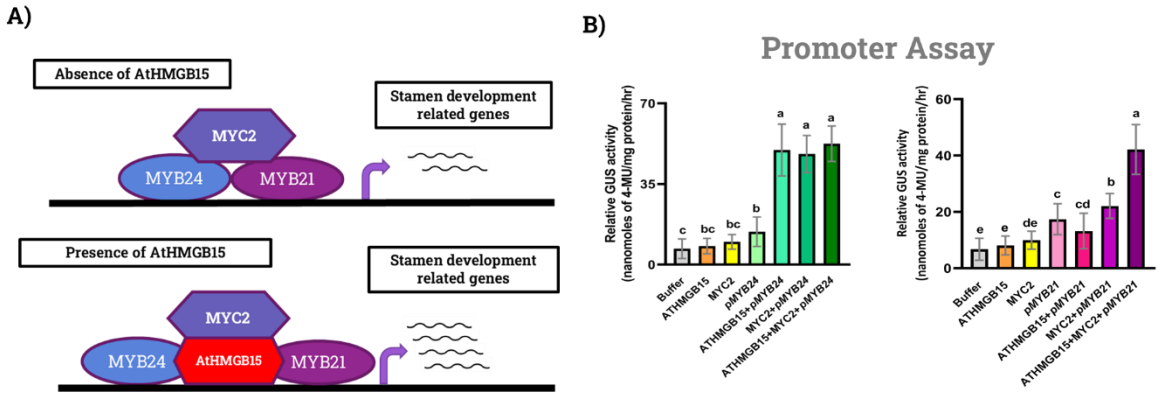

Figure Ch2_12: A) Schematic showing the probable interaction of AtHMGB15 and MYC2 in enhancing the transcription of MYB21/MYB24. B) The 2-kb promoter regions of MYB21 (pMYB21) and MYB24 (pMYB24) were cloned into a GUS reporter construct, and Agrobacterium-mediated infiltration was performed with 35S::AtHMGB15 and 35S::MYC2 in Nicotiana tabacum. GUS reporter assays were conducted 48 hours post-infiltration using MUG as the substrate. Error bars represent the mean ± SD (n=15). Statistical differences between datasets were analyzed by one-way ANOVA followed by Tukey's post hoc test, with significance indicated by letters (P<0.05).

Discussion

Repression of JA Biosynthesis and MYB Transcription in *athmgb15-4* Mutants

Our research highlights the vital role of AtHMGB15 in the regulation of JA-dependent transcription factors, particularly *MYB21* and *MYB24*, which are integral to stamen development. These R2R3-MYB transcription factors (TFs) play crucial roles in promoting male fertility in Arabidopsis by regulating anther dehiscence, filament elongation, and pollen viability. In the *athmgb15-4* mutant, we observed a significant downregulation of *MYB21* and *MYB24*, a result that mirrors findings from previous studies where disrupted JA biosynthesis led to decreased expression of these TFs (Yang et al., 2020, Huang et al., 2020, Huang et al., 2017a). Our analysis suggests that AtHMGB15 directly binds to the promoters of *MYB21* and *MYB24*, functioning as a transcriptional activator.

There are likely two mechanisms contributing to the repression of *MYB21* and *MYB24* in the *athmgb15-4* mutant. First, the disruption of JA biosynthesis in this mutant likely diminishes the transcription of these *MYBs*. Previous studies on *opr3* mutants, which are defective in JA biosynthesis, have demonstrated similar reductions in *MYB21* and *MYB24* expression (Song et al., 2011, Huang et al., 2020). Given that AtHMGB15 positively influences JA signaling pathways, its absence may disrupt upstream regulators like *MYC2*, further contributing to the downregulation of *MYB21 and MYB24*.

Second, the loss of functional *AtHMGB15* may directly impair the transcriptional activation of these *MYB* genes, as AtHMGB15 appears to be an essential cofactor for their expression. AtHMGB15 likely interacts with chromatin and enhances transcription factor binding, ensuring that these MYB TFs are properly expressed in JA-dependent pathways during flower development.

The dual impact of JA biosynthesis repression and the loss of AtHMGB15 function explains many of the developmental defects observed in the *athmgb15-4* mutant. The MYB21 and MYB24 TFs are indispensable for stamen development. In *myb21myb24* double mutants, phenotypes such as short filaments, delayed anther dehiscence, and nonviable pollen result in male sterility (Huang et al., 2020). These findings are consistent with the phenotypic abnormalities we observed in *athmgb15-4* flowers, where approximately 30% exhibited shorter stamen filaments compared to wild-type plants. The shorter filaments hinder proper pollination, as the anthers fail to reach the stigma, resulting in poor fertilization and reduced seed yield. This is a likely consequence of

defective stamen elongation, anther dehiscence, and reduced pollen viability, all of which are linked to diminished MYB21 and MYB24 activity.

Moreover, the role of AtHMGB15 in the MYC2 transcriptional network adds another layer of regulation, where AtHMGB15 may not only activate MYB21 and MYB24, but also modulate broader JA-responsive gene expression. This multifaceted role of AtHMGB15 emphasizes its critical position in coordinating the complex transcriptional networks required for JA signaling and successful stamen development.

Functional Interaction Between AtHMGB15 and MYC2 in JA Signaling

Our study provides new insights into the functional interaction between AtHMGB15 and the MYC2 transcription factor within the context of JA signaling. We demonstrate that AtHMGB15 and MYC2 form a transcriptional activator complex, amplifying MYC2-dependent gene expression. This interaction is particularly significant as AtHMGB15 directly binds to the promoter region of *MYC2*, promoting its transcription. This finding adds a new layer of complexity to *MYC2* regulation, as earlier studies indicated that MYC2 can bind to target genes without the canonical G-box motif, suggesting the need for partner proteins like AtHMGB15 to target non-canonical DNA sequences(Zander et al., 2020).

Our results strongly indicate that AtHMGB15 functions as an essential coactivator required for the full transcriptional activity of MYC2, especially during JA-dependent processes. AtHMGB15 facilitates the transcription of *MYB21 and MYB24*, two critical transcription factors for stamen development. These MYB transcription factors are vital for proper anther dehiscence and pollen viability, processes that are directly linked to male fertility in Arabidopsis. The AtHMGB15-MYC2 activator complex thus plays a crucial role in regulating JA-responsive genes, specifically those involved in reproductive development. This discovery reveals a previously unknown facet of JA signaling, underscoring AtHMGB15 as a key modulator of MYC2 function and transcriptional regulation.

Role of AtHMGB15 in Pollen Development and JA Signaling

Beyond its role as a transcriptional coactivator with MYC2, AtHMGB15 appears to have broader physiological functions in pollen development. Our study shows that AtHMGB15 contributes to the formation of the pollen cell wall by regulating genes involved in cell wall biogenesis. This

novel finding expands the known functional repertoire of AtHMGB15, traditionally classified as a nuclear architectural protein, to include a role in directly influencing transcriptional activation of key developmental pathways. The link between AtHMGB15 and pollen development reveals that this protein is not limited to chromatin remodeling but also actively participates in developmental regulation.

The formation of the AtHMGB15-MYC2 activator complex further underscores its involvement in JA signaling during pollen development. JA is known to regulate various aspects of reproductive development, including anther dehiscence, filament elongation, and pollen maturation. The role of AtHMGB15 in this context suggests that it serves as a key player in orchestrating these JA-dependent developmental processes. By enhancing MYC2 activity, AtHMGB15 indirectly supports the transcription of JA-responsive genes critical for stamen and pollen development.

Implications for Understanding ARID/HMG Nuclear Proteins in Plants

Our findings represent a significant step forward in understanding the diverse roles of ARID/HMG nuclear proteins in plants, particularly AtHMGB15. While these proteins have traditionally been viewed as nuclear architectural proteins involved in chromatin structure and DNA binding, our results highlight AtHMGB15 as a dynamic regulator of gene expression. AtHMGB15 not only influences chromatin accessibility but also acts as a transcriptional activator through its interactions with key transcription factors like MYC2.

The involvement of AtHMGB15 in JA-mediated transcriptional networks essential for flower development and fertility in Arabidopsis emphasizes its broader physiological roles beyond structural functions. These findings open new avenues for exploring the functions of HMG-box proteins in plants and offer potential insights into how these proteins influence other critical developmental and physiological processes through their interactions with transcriptional regulators.

In conclusion, AtHMGB15 is more than just a chromatin remodeler; it is an active participant in transcriptional regulation, particularly in the JA signaling pathway. Its partnership with MYC2 highlights its importance in the regulation of JA-responsive genes, making it a critical player in the broader transcriptional landscape of plant reproductive development. This study lays the groundwork for future research into the multifunctional roles of HMG-box proteins in plants, providing a deeper understanding of their regulatory mechanisms and their potential applications in crop improvement.

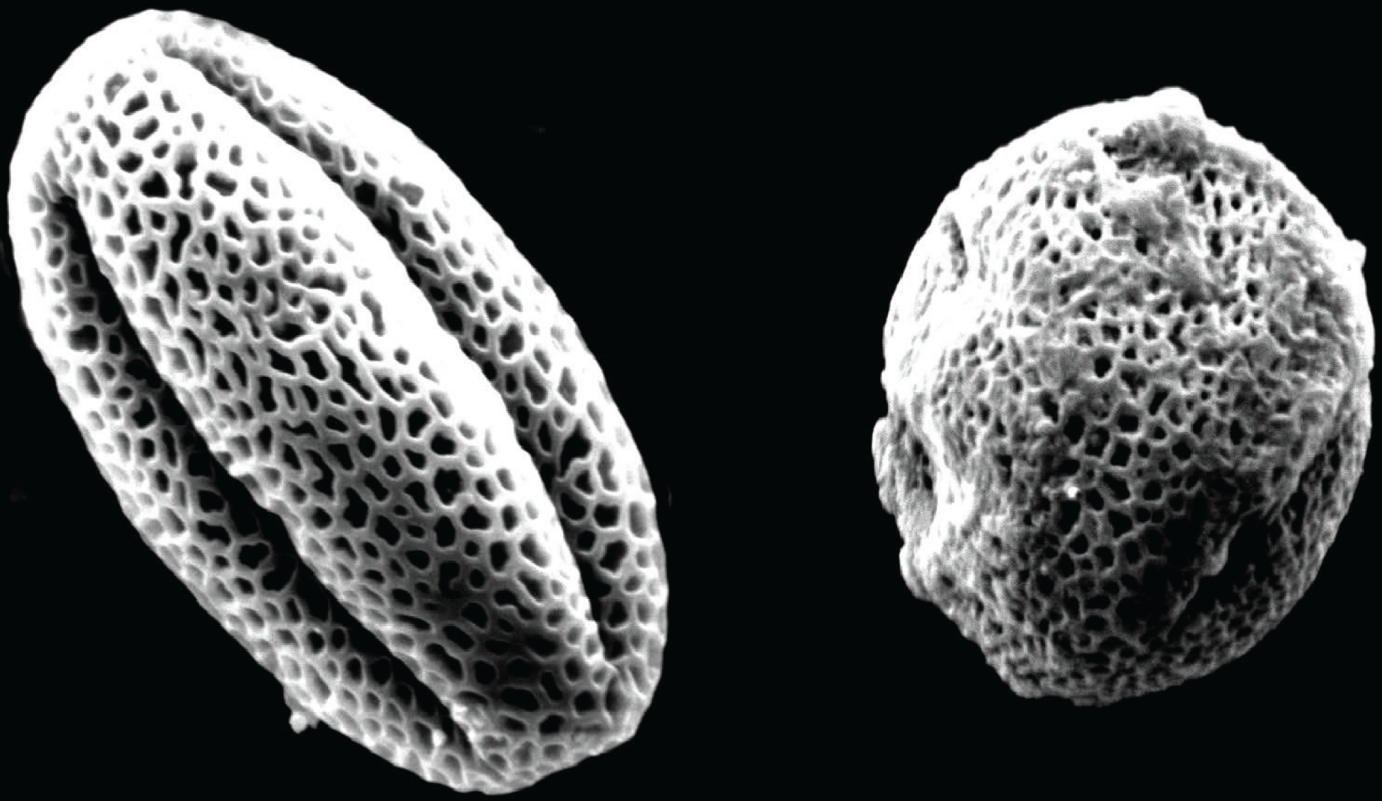

Summary

Our study provides significant insights into the role of the Arabidopsis AtHMGB15 protein in regulating pollen development and jasmonic acid signaling. AtHMGB15 is an ARID/HMG-box protein involved in transcriptional regulation and chromatin remodeling. By examining *athmgb15* insertion mutants, we have elucidated the impact of AtHMGB15 on pollen morphology, JA biosynthesis, and signaling pathways.

The research revealed that *athmgb15* mutants exhibit defective pollen morphology, characterized by distorted cell wall architecture and retarded pollen growth. These morphological defects lead to a significantly reduced seed set, highlighting the essential role of AtHMGB15 in pollen formation and maturation. Our differential gene expression analysis indicated that AtHMGB15 regulates key genes involved in pollen cell wall development. The downregulation of these genes in *athmgb15* mutants likely contributes to the defects in pollen morphology and viability (Xia et al., 2014).

A major finding of this study is that AtHMGB15 plays a crucial role in JA biosynthesis and signaling. JA, a critical phytohormone, regulates multiple aspects of flower development, including anther development, stamen elongation, and pollen maturation (McConn and Browse, 1996, Mandaokar et al., 2006, Ishiguro et al., 2001). Our data showed that athmgb15 mutants have reduced levels of jasmonates due to the downregulation of genes involved in JA biosynthesis and signaling pathways. The restoration of JA signaling and pollen morphology in *athmgb15* mutants upon complementation with full-length AtHMGB15 or exogenous application of jasmonate supports the notion that AtHMGB15 is integral to maintaining proper JA levels (Xie et al., 1998, Feys et al., 1994).

JA signaling involves complex feedback mechanisms that regulate hormone levels and gene expression (Zander et al., 2020, Wasternack et al., 2013). Positive feedback loops enhance JA biosynthesis, while negative feedback loops modulate the activity of key transcription factors (TFs) like MYC2 through repressors such as JAZ proteins (Chini et al., 2016, Chini et al., 2007). Our study demonstrated that AtHMGB15 directly interacts with MYC2 to form an activator complex that enhances MYC2-dependent gene expression. This interaction underscores the role of AtHMGB15 in positively regulating JA signaling by supporting MYC2's transcriptional activity (Kazan and Manners, 2013).

Our findings also revealed that AtHMGB15 influences the transcription of JA biosynthesis genes. We observed decreased expression of these genes and reduced jasmonate levels in athmgb15 mutants, which aligns with the established positive feedback loop where MYC2 activates the transcription of JA biosynthesis genes (Pozo et al., 2008, Dombrecht et al., 2007). The repression of genes responsible for JA derivatives further corroborates the role of AtHMGB15 in maintaining jasmonate concentrations. Specifically, the reduced expression of genes like DAD1 and CYP94B3 in athmgb15 mutants reflects the impact of AtHMGB15 on JA biosynthesis and catabolism (Ishiguro et al., 2001, Koo et al., 2011).

AtHMGB15 also regulates the expression of JA-responsive R2R3-MYB TFs, MYB21 and MYB24, which are crucial for stamen development (Yang et al., 2020, Huang et al., 2020, Huang et al., 2017a). The downregulation of these TFs in athmgb15 mutants, along with the observed short filaments and reduced seed yield, highlights the direct role of AtHMGB15 in activating MYB21 and MYB24 transcription. This regulation is essential for proper stamen growth and pollen viability, further linking AtHMGB15 to JA signaling and floral development (Huang et al., 2020).

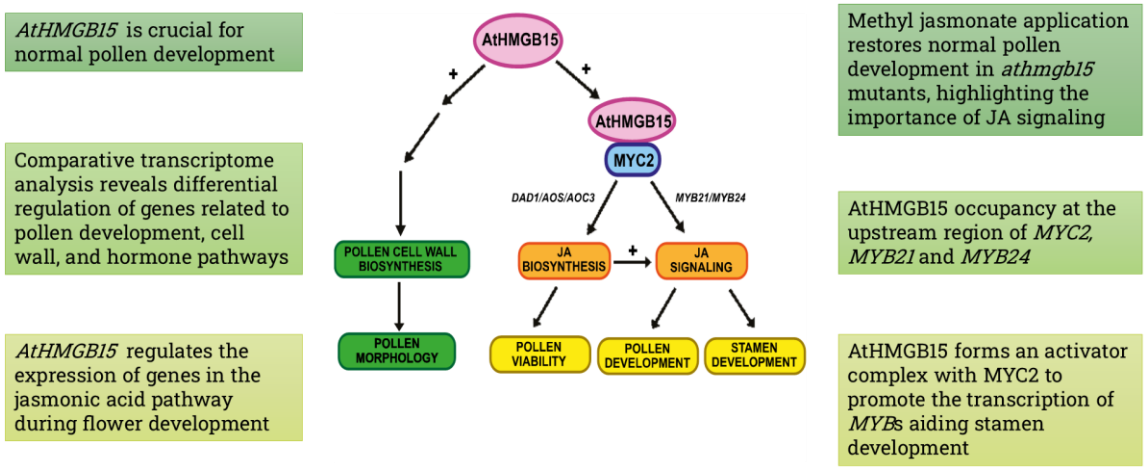

Figure S_1: Schematic concluding the salient features of the thesis and elucidating the role of AtHMGB15 in activating the JA pathways by forming an activation complex with MYC2 to regulate stamen and pollen development.

Our study provides new insights into the interaction between AtHMGB15 and MYC2. We established that AtHMGB15 forms a transcriptional activator complex with MYC2, enhancing its ability to regulate target genes involved in JA signaling. This interaction suggests that AtHMGB15 acts as a necessary coactivator for MYC2, enabling it to bind and activate genes crucial for pollen development (Zander et al., 2020).

Broader Implications and Future Directions

This research highlights the multifaceted role of AtHMGB15 in regulating both chromatin dynamics and gene expression during pollen development. AtHMGB15 is not only a nuclear architectural protein but also a dynamic regulator of transcriptional networks. The findings suggest that AtHMGB15 is essential for integrating JA signaling with transcriptional regulation, impacting pollen morphology, viability, and overall fertility.

Future research should explore the detailed mechanisms of AtHMGB15 interaction with other transcription factors and its role in different developmental stages and stress responses. Additionally, investigations into the broader physiological roles of ARID/HMG-box proteins could provide further insights into their functions in plant development and adaptation.

In summary, AtHMGB15 is a key player in pollen development and JA signaling, functioning through its interaction with MYC2 to regulate gene expression. The study underscores the importance of AtHMGB15 in maintaining jasmonate homeostasis and ensuring the proper development of viable pollen grains. This research advances our understanding of plant transcriptional regulation and offers potential avenues for improving crop fertility and stress resilience.

References

ADAMCZYK, B. J. & FERNANDEZ, D. E. 2009. MIKC* MADS domain heterodimers are required for pollen maturation and tube growth in Arabidopsis. *Plant physiology,* 149**,** 1713-1723.

AGRESTI, A. A. B., M.E. 2003. HMGB proteins and gene expression. *Current opinion in genetics & development,* 13(2), pp.170-178.

ALONI, R., ALONI, E., LANGHANS, M. & ULLRICH, C. I. 2006. Role of auxin in regulating Arabidopsis flower development. *Planta,* 223**,** 315-328.

ALVAREZ-BUYLLA, E. R., BENÍTEZ, M., CORVERA-POIRÉ, A., CADOR, Á. C., DE FOLTER, S., DE BUEN, A. G., GARAY-ARROYO, A., GARCÍA-PONCE, B., JAIMES-MIRANDA, F. & PÉREZ-RUIZ, R. V. 2010. Flower development. *The Arabidopsis Book/American Society of Plant Biologists,* 8.

ANGENENT, G. C., BUSSCHER, M., FRANKEN, J., MOL, J. & VAN TUNEN, A. J. 1992. Differential expression of two MADS box genes in wild-type and mutant petunia flowers. *The Plant Cell,* 4**,** 983-993.

ANTOSCH, M., MORTENSEN, S. A. & GRASSER, K. D. 2012. Plant proteins containing high mobility group box DNA-binding domains modulate different nuclear processes. *Plant physiology,* 159**,** 875-883.

AVANCI, N., LUCHE, D., GOLDMAN, G. H. & GOLDMAN, M. H. D. S. 2010. Jasmonates are phytohormones with multiple functions, including plant defense and reproduction. *Genet Mol Res,* 9**,** 484-505.

AYA, K., UEGUCHI-TANAKA, M., KONDO, M., HAMADA, K., YANO, K., NISHIMURA, M. & MATSUOKA, M. 2009. Gibberellin modulates anther development in rice via the transcriptional regulation of GAMYB. *The Plant Cell,* 21**,** 1453-1472.

BEDI, S. & NAG CHAUDHURI, R. 2018. Transcription factor ABI 3 auto-activates its own expression during dehydration stress response. *FEBS letters,* 592**,** 2594-2611.

BERGER, F. & TWELL, D. 2011. Germline specification and function in plants. *Annual review of plant biology,* 62**,** 461-484.

BIANCHI, M. E. & AGRESTI, A. 2005. HMG proteins: dynamic players in gene regulation and differentiation. *Current opinion in genetics & development,* 15**,** 496-506.

BORG, M. & BERGER, F. 2015. Chromatin remodelling during male gametophyte development. *The Plant Journal,* 83**,** 177-188.

BOWMAN, J. L., SMYTH, D. R. & MEYEROWITZ, E. M. 1989. Genes directing flower development in Arabidopsis. *The Plant Cell,* 1**,** 37-52.

BROOKS, J. & SHAW, G. 1968. Chemical structure of the exine of pollen walls and a new function for carotenoids in nature. *Nature,* 219**,** 532-533.

BROWSE, J. 2009. Jasmonate passes muster: a receptor and targets for the defense hormone. *Annual Review of Plant Biology,* 60**,** 183-205.

BUSTIN, M. 2001a. Chromatin unfolding and activation by HMGN* chromosomal proteins. . *Trends in biochemical sciences,* 26(7), pp.431-437.

BUSTIN, M. 2001b. Revised nomenclature for high mobility group (HMG) chromosomal proteins. *Trends in biochemical sciences* 26(3), pp.152-153.

BUSTIN, M. A. R., R. 1996. High-mobility-group chromosomal proteins: architectural components that facilitate chromatin function. . *Progress in nucleic acid research and molecular biology,* 54, pp.35-100b.

CALDELARI, D., WANG, G., FARMER, E. E. & DONG, X. 2011. Arabidopsis lox3 lox4 double mutants are male sterile and defective in global proliferative arrest. *Plant molecular biology,* 75**,** 25-33.

CATO, L., STOTT, K., WATSON, M. AND THOMAS, J.O. 2008. The interaction of HMGB1 and linker histones occurs through their acidic and basic tails. *Journal of molecular biology,* 384(5), pp.1262-1272.

CECCHETTI, V., ALTAMURA, M. M., FALASCA, G., COSTANTINO, P. & CARDARELLI, M. 2008. Auxin regulates Arabidopsis anther dehiscence, pollen maturation, and filament elongation. *The Plant Cell,* 20**,** 1760-1774.

CHANDLER, J. 2011. The hormonal regulation of flower development. *Journal of Plant Growth Regulation,* 30**,** 242-254.

CHEN, W., LV, M., WANG, Y., WANG, P.-A., CUI, Y., LI, M., WANG, R., GOU, X. & LI, J. 2019. BES1 is activated by EMS1-TPD1-SERK1/2-mediated signaling to control tapetum development in Arabidopsis thaliana. *Nature communications,* 10**,** 4164.

CHENG, H., QIN, L., LEE, S., FU, X., RICHARDS, D. E., CAO, D., LUO, D., HARBERD, N. P. & PENG, J. 2004. Gibberellin regulates Arabidopsis floral development via suppression of DELLA protein function.

CHENG, H., SONG, S., XIAO, L., SOO, H. M., CHENG, Z., XIE, D. & PENG, J. 2009. Gibberellin acts through jasmonate to control the expression of MYB21, MYB24, and MYB57 to promote stamen filament growth in Arabidopsis. *PLoS genetics,* 5**,** e1000440.

CHENG, P., GREYSON, R. & WALDEN, D. 1979. Comparison of anther development in genic male-sterile (ms 10) and in male-fertile corn (Zea mays) from light microscopy and scanning electron microscopy. *Canadian Journal of Botany,* 57**,** 578-596.

CHENG, Y., DAI, X. & ZHAO, Y. 2006. Auxin biosynthesis by the YUCCA flavin monooxygenases controls the formation of floral organs and vascular tissues in Arabidopsis. *Genes & development,* 20**,** 1790-1799.

CHHUN, T., AYA, K., ASANO, K., YAMAMOTO, E., MORINAKA, Y., WATANABE, M., KITANO, H., ASHIKARI, M., MATSUOKA, M. & UEGUCHI-TANAKA, M. 2007. Gibberellin regulates pollen viability and pollen tube growth in rice. *The Plant Cell,* 19**,** 3876-3888.

CHINI, A., FONSECA, S., FERNANDEZ, G., ADIE, B., CHICO, J. M., LORENZO, O., GARCÍA-CASADO, G., LÓPEZ-VIDRIERO, I., LOZANO, F. & PONCE, M. 2007. The JAZ family of repressors is the missing link in jasmonate signalling. *Nature,* 448**,** 666-671.

CHINI, A., GIMENEZ-IBANEZ, S., GOOSSENS, A. & SOLANO, R. 2016. Redundancy and specificity in jasmonate signalling. *Current opinion in plant biology,* 33**,** 147-156.

CHUANG, C.-F., RUNNING, M. P., WILLIAMS, R. W. & MEYEROWITZ, E. M. 1999. The PERIANTHIA gene encodes a bZIP protein involved in the determination of floral organ number in Arabidopsis thaliana. *Genes & development,* 13**,** 334-344.

CLARK, S. E., RUNNING, M. P. & MEYEROWITZ, E. M. 1993. CLAVATA1, a regulator of meristem and flower development in Arabidopsis. *Development,* 119**,** 397-418.

COEN, E. S. 1991. The role of homeotic genes in flower development and evolution. *Annual Review of Plant Biology,* 42**,** 241-279.

COEN, E. S. & MEYEROWITZ, E. M. 1991. The war of the whorls: genetic interactions controlling flower development. *Nature,* 353**,** 31-37.

DEVOTO, A., NIETO-ROSTRO, M., XIE, D., ELLIS, C., HARMSTON, R., PATRICK, E., DAVIS, J., SHERRATT, L., COLEMAN, M. & TURNER, J. G. 2002. COI1 links jasmonate signalling and fertility to the SCF ubiquitin–ligase complex in Arabidopsis. *The Plant Journal,* 32**,** 457-466.

DITTA, G., PINYOPICH, A., ROBLES, P., PELAZ, S. & YANOFSKY, M. F. 2004. The SEP4 gene of Arabidopsis thaliana functions in floral organ and meristem identity. *Current biology,* 14**,** 1935-1940.

DOMBRECHT, B., XUE, G. P., SPRAGUE, S. J., KIRKEGAARD, J. A., ROSS, J. J., REID, J. B., FITT, G. P., SEWELAM, N., SCHENK, P. M. & MANNERS, J. M. 2007. MYC2 differentially modulates diverse jasmonate-dependent functions in Arabidopsis. *The Plant Cell,* 19**,** 2225-2245.

DONG, X., HONG, Z., SIVARAMAKRISHNAN, M., MAHFOUZ, M. & VERMA, D. P. S. 2005. Callose synthase (CalS5) is required for exine formation during microgametogenesis and for pollen viability in Arabidopsis. *The Plant Journal,* 42**,** 315-328.

FARRONA, S., HURTADO, L., BOWMAN, J. L. & REYES, J. C. 2004. The Arabidopsis thaliana SNF2 homolog AtBRM controls shoot development and flowering.

FEYS, B. J., BENEDETTI, C. E., PENFOLD, C. N. & TURNER, J. G. 1994. Arabidopsis mutants selected for resistance to the phytotoxin coronatine are male sterile, insensitive to methyl jasmonate, and resistant to a bacterial pathogen. *The Plant Cell,* 6**,** 751-759.

FIGUEROA, P. & BROWSE, J. 2012. The Arabidopsis JAZ2 promoter contains a G-Box and thymidine-rich module that are necessary and sufficient for jasmonate-dependent activation by MYC transcription factors and repression by JAZ proteins. *Plant and Cell Physiology,* 53**,** 330-343.

FLETCHER, J. C., BRAND, U., RUNNING, M. P., SIMON, R. & MEYEROWITZ, E. M. 1999. Signaling of cell fate decisions by CLAVATA3 in Arabidopsis shoot meristems. *Science,* 283**,** 1911-1914.

GAO, C., QI, S., LIU, K., LI, D., JIN, C., LI, Z., HUANG, G., HAI, J., ZHANG, M. & CHEN, M. 2016. MYC2, MYC3, and MYC4 function redundantly in seed storage protein accumulation in Arabidopsis. *Plant Physiology and Biochemistry,* 108**,** 63-70.

GEISLER, M., BLAKESLEE, J. J., BOUCHARD, R., LEE, O. R., VINCENZETTI, V., BANDYOPADHYAY, A., TITAPIWATANAKUN, B., PEER, W. A., BAILLY, A. & RICHARDS, E. L. 2005. Cellular efflux of auxin catalyzed by the Arabidopsis MDR/PGP transporter AtPGP1. *The Plant Journal,* 44**,** 179-194.

GIBALOVÁ, A., REŇÁK, D., MATCZUK, K., DUPL'ÁKOVÁ, N., CHÁB, D., TWELL, D. & HONYS, D. 2009. AtbZIP34 is required for Arabidopsis pollen wall patterning and the control of several metabolic pathways in developing pollen. *Plant Molecular Biology,* 70**,** 581-601.

GOLDBERG, R. B., BEALS, T. P. & SANDERS, P. M. 1993. Anther development: basic principles and practical applications. *The Plant Cell,* 5**,** 1217.

GÓMEZ, J. F., TALLE, B. & WILSON, Z. A. 2015. Anther and pollen development: a conserved developmental pathway. *Journal of integrative plant biology,* 57**,** 876-891.

GONG, F., WU, X. & WANG, W. 2015. Diversity and function of maize pollen coat proteins: from biochemistry to proteomics. *Frontiers in Plant Science,* 6**,** 199.

GOODWIN, G. H., SANDERS, C. AND JOHNS, E.W. 1973. A new group of chromatin-associated proteins with a high content of acidic and basic amino acids. . *European Journal of Biochemistry,* 38(1), pp.14-19.

GRASSER, K. D. 2003. Chromatin-associated HMGA and HMGB proteins: versatile co-regulators of DNA-dependent processes. . *Plant molecular biology,* 53, pp.281-295.

GRASSER, M., LENTZ, A., LICHOTA, J., MERKLE, T. AND GRASSER, K.D. 2006. The Arabidopsis genome encodes structurally and functionally diverse HMGB-type proteins. . *Journal of molecular biology,* 358(3), pp.654-664.

GRIFFITHS, J., MURASE, K., RIEU, I., ZENTELLA, R., ZHANG, Z.-L., POWERS, S. J., GONG, F., PHILLIPS, A. L., HEDDEN, P. & SUN, T.-P. 2006. Genetic characterization and functional analysis of the GID1 gibberellin receptors in Arabidopsis. *The Plant Cell,* 18**,** 3399-3414.

HACKENBERG, D. & TWELL, D. 2019. The evolution and patterning of male gametophyte development. *current topics in developmental biology,* 131**,** 257-298.

HANSEN, F. T., MADSEN, C. K., NORDLAND, A. M., GRASSER, M., MERKLE, T. & GRASSER, K. D. 2008. A novel family of plant DNA-binding proteins containing both HMG-box and AT-rich interaction domains. *Biochemistry,* 47**,** 13207-13214.

HANSEN, G., VAUBERT, D., HÉRON, J. N., CLÉROT, D., TEMPE, J. & BREVET, J. 1993. Phenotypic effects of overexpression of Agrobacterium rhizogenes T-DNA ORF13 in transgenic tobacco plants are mediated by diffusible factor (s). *The Plant Journal,* 4**,** 581-585.

HEARN, R. 2002. *An investigation of the A6 beta-1, 3-glucanase gene family in Arabidopsis thaliana.* University of Leicester.

HICKS, G. & SUSSEX, I. 1971. Organ regeneration in sterile culture after median bisection of the flower primordia of Nicotiana tabacum. *Botanical Gazette,* 132**,** 350-363.

HONYS, D., REŇÁK, D. & TWELL, D. 2006. Male gametophyte development and function. *Plant Biotechnol,* 1**,** 209-224.

HOU, X., HU, W.-W., SHEN, L., LEE, L. Y. C., TAO, Z., HAN, J.-H. & YU, H. 2008. Global identification of DELLA target genes during Arabidopsis flower development. *Plant Physiology,* 147**,** 1126-1142.

HU, J., MITCHUM, M. G., BARNABY, N., AYELE, B. T., OGAWA, M., NAM, E., LAI, W.-C., HANADA, A., ALONSO, J. M. & ECKER, J. R. 2008. Potential sites of bioactive gibberellin production during reproductive growth in Arabidopsis. *The Plant Cell,* 20**,** 320-336.

HUANG, H., GAO, H., LIU, B., QI, T., TONG, J., XIAO, L., XIE, D. & SONG, S. 2017a. Arabidopsis MYB24 regulates jasmonate-mediated stamen development. *Frontiers in Plant Science,* 8**,** 1525.

HUANG, H., GONG, Y., LIU, B., WU, D., ZHANG, M., XIE, D. & SONG, S. 2020. The DELLA proteins interact with MYB21 and MYB24 to regulate filament elongation in Arabidopsis. *BMC plant biology,* 20**,** 1-9.

HUANG, H., LIU, B., LIU, L. & SONG, S. 2017b. Jasmonate action in plant growth and development. *Journal of experimental botany,* 68**,** 1349-1359.

ISHIGURO, S., KAWAI-ODA, A., UEDA, J., NISHIDA, I. & OKADA, K. 2001. The DEFECTIVE IN ANTHER DEHISCENCE1 gene encodes a novel phospholipase A1 catalyzing the initial step of jasmonic acid biosynthesis, which synchronizes pollen maturation, anther dehiscence, and flower opening in Arabidopsis. *The Plant Cell,* 13**,** 2191-2209.

ITO, T., NG, K.-H., LIM, T.-S., YU, H. & MEYEROWITZ, E. M. 2007. The homeotic protein AGAMOUS controls late stamen development by regulating a jasmonate biosynthetic gene in Arabidopsis. *The Plant Cell,* 19**,** 3516-3529.

IUCHI, S., SUZUKI, H., KIM, Y. C., IUCHI, A., KUROMORI, T., UEGUCHI-TANAKA, M., ASAMI, T., YAMAGUCHI, I., MATSUOKA, M. & KOBAYASHI, M. 2007. Multiple loss-of-function of Arabidopsis gibberellin receptor AtGID1s completely shuts down a gibberellin signal. *The Plant Journal,* 50**,** 958-966.

JENIK, P. D. & IRISH, V. F. 2000. Regulation of cell proliferation patterns by homeotic genes during Arabidopsis floral development. *Development,* 127**,** 1267-1276.

JIA, G., LIU, X., OWEN, H. A. & ZHAO, D. 2008. Signaling of cell fate determination by the TPD1 small protein and EMS1 receptor kinase. *Proceedings of the National Academy of Sciences,* 105**,** 2220-2225.

JIANG, J., ZHANG, Z. & CAO, J. 2013. Pollen wall development: the associated enzymes and metabolic pathways. *Plant biology,* 15**,** 249-263.

KAMALAY, J. C. & GOLDBERG, R. B. 1980. Regulation of structural gene expression in tobacco. *Cell,* 19**,** 935-946.

KAMALAY, J. C. & GOLDBERG, R. B. 1984. Organ-specific nuclear RNAs in tobacco. *Proceedings of the National Academy of Sciences,* 81**,** 2801-2805.

KAUFMANN, K., PAJORO, A. & ANGENENT, G. C. 2010. Regulation of transcription in plants: mechanisms controlling developmental switches. *Nature Reviews Genetics,* 11**,** 830-842.

KAZAN, K. & MANNERS, J. M. 2013. MYC2: the master in action. *Molecular plant,* 6**,** 686-703.

KOLTUNOW, A. M., TRUETTNER, J., COX, K. H., WALLROTH, M. & GOLDBERG, R. B. 1990. Different temporal and spatial gene expression patterns occur during anther development. *The Plant Cell,* 2**,** 1201-1224.

KOO, A. J., COOKE, T. F. & HOWE, G. A. 2011. Cytochrome P450 CYP94B3 mediates catabolism and inactivation of the plant hormone jasmonoyl-L-isoleucine. *Proceedings of the National Academy of Sciences,* 108**,** 9298-9303.

KRIZEK, B. A. 1999. Ectopic expression of AINTEGUMENTA in Arabidopsis plants results in increased growth of floral organs. *Developmental genetics,* 25**,** 224-236.

KRIZEK, B. A. & FLETCHER, J. C. 2005. Molecular mechanisms of flower development: an armchair guide. *Nature Reviews Genetics,* 6**,** 688-698.

LALLEMAND, B., ERHARDT, M., HEITZ, T. & LEGRAND, M. 2013. Sporopollenin biosynthetic enzymes interact and constitute a metabolon localized to the endoplasmic reticulum of tapetum cells. *Plant physiology,* 162**,** 616-625.

LI, H., BACIC, A. & READ, S. M. 1999. Role of a callose synthase zymogen in regulating wall deposition in pollen tubes of Nicotiana alata Link et Otto. *Planta,* 208**,** 528-538.

LI, N., ZHANG, D.-S., LIU, H.-S., YIN, C.-S., LI, X.-X., LIANG, W.-Q., YUAN, Z., XU, B., CHU, H.-W. & WANG, J. 2006. The rice tapetum degeneration retardation gene is required for tapetum degradation and anther development. *The Plant Cell,* 18**,** 2999-3014.

LI, Z., WANG, Y., HUANG, J., AHSAN, N., BIENER, G., PAPROCKI, J., THELEN, J. J., RAICU, V. & ZHAO, D. 2017. Two SERK receptor-like kinases interact with EMS1 to control anther cell fate determination. *Plant Physiology,* 173**,** 326-337.

LIANG, Y., TAN, Z.-M., ZHU, L., NIU, Q.-K., ZHOU, J.-J., LI, M., CHEN, L.-Q., ZHANG, X.-Q. & YE, D. 2013. MYB97, MYB101 and MYB120 function as male factors that control pollen tube-synergid interaction in Arabidopsis thaliana fertilization. *PLoS genetics,* 9**,** e1003933.

LIU, B., DE STORME, N. & GEELEN, D. 2017. Gibberellin induces diploid pollen formation by interfering with meiotic cytokinesis. *Plant physiology,* 173**,** 338-353.

LIU, C., CHEN, H., ER, H. L., SOO, H. M., KUMAR, P. P., HAN, J.-H., LIOU, Y. C. & YU, H. 2008. Direct interaction of AGL24 and SOC1 integrates flowering signals in Arabidopsis.

LIU, C., XI, W., SHEN, L., TAN, C. & YU, H. 2009. Regulation of floral patterning by flowering time genes. *Developmental cell,* 16**,** 711-722.

LIU, X., KIM, Y. J., MÜLLER, R., YUMUL, R. E., LIU, C., PAN, Y., CAO, X., GOODRICH, J. & CHEN, X. 2011. AGAMOUS terminates floral stem cell maintenance in Arabidopsis by directly repressing WUSCHEL through recruitment of Polycomb Group proteins. *The Plant Cell,* 23**,** 3654-3670.

LIU, X., YANG, Y., LIN, W., TONG, J., HUANG, Z. & XIAO, L. 2010. Determination of both jasmonic acid and methyl jasmonate in plant samples by liquid chromatography tandem mass spectrometry. *Chinese Science Bulletin,* 55**,** 2231-2235.

LIU, Y., CUI, S., WU, F., YAN, S., LIN, X., DU, X., CHONG, K., SCHILLING, S., THEIßEN, G. & MENG, Z. 2013. Functional conservation of MIKC*-Type MADS box genes in Arabidopsis and rice pollen maturation. *The Plant Cell,* 25**,** 1288-1303.

MALLIK, R., KUNDU, A. & CHAUDHURI, S. 2018. High mobility group proteins: the multifaceted regulators of chromatin dynamics. *The Nucleus,* 61**,** 213-226.

MALLIK, R., PRASAD, P., KUNDU, A., SACHDEV, S., BISWAS, R., DUTTA, A., ROY, A., MUKHOPADHYAY, J., BAG, S. K. & CHAUDHURI, S. 2020. Identification of genome-wide targets and DNA recognition sequence of the Arabidopsis HMG-box protein AtHMGB15 during cold stress response. *Biochimica et Biophysica Acta (BBA)-Gene Regulatory Mechanisms,* 1863**,** 194644.

MANDAOKAR, A. & BROWSE, J. 2009. MYB108 acts together with MYB24 to regulate jasmonate-mediated stamen maturation in Arabidopsis. *Plant Physiology,* 149**,** 851-862.

MANDAOKAR, A., THINES, B., SHIN, B., MARKUS LANGE, B., CHOI, G., KOO, Y. J., YOO, Y. J., CHOI, Y. D., CHOI, G. & BROWSE, J. 2006. Transcriptional regulators of stamen development in Arabidopsis identified by transcriptional profiling. *The Plant Journal,* 46**,** 984-1008.

MARCHANT, D. B. & WALBOT, V. 2022. Anther development—The long road to making pollen. *The Plant Cell,* 34**,** 4677-4695.

MARCINIAK, K. & PRZEDNICZEK, K. 2019. Comprehensive insight into gibberellin-and jasmonate-mediated stamen development. *Genes,* 10**,** 811.

MASCARENHAS, J. P. 1990. Gene activity during pollen development.

MCBRYANT, S. J., ADAMS, V. H. & HANSEN, J. C. 2006. Chromatin architectural proteins. *Chromosome Research,* 14**,** 39-51.

MCCONN, M. & BROWSE, J. 1996. The critical requirement for linolenic acid is pollen development, not photosynthesis, in an Arabidopsis mutant. *The Plant Cell,* 8**,** 403-416.

MCCORMICK, S. 1993. Male gametophyte development. *The plant cell,* 5**,** 1265.

NAGPAL, P., ELLIS, C. M., WEBER, H., PLOENSE, S. E., BARKAWI, L. S., GUILFOYLE, T. J., HAGEN, G., ALONSO, J. M., COHEN, J. D. & FARMER, E. E. 2005. Auxin response factors ARF6 and ARF8 promote jasmonic acid production and flower maturation.

NIE, J., ZHOU, W., LIU, J., TAN, N., ZHOU, J. M. & HUANG, L. 2021. A receptor-like protein from Nicotiana benthamiana mediates VmE02 PAMP-triggered immunity. *New Phytologist,* 229**,** 2260-2272.

NIU, Q.-K., LIANG, Y., ZHOU, J.-J., DOU, X.-Y., GAO, S.-C., CHEN, L.-Q., ZHANG, X.-Q. & YE, D. 2013. Pollen-expressed transcription factor 2 encodes a novel plant-specific TFIIB-related protein that is required for pollen germination and embryogenesis in Arabidopsis. *Molecular Plant,* 6**,** 1091-1108.

Ó'MAOILÉIDIGH, D. S., GRACIET, E. & WELLMER, F. 2014. Gene networks controlling A rabidopsis thaliana flower development. *New Phytologist,* 201**,** 16-30.

OH, S. A., PARK, K. S., TWELL, D. & PARK, S. K. 2010. The SIDECAR POLLEN gene encodes a microspore-specific LOB/AS2 domain protein required for the correct timing and orientation of asymmetric cell division. *The Plant Journal,* 64**,** 839-850.

OJOLO, S. P., CAO, S., PRIYADARSHANI, S., LI, W., YAN, M., ASLAM, M., ZHAO, H. & QIN, Y. 2018. Regulation of plant growth and development: a review from a chromatin remodeling perspective. *Frontiers in plant science,* 9**,** 1232.

PANDIAN, T. J. 2022. *Evolution and speciation in plants*, CRC Press.

PAPONOV, I. A., TEALE, W. D., TREBAR, M., BLILOU, I. & PALME, K. 2005. The PIN auxin efflux facilitators: evolutionary and functional perspectives. *Trends in plant science,* 10**,** 170-177.

PARISH, R. W. & LI, S. F. 2010. Death of a tapetum: a programme of developmental altruism. *Plant Science,* 178**,** 73-89.

PARK, J. H., HALITSCHKE, R., KIM, H. B., BALDWIN, I. T., FELDMANN, K. A. & FEYEREISEN, R. 2002. A knock-out mutation in allene oxide synthase results in male sterility and defective wound signal transduction in Arabidopsis due to a block in jasmonic acid biosynthesis. *The Plant Journal,* 31**,** 1-12.

PEDERSEN, D. S. & GRASSER, K. D. 2010. The role of chromosomal HMGB proteins in plants. *Biochimica et Biophysica Acta (BBA)-Gene Regulatory Mechanisms,* 1799**,** 171-174.

PLACKETT, A. R., POWERS, S. J., FERNANDEZ-GARCIA, N., URBANOVA, T., TAKEBAYASHI, Y., SEO, M., JIKUMARU, Y., BENLLOCH, R., NILSSON, O. & RUIZ-RIVERO, O. 2012. Analysis of the developmental roles of the Arabidopsis gibberellin 20-oxidases demonstrates that GA20ox1,-2, and-3 are the dominant paralogs. *The Plant Cell,* 24**,** 941-960.

PLACKETT, A. R., THOMAS, S. G., WILSON, Z. A. & HEDDEN, P. 2011. Gibberellin control of stamen development: a fertile field. *Trends in plant science,* 16**,** 568-578.

PNUELI, L., HAREVEN, D., ROUNSLEY, S. D., YANOFSKY, M. F. & LIFSCHITZ, E. 1994. Isolation of the tomato AGAMOUS gene TAG1 and analysis of its homeotic role in transgenic plants. *The Plant Cell,* 6**,** 163-173.

POZO, M. J., VAN DER ENT, S., VAN LOON, L. & PIETERSE, C. M. 2008. Transcription factor MYC2 is involved in priming for enhanced defense during rhizobacteria-induced systemic resistance in Arabidopsis thaliana. *New phytologist,* 180**,** 511-523.

QI, T., HUANG, H., SONG, S. & XIE, D. 2015. Regulation of jasmonate-mediated stamen development and seed production by a bHLH-MYB complex in Arabidopsis. *The Plant Cell,* 27**,** 1620-1633.

QIU, Y., LI, Z. & KÖHLER, C. 2024. Ancestral duplication of MADS-box genes in land plants empowered the functional divergence between sporophytes and gametophytes. *New Phytologist*.

RADOVIC, A., NIKOLIC, D., MILATOVIC, D., ŽIVKOVIC, B. & STEVANOVIC, N. 2016. The effect of plant hormones on pollen germination and pollen tube growth of almond cultivars. *Acta Hortic,* 1139**,** 375-380.

REEVES, P. H., ELLIS, C. M., PLOENSE, S. E., WU, M.-F., YADAV, V., THOLL, D., CHÉTELAT, A., HAUPT, I., KENNERLEY, B. J. & HODGENS, C. 2012. A regulatory network for coordinated flower maturation. *PLoS genetics,* 8**,** e1002506.

RIECHMANN, J. L., HEARD, J., MARTIN, G., REUBER, L., JIANG, C.-Z., KEDDIE, J., ADAM, L., PINEDA, O., RATCLIFFE, O. J., SAMAHA, R. R., CREELMAN, R., PILGRIM, M., BROUN, P., ZHANG, J. Z., GHANDEHARI, D., SHERMAN, B. K. & -L. YU, G. 2000. Arabidopsis Transcription Factors: Genome-Wide Comparative Analysis Among Eukaryotes. *Science,* 290**,** 2105-2110.

RIEU, I., RUIZ-RIVERO, O., FERNANDEZ-GARCIA, N., GRIFFITHS, J., POWERS, S. J., GONG, F., LINHARTOVA, T., ERIKSSON, S., NILSSON, O. & THOMAS, S. G. 2008. The gibberellin biosynthetic genes AtGA20ox1 and AtGA20ox2 act, partially redundantly, to promote growth and development throughout the Arabidopsis life cycle. *The Plant Journal,* 53**,** 488-504.

ROY, A., DUTTA, A., ROY, D., GANGULY, P., GHOSH, R., KAR, R.K., BHUNIA, A., MUKHOBADHYAY, J. AND CHAUDHURI, S. 2016. Deciphering the role of the AT-rich interaction domain and the HMG-box domain of ARID-HMG proteins of Arabidopsis thaliana. *Plant molecular biology,* 92, pp.371-388.

ROY, D., CHAKRABARTY, J., MALLIK, R. & CHAUDHURI, S. 2019. Rice Trithorax factor ULTRAPETALA 1 (OsULT1) specifically binds to “GAGAG” sequence motif present in Polycomb response elements. *Biochimica et Biophysica Acta (BBA)-Gene Regulatory Mechanisms,* 1862**,** 582-597.

RUNNING, M. P. & MEYEROWITZ, E. M. 1996. Mutations in the PERIANTHIA gene of Arabidopsis specifically alter floral organ number and initiation pattern. *Development,* 122**,** 1261-1269.

RUSSELL, S. D. & JONES, D. S. 2015. The male germline of angiosperms: repertoire of an inconspicuous but important cell lineage. *Frontiers in plant science,* 6**,** 173.

SABLOWSKI, R. 2007. Flowering and determinacy in Arabidopsis. *Journal of experimental botany,* 58**,** 899-907.

SANDERS, P. M., BUI, A. Q., WETERINGS, K., MCINTIRE, K., HSU, Y.-C., LEE, P. Y., TRUONG, M. T., BEALS, T. & GOLDBERG, R. 1999. Anther developmental defects in Arabidopsis thaliana male-sterile mutants. *Sexual plant reproduction,* 11**,** 297-322.

SANDERS, P. M., LEE, P. Y., BIESGEN, C., BOONE, J. D., BEALS, T. P., WEILER, E. W. & GOLDBERG, R. B. 2000. The Arabidopsis DELAYED DEHISCENCE1 gene encodes an enzyme in the jasmonic acid synthesis pathway. *The Plant Cell,* 12**,** 1041-1061.

SATINA, S. & BLAKESLEE, A. F. 1941. Periclinal chimeras in Datura stramonium in relation to development of leaf and flower. *American Journal of Botany***,** 862-871.

SCHMIDT, R. J., VEIT, B., MANDEL, M. A., MENA, M., HAKE, S. & YANOFSKY, M. F. 1993. Identification and molecular characterization of ZAG1, the maize homolog of the Arabidopsis floral homeotic gene AGAMOUS. *The Plant Cell,* 5**,** 729-737.

SCHMITZ, K. 1977. K. Esau, Anatomy of seed plants, J. Wiley and Sons, Chichester (1977), 550 S., 321 Abb. 2. Urban & Fischer.

SCHWEIZER, F., FERNÁNDEZ-CALVO, P., ZANDER, M., DIEZ-DIAZ, M., FONSECA, S., GLAUSER, G., LEWSEY, M. G., ECKER, J. R., SOLANO, R. & REYMOND, P. 2013. Arabidopsis basic helix-loop-helix transcription factors MYC2, MYC3, and MYC4 regulate glucosinolate biosynthesis, insect performance, and feeding behavior. *The Plant Cell,* 25**,** 3117-3132.

SCOTT, R. J., SPIELMAN, M. & DICKINSON, H. 2004. Stamen structure and function. *The plant cell,* 16**,** S46-S60.

SHELDON, C. C., ROUSE, D. T., FINNEGAN, E. J., PEACOCK, W. J. & DENNIS, E. S. 2000. The molecular basis of vernalization: the central role of FLOWERING LOCUS C (FLC). *Proceedings of the National Academy of Sciences,* 97**,** 3753-3758.

SHEN, X., MIZUGUCHI, G., HAMICHE, A. & WU, C. 2000. A chromatin remodelling complex involved in transcription and DNA processing. *Nature,* 406**,** 541-544.

SHI, J., CUI, M., YANG, L., KIM, Y.-J. & ZHANG, D. 2015. Genetic and biochemical mechanisms of pollen wall development. *Trends in plant science,* 20**,** 741-753.

SMYTH, D. R., BOWMAN, J. L. & MEYEROWITZ, E. M. 1990. Early flower development in Arabidopsis. *The Plant Cell,* 2**,** 755-767.

SOMMER, H., BELTRAN, J.-P., HUIJSER, P., PAPE, H., LÖNNIG, W.-E., SAEDLER, H. & SCHWARZ-SOMMER, Z. 1990. Deficiens, a homeotic gene involved in the control of flower morphogenesis in Antirrhinum majus: the protein shows homology to transcription factors. *The EMBO Journal,* 9**,** 605-613.

SONG, S., QI, T., HUANG, H., REN, Q., WU, D., CHANG, C., PENG, W., LIU, Y., PENG, J. & XIE, D. 2011. The jasmonate-ZIM domain proteins interact with the R2R3-MYB transcription factors MYB21 and MYB24 to affect jasmonate-regulated stamen development in Arabidopsis. *The Plant Cell,* 23**,** 1000-1013.

SONG, S., QI, T., HUANG, H. & XIE, D. 2013. Regulation of stamen development by coordinated actions of jasmonate, auxin, and gibberellin in Arabidopsis. *Molecular Plant,* 6**,** 1065-1073.

SONG, S., QI, T., WASTERNACK, C. & XIE, D. 2014. Jasmonate signaling and crosstalk with gibberellin and ethylene. *Current Opinion in Plant Biology,* 21**,** 112-119.

SOTOMAYOR, C., CASTRO, J., VELASCO, N. & TORO, R. 2012. Influence of seven growth regulators on fruit set, pollen germination and pollen tube growth of almonds. *Journal of Agricultural Science and Technology. B,* 2**,** 1051.

SPANUDAKIS, E. & JACKSON, S. 2014. The role of microRNAs in the control of flowering time. *Journal of experimental botany,* 65**,** 365-380.

STASWICK, P. E. & TIRYAKI, I. 2004. The oxylipin signal jasmonic acid is activated by an enzyme that conjugates it to isoleucine in Arabidopsis. *The Plant Cell,* 16**,** 2117-2127.

STINTZI, A. & BROWSE, J. 2000. The Arabidopsis male-sterile mutant, opr3, lacks the 12-oxophytodienoic acid reductase required for jasmonate synthesis. *Proceedings of the National Academy of Sciences,* 97**,** 10625-10630.

ŠTROS, M., LAUNHOLT, D. & GRASSER, K. D. 2007. The HMG-box: a versatile protein domain occurring in a wide variety of DNA-binding proteins. *Cellular and Molecular Life Sciences,* 64**,** 2590.

SUN, T. & KAMIYA, Y. 1994. The Arabidopsis GA1 locus encodes the cyclase ent-kaurene synthetase A of gibberellin biosynthesis. *The Plant Cell,* 6**,** 1509-1518.

SUZA, W. P. & STASWICK, P. E. 2008. The role of JAR1 in jasmonoyl-L-isoleucine production during Arabidopsis wound response. *Planta,* 227**,** 1221-1232.

TABATA, R., IKEZAKI, M., FUJIBE, T., AIDA, M., TIAN, C.-E., UENO, Y., YAMAMOTO, K. T., MACHIDA, Y., NAKAMURA, K. & ISHIGURO, S. 2010. Arabidopsis auxin response factor6 and 8 regulate jasmonic acid biosynthesis and floral organ development via repression of class 1 KNOX genes. *Plant and Cell Physiology,* 51**,** 164-175.

TAKAGI, H., HEMPTON, A. K. & IMAIZUMI, T. 2023. Photoperiodic flowering in Arabidopsis: Multilayered regulatory mechanisms of CONSTANS and the florigen FLOWERING LOCUS T. *Plant Communications*.

TAYLOR-TEEPLES, M., LIN, L., DE LUCAS, M., TURCO, G., TOAL, T., GAUDINIER, A., YOUNG, N., TRABUCCO, G., VELING, M. & LAMOTHE, R. 2015. An Arabidopsis gene regulatory network for secondary cell wall synthesis. *Nature,* 517**,** 571-575.

THINES, B., KATSIR, L., MELOTTO, M., NIU, Y., MANDAOKAR, A., LIU, G., NOMURA, K., HE, S. Y., HOWE, G. A. & BROWSE, J. 2007. JAZ repressor proteins are targets of the SCFCOI1 complex during jasmonate signalling. *Nature,* 448**,** 661-665.

TOSUN, F. & KOYUNCU, F. 2007. Effects of some chemical treatments on pollen germination and pollen tube growth in sweet cherries (Prunus avium L.).

TURCZYN, M. 2011. ABC of flower architecture. *POSTEPY BIOLOGII KOMORKI,* 38**,** 673-684.

TWELL, D. 2011. Male gametogenesis and germline specification in flowering plants. *Sexual Plant Reproduction,* 24**,** 149-160.

VAN DER KROL, A. R. & CHUA, N.-H. 1993. Flower development in petunia. *The Plant Cell,* 5**,** 1195.

VEIT, B., SCHMIDT, R. J., HAKE, S. & YANOFSKY, M. F. 1993. Maize floral development: new genes and old mutants. *The plant cell,* 5**,** 1205.

VERELST, W., SAEDLER, H. & MUNSTER, T. 2007. MIKC* MADS-protein complexes bind motifs enriched in the proximal region of late pollen-specific Arabidopsis promoters. *Plant Physiology,* 143**,** 447-460.

VON MALEK, B., VAN DER GRAAFF, E., SCHNEITZ, K. & KELLER, B. 2002. The Arabidopsis male-sterile mutant dde2-2 is defective in the ALLENE OXIDE SYNTHASE gene encoding one of the key enzymes of the jasmonic acid biosynthesis pathway. *Planta,* 216**,** 187-192.

WAHEED, S. & ZENG, L. 2020. The critical role of miRNAs in regulation of flowering time and flower development. *Genes,* 11**,** 319.

WASTERNACK, C., FORNER, S., STRNAD, M. & HAUSE, B. 2013. Jasmonates in flower and seed development. *Biochimie,* 95**,** 79-85.

WASTERNACK, C. & SONG, S. 2017. Jasmonates: biosynthesis, metabolism, and signaling by proteins activating and repressing transcription. *Journal of Experimental Botany,* 68**,** 1303-1321.

WEI, S. & MA, L. 2023. Comprehensive insight into tapetum-mediated Pollen Development in Arabidopsis thaliana. *Cells,* 12**,** 247.

WEISS, J., DELGADO-BENARROCH, L. & EGEA-CORTINES, M. 2005. Genetic control of floral size and proportions. *The International journal of developmental biology,* 49**,** 513-525.

WILS, C. R. & KAUFMANN, K. 2017. Gene-regulatory networks controlling inflorescence and flower development in Arabidopsis thaliana. *Biochimica et Biophysica Acta (BBA)-Gene Regulatory Mechanisms,* 1860**,** 95-105.

WILSON, Z. A. & ZHANG, D.-B. 2009. From Arabidopsis to rice: pathways in pollen development. *Journal of experimental botany,* 60**,** 1479-1492.

WU, J.-Z., LIN, Y., ZHANG, X.-L., PANG, D.-W. & ZHAO, J. 2008. IAA stimulates pollen tube growth and mediates the modification of its wall composition and structure in Torenia fournieri. *Journal of experimental botany,* 59**,** 2529-2543.

WU, M.-F., SANG, Y., BEZHANI, S., YAMAGUCHI, N., HAN, S.-K., LI, Z., SU, Y., SLEWINSKI, T. L. & WAGNER, D. 2012. SWI2/SNF2 chromatin remodeling ATPases overcome polycomb repression and control floral organ identity with the LEAFY and SEPALLATA3 transcription factors. *Proceedings of the National Academy of Sciences,* 109**,** 3576-3581.

XIA, C., WANG, Y. J., LIANG, Y., NIU, Q. K., TAN, X. Y., CHU, L. C., CHEN, L. Q., ZHANG, X. Q. & YE, D. 2014. The ARID-HMG DNA-binding protein A t HMGB 15 is required for pollen tube growth in Arabidopsis thaliana. *The Plant Journal,* 79**,** 741-756.

XIE, D.-X., FEYS, B. F., JAMES, S., NIETO-ROSTRO, M. & TURNER, J. G. 1998. COI1: an Arabidopsis gene required for jasmonate-regulated defense and fertility. *Science,* 280**,** 1091-1094.

XU, J., DING, Z., VIZCAY-BARRENA, G., SHI, J., LIANG, W., YUAN, Z., WERCK-REICHHART, D., SCHREIBER, L., WILSON, Z. A. & ZHANG, D. 2014. ABORTED MICROSPORES acts as a master regulator of pollen wall formation in Arabidopsis. *The Plant Cell,* 26**,** 1544-1556.

XU, L., LIU, F., LECHNER, E., GENSCHIK, P., CROSBY, W. L., MA, H., PENG, W., HUANG, D. & XIE, D. 2002. The SCFCOI1 ubiquitin-ligase complexes are required for jasmonate response in Arabidopsis. *The Plant Cell,* 14**,** 1919-1935.

XU, L. & SHEN, W.-H. 2008. Polycomb silencing of KNOX genes confines shoot stem cell niches in Arabidopsis. *Current Biology,* 18**,** 1966-1971.

YAMAGUCHI, N. 2021. LEAFY, a pioneer transcription factor in plants: A mini-review. *Frontiers in Plant Science,* 12**,** 701406.

YAN, W., CHEN, D. & KAUFMANN, K. 2016. Molecular mechanisms of floral organ specification by MADS domain proteins. *Current Opinion in Plant Biology,* 29**,** 154-162.

YANG, C., VIZCAY-BARRENA, G., CONNER, K. & WILSON, Z. A. 2007. MALE STERILITY1 is required for tapetal development and pollen wall biosynthesis. *The Plant Cell,* 19**,** 3530-3548.

YANG, S.-L., JIANG, L., PUAH, C. S., XIE, L.-F., ZHANG, X.-Q., CHEN, L.-Q., YANG, W.-C. & YE, D. 2005. Overexpression of TAPETUM DETERMINANT1 alters the cell fates in the Arabidopsis carpel

and tapetum via genetic interaction with excess microsporocytes1/extra sporogenous cells. *Plant physiology,* 139**,** 186-191.

YANG, Z., LI, Y., GAO, F., JIN, W., LI, S., KIMANI, S., YANG, S., BAO, T., GAO, X. & WANG, L. 2020. MYB21 interacts with MYC2 to control the expression of terpene synthase genes in flowers of Freesia hybrida and Arabidopsis thaliana. *Journal of Experimental Botany,* 71**,** 4140-4158.

ZANDER, M., LEWSEY, M. G., CLARK, N. M., YIN, L., BARTLETT, A., SALDIERNA GUZMÁN, J. P., HANN, E., LANGFORD, A. E., JOW, B. & WISE, A. 2020. Integrated multi-omics framework of the plant response to jasmonic acid. *Nature plants,* 6**,** 290-302.

ZHAI, Q., ZHANG, X., WU, F., FENG, H., DENG, L., XU, L., ZHANG, M., WANG, Q. & LI, C. 2015. Transcriptional mechanism of jasmonate receptor COI1-mediated delay of flowering time in Arabidopsis. *The Plant Cell,* 27**,** 2814-2828.

ZHANG, D. & LI, H. 2014. Exine export in pollen. *Plant abc transporters.* Springer.

ZHANG, D., LIANG, W., YIN, C., ZONG, J., GU, F. & ZHANG, D. 2010. OsC6, encoding a lipid transfer protein, is required for postmeiotic anther development in rice. *Plant physiology,* 154**,** 149-162.

ZHANG, L., MA, F., DUAN, G., JU, Y., YU, T., ZHANG, Q. & SODMERGEN, S. 2024a. MIKC*-type MADS transcription factors control JINGUBANG expression and the degree of pollen dormancy in Arabidopsis. *Plant Physiology***,** kiae576.

ZHANG, Q. A. W., Y., 2008. High mobility group proteins and their post-translational modifications. *Biochimica et Biophysica Acta (BBA)-Proteins and Proteomics,* 1784(9), pp.1159-1166.

ZHANG, W., SUN, Y., TIMOFEJEVA, L., CHEN, C., GROSSNIKLAUS, U. & MA, H. 2006a. Regulation of Arabidopsis tapetum development and function by DYSFUNCTIONAL TAPETUM1 (DYT1) encoding a putative bHLH transcription factor.

ZHANG, X., BEI, Z., LI, J., MA, H., WANG, C., XU, W., REN, Y., ZHOU, J. & YAN, X. 2024b. Regulatory Mechanisms of Pollen Development: Transcriptomic and Bioinformatic Insights into the Role of β-1, 3 Glucanase Gene (LbGlu1) in Lycium barbarum. *Horticulturae,* 10**,** 512.

ZHANG, X., HE, Y., LI, L., LIU, H. & HONG, G. 2021. Involvement of the R2R3-MYB transcription factor MYB21 and its homologs in regulating flavonol accumulation in Arabidopsis stamen. *Journal of experimental botany,* 72**,** 4319-4332.

ZHANG, X., HENRIQUES, R., LIN, S.-S., NIU, Q.-W. & CHUA, N.-H. 2006b. Agrobacterium-mediated transformation of Arabidopsis thaliana using the floral dip method. *Nature protocols,* 1**,** 641-646.

ZHANG, Z. B., ZHU, J., GAO, J. F., WANG, C., LI, H., LI, H., ZHANG, H. Q., ZHANG, S., WANG, D. M. & WANG, Q. X. 2007. Transcription factor AtMYB103 is required for anther development by regulating tapetum development, callose dissolution and exine formation in Arabidopsis. *The Plant Journal,* 52**,** 528-538.

ZHAO, D.-Z., WANG, G.-F., SPEAL, B. & MA, H. 2002. The excess microsporocytes1 gene encodes a putative leucine-rich repeat receptor protein kinase that controls somatic and reproductive cell fates in the Arabidopsis anther. *Genes & Development,* 16**,** 2021-2031.

ZHOU, J.-J., LIANG, Y., NIU, Q.-K., CHEN, L.-Q., ZHANG, X.-Q. & YE, D. 2013. The Arabidopsis general transcription factor TFIIB1 (AtTFIIB1) is required for pollen tube growth and endosperm development. *Journal of experimental botany,* 64**,** 2205-2218.

ZHU, J., CHEN, H., LI, H., GAO, J. F., JIANG, H., WANG, C., GUAN, Y. F. & YANG, Z. N. 2008. Defective in Tapetal development and function 1 is essential for anther development and tapetal function for microspore maturation in Arabidopsis. *The Plant Journal,* 55**,** 266-277.

ZLATANOVA, J. & VAN HOLDE, K. 1998. Binding to four-way junction DNA: a common property of architectural proteins? *The FASEB Journal,* 12**,** 421-431.

ZOBELL, O., FAIGL, W., SAEDLER, H. & MÜNSTER, T. 2010. MIKC* MADS-box proteins: conserved regulators of the gametophytic generation of land plants. *Molecular biology and evolution,* 27**,** 1201-1211.

Annexure_1: List of Primers

GENE	*GENE ID*	*PRIMER NAME*	*PRIMER SEQUENCE (5'---3')*
PRIMERS FOR VALIDATION OF TRANSCRIPTOME (JA BIOSYNTHESIS GENES)			
DAD1	AT2G44810	AT2G44810-DAD1-F	GGACAAAGAAGAGATCTCGCGGC
		AT2G44810-DAD1-R	TAAGCTGCTAGTGTCGCGATCG
AOS	AT5G42650	AT5G42650-AOS-F	CGATCAAAGCTTCCGGGTCAGAAA
		AT5G42650-AOS-R	GTGGATTCTCGGCGATAAAAGCT
AOC3	AT3G25780	AT3G25780-AOC3-F	GGGCAAGAAGACCGAAAACTCC
		AT3G25780-AOC3-R	CGAATCTGTCACCGCTCTTTTCA
OPR3	AT2G06050	AT2G06050-OPR3-F	ACTCCCGGCGGTTTTCTCA
		AT2G06050-OPR3-R	CGCCACCTGTTTTCCGAGATTG
OPCL1	AT1G20510	AT1G20510-OPCL1-F	CCGAAACAAACCGGTGAGCTTT
		AT1G20510-OPCL1-R	GATTTCAGGATGAGTAAGCAAC
JAR1	AT2G46370	AT2G46370-JAR1-F	CACCTATTCTCACTGGTCACCCTG
		AT2G46370-JAR1-R	TCCCGTTGATATGTACTGCTTGC
CYP94B3	AT3G48520	AT3G48520-CYP94B3-F	ACCGTGCACGTGTTGGTCT
		AT3G48520-CYP94B3-R	CTAACCCTAAACTCACCAACGGG
ST2A	AT5G07010	AT5G07010-ST2A-F	TTAAAGAAGGCAAAACTCGCGAC
		AT5G07010-ST2A-R	CGGTGACGGTTAAGGATGGTGAA
EF1	AT1G07920	AT1G07920-EF1-F	GTAACAAGATGGATGCCAC
		AT1G07920-EF1-R	TCTGGTCAAGAGCCTCAAG
PRIMERS FOR VALIDATION OF TRANSCRIPTOME (JA SIGNALLING AND RESPONSE GENES)			
MYC2	AT1G32640	AT1G32640-MYC2-F	TTGATCTCCGGTGGTGTTGCT
		AT1G32640-MYC2-R	GTTCGCCGAAGGAATACACGC
MYB21	AT3G27810	MYB21-F-AT3G27810	AAGTAGTGGAGGTTCGGGATC
		MYB21-R-AT3G27810	ATTTCCCCGTCGCACATCA
MYB24	AT5G40350	AT5G40350/MYB24-F	TCATTCATGACATGGCTCG
		AT5G40350/MYB24-R	CAAAATGGGGAAATAGGTGG
COI1	AT2G39940	COI1-F-AT2G39940	TGTAAATTGAGCTGCGTCGCGA
		COI1-R-AT2G39940	TTGCCTTTAAGCTTGAGCGACCT
JAZ7	AT2G34600	AT2G34600-JAZ7-F	GATTCTGATTTCCATAGCTCGTT
		AT2G34600-JAZ7-R	TCGAGTCGAATTGTTTGGG
JAZ8	AT1G30135	AT1G30135-JAZ8-F	CAGATGTTACCCATCTTCAGGC
		AT1G30135-JAZ8-R	TTATCGTCGTGAATGGTACGG
JAZ10	AT5G13220	AT5G13220-JAZ10-F	ACGCGTCTCTCGCCAGGTC
		AT5G13220-JAZ10-R	CCTTGCGATGGGAAGATCTC
PRIMERS FOR VALIDATION OF TRANSCRIPTOME (CELL WALL BIOGENESIS GENES)			
MIF21.3	AT5G48140	AT5G48140-F	CACTAACGCATTGTTGAAAGCATTCAATGA
		AT5G48140-R	CAACTTAAACCCATTAATGTTGCGG
CSLD1	AT2G33100	AT2G33100-F	ACGATGACATGGACGTCTCTGGTGATTA
		AT2G33100-R	TTATGATCAAAATCTCCCGTCTGGCTCCTC
DL4030C	AT4G15980	AT4G15980-F	GAGTAGGAAAATGGAAGAGGTTCACCG
		AT4G15980-R	CTACAAGTATTAAGCGCTTCTCTTGTGTGC
HSP90.1	AT5G2640	AT5G52640-F	TAACTCTTCTGATGCTCTTGACAAGATCCG
		AT5G52640-R	TTGTCCTATCATGCTTACATCAGCTCCAG
AT3G07850	AT3G07850	AT3G07850-F	ATGCAGCTACAGCAGTTGAAGATACAGCAA
		AT3G07850-R	AACTCTAGGCTCTCTACCATATACTCACCT
XTH18	AT4G30280	AT4G30280-F	TCTATGCATGTCTATGCGGGTAGCTTC
		AT4G30280-R	CACGTAGTTCCCGGAGACTTAAGAT
F17I5.160	AT4G33970	AT4G33970-F	GTCTCATTTGCCCTAACCGATACAGAA
		AT4G33970-R	ATGCCAGTTCCCCGTGGTGTTAAATG
PRIMERS FOR VALIDATION OF TRANSCRIPTOME (BIOSYTHESIS AND RESPONSE TO HORMONE)			
RRTF1	AT4G34410	RRTF1-F	ACA CGT CTT CAG TTT CAT CTC C
		RRTF1-R	TCA CTG GAA CAT ATC AGC AA
ERF11	AT1G28370	ERF11-F	ATG GCA CCG ACA GTT AAA AC
		ERF11-R	TGG TTT TGG CTT TAG CTC CA
DDF1	AT1G12610	DDF1-F	TGA TGA TAT TAT TCT GGC GGA G
		DDF1-R	TCA AAC ATG CGG ATC TCC CA
DDF2	AT1G63030	DDF2-F	ATG GAA AAC GAC GAT ATC ACC G
		DDF2-R	TAT CTG CCG TCG GAT AAG TT
RGL	AT5G17490	RGL -F	ATG AAA CGA AGC CAT CAA GAA ACG
		RGL -R	TTG AAG GCA TTA CTA GAA GAG GCA
GA2OX6	AT1G02400	GA2ox6 -F	GAG ATT CGA GCA TGA AGG AGA AGA G
		GA2ox6 -R	GTT TCA GAT TTA TCA GCG ACA GC
IQD22	AT4G23060	IQD22- F	CGG TGG TTT AGG AGT CTA TTC GGA G
		IQD22- R	CGG TAG CGA TGG AGT ATG AGG AA
ARF6	AT1G30330	ARF6-F	CAACCGTTGAATGCGCAAGA
		ARF6-R	TGC TGC GAG TAA TCC AAG GGA

WRKY40	AT1G80840	WRKY40-F	CTT CTG ACA CTA CCC TCG T T
		WRKY40-R	CTC CAC ACT TCT CTG AAC CT T
AGL18	AT3G57390	AGL18-F	TGACGCCGAGGTTGCTCTTAT
		AGL18-R	GGGAAACTCATACCTTCAAGCTCC
PRIMERS FOR VALIDATION OF TRANSCRIPTOME (PROTEIN KINASES AND PHOSPHATASES)			
MPK3	AT3G45640	MPK3 -F	TGC GCT TAT TGA CAG AGT T
		MPK3 -R	GGT GAT TCA GAG CTT GTT CAA CA
MKK9	AT1G73500	MKK9 -F	ATG GCT TTA GTA CGT GAA CGT
		MKK9 -R	GAT CCA TGT CGC CGT TAA CT
MAPKKK15	AT5G55090	MAPKKK15-F	ATG GAG GAA CAA AAC TGG AT
		MAPKKK15-R	CTC CCA CCG GAA ACA TAC TC
MAPKKK21	AT4G36950	MAPKKK21-F	ATG GAG TGG ATT CGT AGA GA
		MAPKKK21-R	ACC ACC GGA AGC ATA CTC AA
RBK2	AT3G05140	RBK2-F	TTA GGC TCT CTC CTC CAT GGA
		RBK2-R	AAT ATT CAG GTG CAA AGT ACC C
CPK16	AT2G17890	CPK16-F	CCT TGA AGA GAT GAG GCA GGC
		CPK16-R	CCC TTT CAA GCC AGT TAG CA
PRK4	AT3G20190	PRK4 - F	CAA GCC ATC TTC ACG CG
		PRK4 -R	CGG TTA GGA GTG GCT CAA ATG
PTEN1	AT5G39400	PTEN1-F	GGT TTC AGA ACT TCA GGA GGTT
		PTEN1-R	TGC GTA TGT CAC CAC TAA CTC
PRIMERS FOR CHIP q-PCR			
MYC2	AT1G32640	AT1G32640F-MYC2-CHIP	GCAAGTGAGAATCTCTATCTCC
		AT1G32640R-MYC2-CHIP	CGTTGTTAGCATGTGTTTATCGTG
MYB21	AT3G27810	Chip AT3G27810/MYB21a-F	ATGCATCAAAGAGTCTCCAG
		Chip AT3G27810/MYB21a-R	AATAACACATGCATGGGGAC
MYB24	AT5G40350	Chip AT5G40350/MYB24-F	AGACGAGTTATCTAAAGGGG
		Chip AT5G40350/MYB24-R	CTCAAGTCTGTTGATGCC
CAP	AT1G01310	CV Neg AT1G01310-F	ATGAAGACTCTTCCACAAAACCCT
		CV Neg AT1G01310-R	CTGTTACGACGTCGTATTCTCCTC
AP2-like ethylene responsive TF	AT1G01840	CV Neg AT1G01840-F	AAGTAGCTGAGCTGATATCATCGCTG
		CV Neg AT1G01840-R	CTATCGCCGAGTATCTCTCCTCTTCA
PRIMERS FOR PROMOTOR CLONING FOR GUS ASSAY			
MYC2	AT1G32640	MYC2prom2kb_F	CACCGGATCCCGAGCATGCCAAATCAATC
		MYC2prom2kb_R	CTCGAGGGAGAAAGTCTTCGTAGTGGAG
LOX4	AT1G72520	AT1G72520-F-LOX4prom2kb	CACCGGATCCACACAAACAAAGCCCAAGGG
		LOX4-R-NCO1	GGCCATGGGAAAGAGAGCTTTTCGCCGTC
MYB21	AT3G27810	MYB21-F-ECOR1	CCGAATTCCGACTCGTACCCAAACGTTTA
		MYB21-R-BGL2	CCAGATCTGAAGGTTGTGGAAGGTGAGGTA
MYB24	AT5G40350	AT5G40350-F-MYB24prom2kb	CACCGGATCCATTGGCCAAATTGTTCCCCCT
		AT5G40350-R-MYB24prom2kb	CCCTCGAGGTGGTGGGCAGGTAGCTACTG
MYC2	AT1G32640	MYC2-CDS-F	GGCCATGGATGACTGATTACCGGCTACAACCA
		MYC2-CDS-R	CCGGTCACCTTAACCGATTTTTGAAATCAAA CTT
PRIMER FOR BIFC			
ARID4	AT1G04880	Arid4F-Gateway	CACCATGGCATCAAGCTCTTGTC
		Arid4R-Gateway (101)	GTTCTGCTCAGCAGTCACCG
MYC2	AT1G32640	MYC2-CDS-F	CACCGCTAGCATGACTGATTACCGGCTACAAC
		MYC2-CDS-R	GGCTGCAGTTAACCGATTTTTGAAATCAAAC
PRIMER FOR ELECTROPHORETIC MOBILITY SHIFT ASSAY (EMSA)			
MYC2	AT1G32640	AT1G32640F-MYC2-CHIP	GCAAGTGAGAATCTCTATCTCC
		AT1G32640R-MYC2-CHIP	CGTTGTTAGCATGTGTTTATCGTG
MYB21	AT3G27810	Chip AT3G27810/MYB21a-F	ATGCATCAAAGAGTCTCCAG
		Chip AT3G27810/MYB21a-R	AATAACACATGCATGGGGAC
MYB24	AT5G40350	Chip AT5G40350/MYB24-F	AGACGAGTTATCTAAAGGGG
		Chip AT5G40350/MYB24-R	CTCAAGTCTGTTGATGCC
PRIMER FOR SITE DIRECTED MUTAGENESIS (SDM)			
MYC2	AT1G32640	MYC2-SDFPr	CGACTAAATAACCGAACGCATTTATTAATTTG
		MYC2-SDRPr	GTTTGGTCAAATTAATAAATGCGTTCGGTTAT T
MYB21	AT3G27810	MYB21-SDFPr	CCCTTTTTCAAAACAGATACGCATGACACCAT GTTG
		MYB21-SDRPr	CAATTATAACAACATGGTGTCATGCGTATCTG TTTTG
MYB24	AT5G40350	MYB24-SDFPr	CTAAAGGGGAAGAGAGGACCGCACAAAGCTG TG
		MYB24-SDRPr	TTCTCTTACACAGCTTTGTGCGGTCCTCTCTT C
PRIMER FOR CONSTRUCT OF athmgb15-4-OEA4 (RE) TRANSGENIC			
ARID4	AT1G04880	Arid4F-Gateway	CACCATGGCATCAAGCTCTTGTC

		Arid4R-Gateway (302)	ACTTTTGTCGTCATCGTCTTTGTAGTCGTTCT GCTCAGCAGTCACCG
PRIMER FOR AtHMGB15 EXPRESSION			
ARID4	AT1G04880	Arid4-(F)	AACCATGGCATCAAGCTCTTGTC
		Arid4 HMG (F) Gateway	CACCATGAACACTCTGAACATTTCT
		ARID4-Salk 057612(F2)	ATGTTCCTTCGAATCTCAG
		Arid4 -Arid (R)	CCCTCGAGTCACAGTATTGATCTTGGG
		Arid4 - (R2)	GCCTTCCCTTGGTAAATCAAT
		Arid4 IP (R)	GACACCATGACTCTGTTGCG
		ARID4-Salk 057612(R2)	CACTCTGATCTGATGTGTG
TDNA		LBb1	GCGTGGACCGCTTGCTGCAACT

Annexure2: List of Clones

Routine cloning

Gene of Interest (Insert)	*Vector*	*Resistance*	*Primer(F)/ Restriction enzyme 1*	*Primer(R)/ Restriction enzyme 2*
pMYC2 (200bp)	pGEM®-T Easy	Ampicillin	GCAAGTGAGAATCTCTATCT CC	CGTTGTTAGCATGTGTTTAT CGTG
pMYB24 (200bp)	pGEM®-T Easy	Ampicillin	AGACGAGTTATCTAAAGGGG	CTCAAGTCTGTTGATGCC
pMYB21 (200bp)	pGEM®-T Easy	Ampicillin	ATGCATCAAAGAGTCTCCAG	AATAACACATGCATGGGGAC
MYC2 (full length CDS)	pCambia1304	Kanamycin	Nco1	BstE2

Gateway cloning

Gene of Interest (Insert)	*Vector*	*Resistance*	*Primer(F)/ Restriction enzyme 1*	*Primer(R)/ Restriction enzyme 2*
AtHMGB15 (full length CDS)	pENTR/D-TOPO	Kanamycin	CACCATGGCATCAAGCT CTTGTC	GTTCTGCTCAGCAGTCACCG
MYC2 (full length CDS)	pENTR/D-TOPO	Kanamycin	CACCGCTAGCATGACTG ATTACCGGCTACAAC	GGCTGCAGTTAACCGATTTT TGAAATCAAAC
pMYC2 (2kb upstream)	pENTR/D-TOPO	Kanamycin	BamH1	Xho1
pMYB24 (2kb upstream)	pENTR/D-TOPO	Kanamycin	BamH1	Xho1
pMYB21 (2kb upstream)	pENTR/D-TOPO	Kanamycin	Kpn1	Xho1
AtHMGB15 (full length CDS)	pSITE-cEYFP-N1 (CD3-1651)	Spectinomycin/ Chloramphenicol		
MYC2 (full length CDS)	pSITE-nEYFP-C1 (CD3-1648)	Spectinomycin		
MYC2 (full length CDS)	pGWB618	Spectinomycin	Nhe1	Pst1
pMYC2 (2kb upstream)	pKGWFS7	Spectinomycin	BamH1	Xho1
pMYB24 (2kb upstream)	pKGWFS7	Spectinomycin	BamH1	Xho1
pMYB21 (2kb upstream)	pKGWFS7	Spectinomycin	Kpn1	Xho1
AtHMGB15 (full length CDS)	pMDC84	Kanamycin	CACCATGGCATCAAGCT CTTGTC	GTTCTGCTCAGCAGTCACCG

Annexure_3: List of differentially expressed genes involved in Pollen Development and Related Processes

Gene ID	*Gene Name*	*log2 FC*	*P-value*	*Gene Description*
AT2G07040	*PRK2A*	*-1.12637*	*0.000601*	*Leucine-rich repeat protein kinase family protein*
AT2G15890	*MEE14*	*1.21104*	*5.29E-05*	*maternal effect embryo arrest 14*
AT2G25600	*SPIK*	*-1.30391*	*2.18E-05*	*Shaker pollen inward K+ channel*
AT2G28640	*EXO70H5*	*-1.94839*	*6.76E-05*	*exocyst subunit exo70 family protein H5*
AT2G31500	*CPK24*	*-0.9814*	*0.002177*	*calcium-dependent protein kinase 24*
AT2G33100	*CSLD1*	*-2.52898*	*8.88E-16*	*cellulose synthase-like D1*

AT2G39800	P5CS1	1.3749	4.88E-10	delta1-pyrroline-5-carboxylate synthase 1
AT2G41110	CAM2	-1.13913	2.06E-05	calmodulin 2
AT2G44810	DAD1	-2.01128	5.7E-08	alpha/beta-Hydrolases superfamily protein
AT3G06260	GATL4	-1.2233	4.08E-05	galacturonosyltransferase-like 4
AT3G07970	QRT2	2.05618	4.37E-05	Pectin lyase-like superfamily protein
AT3G08970	ATERDJ3A	-1.18231	0.000418	DNAJ heat shock N-terminal domain-containing protein
AT3G09530	EXO70H3	-1.62208	1.86E-07	exocyst subunit exo70 family protein H3
AT3G12690	AGC1.5	-0.6523	0.003029	AGC kinase 1.5
AT3G13900	AT3G13900	-1.04304	0.001936	ATPase E1-E2 type family protein / haloacid dehalogenase-like hydrolase family protein
AT3G20190	PRK4	-1.30763	3.33E-15	Leucine-rich repeat protein kinase family protein
AT3G21180	ACA9	-0.90583	0.003313	autoinhibited Ca(2+)-ATPase 9
AT3G21700	SGP2	-0.87997	8.64E-06	Ras-related small GTP-binding family protein
AT3G26860	AT3G26860	-1.10424	0.000106	Plant self-incompatibility protein S1 family
AT3G42880	PRK3	-1.56404	7.53E-05	Leucine-rich repeat protein kinase family protein
AT3G45640	MPK3	-1.15654	0.000109	mitogen-activated protein kinase 3
AT1G17420	LOX3	-2.31246	3.14E-10	lipoxygenase 3
AT3G48360	BT2	2.88277	1.04E-14	BTB and TAZ domain protein 2
AT3G48520	CYP94B3	-2.37469	1.8E-14	cytochrome P450, family 94, subfamily B, polypeptide 3
AT3G55610	P5CS2	1.28171	2.06E-05	delta 1-pyrroline-5-carboxylate synthase 2
AT3G57390	AGL18	-0.80995	0.003278	AGAMOUS-like 18
AT1G19180	JAZ1	-1.10051	0.000873	jasmonate-zim-domain protein 1
AT4G13240	ROPGEF9	-1.57761	0.000168	RHO guanyl-nucleotide exchange factor 9
AT4G15200	FH3	-0.98481	7.39E-06	formin 3
AT4G17615	CBL1	-1.68237	8.88E-16	calcineurin B-like protein 1
AT4G24960	HVA22D	-1.29687	1.46E-05	HVA22 homologue D
AT4G26930	MYB97	1.65475	6.9E-05	myb domain protein 97
AT4G38190	CSLD4	-0.91202	0.001839	cellulose synthase like D4
AT5G05690	CPD	0.48334	0.000528	Cytochrome P450 superfamily protein
AT5G12180	CPK17	-1.17293	8.86E-05	calcium-dependent protein kinase 17
AT5G16500	LIP1	-0.97729	0.000897	Protein kinase superfamily protein
AT5G19360	CPK34	-1.51536	1.99E-05	calcium-dependent protein kinase 34
AT5G20690	PRK6	-1.66004	0.000237	Leucine-rich repeat protein kinase family protein
AT5G26050	T1N24.10	1.78722	0.001376	Plant self-incompatibility protein S1 family
AT5G28680	ANX2	-0.8036	1.56E-06	Malectin/receptor-like protein kinase family protein
AT5G39400	PTEN1	-1.0931	0.00022	Calcium/lipid-binding (CaLB) phosphatase
AT5G40260	SWEET8	1.35319	0.001782	Nodulin MtN3 family protein
AT5G45840	K15I22.4	-0.90461	0.000833	Leucine-rich repeat protein kinase family protein
AT5G50260	CEP1	2.65204	2.22E-16	Cysteine proteinases superfamily protein
AT5G63370	CDKG1	-0.48882	4.34E-09	Protein kinase superfamily protein
AT5G64510	TIN1	-1.64892	5.8E-08	tunicamycin induced protein
AT1G35670	CDPK2	0.951308	0.002608	calcium-dependent protein kinase 2
AT1G04880	F13M7.13	-3.5488	3.71E-08	HMG (high mobility group) box protein with ARID/BRIGHT DNA-binding domain-containing protein
AT1G47270	TLP6	-0.96633	4.34E-13	tubby like protein 6
AT1G48020	PMEI1	-1.10763	0.000286	pectin methylesterase inhibitor 1
AT1G50610	PRK5	-1.12251	0.000621	Leucine-rich repeat protein kinase family protein
AT1G05580	CHX23	-1.49881	5.33E-07	cation/H+ exchanger 23
AT1G54280	F20D21.10	-0.87697	0.002845	ATPase E1-E2 type family protein / haloacid dehalogenase-like hydrolase family protein
AT1G61290	SYP124	-1.71978	3.22E-09	syntaxin of plants 124
AT1G64110	DAA1	1.54329	2.19E-05	P-loop containing nucleoside triphosphate hydrolases superfamily protein
AT1G67360	F1N21.18	-0.79266	2.11E-06	Rubber elongation factor protein (REF)
AT1G71880	SUC1	-1.09047	0.00021	sucrose-proton symporter 1
AT1G72520	LOX4	-2.60738	2.22E-16	PLAT/LH2 domain-containing lipoxygenase family protein
AT1G74450	F1M20.13	-1.32644	7.42E-06	BPS1-like protein (DUF793)
AT1G79860	ROPGEF12	-1.07147	0.001092	RHO guanyl-nucleotide exchange factor 12
AT2G02860	SUT2	-0.82584	9.96E-05	sucrose transporter 2

Annexure_4: Summary of 60 upregulated genes common to athmgb15-1 and athmgb15-4 mutants.

Gene ID	Gene Name	log2 FC	P-value	Gene Description
AT1G02580	MEA	2.80852	4.36E-06	SET domain-containing protein
AT1G07610	MT1C	1.7008	2.11E-07	metallothionein 1C
AT1G11690	F25C20.16	2.61753	0.001476	BRANCHLESS TRICHOME-like protein

AT1G18270	T10O22.24	0.734293	8.26E-05	ketose-bisphosphate aldolase class-II family protein
AT1G18830	F6A14.8	2.20249	0.00136	Transducin/WD40 repeat-like superfamily protein
AT1G18860	WRKY61	5.23186	6.19E-11	WRKY DNA-binding protein 61
AT1G19000	F14D16.15	0.612185	0.00042	Homeodomain-like superfamily protein
AT1G20080	SYTB	1.29265	0.0016	Calcium-dependent lipid-binding (CaLB domain) family protein
AT1G23870	TPS9	1.08466	0.000207	trehalose-phosphatase/synthase 9
AT1G28327	F3H9.2	6.08527	4.98E-05	E3 ubiquitin-protein ligase
AT1G35670	CDPK2	0.951308	0.002608	calcium-dependent protein kinase 2
AT1G37130	NIA2	2.11346	1.5E-12	nitrate reductase 2
AT1G52680	F6D8.10	1.44715	0.003143	late embryogenesis abundant protein-related / LEA protein-like protein
AT1G55660	F20N2.9	2.259	0.001557	FBD, F-box and Leucine Rich Repeat domains containing protein
AT1G59890	SNL5	0.53934	0.000717	SIN3-like 5
AT1G69100	F4N2.8	1.96584	1.47E-11	Eukaryotic aspartyl protease family protein
AT1G70290	TPS8	0.785327	0.000224	trehalose-6-phosphatase synthase S8
AT1G72770	HAB1	0.396517	0.000567	HYPERSENSITIVE TO ABA1
AT1G74810	BOR5	1.99744	0.000113	HCO3- transporter family
AT1G77760	NIA1	1.15694	6.83E-05	nitrate reductase 1
AT1G78290	SNRK2-8	0.959954	0.000222	Protein kinase superfamily protein
AT1G80180	F18B13.26	1.14113	0.000246	hypothetical protein AT1G80180
AT2G02120	PDF2.1	2.05689	7.93E-05	Scorpion toxin-like knottin superfamily protein
AT2G28800	ALB3	0.561505	0.002489	63 kDa inner membrane family protein
AT2G29940	ABCG31	1.35939	2.44E-05	pleiotropic drug resistance 3
AT2G30240	ATCHX13	3.40899	1.9E-05	Cation/hydrogen exchanger family protein
AT2G35800	SAMTL	0.972463	0.000998	mitochondrial substrate carrier family protein
AT2G40400	BPG3	0.842406	3.49E-05	DUF399 family protein, putative (DUF399 and DUF3411)
AT2G46220	T3F17.13	0.910065	0.001752	DUF2358 family protein (DUF2358)
AT3G01060	T4P13.26	0.79843	0.003297	lysine-tRNA ligase
AT3G01900	CYP94B2	3.53445	2.97E-05	cytochrome P450, family 94, subfamily B, polypeptide 2
AT3G02480	F16B3.11	1.91565	7.27E-07	Late embryogenesis abundant protein (LEA) family protein
AT3G09240	BSK9	4.24345	4.43E-09	kinase with tetratricopeptide repeat domain-containing protein
AT3G09520	EXO70H4	3.19734	8.54E-06	exocyst subunit exo70 family protein H4
AT3G21870	CYCP2%3B1	1.95144	0.000229	cyclin p2;1
AT3G23270	AT3G23270	1.27425	0.00225	Regulator of chromosome condensation (RCC1) family with FYVE zinc finger domain-containing protein
AT3G28345	ABCB15	2.57054	2.99E-12	ABC transporter family protein
AT3G28840	AT3G28840	2.20155	6.32E-09	hypothetical protein (DUF1216)
AT3G45870	UMAMIT3	1.55453	7.21E-05	nodulin MtN21 /EamA-like transporter family protein
AT3G53800	Fes1B	0.798072	0.001892	Fes1B
AT3G60750	AtTKL1	0.785451	0.000162	Transketolase
AT4G00955	AT4G00955	2.70456	1.42E-07	wall-associated receptor kinase-like protein
AT4G01470	TIP1%3B3	2.09211	0.00016	tonoplast intrinsic protein 1;3
AT4G10220	T9A4.9	2.04282	0.001354	NEP-interacting protein, putative (DUF239)
AT4G13230	F17N18.16	1.9733	0.000636	Late embryogenesis abundant protein (LEA) family protein
AT4G24140	T19F6.130	1.94183	5.81E-05	alpha/beta-Hydrolases superfamily protein
AT4G24680	MOS1	0.369864	0.002257	modifier of snc1
AT4G32375	AT4G32375	4.26237	3.21E-10	Pectin lyase-like superfamily protein
AT4G33010	GLDP1	1.06502	0.002346	glycine decarboxylase P-protein 1
AT5G02840	LCL1	0.745889	0.000868	LHY/CCA1-like 1
AT5G03570	IREG2	2.32284	0.000126	iron-regulated 2
AT5G19560	ROPGEF10	4.76675	7.35E-08	ROP uanine nucleotide exchange factor 10
AT5G26250	T19G15.100	2.11502	0.000683	Major facilitator superfamily protein
AT5G27350	SFP1	2.09483	4.18E-12	Major facilitator superfamily protein
AT5G35970	MEE13.8	1.16671	6E-05	P-loop containing nucleoside triphosphate hydrolases superfamily protein
AT5G40260	SWEET8	1.35319	0.001782	Nodulin MtN3 family protein
AT5G44300	K9L2.6	1.85059	0.000372	Dormancy/auxin-associated family protein
AT5G50210	QS	1.32193	2.6E-05	quinolinate synthase
AT5G57400	MSF19.6	2.17623	0.000161	transmembrane protein

AT5G64940	ATH13	0.771677	0.000924	ABC2 homolog 13

Annexure_5: Summary of 111 down-regulated genes common to athmgb15-1 and athmgb15-4 mutants.

Gene ID	Gene Name	log2 FC	P-value	Gene Description
AT1G01460	PIPK11	-2.34744	1.24E-12	Phosphatidylinositol-4-phosphate 5-kinase, core
AT1G01980	F22M8.11	-1.05833	0.001156	FAD-binding Berberine family protein
AT1G03457	AtBRN2	-1.102	8.31E-06	RNA-binding (RRM/RBD/RNP motifs) family protein
AT1G04880	F13M7.13	-3.5488	3.71E-08	HMG (high mobility group) box protein with ARID/BRIGHT DNA-binding domain-containing protein
AT1G05020	T7A14.11	-1.61579	0.000279	ENTH/ANTH/VHS superfamily protein
AT1G07350	SR45a	-0.99771	0	RNA-binding (RRM/RBD/RNP motifs) family protein
AT1G10620	PERK11	-1.29226	0.001796	Protein kinase superfamily protein
AT1G10680	PGP10	-1.44938	0.002629	P-glycoprotein 10
AT1G12750	RBL6	-0.6153	0.00087	RHOMBOID-like protein 6
AT1G16840	F17F16.27	-0.51795	0.001079	hypothetical protein AT1G16840
AT1G17540	F1L3.25	-1.20519	4.52E-05	kinase with adenine nucleotide alpha hydrolases-like domain-containing protein
AT1G19090	RKF2	-3.69642	1.24E-10	receptor-like serine/threonine kinase 2
AT1G23350	F26F24.23	-1.73771	8.68E-09	Plant invertase/pectin methylesterase inhibitor superfamily protein
AT1G23710	F5O8.26	-1.08494	0.000346	hypothetical protein (DUF1645)
AT1G24110	F3I6.3	-5.09639	9.42E-11	Peroxidase superfamily protein
AT1G30710	T5I8.16	-1.07633	0.000252	FAD-binding Berberine family protein
AT1G44160	T7O23.16	-1.73347	1.58E-07	HSP40/DnaJ peptide-binding protein
AT1G47270	TLP6	-0.96633	4.34E-13	tubby like protein 6
AT1G50610	PRK5	-1.12251	0.000621	Leucine-rich repeat protein kinase family protein
AT1G61290	SYP124	-1.71978	3.22E-09	syntaxin of plants 124
AT1G61860	F8K4.7	-1.8682	6.39E-10	Protein kinase superfamily protein
AT1G62320	F24O1.4	-2.62542	2.71E-06	ERD (early-responsive to dehydration stress) family protein
AT1G66210	T6J19.3	-2.4767	2.89E-15	Subtilisin-like serine endopeptidase family protein
AT1G67480	T1F15.5	-0.6348	2.23E-06	Galactose oxidase/kelch repeat superfamily protein
AT1G67623	F12A21.25	-5.46929	0.000264	F-box family protein
AT1G69840	T17F3.13	-1.03025	2.6E-06	SPFH/Band 7/PHB domain-containing membrane-associated protein family
AT1G71697	CK1	-0.92439	0.001801	choline kinase 1
AT1G72520	LOX4	-2.60738	2.22E-16	PLAT/LH2 domain-containing lipoxygenase family protein
AT1G74010	F2P9.12	-1.23837	8.03E-05	Calcium-dependent phosphotriesterase superfamily protein
AT1G74310	HSP101	-1.38554	1.06E-05	heat shock protein 101
AT1G74450	F1M20.13	-1.32644	7.42E-06	BPS1-like protein (DUF793)
AT1G76600	F14G6.20	-1.2433	0.000153	poly polymerase
AT2G01450	MPK17	-0.80974	2.29E-05	MAP kinase 17
AT2G03840	TET13	-3.93937	9.35E-10	tetraspanin13
AT2G04220	T23O15.16	-2.49835	2.58E-05	DUF868 family protein (DUF868)
AT2G05850	scpl38	-1.85773	1.23E-09	serine carboxypeptidase-like 38
AT2G17660	AT2G17660	-1.6158	9.64E-05	RPM1-interacting protein 4 (RIN4) family protein
AT2G18180	F8D23.4	-1.04514	2.71E-14	Sec14p-like phosphatidylinositol transfer family protein
AT2G19050	T20K24.6	-2.62033	0	GDSL-like Lipase/Acylhydrolase superfamily protein
AT2G21540	SFH3	-0.99197	0	SEC14-like 3

AT2G21990	F7D8.31	-1.85875	2.36E-06	MIZU-KUSSEI-like protein (Protein of unknown function, DUF617)
AT2G22860	PSK2	-1.14872	0.002667	phytosulfokine 2 precursor
AT2G23340	DEAR3	-1.04225	0.00158	DREB and EAR motif protein 3
AT2G24320	T28I24.5	-1.38071	0.000212	alpha/beta-Hydrolases superfamily protein
AT2G25600	SPIK	-1.30391	2.18E-05	Shaker pollen inward K+ channel
AT2G26410	Iqd4	-1.25274	1.27E-06	IQ-domain 4
AT2G26850	F12C20.11	-1.59667	2.23E-08	F-box family protein
AT2G27580	F10A12.25	-1.15069	8.28E-07	A20/AN1-like zinc finger family protein
AT2G28180	ATCHX8	-1.27382	2.02E-05	cation/hydrogen exchanger family protein
AT2G28640	EXO70H5	-1.94839	6.76E-05	exocyst subunit exo70 family protein H5
AT2G32150	F22D22.10	-1.18211	0	Haloacid dehalogenase-like hydrolase (HAD) superfamily protein
AT2G33100	CSLD1	-2.52898	8.88E-16	cellulose synthase-like D1
AT2G37980	T8P21.11	-1.30135	0.000668	O-fucosyltransferase family protein
AT2G38500	T6A23.30	-1.48867	6.69E-06	2-oxoglutarate (2OG) and Fe(II)-dependent oxygenase superfamily protein
AT2G41860	CPK14	-1.2639	1.95E-10	calcium-dependent protein kinase 14
AT2G41880	GK-1	-0.77777	4.3E-05	guanylate kinase 1
AT2G46360	F11C10.5	-1.58463	1.14E-06	hypothetical protein AT2G46360
AT3G02040	SRG3	-1.01676	0.001189	senescence-related gene 3
AT3G02555	AT3G02555	-1.03214	1.45E-06	hypothetical protein AT3G02555
AT3G02970	EXL6	-1.15493	9.05E-05	EXORDIUM like 6
AT3G04630	WDL1	-0.74309	5.26E-07	WVD2-like 1
AT3G04640	F7O18.12	-0.83117	2.83E-07	glycine-rich protein
AT3G05140	RBK2	-4.43805	0	ROP binding protein kinases 2
AT3G05150	T12H1.11	-0.9919	1.66E-05	Major facilitator superfamily protein
AT3G08720	S6K2	-1.03653	6.41E-07	serine/threonine protein kinase 2
AT3G13660	AT3G13660	-1.60101	0.000424	Disease resistance-responsive (dirigent-like protein) family protein
AT3G13900	AT3G13900	-1.04304	0.001936	ATPase E1-E2 type family protein / haloacid dehalogenase-like hydrolase family protein
AT3G16860	COBL8	-1.15602	0.001412	COBRA-like protein 8 precursor
AT3G18220	LPP4	-0.94486	0.003356	Phosphatidic acid phosphatase (PAP2) family protein
AT3G18810	PERK6	-1.16818	8.11E-05	Protein kinase superfamily protein
AT3G20190	PRK4	-1.30763	3.33E-15	Leucine-rich repeat protein kinase family protein
AT3G21570	AT3G21570	-3.8023	0	proline-rich nuclear receptor coactivator
AT3G23170	AT3G23170	-1.6391	4.38E-08	hypothetical protein AT3G23170
AT3G48450	AT3G48450	-1.73993	1.1E-06	RPM1-interacting protein 4 (RIN4) family protein
AT3G52800	AT3G52800	-0.89083	0.001183	A20/AN1-like zinc finger family protein
AT3G57140	SDP1-LIKE	-0.84219	0.000782	sugar-dependent 1-like protein
AT3G57390	AGL18	-0.80995	0.003278	AGAMOUS-like 18
AT3G57450	AT3G57450	-1.76412	4.44E-09	hypothetical protein AT3G57450
AT4G00350	A_IG005I10.20	-1.2641	1.99E-05	MATE efflux family protein
AT4G04610	APR1	-1.02327	0.000558	APS reductase 1
AT4G04980	C17L7.1	-2.35611	0	hypothetical protein AT4G04980
AT4G15200	FH3	-0.98481	7.39E-06	formin 3
AT4G15650	DL3865W	-2.11011	0.000386	kinase-like protein
AT4G16745	AT4G16745	-0.90241	0.00211	Exostosin family protein
AT4G18950	F13C5.120	-0.89039	0.000106	Integrin-linked protein kinase family
AT4G20380	LSD1	-0.85732	5.07E-11	LSD1 zinc finger family protein
AT4G24570	DIC2	-1.09752	0.000191	dicarboxylate carrier 2
AT4G29780	F27B13.20	-1.38359	1.31E-05	nuclease
AT4G30440	GAE1	-1.0017	0.001356	UDP-D-glucuronate 4-epimerase 1
AT4G31780	MGD1	-1.07626	6.49E-10	monogalactosyl diacylglycerol synthase 1
AT4G39180	SEC14	-0.68397	6.92E-06	Sec14p-like phosphatidylinositol transfer family protein
AT5G05140	MUG13.28	-0.87983	0.002665	Transcription elongation factor (TFIIS) family protein

AT5G12180	CPK17	-1.17293	8.86E-05	calcium-dependent protein kinase 17
AT5G13190	GILP	-1.77916	8.71E-10	GSH-induced LITAF domain protein
AT5G17850	MVA3.200	-1.28566	2.54E-07	Sodium/calcium exchanger family protein
AT5G20390	F5O24.280	-1.96947	1.82E-10	Glycosyl hydrolase superfamily protein
AT5G20690	PRK6	-1.66004	0.000237	Leucine-rich repeat protein kinase family protein
AT5G23270	STP11	-2.68864	0	sugar transporter 11
AT5G25430	F18G18.170	-3.86255	4.33E-14	HCO3- transporter family
AT5G25450	F18G18.190	-1.03626	0.00061	Cytochrome bd ubiquinol oxidase, 14kDa subunit
AT5G39420	cdc2cAt	-1.59181	9.8E-08	CDC2C
AT5G40155	AT5G40155	-1.30898	0.001049	Defensin-like (DEFL) family protein
AT5G42490	MDH9.19	-0.793	0.002424	ATP binding microtubule motor family protein
AT5G45840	K15I22.4	-0.90461	0.000833	Leucine-rich repeat protein kinase family protein
AT5G46770	MZA15.19	-1.38336	6.26E-05	hypothetical protein AT5G46770
AT5G48140	MIF21.3	-3.51014	0	Pectin lyase-like superfamily protein
AT5G52640	HSP90.1	-1.15773	0.00018	heat shock-like protein
AT5G54940	MBG8.21	-0.84815	7.58E-06	Translation initiation factor SUI1 family protein
AT5G55980	MDA7.2	-5.82338	4.36E-11	serine-rich protein-like protein
AT5G56160	MDA7.22	-1.29173	2.81E-07	Sec14p-like phosphatidylinositol transfer family protein
AT5G61360	MFB13.14	-1.30813	0.000334	hypothetical protein AT5G61360

Annexure_6: Summary of down-regulated genes common to athmgb15-4 flowers (RNA-seq) vs wildtype seedlings (ChIP on ChIP).

Gene ID	GeneName	Gene ID	GeneName	Gene ID	GeneName
AT1G01140	CIPK9	AT5G47910	RBOHD	AT1G54050	F15I1.13
AT1G01260	F6F3.7	AT5G52310	LTI78	AT1G55450	T5A14.14
AT1G01980	F22M8.11	AT5G54240	MDK4.6	AT1G58420	F9K23.5
AT1G02400	GA2OX6	AT5G54490	PBP1	AT1G62975	AT1G62975
AT1G02930	GSTF6	AT5G55090	MAPKKK15	AT1G66210	T6J19.3
AT1G03457	AtBRN2	AT5G57690	DGK4	AT1G66370	MYB113
AT1G04470	F19P19.7	AT5G59370	ACT4	AT1G67480	T1F15.5
AT1G04880	F13M7.13	AT5G64750	ABR1	AT1G69600	ZFHD1
AT1G05580	CHX23	AT5G65280	GCL1	AT1G69900	T17F3.7
AT1G05710	F3F20.16	AT1G01250	F6F3.6	AT1G70130	F20P5.15
AT1G05820	SPPL5	AT1G04540	T1G11.21	AT1G70270	F17O7.20
AT1G06640	F12K11.27	AT1G11185	AT1G11185	AT1G70790	F15H11.4
AT1G08140	CHX6A	AT1G12750	RBL6	AT1G71000	F15H11.19
AT1G08150	ATCHX5	AT1G14870	PCR2	AT1G72330	ALAAT2
AT1G08290	WIP3	AT1G16440	RSH3	AT1G72920	F3N23.12
AT1G08930	ERD6	AT1G18140	LAC1	AT1G73010	PS2
AT1G10620	PERK11	AT1G18710	MYB47	AT1G74010	F2P9.12
AT1G10680	PGP10	AT1G19380	F18O14.10	AT1G74100	SOT16
AT1G11960	F12F1.17	AT1G20823	F2D10.34	AT1G74310	HSP101
AT1G13970	F16A14.19	AT1G24405	AT1G24405	AT1G74440	F1M20.12
AT1G17420	LOX3	AT1G25250	IDD16	AT1G74450	F1M20.13
AT1G18210	T10F20.22	AT1G28370	ERF11	AT1G74930	ORA47
AT1G23710	F5O8.26	AT1G29690	CAD1	AT1G74950	TIFY10B
AT1G24070	CSLA10	AT1G30135	JAZ8	AT1G75160	F22H5.11
AT1G25240	F4F7.37	AT1G32640	MYC2	AT1G76370	F15M4.13
AT1G27730	STZ	AT1G32928	AT1G32928	AT1G76680	OPR1
AT1G31550	T8E3.19	AT1G43160	RAP2.6	AT1G76970	F22K20.7
AT1G35210	T32G9.25	AT1G47270	TLP6	AT2G01422	AT2G01422
AT1G44160	T7O23.16	AT1G48020	PMEI1	AT2G01450	MPK17

AT1G47280	T3F24.20	AT1G51090	F23H24.15	AT2G07040	PRK2A
AT1G49490	F13F21.7	AT1G56660	F25P12.91	AT2G13800	SERK5
AT1G50110	F2J10.4	AT1G61890	F8K4.9	AT2G17280	F5J6.4
AT1G50610	PRK5	AT1G63860	T12P18.12	AT2G17840	ERD7
AT1G50750	F4M15.2	AT1G64740	TUA1	AT2G18470	PERK4
AT1G51620	F19C24.15	AT1G65970	TPX2	AT2G19980	T2G17.22
AT1G51760	IAR3	AT1G66080	F15E12.12	AT2G21500	F3K23.26
AT1G52700	F6D8.5	AT1G66120	AAE11	AT2G22860	PSK2
AT1G54070	F15I1.15	AT1G66160	CMPG1	AT2G25600	SPIK
AT1G54280	F20D21.10	AT1G67060	F1O19.19	AT2G27500	F10A12.18
AT1G55310	SCL33	AT1G68740	PHO1%3BH1	AT2G29440	GSTU6
AT1G56140	T6H22.26	AT1G71880	SUC1	AT2G31830	5PTase14
AT1G56540	F25P12.101	AT1G73500	MKK9	AT2G33580	LYK5
AT1G58200	MSL3	AT1G74430	MYB95	AT2G33775	RALFL19
AT1G59910	F23H11.22	AT1G80540	T21F11.13	AT2G35930	PUB23
AT1G61120	TPS04	AT1G80840	WRKY40	AT2G38010	T8P21.8
AT1G61290	SYP124	AT2G01180	PAP1	AT2G38240	F16M14.17
AT1G61860	F8K4.7	AT2G01670	NUDT17	AT2G38290	AMT2
AT1G62320	F24O1.4	AT2G02720	T20F6.14	AT2G40116	AT2G40116
AT1G63030	ddf2	AT2G20320	F11A3.13	AT2G40820	T20B5.2
AT1G63090	PP2-A11	AT2G20630	PIA1	AT2G41100	TCH3
AT1G64380	F15H21.12	AT2G22770	NAI1	AT2G43230	F14B2.17
AT1G65390	PP2-A5	AT2G23340	DEAR3	AT2G44810	DAD1
AT1G65480	FT	AT2G25735	AT2G25735	AT2G46370	JAR1
AT1G66090	F15E12.17	AT2G26190	T1D16.17	AT3G01630	F4P13.17
AT1G67640	F12B7.20	AT2G26450	T9J22.12	AT3G02550	LBD41
AT1G68250	T22E19.12	AT2G27080	T20P8.13	AT3G03800	SYP131
AT1G68500	T26J14.7	AT2G27690	CYP94C1	AT3G04640	F7O18.12
AT1G69930	GSTU11	AT2G28085	SAUR42	AT3G05140	RBK2
AT1G70700	TIFY7	AT2G28180	ATCHX8	AT3G05320	T12H1.29
AT1G71110	F23N20.10	AT2G30020	AP2C1	AT3G06260	GATL4
AT1G72510	T10D10.2	AT2G30040	MAPKKK14	AT3G06890	AT3G06890
AT1G73080	PEPR1	AT2G32140	F22D22.11	AT3G07195	AT3G07195
AT1G73210	T18K17.12	AT2G33100	CSLD1	AT3G07850	AT3G07850
AT1G73860	F2P9.27	AT2G33420	F4P9.19	AT3G08710	TH9
AT1G76600	F14G6.20	AT2G34600	JAZ7	AT3G08970	ATERDJ3A
AT1G77450	NAC032	AT2G35765	AT2G35765	AT3G09530	EXO70H3
AT1G78070	F28K19.28	AT2G36020	HVA22J	AT3G10915	AT3G10915
AT1G78280	F3F9.18	AT2G37980	T8P21.11	AT3G11480	BSMT1
AT1G79860	ROPGEF12	AT2G39650	F12L6.31	AT3G12690	AGC1.5
AT1G79910	F19K16.13	AT2G41880	GK-1	AT3G13110	SERAT2%3B2
AT2G01150	RHA2B	AT2G46270	GBF3	AT3G14590	NTMC2T6.2
AT2G06050	OPR3	AT2G46360	F11C10.5	AT3G14870	AT3G14870
AT2G14290	T1O16.12	AT2G46400	WRKY46	AT3G15210	ERF4
AT2G14750	APK	AT3G02040	SRG3	AT3G15530	AT3G15530
AT2G17500	MJB20.6	AT3G02410	ICME-LIKE2	AT3G15540	IAA19
AT2G17890	CPK16	AT3G02555	AT3G02555	AT3G17611	RBL14
AT2G21510	F3K23.27	AT3G03020	F13E7.3	AT3G19240	AT3G19240
AT2G21540	SFH3	AT3G07090	AT3G07090	AT3G19970	AT3G19970
AT2G22500	UCP5	AT3G07760	MLP3.21	AT3G20190	PRK4
AT2G22760	T30L20.2	AT3G09350	Fes1A	AT3G25730	EDF3
AT2G25460	F13B15.12	AT3G10040	HRA1	AT3G25780	AOC3
AT2G26410	Iqd4	AT3G10930	AT3G10930	AT3G26934	AT3G26934
AT2G26420	PIP5K3	AT3G13900	AT3G13900	AT3G27540	AT3G27540
AT2G26850	F12C20.11	AT3G17120	AT3G17120	AT3G36659	AT3G36659
AT2G28580	T8O18.13	AT3G19310	AT3G19310	AT3G42880	PRK3
AT2G28640	EXO70H5	AT3G19550	AT3G19550	AT3G44930	CHX10
AT2G29450	GSTU5	AT3G19830	NTMC2T5.2	AT3G45640	MPK3

AT2G30650	T11J7.4	AT3G21700	SGP2	AT3G48520	CYP94B3
AT2G30830	F7F1.4	AT3G23170	AT3G23170	AT3G49530	NAC062
AT2G32200	F22D22.5	AT3G23250	MYB15	AT3G50060	MYB77
AT2G38500	T6A23.30	AT3G27210	AT3G27210	AT3G50950	ZAR1
AT2G38940	PHT1%3B4	AT3G28153	MMG15.19	AT3G51450	AT3G51450
AT2G41860	CPK14	AT3G43250	AT3G43250	AT3G52010	scpl37
AT2G42760	F7D19.24	AT3G44190	AT3G44190	AT3G52400	SYP122
AT2G44970	T14P1.23	AT3G44260	CAF1a	AT3G54000	AT3G54000
AT2G46500	PI4K GAMMA 4	AT3G48450	AT3G48450	AT3G54800	AT3G54800
AT3G01085	AT3G01085	AT3G52470	AT3G52470	AT3G56180	AT3G56180
AT3G01990	ACR6	AT3G55100	ABCG17	AT3G56600	AT3G56600
AT3G02840	F13E7.22	AT3G57450	AT3G57450	AT3G57390	AGL18
AT3G04220	T6K12.16	AT3G59830	AT3G59830	AT3G57880	AT3G57880
AT3G05500	F22F7.5	AT4G04930	DES-1-LIKE	AT3G58480	AT3G58480
AT3G05610	F18C1.12	AT4G07960	CSLC12	AT3G58790	GAUT15
AT3G05725	AT3G05725	AT4G08630	T3F12.6	AT3G59220	PRN
AT3G10300	AT3G10300	AT4G10380	NIP5%3B1	AT3G60490	AT3G60490
AT3G11690	AT3G11690	AT4G11660	AT-HSFB2B	AT3G61190	BAP1
AT3G11850	AT3G11850	AT4G15980	DL4030C	AT3G62260	AT3G62260
AT3G14200	AT3G14200	AT4G17500	ERF-1	AT3G62720	XT1
AT3G14440	NCED3	AT4G17615	CBL1	AT3G63380	ACA12
AT3G16720	ATL2	AT4G20320	F1C12.230	AT4G00780	A_TM018A10.12
AT3G16860	COBL8	AT4G20830	F21C20.180	AT4G01250	WRKY22
AT3G17060	AT3G17060	AT4G21910	T8O5.120	AT4G02250	T2H3.11
AT3G17690	CNGC19	AT4G21990	APR3	AT4G02650	T10P11.8
AT3G17860	JAZ3	AT4G25830	CASP-like protein 2C1	AT4G04610	APR1
AT3G18220	LPP4	AT4G27350	F27G19.7	AT4G04980	C17L7.1
AT3G18810	PERK6	AT4G27580	T29A15.70	AT4G05010	FBS3
AT3G19150	KRP6	AT4G27657	AT4G27657	AT4G08170	T12G13.10
AT3G21180	ACA9	AT4G28250	EXPB3	AT4G12040	SAP7
AT3G24420	AT3G24420	AT4G32510	L23H3.1	AT4G12720	NUDT7
AT3G43120	SAUR39	AT4G35160	T12J5.30	AT4G12790	T20K18.140
AT3G43860	GH9A4	AT4G35480	RHA3B	AT4G13240	ROPGEF9
AT3G44560	FAR8	AT4G38950	F19H22.50	AT4G16730	TPS02
AT3G45280	SYP72	AT4G39940	AKN2	AT4G17250	DL4660W
AT3G46620	RDUF1	AT5G01700	F7A7.220	AT4G17470	DL4770C
AT3G49580	LSU1	AT5G06320	NHL3	AT4G20380	LSD1
AT3G50760	GATL2	AT5G06710	HAT14	AT4G21570	F17L22.30
AT3G50930	BCS1	AT5G14700	T9L3.2	AT4G22690	CYP706A1
AT3G52770	ZPR3	AT5G15600	SP1L4	AT4G22880	LDOX
AT3G52800	AT3G52800	AT5G15960	KIN1	AT4G23060	IQD22
AT3G55980	SZF1	AT5G16540	ZFN3	AT4G23570	SGT1A
AT3G57140	SDP1-LIKE	AT5G17350	MKP11.31	AT4G24160	T19F6.150
AT3G57530	CPK32	AT5G18310	F20L16.30	AT4G26400	M3E9.170
AT3G60260	AT3G60260	AT5G24310	ABIL3	AT4G27410	RD26
AT4G00350	A_IG005I10.20	AT5G24660	LSU2	AT4G27652	AT4G27652
AT4G02380	SAG21	AT5G24880	F6A4.90	AT4G27654	AT4G27654
AT4G02600	MLO1	AT5G25430	F18G18.170	AT4G29670	ACHT2
AT4G04955	ALN	AT5G38700	MBB18.26	AT4G30440	GAE1
AT4G05120	FUR1	AT5G39400	PTEN1	AT4G31780	MGD1
AT4G10390	F7L13.4	AT5G39420	cdc2cAt	AT4G31800	WRKY18
AT4G11280	ACS6	AT5G43650	BHLH92	AT4G33970	F17I5.160
AT4G11810	T26M18.20	AT5G44640	BGLU13	AT4G34150	F28A23.90
AT4G15200	FH3	AT5G46770	MZA15.19	AT4G34410	RRTF1
AT4G15210	BAM5	AT5G47230	ERF5	AT4G34440	PERK5
AT4G16745	AT4G16745	AT5G48140	MIF21.3	AT4G36500	AP22.75
AT4G17230	SCL13	AT5G49280	K21P3.16	AT4G36950	MAPKKK21
AT4G17490	ERF6	AT5G49520	WRKY48	AT4G39180	SEC14

AT4G19960	KUP9	AT5G52320	CYP96A4	AT5G02580	T22P11.170
AT4G22780	ACR7	AT5G54130	AT5G54130	AT5G06510	NF-YA10
AT4G26260	MIOX4	AT5G54780	MBG8.4	AT5G07990	TT7
AT4G27860	MEB1	AT5G56160	MDA7.22	AT5G08790	ATAF2
AT4G27960	UBC9	AT5G59480	F2O15.10	AT5G12180	CPK17
AT4G28400	F20O9.80	AT5G59580	UGT76E1	AT5G13190	GILP
AT4G30280	XTH18	AT5G60615	AT5G60615	AT5G13700	PAO1
AT4G32630	F4D11.170	AT5G63370	CDKG1	AT5G17490	RGL3
AT4G32800	T16I18.10	AT5G65920	K14B20.9	AT5G18860	NSH3
AT4G33860	F17I5.50	AT5G66620	DAR6	AT5G20390	F5O24.280
AT4G33920	APD5	AT1G01470	LEA14	AT5G20690	PRK6
AT4G34750	F11I11.5	AT1G02810	F22D16.20	AT5G22690	MDJ22.11
AT5G01100	FRB1	AT1G05020	T7A14.11	AT5G24105	AGP41
AT5G02200	FHL	AT1G06620	F12K11.24	AT5G25450	F18G18.190
AT5G05140	MUG13.28	AT1G07330	F22G5.33	AT5G26030	FC1
AT5G07010	ST2A	AT1G07350	SR45a	AT5G28680	ANX2
AT5G07920	DGK1	AT1G09932	AT1G09932	AT5G38120	4CL8
AT5G10260	RABH1e	AT1G09950	RAS1	AT5G40350	MYB24
AT5G10660	MAJ23.20	AT1G11000	MLO4	AT5G41120	MEE6.19
AT5G12000	F14F18.170	AT1G11670	F25C20.18	AT5G41740	MUF8.2
AT5G12020	HSP17.6II	AT1G12610	DDF1	AT5G42380	CML37
AT5G16190	CSLA11	AT1G14200	F7A19.29	AT5G45350	MFC19.1
AT5G16500	LIP1	AT1G14540	PER4	AT5G45840	K15I22.4
AT5G18910	F17K4.160	AT1G15010	T15D22.5	AT5G47730	MCA23.5
AT5G19110	T24G5.10	AT1G16030	Hsp70b	AT5G48655	AT5G48655
AT5G19260	FAF3	AT1G17750	PEPR2	AT5G48850	ATSDI1
AT5G21960	AT5G21960	AT1G18990	F14D16.14	AT5G49152	AT5G49152
AT5G22630	ADT5	AT1G19090	RKF2	AT5G49920	K9P8.6
AT5G24290	MEB2	AT1G19180	JAZ1	AT5G51460	ATTPPA
AT5G24590	TIP	AT1G20310	F14O10.9	AT5G52020	MSG15.10
AT5G25340	F18G18.80	AT1G23110	T26J12.20	AT5G52400	CYP715A1
AT5G26220	AtGGCT2%3B1	AT1G24110	F3I6.3	AT5G52640	HSP90.1
AT5G27520	PNC2	AT1G24330	F3I6.27	AT5G53050	MNB8.11
AT5G28237	AT5G28237	AT1G26480	GRF12	AT5G54095	AT5G54095
AT5G28646	WVD2	AT1G26730	T24P13.11	AT5G54710	K5F14.6
AT5G35735	AT5G35735	AT1G27020	T7N9.8	AT5G56640	MIOX5
AT5G40460	K21I16.3	AT1G27045	ATHB54	AT5G56760	SERAT1%3B1
AT5G41750	MUF8.3	AT1G27770	ACA1	AT5G56980	MHM17.10
AT5G42490	MDH9.19	AT1G28270	RALFL4	AT5G57010	MHM17.13
AT5G42650	AOS	AT1G28380	NSL1	AT5G59550	RDUF2
AT5G44350	K9L2.14	AT1G28480	GRX480	AT5G60860	RABA1f
AT5G45340	CYP707A3	AT1G29980	T1P2.9	AT5G61720	MAC9.3
AT5G46330	FLS2	AT1G32120	F3C3.9	AT5G61900	BON1
AT5G46590	NAC096	AT1G35490	F12A4.11	AT5G62570	calmodulin-binding protein 60a
AT5G47070	K14A3.2	AT1G44120	CELLULOSE SYNTHASE INTERACTIVE 2	AT5G63450	CYP94B1
AT5G47540	MNJ7.13	AT1G50740	F4M15.3	AT5G63770	DGK2
AT5G66675	AT5G66675	AT1G51490	BGLU36	AT5G63790	NAC102
AT5G67180	TOE3	AT1G52580	RBL5	AT5G64790	MXK3.1
AT1G52720	F6D8.3				

Annexure_7: Summary of up-regulated genes common to athmgb15-4 flowers (RNA-seq) vs wildtype seedlings (ChIP on ChIP).

Gene ID	GeneName	Gene ID	GeneName	Gene ID	GeneName
AT1G02820	LEA3	AT5G14200	IMD1	AT1G13700	PGL1

AT1G03090	MCCA	AT5G14260	F18O22.50	AT1G15180	F9L1.12
AT1G04580	AO4	AT5G15780	F14F8.160	AT1G16410	CYP79F1
AT1G05310	YUP8H12.7	AT5G18270	ANAC087	AT1G17020	SRG1
AT1G07390	RLP1	AT5G19190	T24G5.90	AT1G20080	SYTB
AT1G08900	F7G19.22	AT5G19560	ROPGEF10	AT1G20180	T20H2.5
AT1G09570	PHYA	AT5G20250	DIN10	AT1G21240	WAK3
AT1G10470	ARR4	AT5G21930	PAA2	AT1G21400	F24J8.4
AT1G11190	BFN1	AT5G22920	AtRZPF34	AT1G21670	F8K7.9
AT1G11260	STP1	AT5G23010	MAM1	AT1G22120	F2E2.19
AT1G12010	F12F1.12	AT5G24150	SQP1	AT1G23870	TPS9
AT1G13650	F21F23.9	AT5G24470	PRR5	AT1G25440	BBX15
AT1G15290	F9L1.23	AT5G25120	CYP71B11	AT1G25550	AT1G25550
AT1G15950	CCR1	AT5G25260	F21J6.109	AT1G28327	F3H9.2
AT1G17030	F20D23.27	AT5G25630	T14C9.170	AT1G28660	AT1G28660
AT1G18270	T10O22.24	AT5G25840	F18A17.90	AT1G31820	PUT1
AT1G18830	F6A14.8	AT5G27350	SFP1	AT1G33720	CYP76C6
AT1G18860	WRKY61	AT5G30584	AT5G30584	AT1G34760	GRF11
AT1G19000	F14D16.15	AT5G35970	MEE13.8	AT1G42550	PMI1
AT1G19660	AtBBD2	AT5G42820	U2AF35B	AT1G43850	SEU
AT1G19850	MP	AT5G43570	K9D7.7	AT1G44446	CH1
AT1G21580	F24J8.17	AT5G45240	K18C1.12	AT1G49120	CRF9
AT1G22770	GI	AT5G45910	K15I22.11	AT1G53780	T18A20.2
AT1G23390	F26F24.26	AT5G46110	APE2	AT1G56220	F14G9.17
AT1G26230	Cpn60beta4	AT5G47560	TDT	AT1G59890	SNL5
AT1G26820	RNS3	AT5G48160	OBE2	AT1G62510	T3P18.7
AT1G27040	AtNPF4.5	AT5G49360	BXL1	AT1G65113	SCRL2
AT1G32940	SBT3.5	AT5G54190	PORA	AT1G67105	AT1G67105
AT1G33110	T9L6.1	AT5G56870	BGAL4	AT1G67700	F12A21.32
AT1G37130	NIA2	AT5G56970	CKX3	AT1G68050	FKF1
AT1G43790	TED6	AT5G57655	AT5G57655	AT1G68620	F24J5.14
AT1G47470	F16N3.31	AT5G58140	PHOT2	AT1G70100	F20P5.17
AT1G49720	ABF1	AT5G60000	MMN10.25	AT1G70290	TPS8
AT1G52690	LEA7	AT5G60060	MGO3.4	AT1G70890	MLP43
AT1G58180	BCA6	AT5G60680	MUP24.10	AT1G71030	MYBL2
AT1G58190	RLP9	AT5G60770	NRT2.4	AT1G73607	LCR65
AT1G58270	ZW9	AT5G61420	MYB28	AT1G74810	BOR5
AT1G58320	F19C14.14	AT5G63800	MUM2	AT1G78290	SNRK2-8
AT1G60140	TPS10	AT1G01240	F633.5	AT1G79520	T8K14.6
AT1G60160	T13D8.5	AT1G01480	ACS2	AT1G80440	Kelch repeat F-box 20
AT1G61810	BGLU45	AT1G03055	D27	AT1G80660	HA9
AT1G63770	F24D7.4	AT1G03220	F15K9.17	AT2G01280	MEE65
AT1G64050	F22C12.19	AT1G05330	YUP8H12.5	AT2G03140	T18E12.19
AT1G64110	DAA1	AT1G05340	YUP8H12.4	AT2G04037	AT2G04037
AT1G64710	F13O11.3	AT1G07280	F22G5.38	AT2G05100	LHCB2.1
AT1G66760	F4N21.11	AT1G10070	BCAT-2	AT2G05380	GRP3S
AT1G66970	SVL2	AT1G10682	AT1G10682	AT2G15960	F19G14.4
AT1G66980	SNC4	AT1G14700	PAP3	AT2G16505	AT2G16505
AT1G68020	ATTPS6	AT1G15380	GLYI4	AT2G16660	T24I21.7
AT1G68520	BBX14	AT1G21250	WAK1	AT2G16980	F12A24.16
AT1G68570	AtNPF3.1	AT1G21410	SKP2A	AT2G17820	HK1
AT1G69450	F10D13.27	AT1G22750	T22J18.8	AT2G21330	FBA1
AT1G72680	CAD1	AT1G26796	AT1G26796	AT2G25900	ATCTH
AT1G73260	KTI1	AT1G31710	F27M3.9	AT2G26480	UGT76D1
AT1G75460	F1B16.1	AT1G34630	F12K21.3	AT2G27150	AAO3
AT1G75750	GASA1	AT1G49500	F13F21.6	AT2G28170	ATCHX7
AT1G77760	NIA1	AT1G52680	F6D8.10	AT2G28800	ALB3
AT1G78820	F9K20.13	AT1G54790	T22H22.20	AT2G30140	UGT87A2
AT2G14095	AT2G14095	AT1G57760	T8L23.22	AT2G30950	VAR2

AT2G14560	LURP1	AT1G60600	ABC4	AT2G35800	SAMTL
AT2G18050	HIS1-3	AT1G62530	T3P18.9	AT2G36325	AT2G36325
AT2G18300	HBI1	AT1G64860	SIGA	AT2G39400	F12L6.6
AT2G18550	HB21	AT1G66840	PMI2	AT2G41190	T3K9.4
AT2G22980	SCPL13	AT1G68010	HPR	AT2G41560	ACA4
AT2G26690	AtNPF6.2	AT1G69100	F4N2.8	AT2G41850	PGAZAT
AT2G26780	F18A8.15	AT1G70680	F5A18.14	AT2G42190	T24P15.10
AT2G27930	T1E2.15	AT1G72770	HAB1	AT2G46790	PRR9
AT2G28405	LCR32	AT1G77000	SKP2B	AT3G01500	CA1
AT2G28630	KCS12	AT1G77490	TAPX	AT3G01900	CYP94B2
AT2G29090	CYP707A2	AT1G80160	GLYI7	AT3G02930	F13E7.12
AT2G29630	THIC	AT1G80180	F18B13.26	AT3G04760	F7O18.25
AT2G29940	ABCG31	AT2G02120	PDF2.1	AT3G05900	F2O10.14
AT2G30240	ATCHX13	AT2G02710	PLPB	AT3G05950	F2O10.9
AT2G30600	AT2G30610	AT2G04115	AT2G04115	AT3G06850	BCE2
AT2G31810	F20M17.15	AT2G05070	LHCB2.2	AT3G06980	AT3G06980
AT2G31945	AT2G31945	AT2G05540	T20G20.11	AT3G07970	QRT2
AT2G32530	CSLB03	AT2G13360	AGT	AT3G10740	ASD1
AT2G34790	MEE23	AT2G15620	NIR1	AT3G12320	LNK3
AT2G36080	ABS2	AT2G16535	AT2G16535	AT3G14690	CYP72A15
AT2G37130	T2N18.11	AT2G20670	F23N11.1	AT3G15630	AT3G15630
AT2G39800	P5CS1	AT2G22990	SNG1	AT3G22600	glycosylphosphatidylinositol-anchored lipid protein transfer 5
AT2G39930	ISA1	AT2G24205	AT2G24205	AT3G26280	CYP71B4
AT2G42170	T24P15.8	AT2G24820	TIC55-II	AT3G26740	CCL
AT2G42600	PPC2	AT2G25080	GPX1	AT3G28300	AT14A
AT2G43010	PIF4	AT2G25450	F13B15.11	AT3G28980	AT3G28980
AT2G43730	F18O19.16	AT2G29340	F16P2.28	AT3G29240	AT3G29240
AT2G43820	UGT74F2	AT2G34430	LHB1B1	AT3G42850	AT3G42850
AT2G44480	BGLU17	AT2G35950	EDA12	AT3G45245	AT3G45245
AT2G45220	AtPME17	AT2G36630	F13K3.3	AT3G45780	PHOT1
AT3G01060	T4P13.26	AT2G38170	CAX1	AT3G45870	UMAMIT3
AT3G01185	AT3G01185	AT2G39190	ATATH8	AT3G46290	HERK1
AT3G01310	Arabidopsis homolog of yeast Vip1 1	AT2G39410	F12L6.7	AT3G47250	AT3G47250
AT3G05160	T12H1.12	AT2G40370	LAC5	AT3G47340	ASN1
AT3G05630	PLDP2	AT2G42790	CSY3	AT3G48580	XTH11
AT3G06510	SFR2	AT2G45570	CYP76C2	AT3G50980	XERO1
AT3G06530	F5E6.14	AT3G01420	DOX1	AT3G51860	CAX3
AT3G08870	L-type lectin receptor kinase VI.1	AT3G02480	F16B3.11	AT3G53460	CP29
AT3G09220	LAC7	AT3G05155	AT3G05155	AT3G53980	AT3G53980
AT3G09260	PYK10	AT3G05165	AT3G05165	AT3G54500	LNK2
AT3G14210	ESM1	AT3G06433	F24P17.9	AT3G60130	BGLU16
AT3G15510	NAC2	AT3G07350	AT3G07350	AT3G60240	EIF4G
AT3G16857	RR1	AT3G11340	UGT76B1	AT3G63160	OEP6
AT3G18550	BRC1	AT3G13750	BGAL1	AT4G00955	AT4G00955
AT3G20250	PUM5	AT3G14770	SWEET2	AT4G04630	F4H6.15
AT3G24080	AT3G24080	AT3G15840	PIF1	AT4G05070	C17L7.2
AT3G26440	AT3G26440	AT3G17520	AT3G17520	AT4G12290	T4C9.130
AT3G28220	AT3G28220	AT3G19170	PREP1	AT4G13250	NYC1
AT3G28345	ABCB15	AT3G19710	BCAT4	AT4G14760	NET1B
AT3G28770	AT3G28770	AT3G23270	AT3G23270	AT4G15610	CASP-like protein 1D1
AT3G28840	AT3G28840	AT3G25690	CHUP1	AT4G16920	DL4490C
AT3G32980	T15D2.9	AT3G27650	LBD25	AT4G20110	VSR7
AT3G44006	AT3G44006	AT3G30247	AT3G30247	AT4G23300	CRK22
AT3G47800	AT3G47800	AT3G44300	NIT2	AT4G24140	T19F6.130

AT3G48190	ATM	AT3G45060	NRT2.6	AT4G24230	ACBP3
AT3G48200	AT3G48200	AT3G45300	IVD	AT4G24800	ECIP1
AT3G48340	CEP2	AT3G48740	SWEET11	AT4G25650	ACDI-LIKE
AT3G48360	BT2	AT3G56080	AT3G56080	AT4G26150	CGA1
AT3G51540	AT3G51540	AT3G59060	PIL6	AT4G26200	ACS7
AT3G52780	PAP20	AT3G60750	AtTKL1	AT4G28030	T13J8.140
AT3G52840	BGAL2	AT3G62750	BGLU8	AT4G30190	HA2
AT3G55610	P5CS2	AT4G01430	UMAMIT29	AT4G32250	F10M6.110
AT3G56140	AT3G56140	AT4G02280	SUS3	AT4G33010	GLDP1
AT3G57520	SIP2	AT4G04330	RbcX1	AT4G33666	AT4G33666
AT3G60140	DIN2	AT4G04590	F4H6.11	AT4G34860	A/N-InvB
AT3G62730	AT3G62730	AT4G11880	AGL14	AT4G34950	F11I11.190
AT4G00450	CCT	AT4G13230	F17N18.16	AT4G35680	F8D20.190
AT4G01470	TIP1%3B3	AT4G13263	AT4G13263	AT4G35770	SEN1
AT4G01800	AGY1	AT4G13900	RLP49	AT4G37540	LBD39
AT4G02260	RSH1	AT4G15660	DL3870W	AT4G37550	F19F18.40
AT4G04460	T26N6.7	AT4G15760	MO1	AT4G38470	STY46
AT4G09630	T25P22.70	AT4G16160	ATOEP16-2	AT4G39260	CCR1
AT4G10060	F28M11.3	AT4G16810	DL4430C	AT5G02860	F9G14.170
AT4G11650	OSM34	AT4G16890	SNC1	AT5G05740	EGY2
AT4G11890	ARCK1	AT4G18240	SS4	AT5G07080	T28J14.20
AT4G12320	CYP706A6	AT4G26140	BGAL12	AT5G09530	PELPK1
AT4G14130	XTH15	AT4G26530	FBA5	AT5G09660	PMDH2
AT4G14210	PDS3	AT4G27820	BGLU9	AT5G13320	PBS3
AT4G15690	DL3885W	AT4G29905	AT4G29905	AT5G13730	SIG4
AT4G16130	ARA1	AT4G32650	KAT3	AT5G14180	MPL1
AT4G16260	DL4170C	AT4G34320	F10M10.90	AT5G14740	CA2
AT4G16680	DL4365C	AT5G02160	AT5G02160	AT5G15850	COL1
AT4G16740	TPS03	AT5G06110	K16F4.7	AT5G16030	F1N13.170
AT4G16990	RLM3	AT5G13370	T22N19.20	AT5G16150	PGLCT
AT4G17340	TIP2%3B2	AT5G14780	FDH	AT5G16180	CRS1
AT4G18550	DSEL	AT5G23870	MRO11.9	AT5G18980	T16G12.20
AT4G18810	F28A21.220	AT5G26050	T1N24.10	AT5G23980	FRO4
AT4G19160	T18B16.130	AT5G26742	emb1138	AT5G24210	MOP9.2
AT4G19170	NCED4	AT5G38510	MBB18.4	AT5G25130	CYP71B12
AT4G21680	NRT1.8	AT5G38520	MBB18.5	AT5G26250	T19G15.100
AT4G23560	GH9B15	AT5G39590	MIJ24.8	AT5G28770	BZO2H3
AT4G24680	MOS1	AT5G40890	CLC-A	AT5G35630	GS2
AT4G25480	DREB1A	AT5G43450	MWF20.16	AT5G38660	APE1
AT4G27260	WES1	AT5G45930	CHLI2	AT5G39080	MXF12.90
AT4G29305	LCR25	AT5G46060	MCL19.11	AT5G39365	AT5G39365
AT4G30250	F9N11.100	AT5G50950	FUM2	AT5G43630	TZP
AT4G32375	AT4G32375	AT5G51890	MJM18.4	AT5G44190	GLK2
AT4G32810	CCD8	AT5G55110	MCO15.6	AT5G44973	AT5G44973
AT4G34000	ABF3	AT5G64840	ABCF5	AT5G45900	APG7
AT4G34090	F28A23.150	AT5G65210	TGA1	AT5G45980	WOX8
AT4G34830	MRL1	AT5G67390	K8K14.12	AT5G48180	NSP5
AT4G36740	HB40	AT1G02220	NAC003	AT5G48220	MIF21.11
AT4G36850	AP22.27	AT1G02580	MEA	AT5G49740	FRO7
AT4G37990	ELI3-2	AT1G04280	F19P19.28	AT5G50210	QS
AT4G38160	pde191	AT1G06280	LBD2	AT5G50270	K6A12.13
AT5G02840	LCL1	AT1G06570	PDS1	AT5G53440	MYN8.5
AT5G04140	GLU1	AT1G09740	F21M12.12	AT5G53870	ENODL1
AT5G05690	CPD	AT1G11690	F25C20.16	AT5G55700	BAM4
AT5G06220	MBL20.10	AT5G66400	RAB18	AT5G61620	K11J9.15
AT5G07690	MYB29	AT5G67030	ABA1	AT5G63420	emb2746
AT5G11050	MYB64	AT5G67420	LBD37	AT5G64170	LNK1
AT5G12860	DiT1	AT5G13950	MAC12.8	AT5G64570	XYL4

AT5G13360	T22N19.10	AT5G14060	CARAB-AK-LYS	AT5G64940	ATH13
AT5G13650	SVR3				

Annexure_8: List of differentially expressed genes involved in JA Biosynthesis, Response and Signaling.

Gene ID	Gene Name	log2 FC	P-value	Gene Description
AT2G44810	DAD1	-2.01128	5.7E-08	alpha/beta-Hydrolases superfamily protein
AT1G17420	LOX3	-2.31246	3.14E-10	lipoxygenase 3
AT3G48360	BT2	2.88277	1.04E-14	BTB and TAZ domain protein 2
AT3G48520	CYP94B3	-2.37469	1.8E-14	cytochrome P450, family 94, subfamily B, polypeptide 3
AT1G19180	JAZ1	-1.10051	0.000873	jasmonate-zim-domain protein 1
AT1G72520	LOX4	-2.60738	2.22E-16	PLAT/LH2 domain-containing lipoxygenase family protein
AT2G06050	OPR3	-2.04844	0	oxophytodienoate-reductase 3
AT2G26690	AtNPF6.2	0.976826	3.2E-05	Major facilitator superfamily protein
AT2G34600	JAZ7	-2.31716	1.88E-09	jasmonate-zim-domain protein 7
AT2G38240	F16M14.17	-1.73107	1.26E-08	2-oxoglutarate (2OG) and Fe(II)-dependent oxygenase superfamily protein
AT2G39730	RCA	1.03518	2.02E-05	rubisco activase
AT2G46370	JAR1	-1.45007	2.17E-13	Auxin-responsive GH3 family protein
AT3G01310	Arabidopsis homolog of yeast Vip1 1	0.880119	7.42E-05	Phosphoglycerate mutase-like family protein
AT3G11820	SYP121	-0.92794	3.11E-08	syntaxin of plants 121
AT3G15210	ERF4	-1.42947	1.64E-06	ethylene responsive element binding factor 4
AT3G15510	NAC2	1.63294	2.93E-05	NAC domain containing protein 2
AT3G17860	JAZ3	-0.91623	0.001405	jasmonate-zim-domain protein 3
AT3G22275	AT3G22275	-1.98991	1.44E-09	jasmonate ZIM-domain protein
AT3G23250	MYB15	-1.81747	8.37E-08	myb domain protein 15
AT3G25760	AOC1	-1.73544	2.46E-06	allene oxide cyclase 1
AT3G25770	AOC2	-1.82367	3.26E-08	allene oxide cyclase 2
AT3G25780	AOC3	-2.11777	7.35E-12	allene oxide cyclase 3
AT1G17380	JAZ5	-1.87449	0	jasmonate-zim-domain protein 5
AT1G17750	PEPR2	-1.13732	0.001665	PEP1 receptor 2
AT3G51430	YLS2	0.724339	0.000107	Calcium-dependent phosphotriesterase superfamily protein
AT3G51450	AT3G51450	-1.64814	3.84E-08	Calcium-dependent phosphotriesterase superfamily protein
AT3G52400	SYP122	-1.27794	0.000336	syntaxin of plants 122
AT1G18710	MYB47	-1.35594	0.001101	myb domain protein 47
AT4G11280	ACS6	-1.33177	9E-06	1-aminocyclopropane-1-carboxylic acid (acc) synthase 6
AT1G20510	OPCL1	-1.98438	0	OPC-8:0 CoA ligase1
AT4G16740	TPS03	1.07668	3.11E-15	terpene synthase 03
AT4G22880	LDOX	-0.83098	0.000133	leucoanthocyanidin dioxygenase
AT4G34710	ADC2	-0.83832	0.000124	arginine decarboxylase 2
AT4G35770	SEN1	3.99227	0	Rhodanese/Cell cycle control phosphatase superfamily protein
AT5G02840	LCL1	0.745889	0.000868	LHY/CCA1-like 1
AT5G05600	MOP10.14	-1.3086	1.87E-06	2-oxoglutarate (2OG) and Fe(II)-dependent oxygenase superfamily protein
AT5G07010	ST2A	-1.30106	0.000399	sulfotransferase 2A
AT5G07690	MYB29	2.5483	0.000564	myb domain protein 29
AT5G08790	ATAF2	-1.1593	0.000136	NAC (No Apical Meristem) domain transcriptional regulator superfamily protein
AT5G13220	JAZ10	-1.59693	0	jasmonate-zim-domain protein 10
AT5G17490	RGL3	-1.02382	0.002701	RGA-like protein 3

AT5G18860	*NSH3*	*-0.57288*	*0.003219*	*inosine-uridine preferring nucleoside hydrolase family protein*
AT5G40350	*MYB24*	*-0.78894*	*0.000583*	*myb domain protein 24*
AT5G42650	*AOS*	*-1.98559*	*6.93E-11*	*allene oxide synthase*
AT5G45110	*NPR3*	*-1.18997*	*2.64E-05*	*NPR1-like protein 3*
AT5G47220	*ERF2*	*-1.26707*	*6.02E-05*	*ethylene responsive element binding factor 2*
AT1G28480	*GRX480*	*-2.46458*	*2.88E-09*	*Thioredoxin superfamily protein*
AT5G54060	*UF3GT*	*-1.82756*	*0.000101*	*UDP-glucose:flavonoid 3-o-glucosyltransferase*
AT5G61420	*MYB28*	*1.02702*	*0.000525*	*myb domain protein 28*
AT1G30135	*JAZ8*	*-2.30401*	*2.04E-11*	*jasmonate-zim-domain protein 8*
AT1G32640	*MYC2*	*-1.2995*	*0.000171*	*Basic helix-loop-helix (bHLH) DNA-binding family protein*
AT1G43160	*RAP2.6*	*-1.4916*	*8.19E-07*	*related to AP2 6*
AT1G44350	*ILL6*	*-1.16789*	*8.98E-05*	*IAA-amino acid hydrolase ILR1-like 6*
AT1G61120	*TPS04*	*-1.6229*	*0.000226*	*terpene synthase 04*
AT1G61340	*FBS1*	*-1.33594*	*1.08E-07*	*F-box family protein*
AT1G66370	*MYB113*	*-2.41043*	*0.001922*	*myb domain protein 113*
AT1G70700	*TIFY7*	*-0.86371*	*1.53E-08*	*TIFY domain/Divergent CCT motif family protein*
AT1G71030	*MYBL2*	*1.62189*	*6.05E-09*	*MYB-like 2*
AT1G72450	*JAZ6*	*-1.12383*	*7.67E-05*	*jasmonate-zim-domain protein 6*
AT1G73080	*PEPR1*	*-1.08841*	*0.002434*	*PEP1 receptor 1*
AT1G74100	*SOT16*	*-1.13402*	*0.000117*	*sulfotransferase 16*
AT1G74430	*MYB95*	*-0.76474*	*0.000877*	*myb domain protein 95*
AT1G74840	*F25A4.19*	*0.642012*	*0.000332*	*Homeodomain-like superfamily protein*
AT1G74950	*TIFY10B*	*-1.11141*	*6.56E-05*	*TIFY domain/Divergent CCT motif family protein*

Conferences and Workshops

2024	*Attended 3rd Plant Cell Atlas Symposium*
2024	*Oral and Poster Presentation at ICAR 2024 (University of California San Diego, USA)- Talk dated 18th July 2024*
2024	*Oral Presentation at SEB Prague 2024 (Prague, Czech Republic) Talk dated 3rd July 2024 (doi.org/10.48448/rpy5-a375)*
2024	*Attended Plant Cell Atlas- Spatial Omics Workshop dated 9th May 2024*
2024	*Member of ASPB Early Career Plant Scientists (ASPB-ECPS)*
2024	*Member of the Society of Experimental Biologists (SEB)*
2023	*Member of the American Society of Plant Biologists (ASPB)*
2023	*Member of the North American Arabidopsis Steering Committee (NAASC)*
2022	*Poster Presentation at SBC Conference 2022, Kolkata*
2022	*Poster Presentation in Recent Trends in Science, Bose Institute*
2019	*Attended workshop on Electron Microscopy, AIIMS, New Delhi*
2019	*Member of Organizing and Volunteering team at YSC IISF 2019, Kolkata*
2018	*Participated in the Indo-Japan Conference on Epigenetics, 2018, Bose Institute*

Awards and Fellowships

2024	*International Travel Award by ITS-SERB (ANRF)*
2024	*International Travel Grant Award by CSIR*
2024	*Awarded Equity fund and Registration fee waiver to attend ICAR 2024*
2024	*ASPB-ECPS Virtual Viewing Award to Plant Biology 2024*
2022	*Best Poster Award in Recent Trends in Science*
2017	*University Gold Medal for M.Sc. in Botany*
2017	*DST-inspire Fellowship Award (Provisional)*
2017	*CSIR-UGC NET Fellowship (AIR-49)*

Mentorship and Teaching

I have served as President of the Bose Institute Research Scholars Forum for the tenure 2018-2020. Since 2019, I have been mentoring postgraduate trainees, Ms. Asmita Chakrabarty (2019), Ms. Mouli Naskar (2020), Ms. Paroma Mitra (2021) and Ms. Ayantika Nandi (2022). Notably, three of them were motivated to pursue their Ph.D. program under my guidance. Ms. Nandi is now a Graduate student of Prof. Shubho Chaudhuri's Lab group.

Publications and Reprints

2024 Sachdev S, Biswas R, Roy A, Nandi A, Roy V, Basu S, Chaudhuri S. The Arabidopsis ARID-HMG DNA-BINDING PROTEIN 15 modulates JA signaling by regulating MYC2 during pollen development. Plant Physiology

10.1093/plphys/kiae355

2020 Majumdar, S., Sachdev, S., & Kundu, R. (2020). Salicylic acid mediated reduction in grain cadmium accumulation and amelioration of toxicity in Oryza sativa L. cv Bandana. Ecotoxicology and environmental safety, 205, 111167

10.1016/j.ecoenv.2020.111167

2020 Mallik, R., Prasad, P., Kundu, A., Sachdev, S., Biswas, R., Dutta, A., Roy, A., Mukhopadhyay, J., Bag, S.K., & Chaudhuri, S. (2020). Identification of genome-wide targets and DNA recognition sequence of the Arabidopsis HMG-box protein AtHMGB15 during cold stress response. Biochimica et biophysica acta. Gene regulatory mechanisms, 194644.

doi.org/10.1016/j.bbagrm.2020.194644

Plant Physiology®

Plant Physiology, 2024, 196, 996–1013
https://doi.org/10.1093/plphys/kiae355
Advance access publication 26 June 2024
Research Article

The *Arabidopsis* ARID–HMG DNA-BINDING PROTEIN 15 modulates jasmonic acid signaling by regulating MYC2 during pollen development

Sonal Sachdev,[1] Ruby Biswas,[1] Adrita Roy,[1] Ayantika Nandi,[1] Vishal Roy,[1] Sabini Basu,[1] and Shubho Chaudhuri[1,*]

[1]Department of Biological Sciences, Bose Institute, Unified Academic Campus, EN 80, Sector V, Kolkata 700091, WB, India
*Author for correspondence: shubho@jcbose.ac.in (S.C.)
The author responsible for distribution of materials integral to the findings presented in this article in accordance with the policy described in the Instructions for Authors (https://academic.oup.com/plphys/pages/General-Instructions) is Shubho Chaudhuri.

Abstract

The intricate process of male gametophyte development in flowering plants is regulated by jasmonic acid (JA) signaling. JA signaling initiates with the activation of the basic helix–loop–helix transcription factor (TF), MYC2, leading to the expression of numerous JA-responsive genes during stamen development and pollen maturation. However, the regulation of JA signaling during different stages of male gametophyte development remains less understood. This study focuses on the characterization of the plant ARID–HMG DNA-BINDING PROTEIN 15 (*AtHMGB15*) and its role in pollen development in *Arabidopsis* (*Arabidopsis thaliana*). Phenotypic characterization of a T-DNA insertion line (*athmgb15-4*) revealed delayed bolting, shorter siliques, and reduced seed set in mutant plants compared to the wild type. Additionally, *AtHMGB15* deletion resulted in defective pollen morphology, delayed pollen germination, aberrant pollen tube growth, and a higher percentage of nonviable pollen grains. Molecular analysis indicated the downregulation of JA biosynthesis and signaling genes in the *athmgb15-4* mutant. Quantitative analysis demonstrated that JA and its derivatives were ∼10-fold lower in *athmgb15-4* flowers. Exogenous application of methyl jasmonate could restore pollen morphology and germination, suggesting that the low JA content in *athmgb15-4* impaired JA signaling during pollen development. Furthermore, our study revealed that AtHMGB15 physically interacts with MYC2 to form a transcription activation complex. This complex promotes the transcription of key JA signaling genes, the R2R3-MYB TFs *MYB21* and *MYB24*, during stamen and pollen development. Collectively, our findings highlight the role of AtHMGB15 as a positive regulator of the JA pathway, controlling the spatiotemporal expression of key regulators involved in Arabidopsis stamen and pollen development.

Introduction

The development of male gametophytes in angiosperms is a highly coordinated process, requiring the integration of various plant hormone signaling pathways (Mascarenhas 1990; Wilson and Zhang 2009; Marciniak and Przedniczek 2019). The spatiotemporal activity of key hormone signaling factors regulates the pollen maturation, anther dehiscence, release of pollen grains to the surface of the stigma, and pollen tube germination, for successful fertilization. The differentiation of sporogenous cells (pollen mother cell) in the anther gives rise to haploid microspores through meiosis. Subsequent development involves mitotic divisions and the formation of the pollen cell wall through programmed cell death of the tapetum layer (McCormick 2004; Zhang et al. 2007). The degeneration of the tapetum layer is essential for anther dehiscence and the release of mature pollen. In self-pollinating plants, anther dehiscence and the release of pollen onto the stigma depend upon the appropriate length of the stamen filament. The anthers in these self-pollinating plants are positioned at an equivalent height or above the stigma papillae, ensuring efficient pollen transfer and fertilization. Any abnormalities during pollen maturation, stamen elongation, or anther dehiscence can lead to reduced fertility or complete male sterility.

Plant hormone jasmonic acid (JA) and its derivatives are indispensable for the development of stamen and male gametophyte maturation (Huang et al. 2017b). Arabidopsis (*Arabidopsis thaliana*) mutants deficient in JA biosynthesis, viz. FATTY ACID DESATURASE 3/7/8 (*fad3fad7fad8*), DEFECTIVE IN ANTHER DEHISENCE 1 (*dad1*), LIPOOXYGENASE 3/4 (*lox3–lox4*), ALLENE OXIDE SYNTHASE (*aos*), and 12-OXOPHYTODIENOIC ACID REDUCTASE 3 (*opr3*), exhibit male sterility due to arrested stamen development at anthesis (McConn and Browse 1996; Stintzi and Browse 2000; Ishiguro et al. 2001; Park et al. 2002; Caldelari et al. 2011). These mutants have indehiscent anthers or short filaments that fail to reach the stigma surface. Although the pollen grain from these mutants initially develops normally to produce tricellular gametophyte, they lose viability during later stages (Acosta and Przybyl 2019). However, the application of exogenous JA can restore fertility in these JA biosynthesis-deficient mutants (Park et al. 2002). CORONATINE INSENSITIVE1 (COI1), an F-box protein is a part of SKP1-CULLIN1-F-box-type (SCF) E3 ubiquitin ligase complex SCF^{COI1} and a crucial component of JA signaling, forms a complex with transcriptional repressors Jasmonate ZIM-domain (JAZ) in the presence of JA-isoleucine (JA-Ile) derivative. The 26S proteasome mediates the degradation of JAZ repressor and releases the MYC transcription factor (TF) for the expression of JA-responsive genes (Xie et al. 1998; Devoto et al. 2002; Chini et al. 2007; Thines et al. 2007; Zhai et al. 2015). *coi1* mutants exhibit impaired stamen maturation and male sterility. However, unlike JA biosynthesis-deficient

Received January 18, 2024. Accepted May 7, 2024.

mutants, exogenous application of JA fails to rescue fertility in *coi1* mutants (Feys et al. 1994; Xu et al. 2002).

The MYC2 TF, a member of the basic helix–loop–helix family, is a central regulator of the JA response. MYC2 activates the transcription of JA-responsive genes by binding to G-box motifs present in their promoter regions (Dombrecht et al. 2007; Pozo et al. 2008; Figueroa and Browse 2012; Kazan and Manners 2013). Previous studies have shown that *MYC2* along with *MYC3*, *MYC4*, and *MYC5* redundantly regulates stamen development and seed production (Qi et al. 2015; Gao et al. 2016). While the single and double mutants showed no defect in stamen development, the triple mutants *myc2myc3myc4*, *myc2myc4myc5*, and *myc3myc4myc5* exhibited delayed stamen development (Dombrecht et al. 2007; Schweizer et al. 2013). The anthers of these triple mutants fail to dehisce at the floral stage13, and pollen grains are unable to germinate in vitro; however, anther dehiscence and pollen maturation occur at the later stage of flower development. Quadruple mutants, in comparison with triple mutants, exhibit more severe defects in stamen development, characterized by short stamen filaments, indehiscent anthers, and nonviable pollen grains (Qi et al. 2015).

MYC2 TF coordinates JA signaling through R2R3-type MYB TFs, specifically MYB21 and MYB24, during stamen maturation (Song et al. 2011). MYB21 and MYB24 physically interact with MYC2 forming the MYC–MYB complex for transcription activation while also interacting with JAZ to attenuate their activity (Yang et al. 2020; Zhang et al. 2021). The phytohormone gibberellin (GA) has been shown to regulate the expression of *MYB21/24* and promote stamen growth (Cheng et al. 2009). Studies indicate that DELLA inhibits JA biosynthesis by suppressing the expression of *DAD1* and *LOX1*. DELLA also interacts with MYB21/24 in the absence of GA and represses their transcriptional activity (Cheng et al. 2009). GA triggers the ubiquitination of DELLA and upregulates the expression of JA biosynthesis genes *DAD1* and *LOX1* (Huang et al. 2020). The increased concentration of JA will induce the expression of *MYB21* and *MYB24* (Vera-Sirera et al. 2016; Huang et al. 2020). Thus, GA and JA signaling synergistically modulate stamen elongation by regulating MYC–MYB signaling (Song et al. 2014; Chini et al. 2016). *myb21* mutants have short filaments that are unable to reach the pistil's stigma resulting in complete male sterility (Mandaokar et al. 2006). However, *myb21* pollen grains are viable. *myb24* mutants are completely fertile, whereas the *myb21myb24* double mutants exhibit impaired stamen development and complete sterility highlighting the essential role of *MYB21* in filament elongation and *MYB24* in pollen viability and anther dehiscence (Mandaokar et al. 2006; Mandaokar and Browse 2009; Song et al. 2011; Huang et al. 2017b).

AtHMGB15 belongs to a unique group of nuclear architectural proteins, containing 2 DNA-binding domains, namely ARID and HMG-box (Štros et al. 2007). Biochemical analysis shows that ARID–HMG proteins bind to different DNA topological structures preferably in the AT-rich region (Hansen et al. 2008; Roy et al. 2016). Previous research has demonstrated the involvement of AtHMGB15 in pollen tube growth (Xia et al. 2014). Approximately 10% of the pollen grains of the Ds insertion line of *AtHMGB15* (*athmgb15-1*) have defective morphology. Comparative transcriptome analysis between wild-type and *athmgb15-1* pollen showed alteration of genes specific for pollen. Additionally, AtHMGB15 was found to interact with two MIKC* TFs, namely AGL66 and AGL104. However, the mechanistic role of AtHMGB15 in pollen development remained unclear. In this study, we characterized the T-DNA insertion mutant of *AtHMGB15* (*athmgb15-4*), where the insertion is in the first exon. Our findings demonstrate that ~30% of pollen grains from *athmgb15-4* plants exhibit defective morphology, characterized by a round shape, and disrupted reticulate ornamentation. Transcriptome analysis revealed substantial repression of JA biosynthesis and signaling in *athmgb15-4* flowers. Collectively, our results provide comprehensive insights into the mechanistic role of the ARID–HMG protein AtHMGB15 in pollen development, specifically in regulating key master regulators of the JA pathway.

Results

Isolation and characterization of *athmgb15-4* mutant lines

The *athmgb15-4* mutant was identified from a screening of the T-DNA insertion line of Arabidopsis ecotype Col-0 from the GABI-Kat collection (GABI_351D08). GABI_351D08 has the T-DNA insertion annotated at exon 1 of the gene *At1g04880* (Fig. 1A, i). The T-DNA insertion carries a sulfadiazine-resistant marker. The homozygous *athmgb15-4* lines were generated through the self-crossing of heterozygous *athmgb15-4* plants followed by the selection of sulfadiazine resistance progeny. The homozygous lines were confirmed by PCR (Fig. 1A, ii), and the T-DNA insertion was validated through Southern blot (Supplementary Fig. S1). RT-qPCR analysis demonstrated a significant downregulation of *AtHMGB15* expression in the *athmgb15-4* mutant plants (Fig. 1A, iii). Previously, our group had reported the absence of the AtHMGB15 protein in the same mutant line (Mallik et al. 2020). Homozygous seeds were collected for subsequent investigations.

At the rosette stage, *athmgb15-4* plants did not exhibit any phenotypic differences compared to wild-type plants, except for a shorter primary root length in *athmgb15-4* (Fig. 1B, i and Supplementary Fig. S2). Additionally, *athmgb15-4* plants showed a significant delay in flowering compared to wild type (Fig. 1B, ii and Supplementary Fig. S3). Under regular growth conditions (long days), the number of rosette leaves at bolting for wild type was 14 compared to 20 for *athmgb15-4*. Further, *athmgb15-4* takes around 37 days for flowering compared to 27 days for wild-type plants (Fig. 1B, iv, v). Approximately 45% ($P \leq 0.05$) of seedlings of wild type initiated bolting after 30 days post-germination (dpg), whereas only 8% ($P \leq 0.05$) of *athmgb15-4* plants exhibited bolting (Fig. 1B, iii). The seeds of *athmgb15-4* mutant plants showed no marked difference when compared with wild type; they were viable and exhibited normal germination, like the wild type. However, mutant siliques were shorter in length compared to wild type (Fig. 1C, i, ii, iv) and contained fewer fertilized ovules, resulting in reduced seed yield compared to wild-type plants (Fig. 1C, iii, v).

Comparative transcriptome between wild type and *athmgb15-4* showed differential regulation of genes belonging to pollen development, cell wall, and hormone pathways

Earlier studies have shown that expression of *AtHMGB15* is highly tissue-specific with maximum expression observed in pollen grain (Xia et al. 2014). To gain insights into the role of AtHMGB15 in pollen development, we conducted a comparative transcriptome analysis between wild-type and *athmgb15-4* flowers of stage 13 (Sanders et al. 1999). The gene ontology (GO) term enrichment analysis using differentially expressed genes (DEGs) revealed enrichment of pollen tube development, cell growth and its regulation, cell wall development, biogenesis and organization, hormone-mediated signaling pathway and response, response to JA, and biosynthetic and metabolic process for biological process

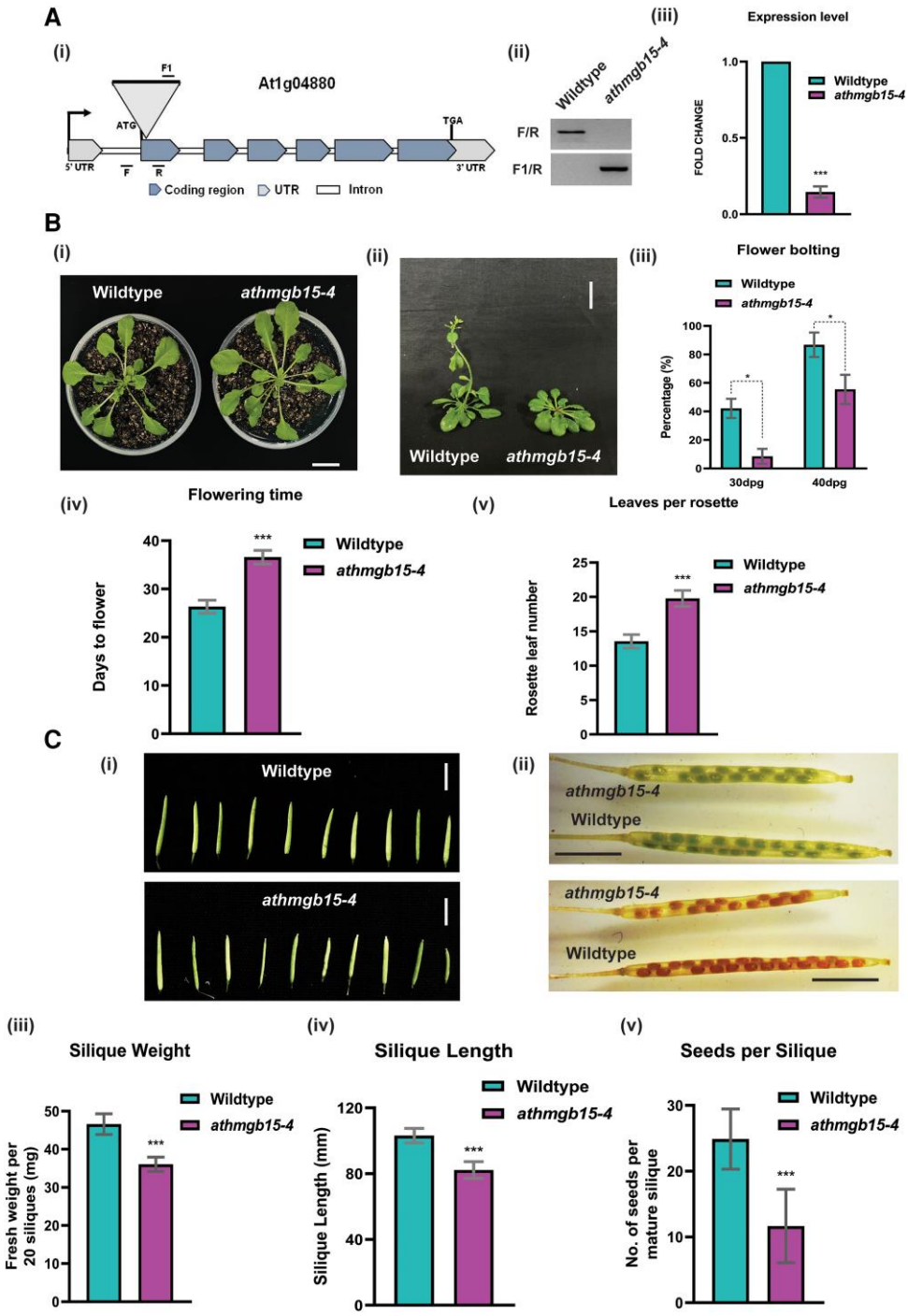

Figure 1. Phenotypic characterization of *athmgb15-4* mutant. **A)** (i) Schematic showing the position of T-DNA insertion in the 1st exon of *AtHMGB15* (At1g04880) and the position of PCR primers used for mutant screening. Black arrow indicates the transcription start site. (ii) PCR confirmation of *athmgb15-4* homozygous line. (iii) RT-qPCR showing significant reduction of *AtHMGB15* transcript in *athmgb15-4* lines. The fold change was represented with respect to wild type. Error bars represent mean ± SD ($n = 3$); significance was calculated by paired two-tailed Student's *t*-test. Asterisks represent significant differences between wild type and *athmgb15-4*, ***$P < 0.001$. **B)** (i) Wild type and *athmgb15-4* at the rosette stage. Scale bar = 2 cm. (ii) Delayed flowering of *athmgb15-4* compared to wild type. Scale bar = 2 cm. (iii) Quantitative analysis of flower bolting between *athmgb15-4* and wild type. The experiments were done from seeds of 4 to 5 independent harvests. Data were collected from 100 plants of each batch. Error bars represent mean ± SD ($n = 400$), and significance was calculated by paired two-tailed Student's *t*-test. Asterisks represent significant differences between wild type and *athmgb15-4*, *$P < 0.05$. dpg, days post-germination. (iv) Days from germination to flowering. Error bars represent mean ± SD ($n = 27$), and significance was calculated by paired two-tailed Student's *t*-test. Asterisks represent significant differences between wild type and *athmgb15-4*, ***$P < 0.001$. (v) Number of rosette leaves at bolting. Error bars represent mean ± SD ($n = 27$), and significance was calculated by paired two-tailed Student's *t*-test. Asterisks represent significant differences between wild type and *athmgb15-4*, ***$P < 0.001$. **C)** (i) Comparative silique length of wild type and *athmgb15-4*. Scale bar = 5 mm. (ii) Comparison of seed set between wild type and *athmgb15-4*. Scale bar = 2.5 mm. (iii) Quantitative silique fresh weight between *athmgb15-4* and wild type. Measurement was taken using 20 siliques for each observation. Error bars represent mean ± SD ($n = 20$). (iv) Quantitative silique length between *athmgb15-4* and wild type. Measurement was taken using 20 siliques for each observation. Error bars represent mean ± SD ($n = 20$). (v) Seed numbers were counted from mature siliques of wild type and *athmgb15-4*. Error bar represents mean ± SD ($n = 30$). The significance of all these results was analyzed by paired two-tailed Student's *t*-test Asterisks represent significant differences between wild type and *athmgb15-4*, ***$P < 0.001$.

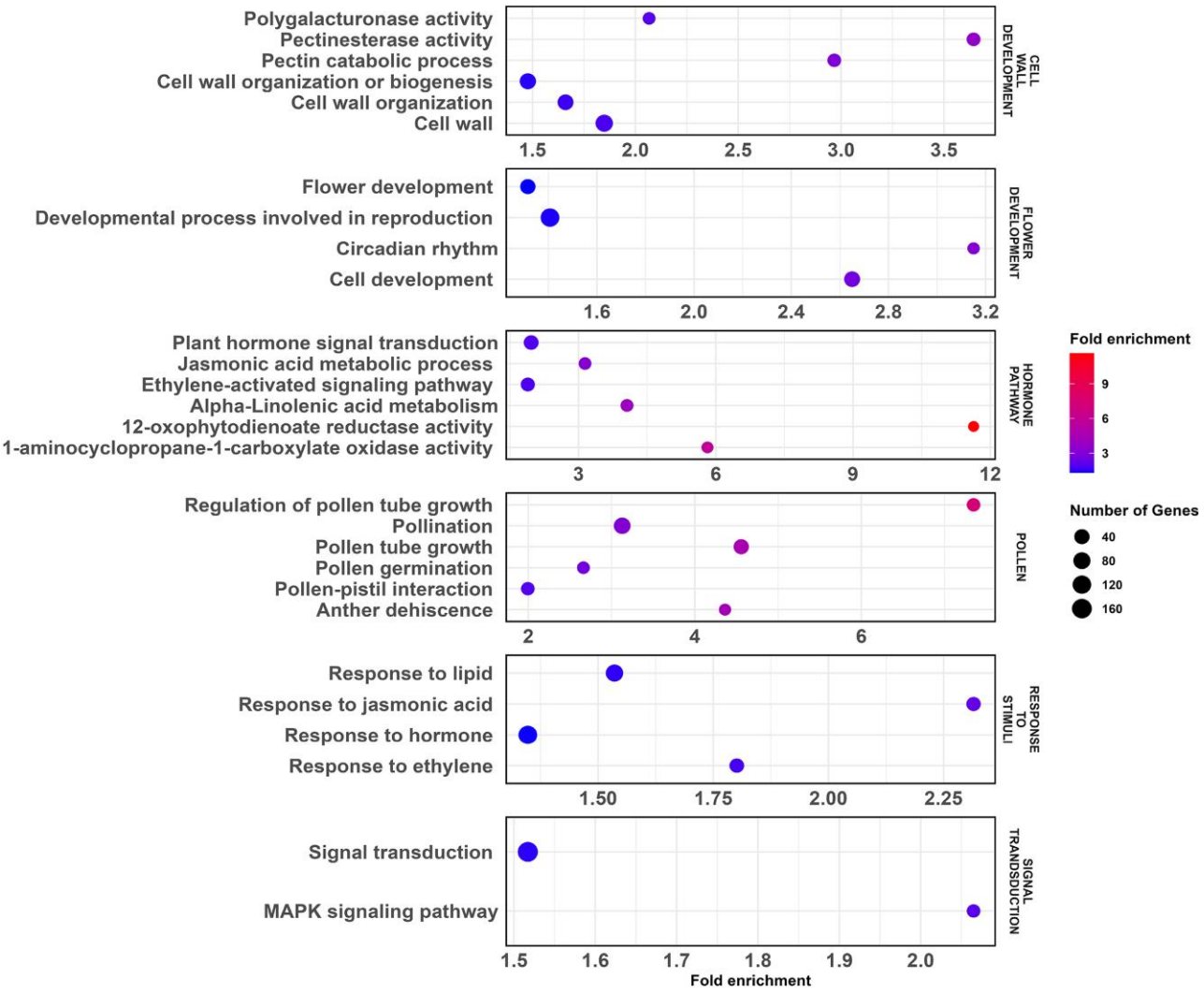

Figure 2. The GO and KEGG enrichment analysis. Bubble plot showing the enriched terms from the biological process, molecular function, cell component, and KEGG pathways between wild-type and *athmgb15-4* DEG datasets. The significantly enriched terms are plotted using the False Discovery Rate enrichment and number of genes and are categorized under 6 subcategories relevant to our study, namely, cell wall development, hormone pathway, response to stimuli, flower development, pollen, and signal transduction.

(Fig. 2 and Supplementary Fig. S4). Additionally, Kyoto Encyclopedia of Genes and Genomes (KEGG) analysis highlighted the enrichment of α-linolenic acid metabolism, carotenoid biosynthesis, and biosynthesis of secondary metabolites as some of the pathways enriched in our dataset (Supplementary Fig. S5). To validate our result, we selected candidate genes and performed RT-qPCR analysis (Supplementary Fig. S6).

Previously published microarray data from Xia et al. using *athmgb15-1* and wild-type pollen grains have shown genes responsible for cell growth, pollen development, and pollen tube growth, cell wall synthesis, and cellular transport as some of the important ones that are differentially enriched. We next compared our transcriptome with Xia et al. and found 171 DEGs common in both the datasets. Of these, 111 DEGs represent downregulated, and 60 represent upregulated. Further analysis showed that these 111 downregulated genes represent GO biological processes such as pollen tube growth and development, pollination, cell growth, and protein phosphorylation. Notably, there was no GO enrichment related to the JA pathway except the *LOX4* gene which was found downregulated even in Xia et al. dataset (Supplementary Fig. S7A to C and Tables S1 and S2). This discrepancy can be attributed to the difference in tissue types used for the transcriptome studies; Xia et al. used pollen grains, while we used stage 13 flower. Nevertheless, previous studies have established the role of jasmonate during the initiation of pollen development particularly during anther development at around stages 12 to 13 of flower development (Sanders et al. 1999).

In our previous study, we conducted a whole-genome ChIP-on-chip assay using 14-day-old Arabidopsis seedlings to identify the targets of AtHMGB15. Comparing our DEGs with the ChIP-on-chip data, we identified ~1,090 common loci between the 2 datasets. GO analysis of these common loci unveiled the significant enrichment of genes belonging to stress response, response to JA, and pollen development in terms of biological processes (Supplementary Fig. S7 D to F and Tables S3 and S4). Collectively, our transcriptome analysis and previous findings indicate that AtHMGB15 directly or indirectly regulates the transcription of genes involved in the pollen development pathway, possibly by modulating hormone signaling.

athmgb15-4 plants have defective pollen morphology and delayed pollen germination rate

To investigate the role of AtHMGB15 on pollen development, we initially studied pollen grain morphology of *athmgb15-4* mutants and wild-type plants using scanning electron microscopy (SEM). Our observations revealed that wild-type pollen grains exhibited an ellipsoidal shape (Fig. 3A), while *athmgb15-4* pollen grains displayed a mixture of shapes, including ~25% to 30% with circular or irregular shapes (Fig. 3B and Supplementary Fig. S8A). Additionally, the outermost exine wall of wild-type pollen grains had a typical reticulate pattern of ornamentation, which was completely absent in the defective pollen grains of mutant plants. To gain further insights into the abnormal cell wall morphology of *athmgb15-4* plants, we analyzed the transcriptome data for genes associated with cell wall biosynthesis. Our RNA-seq analysis revealed significant downregulation of genes involved in cell wall biosynthesis in *athmgb15-4* flowers, including pectin lyase, cellulose synthase, pectin methylesterase, and extensin, which are known to play crucial roles in pollen development (Fig. 3C and Supplementary Fig. S6C). Interestingly, most of the cell wall validated genes, *viz.* pectin lyase (At5g48140 and At3g07850), pectin methyltransferase (At4g15980), cellulose synthase (At2g33100), and xyloglucan endotransglucosylase (AT4G30280), showed AtHMGB15 binding as per our ChIP-on-chip data (Mallik et al. 2020) (Supplementary Table S3).

Subsequently, we examined the pollen germination rate of wild-type and *athmgb15-4* pollen grains. The time kinetics of in vitro pollen tube germination shows that within 4 h, more than 50% of pollen grains ($P \leq 0.005$) were germinated for wild-type pollen grains and by 6 h almost 80% ($P \leq 0.005$) germination was achieved (Fig. 3D, i, iii). Interestingly, only 40% ($P \leq 0.005$) germination of *athmgb15-4* pollen grains was observed after 24 h in pollen germination media (Fig. 3D, ii, iii). These results indicate that the mutation of *AtHMGB15* leads to severe defects in pollen morphology and causes significant delays in the germination rate of pollen tubes. Some of the pollen grains from *athmgb15-4* that show tube growth comparable to wild type may be considered normal ellipsoidal in shape (like wild type). However, this percentage is less in the mutant compared to the wild type, based on our in vitro germination assay (Supplementary Fig. S8B). To assess the viability of *athmgb15-4* pollen grains compared to wild type, we performed fluorescein diacetate (FDA) and propidium iodide (PI) staining. While FDA is permeable to the cell membrane and can stain live cells, PI is impermeable and can stain DNA only when the cell integrity is compromised. Thus, PI-stained cells are considered dead cells. Comparison of the staining patterns revealed a higher percentage of nonviable pollen grains (55%, $P \leq 0.005$) in *athmgb15-4* mutants compared to wild type (30%, $P \leq 0.05$) (Fig. 3E), justifying the lower germination rate observed in the mutant plants. Thus, our data strongly indicate that the AtHMGB15 function is essential for the development of viable pollen grains in *Arabidopsis*.

AtHMGB15 regulates the expression of genes involved in the JA pathway during flower development

KEGG analysis of RNA-seq data has identified enrichment of the α-linolenic acid metabolism pathway from the differential expressed gene pool (Fig. 2, and Supplementary Fig. S5). α-Linolenic acid is the precursor of the plant phytohormone, JA. JA and its derivatives have been shown to regulate many developmental processes including stamen and flower development (Wasternack and Hause 2013; Jang et al. 2020). We examined the expression of JA biosynthesis and signaling genes in *athmgb15-4* flowers using RT-qPCR. As shown in Fig. 4, A, the relative fold change for genes involved in JA biosynthesis and JA signaling was significantly downregulated in *athmgb15-4* flowers compared to wild type. Furthermore, the expression levels of JA-related genes were moderately downregulated in another T-DNA mutant of *AtHMGB15* (SALK_057612C_9 and SALK_057612C_15) (Supplementary Fig. S9). These *athmgb15* mutants harbor T-DNA insertion in the promoter region. Collectively, the transcriptome and RT-qPCR analyses suggested the transcriptional activator role of AtHMGB15 for the expression of JA biosynthesis and signaling genes during flower development. Comparing our transcriptome and earlier published ChIP-on-chip data (Mallik et al. 2020), it was observed that most of the validated genes associated with JA response, *viz. LOX3*, *AOS*, *DAD1*, *AOC3*, *JAR1*, *JAZ1*, *JAZ3*, *JAZ8*, and *MYC2*, have AtHMGB15-binding site (Supplementary Table S3).

To further establish the regulation of *AtHMGB15* in JA signaling during pollen development, we raised complementation lines using 35S::*AtHMGB15* in *athmgb15-4* background. Stable homozygous lines were selected (*athmgb15-4-OE*$_{A4}$), and the expression of *AtHMGB15* was analyzed using RT-qPCR (Fig. 4B, iii). These complementation lines were stable and recovered the delayed bolting and small silique size phenotype of *athmgb15-4* mutant (Fig. 4B, i, ii). Moreover, a comparison of pollen tube germination rates showed a significantly higher population of germinated pollen grains in the *athmgb15-4-OE*$_{A4}$ compared to *athmgb15-4* (Fig. 4C, i, ii). Additionally, more than 95% ($P \leq 0.05$) of pollen grains in *athmgb15-4-OE*$_{A4}$ exhibited an ellipsoidal shape, indicating complete recovery of pollen morphology (Fig. 4D). RT-qPCR results revealed higher expression of JA biosynthesis and signaling genes in the complementation line compared to the mutant (Fig. 4E). The expression of JA biosynthesis genes in the complementation line was comparable to wild type; however, the expression of JA signaling genes was higher than wild type. The molecular and phenotypic analyses of complementation lines strongly demonstrate that *AtHMGB15* is essential in JA-regulated signaling events during pollen development.

athmgb15 flowers showed low levels of JA and its derivatives

The downregulation of JA biosynthesis genes in *athmgb15-4* mutants suggests a low intrinsic level of JA and its derivatives. To assess the hormone level, we next estimated the in vivo level of jasmonate in the flowers of wild-type, *athmgb15-4*, and *athmgb15-4-OE*$_{A4}$ lines. As shown in Fig. 5A, the levels of JA along with two of its derivatives, namely methyl jasmonate (MeJA) and JA-Ile, are almost 10-fold ($P \leq 0.05$) lower in *athmgb15-4* flowers compared to wild type. Remarkably, the low level of JA and its derivatives were restored in *athmgb15-4-OE*$_{A4}$ complementation lines.

Considering the reduced JA levels in *athmgb15-4* flowers, the effect of exogenous MeJA application on these flowers was examined by evaluating the pollen tube germination post-48 h treatment. The result revealed that the application of exogenous treatment of MeJA on buds and young flowers restores the pollen tube germination of *athmgb15-4* pollen grains, and the rate is equivalent to that of wild-type pollen grains (Fig. 5B and C). We checked the expression of JA biosynthesis and signaling genes post-exogenous MeJA application in the young flowers. Our results indicate that there was a significant increase in the expression of *AOS*, *OPR3*, *MYC2*, *JAZ1*, and *JAZ10*

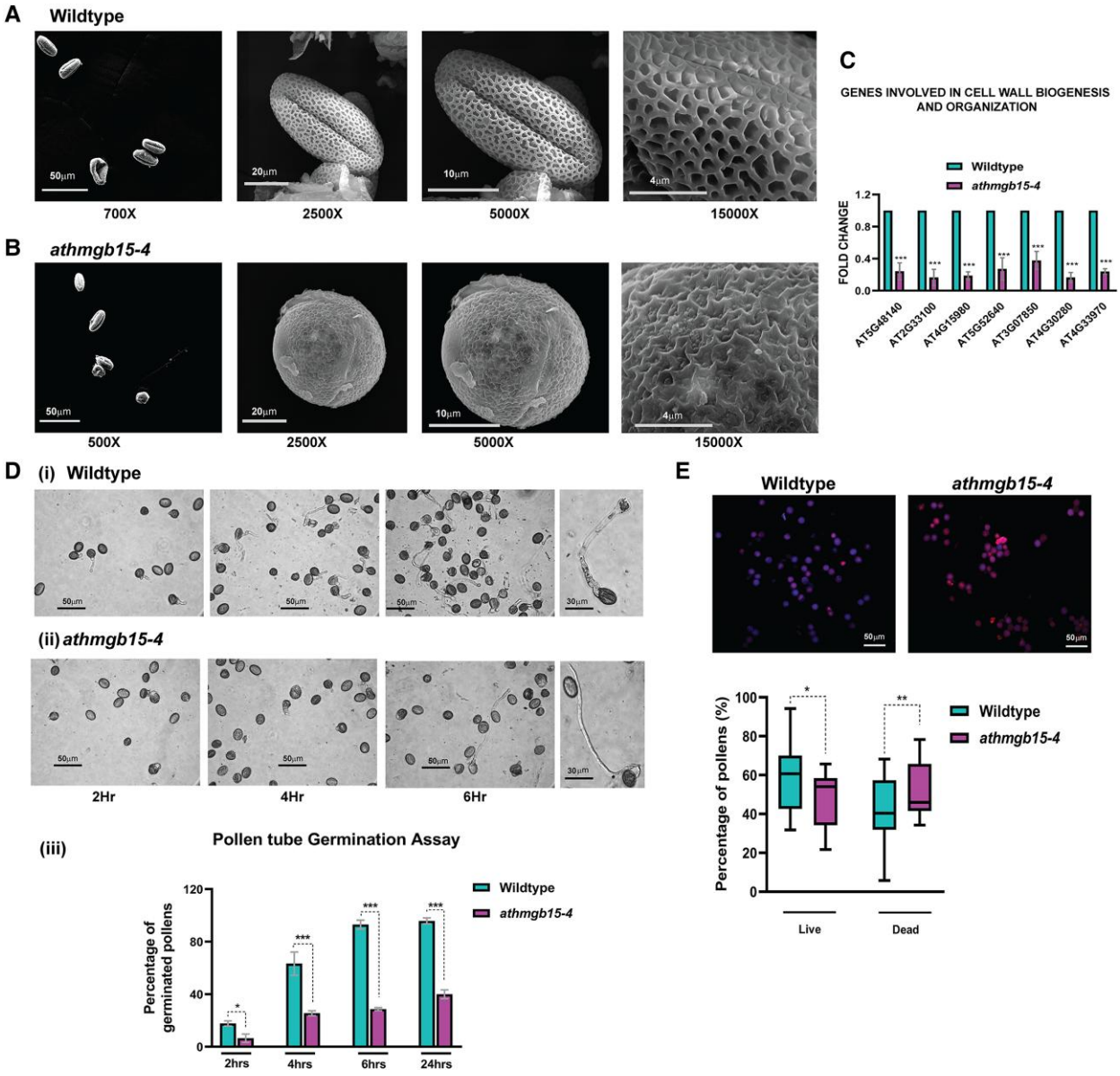

Figure 3. Defective pollen morphology and pollen germination rate of *athmgb15-4* compared to wild type. **A)** SEM of pollen grains isolate from wild type showing ellipsoidal shape with reticulate ornamentations. **B)** Representation of defective pollen morphology of *athmgb15-4* mutant having a circular shape with irregular ornamentation. The experiment was repeated at least 10 times with pollen grains isolated from different batches of wild type and *athmgb15-4*. **C)** Expression of differentially regulated cell wall biosynthesis genes between wild type and *athmgb15-4* using RT-qPCR. The fold change was represented with respect to wild type. Error bars represent mean ± SD ($n = 8$). The significance was analyzed by paired two-tailed Student's *t*-test. Asterisks represent significant differences between wild type and *athmgb15-4*, $^{***}P < 0.001$. **D)** Freshly isolated pollen grains from (i) wild type and (ii) *athmgb15-4* were subjected to in vitro germination for different time periods. (iii) Graphical representation of rate of pollen germination of wild type and *athmgb15-4* at the given time points. Error bars represent mean ± SD ($n = 10$). The significance was analyzed by paired two-tailed Student's *t*-test. Asterisks represent significant differences between wild type and *athmgb15-4*, $^{*}P < 0.05$, $^{***}P < 0.001$. **E)** Pollen viability was measured using FDA and PI. FDA-stained cells are blue denoting live pollen grains, the PI-stained cells are red denoting dead pollen grains, and the purple-colored pollen grains are sterile in nature. The excitation wavelength used for the fluorescence microscope to observe PI was 535 nm, with an exposure duration of 100 ms and the gain at 1×. The excitation wavelength for FDA was 488 nm, with an exposure duration of 200 ms and the gain at 1.5×. Box plot representation of pollen viability between wild type and *athmgb15-4*. Whiskers represent mean ± SD ($n = 12$). The significance was analyzed by paired two-tailed Student's *t*-test. Asterisks represent significant differences as indicated, $^{*}P < 0.05$, $^{**}P < 0.01$. The center line of the box denotes the median. Box limits denotes the upper quartile (Q1) and the lower quartile (Q3). The whiskers extend to the maximum and minimum data values.

(Fig. 5D and Supplementary Fig. S10) in wild-type and *athmgb15-4* flowers after exogenous MeJA application. Thus, restoration of mutant pollen phenotype and induction of JA signaling genes by exogenous MeJA application indicates that the low endogenous level of JA in *athmgb15-4* plants is responsible for the reduced expression of JA signaling genes during pollen development.

AtHMGB15 acts as a transcription activator for the expression of *MYC2*

Transcriptome and RT-qPCR analyses revealed the downregulation of the key TFs of JA signaling, *viz. MYC2*, *MYB21*, and *MYB24*, in *athmgb15-4* mutant flowers. We next aimed to investigate whether AtHMGB15 acts as a transcription activator for the expression of these genes.

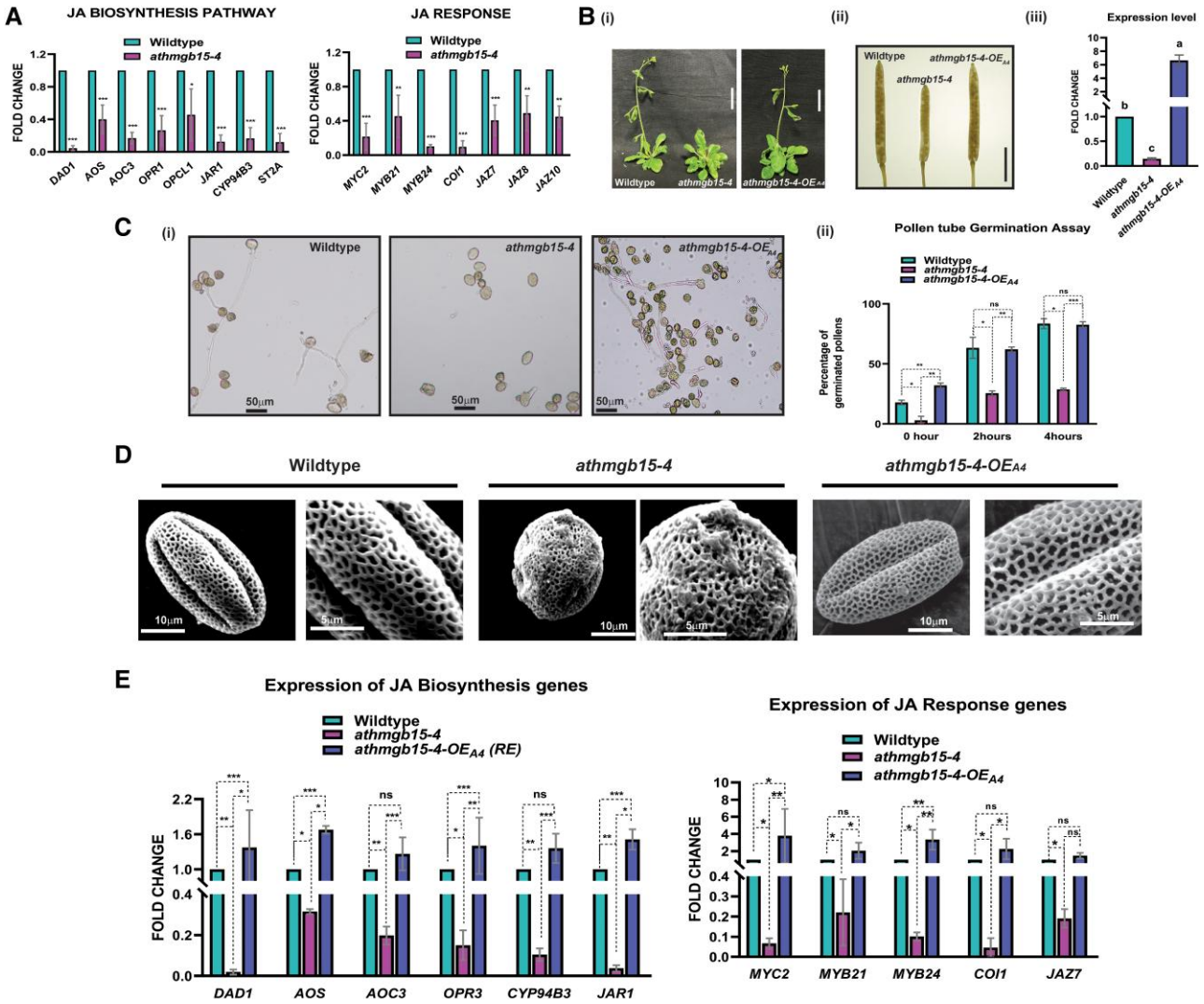

Figure 4. Complementation of *athmgb15-4* mutant line with *AtHMGB15* restores pollen morphology and pollen tube germination. **A)** Expression of differentially regulated JA biosynthesis and signaling genes was analyzed between wild type and *athmgb15-4* using RT-qPCR. The fold change was represented with respect to wild type. Error bars represent mean ± SD ($n = 6$). The significance for each gene was analyzed by paired two-tailed Student's *t*-test. Asterisks represent significant differences between wild type and *athmgb15-4*, $^{*}P < 0.05$, $^{**}P < 0.01$, $^{***}P < 0.001$. **B)** (i) Comparative flower bolting between wild type, *athmgb15-4*, and *athmgb15-4-OE$_{A4}$*. Scale bar = 2 cm. (ii) Silique length of wild type, *athmgb15-4*, and *athmgb15-4-OE$_{A4}$*. Scale bar = 4 mm. (iii) RT-qPCR to check *AtHMGB15* transcript level in wild type, *athmgb15-4*, and *athmgb15-4-OE$_{A4}$*. The fold change was represented with respect to wild type. Error bars represent mean ± SD ($n = 6$). Letters indicate significant differences according to a one-way ANOVA with Tukey's post hoc test ($P < 0.05$). **C)** (i) Comparative in vitro pollen germination between wild type, *athmgb15-4*, and *athmgb15-4-OE$_{A4}$*. (ii) Quantification of the rate of pollen germination. Error bars represent mean ± SD ($n = 6$). The significance for each time point was analyzed by one-way ANOVA with Fisher's LSD post hoc test. Asterisks represent significant differences as indicated ($^{*}P < 0.05$, $^{**}P < 0.01$, $^{***}P < 0.001$, *ns*, *not significant*). **D)** SEM analysis of pollen morphology. **E)** Expression of JA biosynthesis and signaling genes in wild-type, *athmgb15-4*, and *athmgb15-4-OE$_{A4}$* flowers. The fold change for each gene was represented with respect to wild type. Error bars represent mean ± SD ($n = 8$). The significance for each gene was analyzed by one-way ANOVA with Tukey's post hoc test. Asterisks represent significant differences as indicated ($^{*}P < 0.05$, $^{**}P < 0.01$, $^{***}P < 0.001$, *ns*, *not significant*).

AtHMGB15 occupancy at the upstream region of *MYC2*, *MYB21*, *and MYB24*

To explore the potential interaction between AtHMGB15 and the upstream regions of these genes, a ChIP assay was performed using the custom-made (Thermo Scientific, India) affinity-purified anti-AtHMGB15 antibody and the immunoprecipitated DNA was subjected to qPCR. It is noteworthy that the antibody that was used for ChIP analysis was previously validated in the whole-genome ChIP-on-chip study (Mallik et al. 2020). However, we have further performed a western blot with flower samples of stage 13 to further revalidate the antibody (Supplementary Fig. S11). All our ChIP data were normalized with 2 loci, namely At1g01840 and At1g01310, showing no AtHMGB15 occupancy from our previous study (Mallik et al. 2020). The primers were designed from *in silico* analysis of promoter/upstream region of *MYC2*, *MYB21*, and *MYB24* that contain AtHMGB15-binding site A(A/C)–ATA–(A/T)(A/T) (Mallik et al. 2020). The qPCR analysis showed AtHMGB15 occupancy at the promoter/upstream region of *MYC2*, *MYB21*, as well as *MYB24* (Fig. 6A). To test whether AtHMGB15 directly binds to the promoter/upstream region of *MYC2*, *MYB21*, and *MYB24*, we performed an electrophoretic mobility shift assay (EMSA) using the same 200-bp DNA fragments that were used for ChIP validation of AtHMGB15 binding. EMSA experiments confirmed the direct binding of AtHMGB15 protein at the promoter regions of *MYC2*, *MYB21*, and *MYB24* (Fig. 6B). There was no binding with the 200-bp DNA fragment corresponding to At1g01310

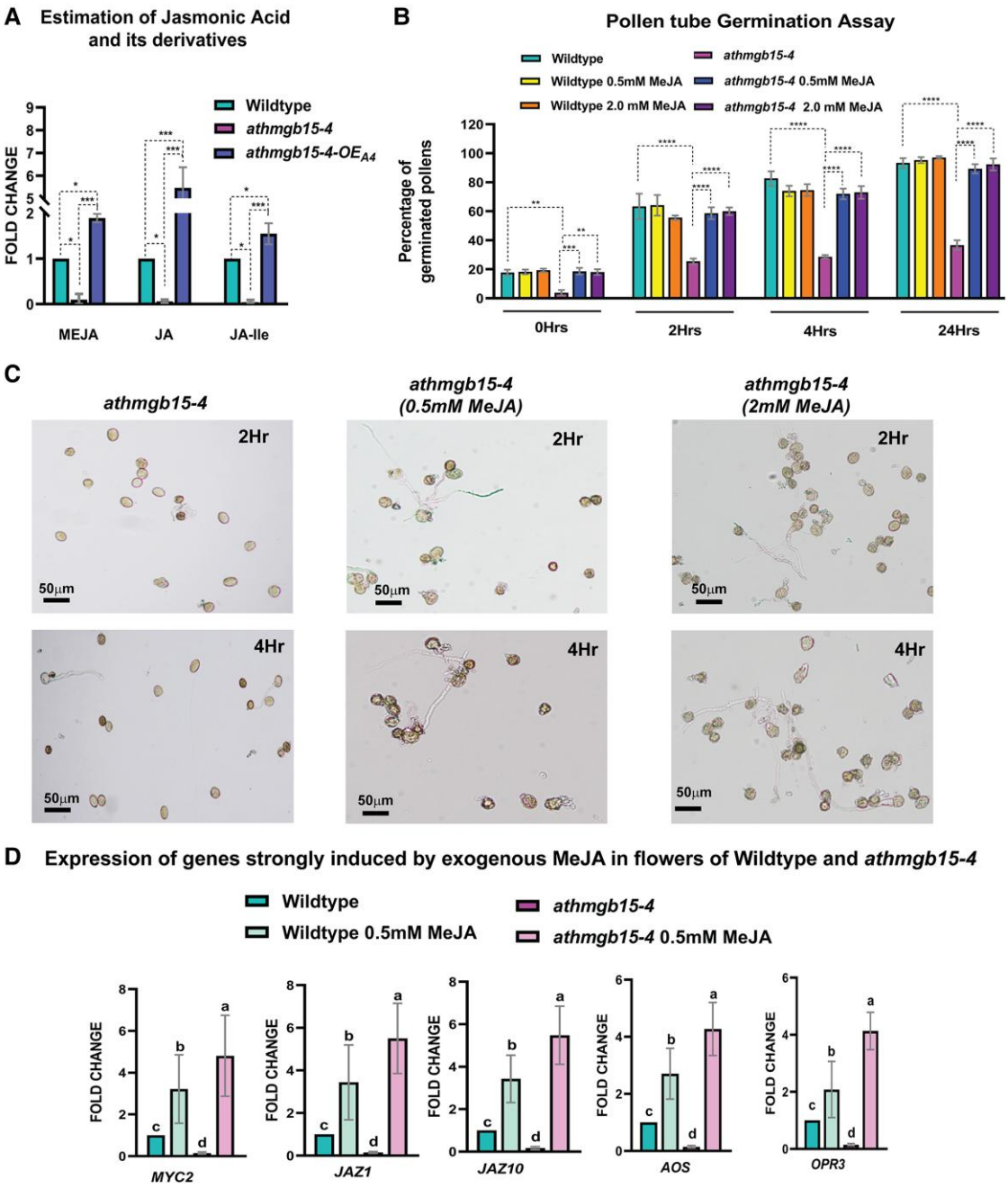

Figure 5. *athmgb15-4* mutants have reduced levels of JA and its derivatives. **A)** JA and its derivatives were measured from the flowers of wild type, *athmgb15-4*, and *athmgb15-4-OEA4* and represented as fold change with respect to wild type. Error bars represent mean ± SD ($n = 3$). The significance was analyzed by one-way ANOVA with Fisher's LSD post hoc test. Asterisks represent significant differences as indicated (*$P < 0.05$ and ***$P < 0.001$). JA, jasmonic acid; MeJA, methyl jasmonate; JA-Ile, jasmonic acid isoleucine. **B)** Quantification of the rate of pollen tube germination in the presence of different concentrations of methyl jasmonate. Error bars represent mean ± SD ($n = 3$). The significance was analyzed by two-way ANOVA with Tukey's post hoc test. Asterisks represent significant differences as indicated (**$P < 0.01$, ***$P < 0.001$, and ****$P < 0.0001$). **C)** Restoration of in vitro pollen germination of *athmgb15-4* on treatment with exogenous MeJA (0.5 and 2 mM). **D)** Expression of genes strongly induced by exogenous MeJA (0.5 mM) in flowers of wild type and *athmgb15-4*. The fold change was represented with respect to wild type. Error bars represent mean ± SD ($n = 6$). Letters indicate significant differences according to a one-way ANOVA with Tukey's post hoc test ($P < 0.05$).

(negative control). Furthermore, site-directed mutagenesis (SDM) causing mutation of the AT-rich binding motif resulted in a significant reduction in AtHMGB15 binding, with binding observed only at high protein concentrations (Supplementary Fig. S12). Moreover, previous ChIP-on-chip data also supported the presence of AtHMGB15 at the *MYC2* and *MYB24* loci, further suggesting its role in regulating the transcription of JA signaling genes.

AtHMGB15 activates the transcription of *MYC2*

The binding of AtHMGB15 at the promoter/upstream region of *MYC2* prompted us to investigate whether AtHMGB15 regulates the transcription of *MYC2*. For this, ~2-kb promoter/upstream region of *MYC2* was cloned in pCambia1304 replacing 35S promoter to generate pMYC2::GUS reporter construct. The constructs were infiltrated into *Nicotiana benthamiana* plants to examine the promoter activity (pMYC2) by measuring GUS activity in the absence

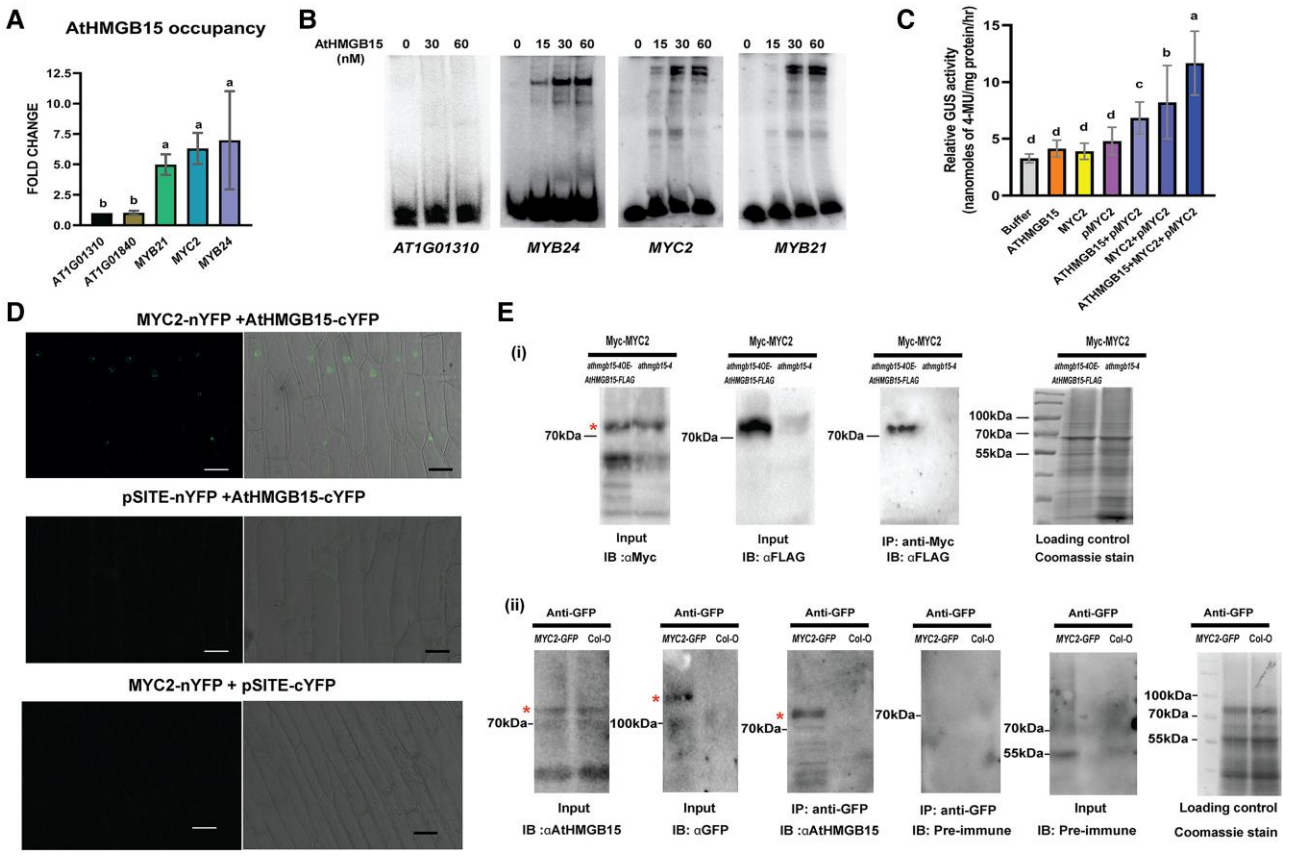

Figure 6. AtHMGB15 acts as a transcriptional activator for the expression of *MYC2*. **A)** ChIP analysis shows AtHMGB15 occupancy at the promoter/upstream of *MYC2*, *MYB21*, and *MYB24*. The data were normalized with no binding regions corresponding to At1g01310. Error bars represent mean ± SD ($n = 5$). Letters indicate significant differences according to a one-way ANOVA with Tukey's post hoc test ($P < 0.05$). **B)** EMSA was performed using ^{32}P-labeled DNA fragments of At1g01310, *MYB24*, MYC2, and *MYB21* and increasing concentration of recombinant AtHMGB15 (15 to 60 nM). **C)** 2 kb promoter region of *MYC2* (pMYC2) was cloned with GUS reporter, and *Agrobacterium*-mediated infiltration was done with 35S::*AtHMGB15*, and 35S::*MYC2* in *Nicotiana tabacum*. GUS reporter gene assay was done after 48 h using MUG. Error bars represent mean ± SD ($n = 15$). Letters indicate significant differences between the represented datasets according to a one-way ANOVA with Tukey's post hoc test ($P < 0.05$). **D)** BiFC confirming the interaction between AtHMGB15 and MYC2 in onion epidermal cells using split Yellow Fluorescent Protein (YFP). *AtHMGB15-cYFP + pSITE-nYFP-C1* and *MYC2-nYFP + pSITE-cYFP-N1* were used as control. Scale bar = 50 μm. **E)** (i) Co-immunoprecipitation (co-IP) assay confirming interaction of AtHMGB15 and MYC2. Total protein from leaves of *athmgb15-4OE$_{A4}$-FLAG* and *athmgb15-4* transiently expressing Myc-MYC2 was extracted and subjected to immunoprecipitation with anti-Myc antibody, followed by immunoblot analysis with anti-FLAG (IB: αFLAG) antibodies to detect AtHMGB15-Flag and anti-Myc (IB: αMyc) antibodies to detect Myc-MYC2. Extract of *athmgb15-4* leaves only expressing Myc-MYC2 was used as a control. Coomassie blue staining for Rubisco was used to ascertain even protein loading in each lane. (ii) Co-immunoprecipitation (co-IP) assay confirming interaction of AtHMGB15 and MYC2 in vivo. Total protein from seedlings of MYC2-GFP was extracted and immunoprecipitated with anti-GFP magnetic beads, followed by immunoblot analysis with anti-AtHMGB15 (IB: αAtHMGB15) and anti-GFP (IB: αGFP) antibodies and preimmune sera. Extract of wild-type seedlings was used as control. Coomassie blue staining for Rubisco was used to ensure even protein loading in each lane (* indicates the band of interest).

and presence of AtHMGB15. AtHMGB15 is not a TF but can modulate transcription when associated with a TF. Moreover, previous studies have identified the MYC2-binding site at the promoter of MYC2 gene (Zander et al. 2020). Thus, we presumed that AtHMGB15 is a coactivator coupled with the TF MYC2 to regulate transcription. To test this hypothesis, we measured the promoter activity of *MYC2* in the presence of both the proteins, namely MYC2 and AtHMGB15. As shown in Fig. 6C, the promoter activity was higher in the presence of AtHMGB15 (p*MYC2* + AtHMGB15) compared to the control (p*MYC2*). Similarly, we have observed an increase in p*MYC2* activity in the presence of MYC2 (p*MYC2* + MYC2) compared to the control, supporting the earlier finding that MYC2 regulates its transcription. Interestingly, the p*MYC2* activity increased significantly in the presence of both MYC2 and AtHMGB15 protein (p*MYC2* + MYC2 + AtHMGB15) compared to when measured with individual proteins. The increase of pMYC2 activity in the presence of both the proteins, namely AtHMGB15 and MYC2, indicates that AtHMGB15 along with MYC2 TF positively activates the transcription of *MYC2*.

AtHMGB15 interacts with *MYC2* protein to form the activator complex

To further explore the physical interaction between AtHMGB15 and MYC2, a BiFC assay was conducted using co-infiltration of *Agrobacterium* carrying MYC2-nYFP and AtHMGB15-cYFP constructs into the onion epidermis. The results revealed reconstitution of the Yellow Fluorescent Protein (YFP) signal in the nucleus, particularly in the nucleolus, indicating the physical interaction between AtHMGB15 and MYC2 *in planta* (Fig. 6D). No YFP fluorescence was observed in the control combinations.

To further validate this physical interaction, we performed a transient co-immunoprecipitation using Myc-tagged MYC2 and C-terminal Flag-tagged AtHMGB15. We raised transgenic *Arabidopsis* overexpressing AtHMGB15-flag in *athmgb15-4* background. These

transgenic plants were used for Agrobacterium infiltration using the Myc-MYC2 construct. As a control, Myc-MYC2 constructs were infiltrated in *athmgb15-4* plants. The complex was immunoprecipitated using an anti-Myc antibody and detected with an anti-flag antibody. The Western blot analysis indicates that Myc-tagged MYC2 immunoprecipitated AtHMGB15-Flag (Fig. 6E). Alternatively, we infiltrated *Myc-MYC2* into the leaves of *AtHMGB15-Flag* and performed immunoprecipitation assay with anti-FLAG affinity beads to pull down the protein complex. To detect its interactors, we used an anti-Myc antibody. We infiltrated *pGWB618* (empty vector) in the leaves of *AtHMGB15-Flag* as control (Supplementary Fig. S13).

To confirm the interaction between MYC2 and AtHMGB15 *in planta*, co-immunoprecipitation assay was performed using transgenic plants expressing MYC2-GFP. The complex was pulled down with anti-GFP magnetic beads, and AtHMGB15 was detected in the precipitated complex using AtHMGB15 antibody (Mallik et al. 2020). The results confirmed positive interaction between MYC2 and AtHMGB15, in vivo. *Arabidopsis* Col-0 was used as control in this assay (Fig. 6E, ii). These experimental findings indicate the physical interaction of AtHMGB15 with MYC2 protein to form an activator complex to promote the transcription of the MYC2 TF.

AtHMGB15 promotes the transcription of *MYB*s

MYC2 has been shown to interact with R2R3-MYB TFs, MYB21, and MYB24 to regulate anther and pollen development in a JA-dependent manner (Goossens et al. 2017). Our RT-qPCR analysis confirmed the expression of *MYB21* and *MYB24* is downregulated in *athmgb15* mutants. Additionally, the *in silico* analysis revealed the presence of MYC2-binding sites at the promoter region of *MYB24*. Since AtHMGB15 and MYC2 form a transcription activator complex, we next investigated whether this complex regulates the transcription of R2R3-MYB TFs. To explore this possibility, we examined the expression of *MYB21* and *MYB24* in the flowers of 2 previously characterized *myc2* knockout lines, namely *myc2-2* and *jin1-2* (Boter et al. 2004; Lorenzo et al. 2004). Our results demonstrated a significant downregulation of *MYB21* and *MYB24* expression in these *myc2* mutant lines (Fig. 7A, i). Furthermore, the expression of JA biosynthesis gene *OPR3*, which was previously shown to be MYC2-dependent (Mandaokar et al. 2006), was downregulated in these mutants. We analyzed the JA content of *myc2* mutants and observed a significant reduction in jasmonate levels (Fig. 7A, ii).

Subsequently, we investigated the promoter activity of *MYB21* and *MYB24* in the presence of AtHMGB15 and MYC2 TFs. The promoter activity of pMYB24 was significantly upregulated in the

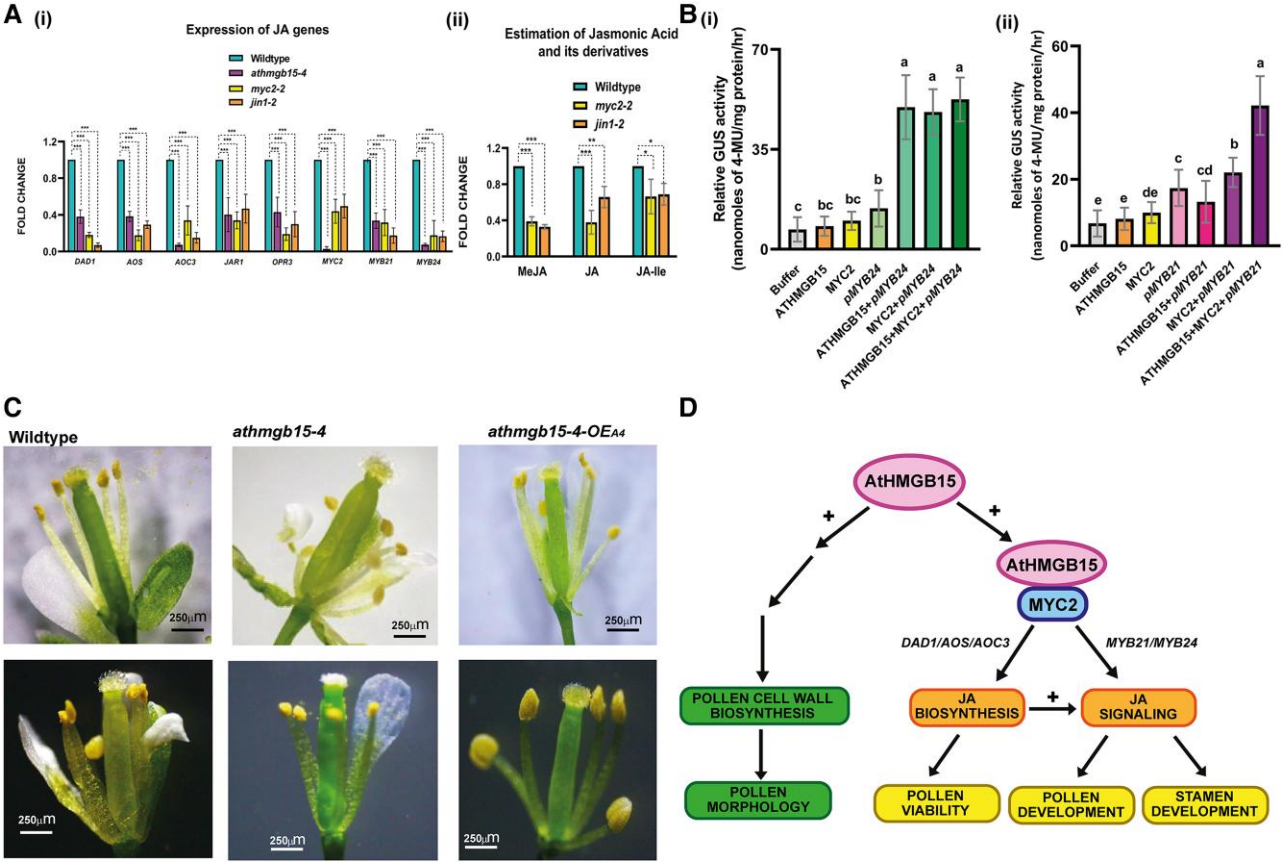

Figure 7. AtHMGB15 promotes transcription of *MYB*s. **A)** (i) Expression of JA genes in *MYC2* knockout mutants *myc2-2* and *jin1-2*, and *athmgb15-4* using RT-qPCR. The fold change was represented with respect to wild type. Error bars represent mean ± SD ($n = 4$). The significance for each gene was analyzed by one-way ANOVA with Tukey's post hoc test. Asterisks represent significant differences as indicated (***$P < 0.001$). (ii) Comparative JA and its derivatives content in flowers of wild type and *MYC2* knockout mutants *myc2-2* and *jin1-2*. Error bars represent mean ± SD ($n = 3$). The fold change for each gene was represented with respect to wild type. The significance for each gene was analyzed by one-way ANOVA with Tukey's post hoc test. Asterisks represent significant differences as indicated (*$P < 0.05$, **$P < 0.01$, and ***$P < 0.001$). **B)** (i and ii) 2-kb promoter regions of *MYB21* (pMYB21) and *MYB24* (pMYB24) were cloned with GUS reporter and *Agrobacterium*-mediated infiltration was done with *35S::AtHMGB15* and *35S::MYC2* in *N. tabacum*. GUS reporter gene assay was done after 48 h using MUG. Error bars represent mean ± SD ($n = 15$). Letters indicate significant differences between the represented datasets according to a one-way ANOVA with Tukey's post hoc test ($P < 0.05$). **C)** Comparison of stamen phenotype between wild type, *athmgb15*, and *athmgb15-4-OEA4*. Scale bar = 250 μm. **D)** Proposed model elucidating the role of AtHMGB15 in activating the JA pathways by forming an activation complex with MYC2 to regulate stamen and pollen development.

presence of AtHMGB15 and MYC2 independently; however, in the presence of both proteins, there was no additional increase in promoter activity (Fig. 7B, i). For p*MYB21*, an increase in promoter activity was observed only in the presence of MYC2 protein (Fig. 7B, ii). There was no increase in promoter activity in the presence of AtHMGB15, although strong DNA-binding activity of AtHMGB15 was observed in the promoter region. Interestingly, the activity of pMYB21 increased significantly in the presence of both AtHMGB15 and MYC2, suggesting the formation of an activation complex between these 2 proteins to activate p*MYB21*.

Since R2R3 TFs were needed for the elongation of stamen during flower development, we further analyzed the flower morphology of *athmgb15-4* and compared it to wild-type Arabidopsis flower. Our observation suggests that around 30% of *athmgb15-4* flowers have shorter stamen filaments compared to wild type (Fig. 7C and Supplementary Fig. S14). This may be one of the reasons for poor fertilization and low seed yield in *athmgb15* mutants. The complementation lines on the other hand showed a similar stamen phenotype as compared to wild type. Taken together, these findings suggest that AtHMGB15 regulates the transcription of R2R3-MYB TFs during flower development, thereby regulating the growth and development of stamens and pollen grains.

Discussion

AtHMGB15 insertion mutants have defective pollen morphology

Optimal pollen development and functional floral organs are crucial for efficient pollination and genetic diversity. These complex processes are precisely regulated by endogenous cues. In this study, we have investigated the role of the *Arabidopsis* ARID/HMG group of transcriptional regulators, AtHMGB15, in pollen development. A previous study by Xia et al. (2014) using a Ds insertion line and our study using another T-DNA mutant allele of *AtHMGB15* similarly showed defective pollen morphology and retarded pollen growth in mutant plants. These allelic mutants of *athmgb15* have a significant reduction in the seed set. Given the impaired pollen morphology and viability resulting from the absence of functional AtHMGB15, we aimed to explore its involvement in pollen formation and maturation during *Arabidopsis* floral development. Pollen development initiates after meiosis of sporogenous cells corresponding to stage 10 of floral development and continues through stages 12 to 13 till the completion of the pollen cell wall (Sanders et al. 1999). Subsequently, filament elongation and anther dehiscence occur, enabling the release of viable pollen grains for germination (Goldberg et al. 1993; Scott et al. 2004). In this investigation, we initially examined the differential gene expression between wild type and *athmgb15-4* mutant during the early stages of flower development, to identify AtHMGB15-regulated targets involved in the pollen development process. Our findings revealed the downregulation of genes responsible for pollen cell wall development in the *athmgb15* mutant. The reduced expression of cell wall-related genes provides a plausible explanation for the defective morphology and distorted cell wall architecture observed in *athmgb15* pollen grains.

AtHMGB15 regulates JA biosynthesis and signaling during pollen development

A significant finding in our study is the differential expression of genes responsible for α-linolenic acid metabolism and response to JA. As previously mentioned, α-linolenic acid serves as a precursor of plant phytohormone, JA. Our RT-qPCR data showed significant downregulation of genes responsible for JA biosynthesis and response pathways in *athmgb15* mutant flowers. This downregulation of JA biosynthesis genes leads to a substantial decrease in jasmonate levels in the *athmgb15-4* mutant. Interestingly, the complementation of *athmgb15-4* with full-length *AtHMGB15* or exogenous application of jasmonate completely restores impaired JA signaling and pollen morphology of *athmgb15-4*, indicating that the defect lies in JA biosynthesis for this phenotype.

Previous studies have established that phytohormone JA is one of the major plant hormones required for different stages of flower development, including regulation of anther development, stamen elongation, dehiscence, flower opening, and pollen development (McConn and Browse 1996; Ishiguro et al. 2001; Mandaokar et al. 2006; Mandaokar and Browse 2009; Qi et al. 2015; Huang et al. 2017a, 2017b; Huang et al. 2020). Mutants, deficient in JA biosynthesis and signaling, were found to have reduced fertility or are male sterile (Feys et al. 1994; Xie et al. 1998; Ishiguro et al. 2001; Park et al. 2002; Cheng et al. 2009). Collectively, the low jasmonate content observed in *athmgb15-4* indicates that AtHMGB15 plays a crucial role in regulating the JA pathway for the development of viable pollen grains in *Arabidopsis*.

AtHMGB15-mediated regulation of JA signaling in *athmgb15-4* plants

Attenuation of JA signaling at specific developmental stages is crucial for the proper growth and fitness of plants. This regulation involves intricate interactions between JA biosynthesis and signaling through positive and negative feedback loops (Wasternack and Hause 2013; Wasternack 2019; Zander et al. 2020). Positive feedback stimulates JA biosynthesis to activate JA signaling, while the negative loop controls the activity of TFs such as MYC2 by inducing the expression of negative repressors like *JAZ* or *JAZ* splice variants (Chini et al. 2007; Pauwels and Goossens 2011; Song et al. 2011, 2014; Chini et al. 2016). The basic helix–loop–helix TF MYC2 serves as the master regulator of JA signaling (Kazan and Manners 2013). The transcriptional activity of MYC2, responsible for JA-responsive gene expression, is tightly controlled by the SCFCOI1–JAZ complex. The physical interaction of JAZ1 with MYC2 attenuates the transcriptional activity of MYC2 (Xu et al. 2002; Chini et al. 2007; Acosta and Przybyl 2019), which is released by jasmonate-induced SCF^{COI1}-dependent proteasomal degradation of JAZ (Devoto et al. 2002; Thines et al. 2007; Kazan and Manners 2008). Intriguingly, MYC2 targets its own promoter, as well as the promoters of JAZ genes, during jasmonate response, indicating that MYC2 activates its own transcription and that of its negative regulator, JAZ (Dombrecht et al. 2007; Kazan and Manners 2013; Zander et al. 2020). This tight regulation leads to a negative feedback loop in JA signaling where JA-dependent destruction of MYC2 repressor followed by MYC2-dependent activation of *JAZ* repressor regulates the appropriate amplitude of JA signaling during various development processes (Chini et al. 2007).

Our findings demonstrate that AtHMGB15 directly binds to the promoter of *MYC2* and interacts with MYC2 to form the activator complex that positively regulates the transcription of *MYC2*. Since the expression of *MYC2* is compromised in *athmgb15* mutant, expression of most of the *JAZ* genes (*JAZ1*, *5*,*6*,*7*,*8*, and *10*) was found to be downregulated in these plants (Supplementary Fig. S6). The downregulation of both *MYC2* and *JAZ* suggests that fine-tuning of JA signaling is severely affected in *athmgb15* mutants.

Regulation of JA biosynthesis

Studies have revealed that JA biosynthesis is regulated by a positive feedback loop through the SCF^{COI1}–JAZ regulatory module in the presence of jasmonate derivative (Devoto et al. 2002). The JA-dependent release of MYC2 binds to JA-responsive elements (G-box) present in the promoters of JA biosynthesis genes such as *AOS*, *AOC3*, *OPR3*, *OPRL1*, *LOX3*, and *LOX4* to promote their transcription (Dombrecht et al. 2007; Pozo et al. 2008; Figueroa and Browse 2012; Kazan and Manners 2013). Additionally, a previous transcriptome study has shown the downregulation of JA biosynthesis genes in *MYC2* mutant *jin1-8* plants (Lorenzo et al. 2004), further supporting the role of MYC2 in the transcription of JA biosynthesis genes. In this study, we have observed a decrease in the expression of JA biosynthesis genes and low jasmonate content in *MYC2* mutants *myc2-2* and *jin1-2*, supporting that MYC2 regulates transcription of JA biosynthesis. Since AtHMGB15 positively regulates the *MYC2* expression, we reasoned that the low expression of JA biosynthesis genes is due to the downregulation of *MYC2* gene expression in *athmgb15-4*. Our data align with previous studies showing MYC2 controls JA biosynthesis genes through a positive feedback loop (Van Moerkercke et al. 2019).

DAD1 is a chloroplastic phospholipase A1 lipase that is involved in the initial step of JA biosynthesis for the formation of α-linolenic acid. The *dad1* mutants were defective in anther dehiscence, pollen maturation, and flower bud development (Ishiguro et al. 2001; Peng et al. 2013). The expression of *DAD1* is regulated by the homeotic protein AGAMOUS and the auxin-responsive factors ARF6 and ARF8 (Nagpal et al. 2005; Tabata et al. 2010). Our study shows a small change in the expression of *ARF6* but no change in the expression of *AGAMOUS* or *ARF8*. However, the expression of *COI1* was found to be severely repressed in *athmgb15* mutants. A previous study has shown that wound-induced *DAD1* expression is lower in JA biosynthesis mutants *aos* and *opr3*, and completely abolished in *coi1*, suggesting that *DAD1* expression is regulated by both coronatine insensitive (COI)-dependent and independent mechanisms (Hyun et al. 2008; Ruduś et al. 2014). Considering the repression of *COI1* in *athmgb15-4*, we propose that the transcription of *DAD1* is possibly *COI1*-dependent during the pollen development process.

JAR1, CYP94B3, and ST2A are JA catabolic enzymes required for the formation of JA derivatives JA-Ile, 12-hydroxy-JA-Ile, and 12-HSO4-JA, respectively (Ruan et al. 2019; Wasternack 2019). JA serves as the substrate for JA-Ile formation by JAR1. Similarly, JA-Ile is hydroxylated by CYP94B3, and STA2 uses 12-OH-JA for sulfated derivate (Wasternack and Hause 2013). In each case, it appears that the biosynthesis of JA catabolites depends upon the availability of its substrate and the level of these derivatives through positive feedback. Consistent with these findings, we propose that the low level of JA derivatives is due to the reduced JA content in *athmgb15-4* plants. Consequently, the expression of genes responsible for the formation of JA derivatives was found repressed in *athmgb15* mutants. Furthermore, Koo et al. have demonstrated that the expression of *CYP94B3* is dependent on COI1, as the expression is completely diminished in the *coi1* mutant. Therefore, reduced expression of *CYP94B3* in *athmgb15* mutant may be due to downregulation of *COI1* gene expression and substrate availability (Koo et al. 2011). These collective observations establish the significance of AtHMGB15-mediated regulation in maintaining an appropriate jasmonate concentration during pollen development.

Repression of JA biosynthesis and signaling resulted in downregulation of JA-responsive TF *MYB21* and *MYB24* in *athmgb15* mutant

The R2R3-MYB TFs, MYB21 and MYB24, are considered a critical regulator of JA signaling during stamen development (Huang et al. 2017b, 2020; Yang et al. 2020). In this study, we observed a downregulation of *MYB21* and *MYB24* expression in the *athmgb15-4* mutant. Additionally, we found that AtHMGB15 binds to the promoter of *MYB24* and *MYB21* to activate their transcription. There may be 2 possible reasons for the repression of MYBs in the *athmgb15-4* mutant. Firstly, repression of JA biosynthesis in *athmgb15-4* causes downregulation of *MYB21* and *MYB24* expression, as previously shown in *opr3* mutants (Song et al. 2011; Huang et al. 2020). Furthermore, the absence of functional AtHMGB15 may contribute to the downregulation of MYB21 and MYB24, as AtHMGB15 transcriptionally activates their expression. Genetic analysis has indicated that *MYB21* and *MYB24* are indispensable for stamen growth and development and *myb21myb24* double mutant is completely male sterile with short filaments, delayed anther dehiscence, and nonviable pollen grains (Huang et al. 2020). Consistently, we have observed short filaments in around 30% of *athmgb15-4* flowers. The short filaments may be one possible reason for having defective pollination as anthers fail to reach stigma leading to lower seed yields in *athmgb15-4* mutant.

AtHMGB15 and MYC2 form the activator complex for regulating JA-responsive transcription

Our study reveals an intriguing finding regarding the interaction between the AtHMGB15 protein and the MYC2 TF. We provide evidence demonstrating that AtHMGB15, in conjunction with MYC2, activates the transcription of *MYC2*. Interestingly, previous research by Zander et al. has identified that MYC2 binds many targets that do not have canonical G-box DNA sequence motifs. This suggests that MYC2 may indirectly bind to numerous targets through its interaction with the partner protein AtHMGB15. Our study indicates that AtHMGB15 acts as a necessary partner for MYC2 activity. The interaction between MYC2 and AtHMGB15 suggests that these 2 proteins form a transcriptional activator complex for MYC2-dependent gene expression during JA signaling.

In this study, we provide mechanistic insights into the role of ARID/HMG group nuclear proteins in pollen development. We identify the involvement of AtHMGB15 in the formation of pollen cell wall by positively regulating the expression of cell wall genes. Moreover, we demonstrate the contribution of AtHMGB15 to JA signaling by forming an activator complex with the MYC2 TF, thereby activating JA-dependent gene expression during pollen development (Fig. 7D). Our findings shed light on the physiological roles of plant ARID/HMGs, particularly in gene regulation and chromatin remodeling. The present study shall be a step forward in this direction and establish a role of AtHMGB15 in transcription activation other than being an HMG-box group of nuclear architectural protein.

Materials and methods

Plant materials and growth conditions

Arabidopsis (*A. thaliana*) ecotype Columbia-O (Col) was used in this study. All the mutants and over-expression lines used in this study were in the Col background. The T-DNA insertion line of AtHMGB15 (GABI_351D08) was obtained from the Eurasian Arabidopsis Stock Centre (NASC), and the T-DNA insertion line of AtHMGB15 (SALK057612C) was obtained from the Arabidopsis

Biological Resource Centre (ABRC). SALK_083483 (*atmyc2-2*) and SALK_061267 (*atjin1-2*) and *35S:MYC2-GFP* lines were also procured for the study. The seeds were grown on Murashige and Skoog agar plates at 22 °C under 16-h:8-h light (~150 ± 10 μmol m^{-2} s^{-1}) and dark cycles in the growth chamber. 20-day-old seedlings were transferred to soil pots in the greenhouse with 60% relative humidity. Freshly opened flowers were collected every day between 9:00 AM and 11:00 AM IST during the flowering stage (flowering stage 13) for downstream experiments. Pictures of wild-type, *athmgb15-4* mutant, and *athmgb15-4-OE$_{A4}$* (RE) plants at various growth stages (rosette, inflorescence bolting, fully mature plant with flower and silique stage) were taken using a digital camera. Individual organs such as the flowers and siliques were isolated and investigated for Leica stereo-zoom microscope S9i.

Generation of transgenic plants

The coding sequence of *AtHMGB15* was cloned under 35S in pMDC84 using the gateway cloning system (Invitrogen). This construct was used to generate complementation lines constructed in the *athmgb15-4* mutant background. Plant transformation was performed by *Agrobacterium tumefaciens*-mediated floral dip method, and transgenic plants (Zhang et al. 2006) were selected by hygromycin selection. The complementation lines were confirmed by PCR for insertion and RT-qPCR for expression. The plants were progressed to the T3 generation before they were used for analysis. The list of primers used for this study is presented in Supplementary Table S5.

RNA extraction, Illumina sequencing, and RT-qPCR

Total RNA was isolated from 200 mg of young flowers (flowering stages 12 to 13) of wild type and *athmgb15-4* mutant using RNASure Mini Kit (Nucleopore-Genetix). RNA isolated from three such replicates was pooled and used for Illumina NextSeq 500 sequencing at Eurofins Genomics India Pvt. Ltd. using 2 × 75 bp chemistry generating 30 million paired end reads per sample. Processing of raw read, adaptor removal using Trimmomatic v0.35, and mapping of read to Arabidopsis genome (TAIR10) using TopHat v2.1.1 were performed. The differential gene expression analysis was carried out using Cufflink v1.3.0 where threshold fold change was set (FC) values >0 along with *P* value threshold of 0.05 and threshold fold change was set (FC) values > ± 1 with *P* value cutoff filter of 0.05, which were considered as differentially expressed genes. The data are available in the NCBI Sequence Read Archive repository under the accession ID: PRJNA874885.

For the replicates, total RNA was isolated from 200 mg of young as mentioned above. RNA quality was measured using an Agilent Tape station (RIN > 7) by Theomics International Pvt. Ltd. Total RNA integrity was checked by Agilent Bioanalyzer 2100, and samples with clean rRNA peaks only were used for further investigation. Libraries for RNA-seq were prepared according to the KAPA stranded RNA-seq kit with RiboErase (KAPA Biosystems, Wilmington, MA, USA) system. Final library quality and quantity were analyzed by Agilent Bioanalyzer 2100 and Life Technologies Qubit3.0 Fluorometer, respectively. The libraries were size selected for 140 bp ± 10% fragments and sequenced on Illumina Novoseq 6000 to an average depth of 20 million reads using 2 × 150 bp chemistry. Mapping of reads to *Arabidopsis* genome (TAIR10) was performed as mentioned earlier. The data are available in NCBI Sequence Read Archive repository under the accession ID: PRJNA974968.

RT-qPCR was performed, and relative fold change for the gene of interest was calculated with respect to housekeeping gene *AtEF1α* transcript (At1g07920) level using the $2^{-\Delta\Delta CT}$ method. The primers used in the analysis are enlisted in Supplementary Table S5.

Bioinformatics analysis

The ShinyGO v0.77 program was used for the GO annotation analysis of DEGs in terms of Biological Process, Molecular Function, and Cellular Components ontologies. Significantly enriched GO and KEGG pathways of the differentially expressed genes were carried out using ShinyGO v0.77 program. Venny v2.0. was used to generate Venn diagrams for comparison between various datasets. The promoter sequence of *MYC2*, *MYB24*, and *MYB21* was analyzed using PlantPAN 3.0.

Chromatin immunoprecipitation and ChIP-qPCR

Nuclei from the 700 mg of wild-type flower tissue were isolated using the Plant Nuclei isolation kit (Sigma #CELLYTPN1) using the manufacturer's protocol. The chromatin immunoprecipitation assay was performed as described previously by Mallik et al. (2020), and immunoprecipitated DNA was analyzed by ChIP-qPCR. The data were normalized with respect to input, and fold change was calculated against previously characterized 2 loci *At1g01840* and *At1g01310* using the $2^{-\Delta\Delta CT}$ method. Three independent biological replicate samples were used for qPCR experiments, where each sample was collected from ≥80 wild-type plants in the flowering stage. The primer list for the ChIP study is attached in Supplementary Table S5.

Electrophoretic mobility shift assay

EMSA was performed using the protocol described previously (Roy et al. 2016; Mallik et al. 2020). The DNA binding studies were done with PCR fragments obtained from the selected genes by ChIP-qPCR study. The DNA fragments (200 bp) from the promoter/upstream region of *MYC2*, *MYB21*, and *MYB24* containing previously identified AtHMGB15-binding site "A(A/C)–ATA–(A/T)(A/T)" were PCR amplified, and fragments were end labeled with γ^{32}P ATP (3,500 Ci/mmol) using T4 polynucleotide kinase (Thermo Scientific, #EK0031) and purified. 5×10^4 cpm γ^{32}P-labeled DNA (~7 fmol) was mixed with increasing concentrations (15 to 60 nM) of the full-length AtHMGB15 in the presence of 1× EMSA buffer containing 10 mM Tris–HCl (pH 7.5), 5 mM NaCl, 0.1 mM EDTA, 0.5 mM $MgCl_2$, 0.1 mM DTT, 5% (v/v) glycerol, and 1.25 μg/ml poly dI–dC. The DNA–protein mixture was incubated for 1 h on ice and analyzed by 5% (v/v) native PAGE supplemented with 5% (v/v) glycerol in 0.5× TBE at 4 °C.

Site-directed mutagenesis

SDM was done according to the protocol described previously (Roy et al. 2016). Two synthetic partial overlapping primers containing the desired mutation were designed (Supplementary Table S5 and Fig. S12) and extended using Pfu turbo, thereby generating mutated plasmids. The PCR products were treated with 1 μl of DpnI endonuclease (10 U/μl, Agilent) at 37 °C for 1 to 2 h and transformed into competent DH5α cells. The mutation was verified by sequencing. The mutated fragments of *MYC2*, *MYB21*, and *MYB24* were then amplified from the clones, and EMSA was performed as described earlier.

Scanning electron microscopy

Pollen grains were isolated from anthers of dried flowers of wild type, *athmgb15-4* mutant, and *athmgb15-4-OE$_{A4}$* (*RE*) and refined by passing them through a series of fine mesh with decreasing porosity. The pollen grains were brushed onto the brass stub with a carbon tape and subjected to gold coating in Edward gold sputter coater. The coated samples were visualized in SEM (FEI 200) under an accelerating voltage of 5, 10, and 20 kV.

Pollen germination and viability assay

Pollen germination assay was done as described previously (Li 2011). Pollen was isolated from mature wild-type, *athmgb15-4*, and *athmgb15-4-OE$_{A4}$* (*RE*) flowers by drying them and then suspending them in a pollen germination medium containing 20% (*w/v*) sucrose, 100 mM boric acid, 1 M $CaCl_2$, 200 mM Tris–MES, 1 M $MgSO_4$, 30% (*w/v*) PEG 4000, and 500 mM KCl of pH 5.6 to 6. Pollen germination was observed after 2, 4, 6, and 24 h and visualized by a microscope (Nikon ECLIPSE Ni). Double staining with FDA and PI was performed using the method described earlier (Chang et al. 2014). A drop containing the stained pollen grains was viewed under a fluorescence microscope (Nikon ECLIPSE Ni). FDA-stained cells are blue denoting live pollen grains, the PI-stained cells are red denoting dead pollen grains, and the purple-colored pollen grains are sterile in nature. The excitation wavelength used for the fluorescence microscope to observe PI was 535 nm, with an exposure duration of 100 ms and the gain at 1×. The excitation wavelength for FDA was 488 nm, with an exposure duration of 200 ms and the gain at 1.5×.

Hormone estimation

JA content was estimated using electron spray ionization coupled with mass spectroscopy (ESI-MS) as described previously (Liu et al. 2010). 500 mg of fresh flower tissue from wild-type, *athmgb15-4*, and *athmgb15-4-OE$_{A4}$* (*RE*) plants along with *myc2-2* and *jin1-2* was homogenized in liquid N_2 and extracted overnight with methanol (HPLC grade) at 4 °C. The homogenates were centrifuged, diluted with water (HPLC grade), and subjected to the Sep-Pak C18 cartridge (Pierce #89870). SPE cartridge was washed with 20% (*v/v*) and 30% (*v/v*) methanol and finally eluted with 100% (*v/v*) methanol. The eluant was 10 times diluted with methanol and analyzed by ESI-MS. Analytical standards of MeJA (Sigma #392707), JA (Sigma #J2500), and JA-Ile (Cayman Chemical #10740) were used. The relative abundance of all three derivatives in the wild-type, *athmgb15-4*, and *athmgb15-4-OE$_{A4}$* (*RE*) samples was obtained and expressed as fold change with respect to wild type.

Hormone treatment

For MeJA treatment, the wild-type and *athmgb15-4* plants were grown in soil. At the onset of flowering, 0.5 and 2 mM MeJA (Sigma #392707) was sprayed directly onto the flower buds twice a day for 2 consecutive days. The treated flowers were harvested and used for pollen germination assay (Park et al. 2002). RNA isolation, cDNA synthesis, and RT-qPCR were performed with flowers treated with exogenous MeJA (0.5 mM) and harvested at 4 h post-treatment.

GUS assay

GUS assay was performed as described previously (Bedi and Nag Chaudhuri 2018). 2-kb promoter regions of *MYC2*, *MYB21*, and *MYB24* were cloned into pKGWFS7 vector, containing GUS as the reporter gene, by the Gateway cloning (Invitrogen). Similarly, the full-length coding sequence of *AtHMGB15* and *MYC2* was cloned in pMDC84 and pCambia1304, respectively. Overnight culture of *Agrobacterium tumefaciens* strain EHA105 containing *pMYC2*, *pMYB21*, and *pMYB24* was mixed individually with different combinations of Agrobacterium strain containing 35S::AtHMGB15 and 35S::MYC2 at OD_{600}0.8 and infiltrated into the leaves of 6-wk-old *N. benthamiana* plants. The leaf samples were incubated for 48 h and homogenized, and GUS activity was measured using 1 mM 4-Methylumbelliferyl-β-D-glucuronide (MUG) at fluorescence at 455 nm (excitation at 365 nm) in a fluorimeter (Thermo Scientific Varioskan Flash). The total protein concentration of extracted leaf samples was measured by the Bradford method at 595 nm. GUS activity was represented as nanomoles of 4-MU produced per mg of protein, and the total data were obtained from 15 sets of biological repeats.

BiFC

For BiFC assay, the full-length coding sequences of *AtHMGB15* and *MYC2* were cloned through Gateway cloning system (Invitrogen) into the binary vector pSITE-cEYFP-N1 (CD3-1651) and pSITE-nEYFP-C1 (CD3-1648), respectively. *Agrobacterium* strain (EHA105) transformed with the cloned vectors along with the empty vectors as control was infiltrated into the onion epidermis as done previously (Roy et al. 2019). The inner epidermal peels were isolated and subjected to wash with 1× PBS for 16 h, mounted on a slide, and observed for interaction under the confocal microscope (Stellaris 5, Leica). The laser used for the fluorescence microscopy was 488 nm with a collection bandwidth of 513 to 560 nm. The gain was set at 86 with 2% intensity.

Co-immunoprecipitation and immunoblotting

Co-immunoprecipitation was followed as previously described with experimental modifications (Nie et al. 2021). Full-length CoDing Sequence of *MYC2* was cloned into *pGWB618* having Myc tag. The positive clone was transformed into the *A. tumefaciens* strain EHA105. The bacterial cells were pelleted and resuspended to at final OD_{600} at 0.3, in resuspension buffer (10 mM $MgCl_2$, 10 mM MES, 200 μM acetosyringone, pH 5.7) in the dark for 3 h at room temperate prior to infiltration. The resuspended cells were infiltrated in the leaves of *athmgb15-4* (control) and *athmgb15-4-OE$_{A4\text{-}FLAG}$*. Infected leaves were harvested at 48 h after infiltration and frozen in liquid nitrogen. Total proteins were extracted from infected leaves using extraction buffer (3 ml/g of leaf) containing 50 mM Tris–HCl (pH 7.4), 1 mM EDTA, 150 mM NaCl, 5% (*v/v*) glycerol, 0.5% (*v/v*) Triton X-100, 1 mM PMSF, and 1× Protease Inhibitor Cocktail Tablets (Roche). After centrifugation at 20,000 g for 30 min, the extracts were precleared with protein A^{plus} agarose beads (BB#-PA001PD) to reduce nonspecific interactions. The input sample was collected from pre-cleaned extract. The complex was immunoprecipitated using Anti-Myc antibody (abcam #9E10) overnight at 4 °C and pulled down using Magna ChIP Protein A + G Magnetic beads (Millipore #16-663). The co-immunoprecipitated protein samples were extracted from the beads using 2× SDS sample buffer, boiled, and separated in a 10% (*v/v*) SDS–PAGE followed by transfer to a PVDF membrane. The co-immunoprecipitation was detected using anti-FLAG M2 antibody (Sigma-Aldrich #F1804) and anti-Myc antibody (abcam #9E10). The blot was detected with Enhanced Chemiluminescence substrate (Bio-Rad).

Alternatively, in the leaves of *athmgb15-4-OE$_{A4\text{-}FLAG}$*, the Myc-MYC2 and PGWB618 (control) were infiltrated. The procedure was followed as above; instead, the complex was pulled down

against Anti-FLAG Affinity beads (abcam #270704) and detected against anti-Myc antibody and anti-FLAG M2 antibody (control).

Co-immunoprecipitation was carried out with Arabidopsis overexpressing MYC2-GFP lines and Col-0 plants (control). The total protein was extracted as described above. The extract was pulled down using anti-GFP nanobody Magnetic beads (Antibodies.com #A310039), and the AtHMGB15 was detected using custom-made affinity-purified anti-AtHMGB15 (Thermo Scientific) antibody. MYC2-GFP was detected using anti-GFP (Plant specific) antibody (Antibodies.com #A50024). Western blot using preimmune Sera was used as experimental controls. The co-immunoprecipitation experiments were repeated at least 3 times.

Quantification and statistical analysis

Statistical analysis was performed using GraphPad Prism8 (GraphPad Software) and IBM SPSS Statistics (v29.0.2.0). The values shown in the figures are either means of 3 or more experimental replicates or means of 3 or more independent experiments as specified in each figure caption. Student's *t*-test and one-way and two-way analysis of variance (ANOVAs) were performed in GraphPad Prism and IBM SPSS Statistics. Details of statistical tests are indicated in each figure legend.

Accession numbers

Sequence data from this article can be found in The *Arabidopsis* Information Resource (TAIR) under the accession numbers *AtHMGB15* (AT1G04880), *MYC2* (AT1G32640), *MYB24* (AT5G40350), *MYB21* (AT3G27810), and *EF1* (AT1G07920). The accession numbers of genes are mentioned in Supplementary Table S5.

Acknowledgments

The authors sincerely thank Dr Sreeramaiah Gangappa (IISER, Kolkata) for the seeds of SALK_083483 (*atmyc2-2*), SALK_061267 (*atjin1-2*), *35S:MYC2-GFP* line, and pGWB618 vector and Dr Anindita Seal (Department of Biotechnology, University of Calcutta) for BiFC vectors.

Author contributions

S.C. conceptualized the idea, supervised the project, and was involved in funding acquisition. S.S. performed all the experiments related to raising transgenic and morphological studies, RT-qPCR, pollen germination assay, ChIP, EMSA, SDM, BiFC, Co-immunoprecipitation assay and immunoblotting, SEM, hormone estimation, preparation of samples for RNA-seq, analysis of RNA-seq data (accession ID: PRJNA874885 and PRJNA974968), promoter assay, hormone treatment, and screening of SALK_057612C_15 and SALK_057612C_9 mutants. R.B. performed the experiments on pollen viability, pollen germination, promoter assay, and flower morphology and assisted S.S. in EMSA, SEM, ChIP, and analyzing RNA-seq (accession ID: PRJNA874885). A.R. screened *athmgb15-4* mutant line, standardization of pollen SEM, and prepared samples for RNA-seq. A.N. assisted S.S. in screening of SALK_057612C_15 and SALK_057612C_9 mutants and assisted R.B. in flower morphology. V.R. assisted S.S. in analyzing RNA-seq data (accession ID: PRJNA974968). S.B. assisted S.S. in EMSA. S.S. contributed to the critical revision of the manuscript. S.C. wrote the original draft, and all the authors read, edited, and reviewed it.

Supplementary data

The following materials are available in the online version of this article.

Supplementary Table S1. Summary of 111 downregulated genes common to *athmgb15-1* and *athmgb15-4* mutants.

Supplementary Table S2. Summary of 60 upregulated genes common to *athmgb15-1* and *athmgb15-4* mutants.

Supplementary Table S3. Summary of downregulated genes common to *athmgb15-4* flowers (RNA-seq) vs wild-type seedlings (ChIP-on-chip).

Supplementary Table S4. Summary of upregulated genes common to *athmgb15-4* flowers (RNA-seq) vs wild-type seedlings (ChIP-on-chip).

Supplementary Table S5. List of primers.

Supplementary Figure S1. Confirmation of *athmgb15-4* homozygous line was done by Southern blot.

Supplementary Figure S2. *athmgb15-4* mutant shows retarded primary root growth.

Supplementary Figure S3. *athmgb15-4* shows delayed flowering compared to wild type.

Supplementary Figure S4. Gene ontology analysis of differentially enriched genes.

Supplementary Figure S5. KEGG ontology analysis of differentially enriched genes.

Supplementary Figure S6. Analysis of transcriptome data and validation of selected genes.

Supplementary Figure S7. Comparative analysis of DEGs (flower tissue) with Xia et al. (2014) (pollen tissue) and Mallik et al. (2020) (seedling tissue) datasets.

Supplementary Figure S8. Representative pollen grains isolated from wild type and the *athmgb15-4* mutant.

Supplementary Figure S9. Isolation and characterization of the homozygous line of *AtHMGB15* from SALK_057612C.

Supplementary Figure S10. Relative expression of JA biosynthesis and JA signaling genes post-MeJA treatment of the *athmgb15-4* mutant.

Supplementary Figure S11. Western blot using total protein from flower tissue of wild type and *athmgb15-4*.

Supplementary Figure S12. DNA binding analysis of *MYC2*, *MYB24*, and *MYB21* using recombinant AtHMGB15 protein.

Supplementary Figure S13. Co-immunoprecipitation (co-IP) assay confirming interaction of AtHMGB15 and MYC2.

Supplementary Figure S14. Representative flowers isolated from wild type, *athmgb15-4*, and *athmgb15-4-OE*$_{A4}$ lines (RE).

Funding

This work was supported by the Science and Engineering Research Board (SERB), Department of Science and Technology, Government of India (SERB/2017/000768 and CRG/2022/001524). S.S. sincerely acknowledges the University Grants Commission (UGC), Government of India, for her fellowship [UGC-Ref. No.: 749/(CSIR-UGC NET DEC. 2016)]. The authors sincerely acknowledge the Bose Institute for institutional support.

Conflict of interest statement. The authors declared no conflict of interest.

Data availability

The datasets generated during this current study are available in the NCBI Sequence Read Archive repository (https://www.ncbi.nlm.nih.gov/sra/PRJNA874885) under the accession ID:

PRJNA874885. The replicates are available in the NCBI Sequence Read Archive repository (https://www.ncbi.nlm.nih.gov/sra/PRJNA974968) under the accession ID: PRJNA974968.

References

Acosta IF, Przybyl M. Jasmonate signaling during Arabidopsis stamen maturation. *Plant Cell Physiol*. 2019:60(12):2648–2659. https://doi.org/10.1093/pcp/pcz201

Bedi S, Nag Chaudhuri R. Transcription factor ABI 3 auto-activates its own expression during dehydration stress response. *FEBS Lett*. 2018:592(15):2594–2611. https://doi.org/10.1002/1873-3468.13194

Boter M, Ruíz-Rivero O, Abdeen A, Prat S. Conserved MYC transcription factors play a key role in jasmonate signaling both in tomato and Arabidopsis. *Genes Dev*. 2004:18(13):1577–1591. https://doi.org/10.1101/gad.297704

Caldelari D, Wang G, Farmer EE, Dong X. Arabidopsis lox3 lox4 double mutants are male sterile and defective in global proliferative arrest. *Plant Mol Biol*. 2011:75(1-2):25–33. https://doi.org/10.1007/s11103-010-9701-9

Chang F, Zhang Z, Jin Y, Ma H. Cell biological analyses of anther morphogenesis and pollen viability in Arabidopsis and rice. In: Riechmann JL, Wellmer F, editors. *Flower development: methods and protocols*. New York (NY): Springer; 2014. p. 203–216

Cheng H, Song S, Xiao L, Soo HM, Cheng Z, Xie D, Peng J. Gibberellin acts through jasmonate to control the expression of MYB21, MYB24, and MYB57 to promote stamen filament growth in Arabidopsis. *PLoS Genet*. 2009:5(3):e1000440. https://doi.org/10.1371/journal.pgen.1000440

Chini A, Fonseca S, Fernandez G, Adie B, Chico J, Lorenzo O, García-Casado G, López-Vidriero I, Lozano F, Ponce M. The JAZ family of repressors is the missing link in jasmonate signalling. *Nature*. 2007:448(7154):666–671. https://doi.org/10.1038/nature06006

Chini A, Gimenez-Ibanez S, Goossens A, Solano R. Redundancy and specificity in jasmonate signalling. *Curr Opin Plant Biol*. 2016:33:147–156. https://doi.org/10.1016/j.pbi.2016.07.005

Devoto A, Nieto-Rostro M, Xie D, Ellis C, Harmston R, Patrick E, Davis J, Sherratt L, Coleman M, Turner JG. COI1 links jasmonate signalling and fertility to the SCF ubiquitin–ligase complex in Arabidopsis. *Plant J*. 2002:32(4):457–466. https://doi.org/10.1046/j.1365-313X.2002.01432.x

Dombrecht B, Xue GP, Sprague SJ, Kirkegaard JA, Ross JJ, Reid JB, Fitt GP, Sewelam N, Schenk PM, Manners JM, *et al*. MYC2 differentially modulates diverse jasmonate-dependent functions in Arabidopsis. *Plant Cell*. 2007:19(7):2225–2245. https://doi.org/10.1105/tpc.106.048017

Feys BJ, Benedetti CE, Penfold CN, Turner JG. Arabidopsis mutants selected for resistance to the phytotoxin coronatine are male sterile, insensitive to methyl jasmonate, and resistant to a bacterial pathogen. *Plant Cell*. 1994:6(5):751–759. https://doi.org/10.2307/3869877

Figueroa P, Browse J. The Arabidopsis JAZ2 promoter contains a G-Box and thymidine-rich module that are necessary and sufficient for jasmonate-dependent activation by MYC transcription factors and repression by JAZ proteins. *Plant Cell Physiol*. 2012:53(2):330–343. https://doi.org/10.1093/pcp/pcr178

Gao C, Qi S, Liu K, Li D, Jin C, Li Z, Huang G, Hai J, Zhang M, Chen M. MYC2, MYC3, and MYC4 function redundantly in seed storage protein accumulation in Arabidopsis. *Plant Physiol Biochem*. 2016:108:63–70. https://doi.org/10.1016/j.plaphy.2016.07.004

Goldberg RB, Beals TP, Sanders PM. Anther development: basic principles and practical applications. *Plant Cell*. 1993:5(10):1217. https://doi.org/10.1105/tpc.5.10.1217

Goossens J, Mertens J, Goossens A. Role and functioning of bHLH transcription factors in jasmonate signalling. *J Exp Bot*. 2017:68(6):1333–1347. https://doi.org/10.1093/jxb/erw440

Hansen FT, Madsen CK, Nordland AM, Grasser M, Merkle T, Grasser KD. A novel family of plant DNA-binding proteins containing both HMG-box and AT-rich interaction domains. *Biochemistry*. 2008:47(50):13207–13214. https://doi.org/10.1021/bi801772k

Huang H, Gao H, Liu B, Qi T, Tong J, Xiao L, Xie D, Song S. Arabidopsis MYB24 regulates jasmonate-mediated stamen development. *Front Plant Sci*. 2017a:8:1525. https://doi.org/10.3389/fpls.2017.01525

Huang H, Gong Y, Liu B, Wu D, Zhang M, Xie D, Song S. The DELLA proteins interact with MYB21 and MYB24 to regulate filament elongation in Arabidopsis. *BMC Plant Biol*. 2020:20(1):1–9. https://doi.org/10.1186/s12870-020-2274-0

Huang H, Liu B, Liu L, Song S. Jasmonate action in plant growth and development. *J Exp Bot*. 2017b:68(6):1349–1359. https://doi.org/10.1093/jxb/erw495

Hyun Y, Choi S, Hwang H-J, Yu J, Nam S-J, Ko J, Park J-Y, Seo YS, Kim EY, Ryu SB. Cooperation and functional diversification of two closely related galactolipase genes for jasmonate biosynthesis. *Dev Cell*. 2008:14(2):183–192. https://doi.org/10.1016/j.devcel.2007.11.010

Ishiguro S, Kawai-Oda A, Ueda J, Nishida I, Okada K. The DEFECTIVE IN ANTHER DEHISCENCE1 Gene Encodes a Novel Phospholipase A1 catalyzing the initial step of jasmonic acid biosynthesis, which synchronizes pollen maturation, anther dehiscence, and flower opening in Arabidopsis. *Plant Cell*. 2001:13(10):2191–2209. https://doi.org/10.1105/tpc.010192

Jang G, Yoon Y, Choi YD. Crosstalk with jasmonic acid integrates multiple responses in plant development. *Int J Mol Sci*. 2020:21(1):305. https://doi.org/10.3390/ijms21010305

Kazan K, Manners JM. Jasmonate signaling: toward an integrated view. *Plant Physiol*. 2008:146(4):1459–1468. https://doi.org/10.1104/pp.107.115717

Kazan K, Manners JM. MYC2: the master in action. *Mol Plant*. 2013:6(3):686–703. https://doi.org/10.1093/mp/sss128

Koo AJ, Cooke TF, Howe GA. Cytochrome P450 CYP94B3 mediates catabolism and inactivation of the plant hormone jasmonoyl-L-isoleucine. *Proc Natl Acad Sci*. 2011:108(22):9298–9303. https://doi.org/10.1073/pnas.1103542108

Li X. Arabidopsis pollen tube germination. *Bio Protoc*. 2011:1(10):e73. https://doi.org/10.21769/BioProtoc.73

Liu X, Yang Y, Lin W, Tong J, Huang Z, Xiao L. Determination of both jasmonic acid and methyl jasmonate in plant samples by liquid chromatography tandem mass spectrometry. *Chin Sci Bull*. 2010:55(21):2231–2235. https://doi.org/10.1007/s11434-010-3194-4

Lorenzo O, Chico JM, Saénchez-Serrano JJ, Solano R. JASMONATE-INSENSITIVE1 encodes a MYC transcription factor essential to discriminate between different jasmonate-regulated defense responses in Arabidopsis. *Plant Cell*. 2004:16(7):1938–1950. https://doi.org/10.1105/tpc.022319

Mallik R, Prasad P, Kundu A, Sachdev S, Biswas R, Dutta A, Roy A, Mukhopadhyay J, Bag SK, Chaudhuri S. Identification of genome-wide targets and DNA recognition sequence of the Arabidopsis HMG-box protein AtHMGB15 during cold stress response. *Biochim Biophys Acta (BBA)-Gene Regulatory Mech*. 2020:1863(12):194644. https://doi.org/10.1016/j.bbagrm.2020.194644

Mandaokar A, Browse J. MYB108 acts together with MYB24 to regulate jasmonate-mediated stamen maturation in Arabidopsis. *Plant Physiol*. 2009:149(2):851–862. https://doi.org/10.1104/pp.108.132597

Mandaokar A, Thines B, Shin B, Markus Lange B, Choi G, Koo YJ, Yoo YJ, Choi YD, Choi G, Browse J. Transcriptional regulators of stamen development in Arabidopsis identified by transcriptional profiling. *Plant J*. 2006:46(6):984–1008. https://doi.org/10.1111/j.1365-313X.2006.02756.x

Marciniak K, Przedniczek K. Comprehensive insight into gibberellin- and jasmonate-mediated stamen development. *Genes (Basel)*. 2019:10(10):811. https://doi.org/10.3390/genes10100811

Mascarenhas JP. Gene activity during pollen development. *Ann Rev Plant Biol*. 1990:41(1):317–338. https://doi.org/10.1146/annurev.pp.41.060190.001533

McConn M, Browse J. The critical requirement for linolenic acid is pollen development, not photosynthesis, in an Arabidopsis mutant. *Plant Cell*. 1996:8(3):403–416. https://doi.org/10.2307/3870321

McCormick S. Control of male gametophyte development. *Plant Cell*. 2004:16(suppl_1):S142–S153. https://doi.org/10.1105/tpc.016659

Nagpal P, Ellis CM, Weber H, Ploense SE, Barkawi LS, Guilfoyle TJ, Hagen G, Alonso JM, Cohen JD, Farmer EE. Auxin response factors ARF6 and ARF8 promote jasmonic acid production and flower maturation. *Development*. 2005:132(18):4107–4118. https://doi.org/10.1242/dev.01955

Nie J, Zhou W, Liu J, Tan N, Zhou JM, Huang L. A receptor-like protein from *Nicotiana benthamiana* mediates VmE02 PAMP-triggered immunity. *New Phytolog*. 2021:229(4):2260–2272. https://doi.org/10.1111/nph.16995

Park JH, Halitschke R, Kim HB, Baldwin IT, Feldmann KA, Feyereisen R. A knock-out mutation in allene oxide synthase results in male sterility and defective wound signal transduction in Arabidopsis due to a block in jasmonic acid biosynthesis. *Plant J*. 2002:31(1):1–12. https://doi.org/10.1046/j.1365-313X.2002.01328.x

Pauwels L, Goossens A. The JAZ proteins: a crucial interface in the jasmonate signaling cascade. *Plant Cell*. 2011:23(9):3089–3100. https://doi.org/10.1105/tpc.111.089300

Peng YJ, Shih CF, Yang JY, Tan CM, Hsu WH, Huang YP, Liao PC, Yang CH. A RING-type E 3 ligase controls anther dehiscence by activating the jasmonate biosynthetic pathway gene DEFECTIVE IN ANTHER DEHISCENCE 1 in Arabidopsis. *Plant J*. 2013:74(2):310–327. https://doi.org/10.1111/tpj.12122

Pozo MJ, Van Der Ent S, Van Loon L, Pieterse CM. Transcription factor MYC2 is involved in priming for enhanced defense during rhizobacteria-induced systemic resistance in Arabidopsis thaliana. *New Phytol*. 2008:180(2):511–523. https://doi.org/10.1111/j.1469-8137.2008.02578.x

Qi T, Huang H, Song S, Xie D. Regulation of jasmonate-mediated stamen development and seed production by a bHLH-MYB complex in Arabidopsis. *Plant Cell*. 2015:27(6):1620–1633. https://doi.org/10.1105/tpc.15.00116

Roy D, Chakrabarty J, Mallik R, Chaudhuri S. Rice Trithorax factor ULTRAPETALA 1 (OsULT1) specifically binds to "GAGAG" sequence motif present in Polycomb response elements. *Biochim Biophys Acta – Gene Regul Mech*. 2019:1862(5):582–597.

Roy A, Dutta A, Roy D, Ganguly P, Ghosh R, Kar RK, Bhunia A, Mukhopadhyay J, Chaudhuri S. Deciphering the role of the AT-rich interaction domain and the HMG-box domain of ARID-HMG proteins of Arabidopsis thaliana. *Plant Mol Biol*. 2016:92(3):371–388. https://doi.org/10.1007/s11103-016-0519-y

Ruan J, Zhou Y, Zhou M, Yan J, Khurshid M, Weng W, Cheng J, Zhang K. Jasmonic acid signaling pathway in plants. *Int J Mol Sci*. 2019:20-(10):2479. https://doi.org/10.3390/ijms20102479

Ruduś I, Terai H, Shimizu T, Kojima H, Hattori K, Nishimori Y, Tsukagoshi H, Kamiya Y, Seo M, Nakamura K. Wound-induced expression of DEFECTIVE IN ANTHER DEHISCENCE1 and DAD1-like lipase genes is mediated by both CORONATINE INSENSITIVE1-dependent and independent pathways in Arabidopsis thaliana. *Plant Cell Rep*. 2014:33(6):849–860. https://doi.org/10.1007/s00299-013-1561-8

Sanders PM, Bui AQ, Weterings K, McIntire K, Hsu Y-C, Lee PY, Truong MT, Beals T, Goldberg R. Anther developmental defects in *Arabidopsis thaliana* male-sterile mutants. *Sex Plant Reprod*. 1999:11(6):297–322. https://doi.org/10.1007/s004970050158

Schweizer F, Fernández-Calvo P, Zander M, Diez-Diaz M, Fonseca S, Glauser G, Lewsey MG, Ecker JR, Solano R, Reymond P. Arabidopsis basic helix-loop-helix transcription factors MYC2, MYC3, and MYC4 regulate glucosinolate biosynthesis, insect performance, and feeding behavior. *Plant Cell*. 2013:25(8):3117–3132. https://doi.org/10.1105/tpc.113.115139

Scott RJ, Spielman M, Dickinson H. Stamen structure and function. *Plant Cell*. 2004:16(suppl_1):S46–S60. https://doi.org/10.1105/tpc.017012

Song S, Qi T, Huang H, Ren Q, Wu D, Chang C, Peng W, Liu Y, Peng J, Xie D. The jasmonate-ZIM domain proteins interact with the R2R3-MYB transcription factors MYB21 and MYB24 to affect jasmonate-regulated stamen development in Arabidopsis. *Plant Cell*. 2011:23(3):1000–1013. https://doi.org/10.1105/tpc.111.083089

Song S, Qi T, Wasternack C, Xie D. Jasmonate signaling and crosstalk with gibberellin and ethylene. *Curr Opin Plant Biol*. 2014:21:112–119. https://doi.org/10.1016/j.pbi.2014.07.005

Stintzi A, Browse J. The Arabidopsis male-sterile mutant, opr3, lacks the 12-oxophytodienoic acid reductase required for jasmonate synthesis. *Proc Natl Acad Sci*. 2000:97(19):10625–10630. https://doi.org/10.1073/pnas.190264497

Štros M, Launholt D, Grasser KD. The HMG-box: a versatile protein domain occurring in a wide variety of DNA-binding proteins. *Cell Mol Life Sci*. 2007:64(19-20):2590–2606. https://doi.org/10.1007/s00018-007-7162-3

Tabata R, Ikezaki M, Fujibe T, Aida M, Tian C-e, Ueno Y, Yamamoto KT, Machida Y, Nakamura K, Ishiguro S. Arabidopsis auxin response factor6 and 8 regulate jasmonic acid biosynthesis and floral organ development via repression of class 1 KNOX genes. *Plant Cell Physiol*. 2010:51(1):164–175. https://doi.org/10.1093/pcp/pcp176

Thines B, Katsir L, Melotto M, Niu Y, Mandaokar A, Liu G, Nomura K, He S, Howe G, Browse J. JAZ repressor proteins are targets of the SCF (COI1) complex during jasmonate signalling. *Nature*. 2007:448(7154):661–665. https://doi.org/10.1038/nature05960

Van Moerkercke A, Duncan O, Zander M, Šimura J, Broda M, Vanden Bossche R, Lewsey MG, Lama S, Singh KB, Ljung K, *et al.* A MYC2/MYC3/MYC4-dependent transcription factor network regulates water spray-responsive gene expression and jasmonate levels. *Proc Natl Acad Sci*. 2019:116(46):23345–23356. https://doi.org/10.1073/pnas.1911758116

Vera-Sirera F, Gomez MD, Perez-Amador MA. DELLA proteins, a group of GRAS transcription regulators that mediate gibberellin signaling. In: Gonzalez D, editor. Plant transcription factors. USA: Elsevier; 2016. p. 313–328. https://doi.org/10.1016/B978-0-12-800854-6.00020-8

Wasternack C. Termination in jasmonate signaling by MYC2 and MTBs. *Trends Plant Sci*. 2019:24(8):667–669. https://doi.org/10.1016/j.tplants.2019.06.001

Wasternack C, Hause B. Jasmonates: biosynthesis, perception, signal transduction and action in plant stress response, growth and development. An update to the 2007 review in Annals of Botany. *Ann Bot*. 2013:111(6):1021–1058. https://doi.org/10.1093/aob/mct067

Wilson ZA, Zhang D-B. From Arabidopsis to rice: pathways in pollen development. *J Exp Bot*. 2009:60(5):1479–1492. https://doi.org/10.1093/jxb/erp095

Xia C, Wang YJ, Liang Y, Niu QK, Tan XY, Chu LC, Chen LQ, Zhang XQ, Ye D. The ARID-HMG DNA-binding protein A t HMGB 15 is required for pollen tube growth in Arabidopsis thaliana. *Plant J*. 2014:79(5):741–756. https://doi.org/10.1111/tpj.12582

Xie D-X, Feys BF, James S, Nieto-Rostro M, Turner JG. COI1: an Arabidopsis gene required for jasmonate-regulated defense and fertility. *Science*. 1998:280(5366):1091–1094. https://doi.org/10.1126/science.280.5366.1091

Xu L, Liu F, Lechner E, Genschik P, Crosby WL, Ma H, Peng W, Huang D, Xie D. The SCFCOI1 ubiquitin-ligase complexes are required for jasmonate response in Arabidopsis. *Plant Cell*. 2002:14(8):1919–1935. https://doi.org/10.1105/tpc.003368

Yang Z, Li Y, Gao F, Jin W, Li S, Kimani S, Yang S, Bao T, Gao X, Wang L. MYB21 interacts with MYC2 to control the expression of terpene synthase genes in flowers of *Freesia hybrida* and *Arabidopsis thaliana*. *J Exp Bot*. 2020:71(14):4140–4158. https://doi.org/10.1093/jxb/eraa184

Zander M, Lewsey MG, Clark NM, Yin L, Bartlett A, Saldierna Guzmán JP, Hann E, Langford AE, Jow B, Wise A. Integrated multi-omics framework of the plant response to jasmonic acid. *Nat Plants*. 2020:6(3):290–302. https://doi.org/10.1038/s41477-020-0605-7

Zhai Q, Zhang X, Wu F, Feng H, Deng L, Xu L, Zhang M, Wang Q, Li C. Transcriptional mechanism of jasmonate receptor COI1-mediated delay of flowering time in Arabidopsis. *Plant Cell*. 2015:27(10):2814–2828. https://doi.org/10.1105/tpc.15.00619

Zhang X, He Y, Li L, Liu H, Hong G. Involvement of the R2R3-MYB transcription factor MYB21 and its homologs in regulating flavonol accumulation in Arabidopsis stamen. *J Exp Bot*. 2021:72(12):4319–4332. https://doi.org/10.1093/jxb/erab156

Zhang X, Henriques R, Lin S-S, Niu Q-W, Chua N-H. Agrobacterium-mediated transformation of Arabidopsis thaliana using the floral dip method. *Nat Protocols*. 2006:1(2):641–646. https://doi.org/10.1038/nprot.2006.97

Zhang ZB, Zhu J, Gao JF, Wang C, Li H, Li H, Zhang HQ, Zhang S, Wang DM, Wang QX. Transcription factor AtMYB103 is required for anther development by regulating tapetum development, callose dissolution and exine formation in Arabidopsis. *Plant J*. 2007:52(3):528–538. https://doi.org/10.1111/j.1365-313X.2007.03254.x

BBA - Gene Regulatory Mechanisms 1863 (2020) 194644

Contents lists available at ScienceDirect

BBA - Gene Regulatory Mechanisms

journal homepage: www.elsevier.com/locate/bbagrm

Research paper

Identification of genome-wide targets and DNA recognition sequence of the *Arabidopsis* HMG-box protein AtHMGB15 during cold stress response

Rwitie Mallik[a], Priti Prasad[b,c,1], Anindya Kundu[a,1], Sonal Sachdev[a], Ruby Biswas[a], Arkajyoti Dutta[d], Adrita Roy[a], Jayanta Mukhopadhyay[d], Sumit K. Bag[b,c], Shubho Chaudhuri[a,*]

[a] Division of Plant Biology, Bose Institute, P1/12 C.I.T Scheme VII M, Kolkata 700054, India
[b] Academy of Scientific and Innovative Research (AcSIR), CSIR-NBRI Campus, Lucknow, India
[c] Computational Biology Lab, Council of Scientific and Industrial Research - National Botanical Research Institute (CSIR-NBRI), Rana Pratap Marg, Lucknow, Uttar Pradesh 226001, India
[d] Department of Chemistry, Bose Institute, P1/12 C.I.T Scheme VII M, Kolkata 700054, India

ARTICLE INFO

Keywords:
Arabidopsis thaliana
ARID-HMG
AtHMGB15
ChIP-chip
Cold stress
DNaseI footprinting

ABSTRACT

AtHMGB15 belongs to a group of ARID-HMG proteins which are plant specific. The presence of two known DNA binding domains: AT rich interacting domain (ARID) and High Mobility Group (HMG)-box, in one polypeptide, makes this protein intriguing. Although proteins containing individual HMG and ARID domains have been characterized, not much is known about the role of ARID-HMG proteins. Promoter analysis of AtHMGB15 showed the presence of various stress responsive *cis* regulatory elements along with MADS-box containing transcription factors. Our result shows that the expression of AtHMGB15 increased significantly upon application of cold stress. Using ChIP-chip approach, we have identified 6128 and 4689 significantly enriched loci having AtHMGB15 occupancy under control and cold stressed condition respectively. GO analysis shows genes belonging to abiotic stress response, cold response and root development were AtHMGB15 targets during cold stress. DNA binding and footprinting assays further identified A(A/C)–ATA—(A/T)(A/T) as AtHMGB15 binding motif. The enriched probe distribution in both control and cold condition shows a bias of AtHMGB15 binding towards the transcribed (gene body) region. Further, the expression of cold stress responsive genes decreased in *athmgb15* knockout plants compared to wild-type. Taken together, binding enrichment of AtHMGB15 to the promoter and upstream to stress loci suggest an unexplored role of the protein in stress induced transcription regulation.

1. Introduction

Plants are subjected to various kinds of adverse environmental stresses throughout their lifespan. Being sessile organisms, plants can cope with such conditions by changing the cellular processes within themselves through reprogramming of the transcriptome. These stress dependent changes in plants are needed to act against adverse environmental condition for maintaining the overall stability during stress situations. However, the compact chromatin structure in eukaryotic cell imposes various constraints to many DNA dependent processes such as transcription, replication, repair, recombination and transposition. This problem is overcome by the unique aspect of plasticity present in the eukaryotic chromatin. Even though the DNA is very tightly packed, it is rendered accessible for carrying out various DNA dependent processes. This dynamicity of the genome architecture is extremely fascinating and has become one of the most studied aspects in chromatin biology in the last few decades.

Preliminary DNA packaging begins with the coiling of DNA with the aid of the histone octamer where it forms the bead on the string arrangement [1]. Following this, the DNA undergoes rounds of supercoiling to finally attain the condensed form of the chromatin [2,3]. DNA binding proteins that aid in stabilizing the DNA structure during this packaging form the 'Architectural group of proteins' that promotes wrapping, bending and bridging [4]. Similarly, to make the packaged DNA accessible for different nuclear factors, alteration of compact chromatin structure to a more open configuration is required. This

Abbreviations: HMG, High Mobility Group; ARID, AT rich interaction domain

* Corresponding author.
E-mail address: shubho@jcbose.ac.in (S. Chaudhuri).

[1] Equal contribution.

https://doi.org/10.1016/j.bbagrm.2020.194644
Received 28 May 2020; Received in revised form 12 September 2020; Accepted 7 October 2020
Available online 14 October 2020

plasticity is achieved through chromatin remodelling mainly through three methods: by i) modulation of interactions between an architectural protein and DNA [5], ii) modulating the higher-order folding of the genome by antagonizing or cooperative action of architectural proteins [6–8] and iii) energy dependent displacement of DNA wrappers [9,10]. The High Mobility Group of proteins are the group of architectural proteins involved in modulating chromatin structure and organizing the efficient participation of other proteins in various nuclear activities such as transcription, replication and DNA repair [11–14]. Based on the type of DNA binding domain, HMG proteins are grouped into three distinct classes HMGA, HMGB and HMGN [12]. In plants, with the exception of HMGN, proteins belonging to both HMGA and HMGB families have been characterized [15]. Other than classical HMGB type proteins, plants have three more types of HMG-box containing proteins a) structure-specific recognition protein1 (SSRP1), b) proteins containing three copies of HMG-box (3xHMG) and c) proteins with both AT-rich interaction domain and HMG-box domain (ARID-HMG) [16]. Among the different types of the HMG proteins, the 3xHMG box proteins and the ARID HMG proteins are found exclusively in plants. Interestingly, the presence of two DNA binding domains: ARID and HMG in ARID-HMG group make it a unique member among the plant HMGB-box proteins.

The ARID domain was first identified in Bright, a mouse B-cell-specific transcription factor [17] and DRI gene of Drosophila [18]. Initially characterized as the AT-rich DNA binding domain; subsequent studies have revealed that many ARID domain containing proteins can bind DNA in a non-sequence specific manner [19]. The ARID domain containing proteins have been implicated in a wide variety of roles, including chromatin remodelling, transcription, and cell growth [20]. In *Arabidopsis*, 7 ARID domain containing proteins have been identified and have been grouped into the ARID transcription factor family (https://agris-knowledgebase.org/AtTFDB/). Among these 7 proteins, 4 members belong to the novel ARID-HMG group namely AtHMGB9, AtHMGB10, AtHMGB11 and AtHMGB15. Molecular characterization indicates that ARID-HMG protein can bind to various DNA structures and facilitate DNA bending [21,22]. It is likely that the presence of two DNA binding motifs in ARID-HMG proteins can promote transcription either by modulating the chromatin accessibility or by acting as transcription activators.

Previous studies of plant ARID-HMG group were focused mainly on the biochemical properties of the protein. However, there was less information available to understand the physiological role of this group of proteins. Only a recent study has shown that one member of *Arabidopsis* ARID-HMG family, *AtHMGB15*, is highly expressed in pollen and plays a significant role in pollen tube growth [23]; however, the milieu of roles that might be played by this protein remains unexplored. The advent of ChIP coupled with microarray or sequencing techniques, revolutionized detection of transcription factor binding sites, and aided greatly in gaining insights into their functional roles. In this paper, we are reporting for the first time, about a genome-wide DNA binding study of AtHMGB15. In-silico sequence analysis revealed the presence of stress-responsive element about 500 bp upstream of the transcription start site of *AtHMGB15* gene. Expression analysis showed that *AtHMGB15* is upregulated during various stresses condition, with the maximum upregulation during cold stress. The genome-wide DNA binding study indicates that 6128 loci were significantly enriched in the control data set, whereas 4689 loci were enriched during cold stress response. The genome-wide distribution of AtHMGB15 shows that its occupancy is highly enriched in the euchromatin region with maximum enrichment in gene bodies. Further, *in vitro* and *in vivo* DNA binding studies show that AtHMGB15 prefers to bind AT rich sequence with a motif A(A/C)–ATA—(A/T)(A/T). Further, the integration of gene expression data with the AtHMGB15 ChIP-chip results led to the identification of target genes that were differentially regulated under cold stress. Moreover, transcription studies have shown that expression of many known cold responsive genes that have AtHMGB15 occupancy were differentially regulated in AtHMGB15 knockout mutants. Collectively, the genome-wide analysis of AtHMGB15 targets during cold stress response and integration with gene expression led us to the unravelling of previously unexplored aspects of the protein.

2. Materials and methods

2.1. Plant material and treatment condition

Arabidopsis thaliana ecotype Columbia (Col-0) seeds, after cold (4 °C) stratification, were germinated under 16 h light (~150 ± 10 μmol m^{-2} s^{-1}) and 8 h dark at 22 °C on MS Agar plates. 22 days old Arabidopsis seedlings were subjected to various stress treatment such as cold, salinity, ABA treatment and dehydration for different time period, according to Yamaguchi-Shinozaki et al. [24] with some modifications. Briefly, for cold stress treatment, Arabidopsis seedlings were subjected to 4 °C under dim light condition for specific time periods. For ABA and salinity stress, Arabidopsis seedlings were hydroponically treated with 100 μM ABA treatment (for 22 h) and 150 mM NaCl (for 16 h) at 22 °C respectively. For dehydration stress, Arabidopsis seedlings were air dried on 3MM filter paper for 30 min. 22 days old Arabidopsis seedlings were subjected to heat stress according to Sakuma et al. with brief modification [25]. The seedlings were incubated at 42 °C for 1 h. 22 days old Arabidopsis seedlings were subjected to UVB for 1 h as described previously [26].

T-DNA insertion lines of *Arabidopsis* ecotype Col-0 lines at AtHMGB15 locus were procured from GABI-Kat collection (351D08). The T-DNA insertion was screened by the presence of sulfadiazine (Sul^r) resistance. The homozygous lines were obtained by self-crossing heterozygous lines (*AtHMGB15/+*) and screening the seeds for Sul^r resistance. *athmgb15* homozygous lines were confirmed by Southern and Northern Blot.

2.2. RNA extraction and q-PCR

RNA extraction and q-PCR was done according to Roy et al. [21]. Three independent sets of Control and stressed (Cold, ABA, UV, heat, salt, drought) samples were used to isolate RNA and 3 μg of total RNA was used to prepare cDNA using Revert-aid RT (Thermo Scientific). Relative fold change for the gene of interest was calculated with respect to AtEF 1α transcript (*At1g07920*) level using $2^{-\Delta\Delta}$ method. The significance of the results was analysed by Student's *t*-test (* denotes $P \leq 0.05$). For gene expression analysis of AtHMGB15 bound genes, three independent sets of wild type and *athmgb15* (Control, Cold 2 h, 4 h, 8 h, 12 h and 24 h) samples were used to isolate RNA and 5 μg of total RNA was used to prepare cDNA using Revert-aid RT (Thermo Scientific). Relative fold change for the gene of interest was calculated with respect to AtEF 1α transcript (*At1g07920*) level or Tubulin (*At1G04820*) using $2^{-\Delta\Delta}$ method. The significance of the results was analysed by two way ANOVA followed by Dunnet's multiple comparison test (* denotes $P \leq 0.05$). The primers used are listed in Supporting Table S5.

2.3. Chromatin immunoprecipitation

Nuclei isolation was performed using plant nuclei isolation kit (Sigma, # CELLYTPN 1) according to the manufacturer's protocol and chromatin immunoprecipitation assay was done as previously described by Roy et al. [27] with a few modifications. The chromatin preparation was subjected to sonication using a water bath sonicator (Diagenode Bioruptor) so that fragments ranging from 750 bp to 200 bp were generated. ChIP was performed with custom made affinity purified AtHMGB15 antibody, and the DNA protein complexes were pulled down using Magna ChIP Protein A + G Magnetic beads (Millipore, # 16-663). Two independent replicates of control and cold stress treated (2 h) samples were used for ChIP-chip studies where each set contained ≥60 22-days old seedlings.

2.4. Microarray analysis

We worked with Genotypic Technology Pvt. Ltd. (Bengaluru, India) to perform the DNA microarray. Labeling, hybridization, and image analyses were all performed at Genotypic life sciences. The custom Agilent binding array includes a total of 415,056 probes each 60 bp in length, that target 98% of the protein coding genes of *Arabidopsis thaliana* covering 5 kb upstream to 2 kb downstream from the transcriptional start sites. Supporting Table S5 contains the list of protein coding genes represented in this custom array. The data obtained was normalized using Median Blanks subtraction and Intra-array (intensity-dependent) Lowess normalization methods. To define regions associated with AtHMGB15, Whitehead Per-Array Neighbourhood algorithm was used (Agilent Genomic Workbench Lite Edition 6.5). The algorithm samples every probe and its immediate upstream or downstream neighbouring probe to identify robust regions of increased probe signals. It does so by examining groups of probe triplets where each probe is significantly enriched ($P < 0.05$) and the maximum distance for two probes to be considered as neighbours is 100 bp. The central probe is then assigned a p xbar value which is the average *p*-value for the central probe and its neighbours in each triplet set. The p xbar significance level is set to 0.05. Genes associated with significant regions were annotated using TAIR 10, and are therefore considered target genes of AtHMGB15. Each target gene was assigned a p xbar $_{min}$ value corresponding to the lowest p xbar among all the probes that fall in one gene. The complete microarray data were uploaded to Gene Expression Omnibus [28] with accession number GSE140593.

2.5. Bioinformatic analysis

The promoter sequence of AtHMGB15 was analysed using PlantPAN 3.0.The functional categorization of all bound genes in control only, cold only and constant binding data set was done using AgriGO (http://bioinfo.cau.edu.cn/agriGO/). The GO terms were assigned significance using the Fisher test. The output generated from AgriGO was represented as a heat map. The enriched, cold regulated gene networking was obtained using STRING 11 software. For motif analysis, 6128 genes that were significantly enriched (pxbar < 0.05) in control and 4689 genes in cold data set were used for analysis. The probes corresponding to these genes were classified as intergenic (promoter and downstream) or gene body probes depending upon the location of the probe from the nearest annotated TSS. Each set was then analysed using MEME-ChIP (http://meme-suite.org/tools/meme-chip). The DREME tool of the MEME ChIP suite generated the de novo DNA binding motifs output. To check the probe binding intensity over the genome, significant probes of control and cold datasets were visualised over the Arabidopsis genome in a 2Kb window on either side of the gene body through the ngs.plot tool [29]. Circular visualization of probe intensity of each gene along with the gene density and their DHS score [30] were carried out by the circa tool for both datasets.

2.6. ChIP-qPCR

To validated the ChIP-chip data, ChIP-qPCR was carried out. For the control data set the immunoprecipitated (IP) DNA from control samples were normalized with respect to input and fold change was calculated against a negative control region (p xbar > 0.05 with very low normalized signal ratio) using $2^{-\Delta\Delta}$ method. For the cold only data set the IP DNA from cold samples was normalized with respect to input and fold change was calculated against IP DNA from control samples for a given set of primer. Power up SYBR green PCR master mix (Applied biosystems, #A25742) and gene specific primers were used for the reactions in an Applied Biosystems 7500 FAST machine. Three independent replicates of control and cold stress treated (2 h) samples were used for qPCR experiments, where each sample contained ≥60 seedlings. The significance of the results was analysed by Student's *t*-test (* denotes $P \leq 0.05$). The primers used for ChIP analysis are listed in Supporting Table S5.

2.7. Immunoprecipitation assay and Western Blot

Nuclear protein from control and cold treated seedlings was isolated using plant nuclei isolation kit, as mentioned above. The extract was then precleaned with pre-immune serum and immunoprecipitated with 1 μg of purified anti-AtHMGB15 antibody at 4 °C. The complex was captured by 40 μl of protein A-Sepharose beads, washed and suspended in 2× Laemmli buffer. The samples were analysed by 10% SDS-PAGE and immunoblotted using anti-AtHMGB15 antibody. To overcome masking of the band of interest, we used a secondary antibody (Abcam # ab99697) that reacts with the light chain of native Rabbit IgG primary antibodies and does not bind to the reduced and denatured Rabbit IgG heavy chain band (50kD). This eliminates the detection of denatured primary heavy and/or light chains during western blotting. 150 ng of whole cell extract were analysed by 10% SDS-PAGE and western blotting was performed using anti-AtHMGB15 and anti-ubiquitin (Santa Cruz # sc-8017) antibodies.

2.8. Protein cloning and purification

The sequence encoding the full length AtHMGB15(At1G04880) cDNA was amplified, cloned and expressed as described previously by Roy et.al [21]. Primers were also designed to amplify individual DNA binding domain: AtHMGB15-ARID domain (30aa to 121aa) and AtHMGB15-HMG box domain (262aa to 331aa). All primers used for cloning are listed in Supporting Table S5. The domains were cloned into pMAL-c2X (NEB) expression vector and expressed as MBP tagged fusion protein in the presence of 0.5 mM IPTG at 28 °C. The MBP tagged recombinant proteins were purified using Amylose resin affinity chromatography. Briefly, cells were lysed in buffer containing 20 mM Tris pH 7.2, 200 mM NaCl, 1 mM EDTA and 1 mM PMSF. The column was washed stepwise using the lysis buffer with 2.5 to 5 mM Maltose and eluted with lysis buffer containing 10 mM Maltose. The eluted fractions were pooled and dialysed against 50 mM Tris-HCl (pH 7.2), 300 mM NaCl, 2.5 mM EDTA, 5% glycerol, 1 mM DTT and 1 mM PMSF. The dialysed proteins were checked for purity by SDS-PAGE, and the concentrations were determined using Bradford reagent.

2.9. Fluorescence anisotropy

Fluorescence Anisotrop was performed as described previously [21]. Equimolar amounts of the single stranded unlabelled reverse primer and the Cy5 labelled forward primer were annealed in buffer [50 mM Tris-Cl (pH 8) and 100 mM NaCl] by heating to 95 °C and kept overnight followed by cooling to 25 °C. The double stranded DNA was then run on 10% acrylamide gel in 0.5× TBE buffer, excised and eluted in 10 mM Tris-Cl (pH 8). 1.6 μg/μl of Cy5 labelled (1.2pM) double stranded oligonucleotide containing either CMAAAB or HWTATAT motif was incubated with increasing concentration of ATHMGB15 protein (24, 48, 72, 96, 120 and 168 nM) in 70 μl reaction volume at 37 °C. Fluorescence anisotropy was monitored at 630 nm excitation and 670 nm emission using PTI fluorescence master QM400 system fitted with automatic polarizers. Normalized fluorescence anisotropy increments (ΔA/A0) were plotted against protein concentration, where A and A0 denote anisotropy of Cy5-DNA with and without protein respectively and ΔA = A-A0. The dissociation constant (Kd) was determined using Sigma Plot by fitting the curve with three parameter sigmoidal function {f = a/(1 + exp.(−(X-X0)/b))} where f is the complex concentration, X is the concentration of ATHMGB15 and X0 is the half-saturation constant.

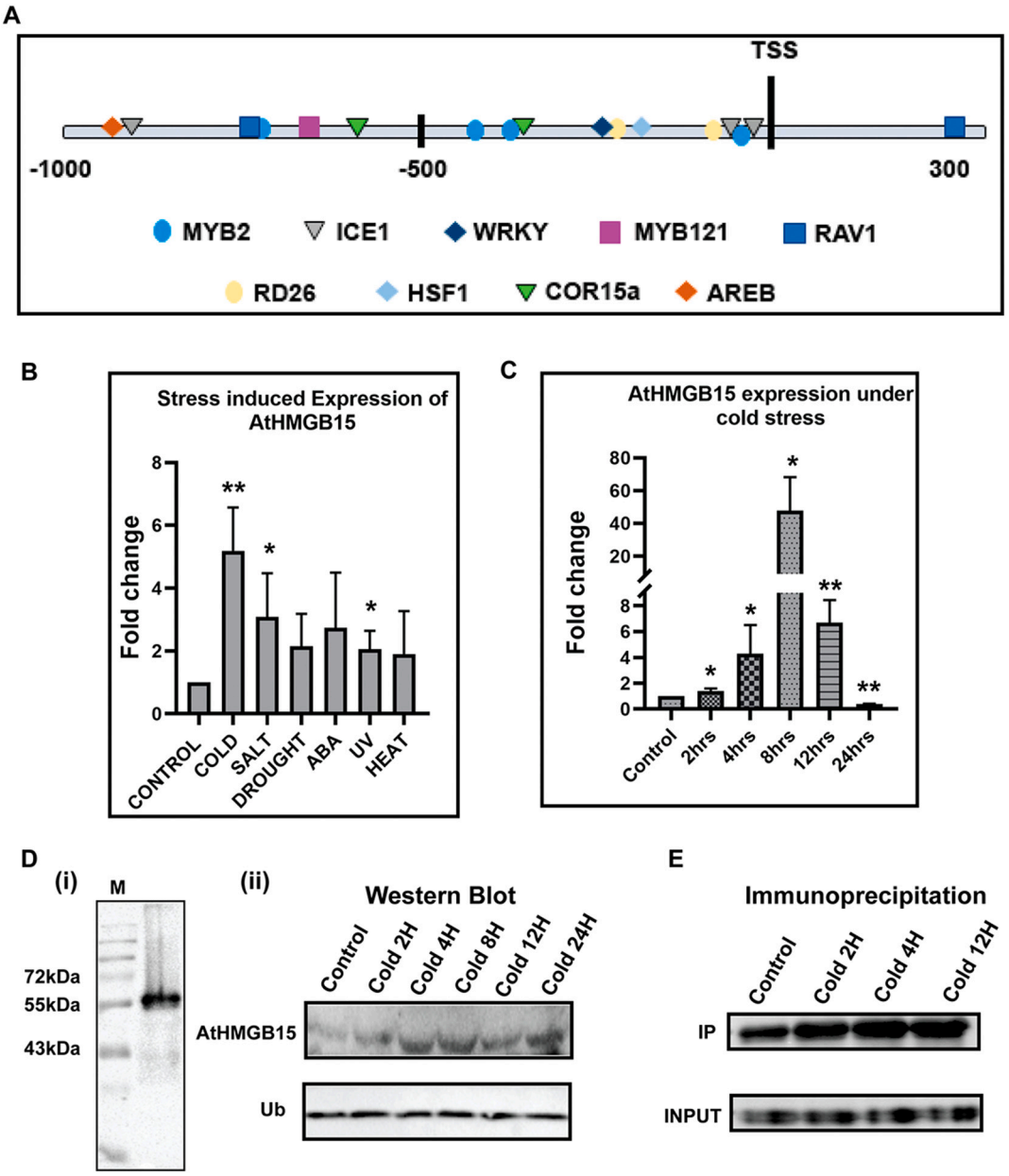

Fig. 1. AtHMGB15 induction in response to abiotic stress.
A. Schematic representation of transcription factors binding sites at the promoter/upstream region of AtHMGB15 gene. **B**. Real time quantification of AtHMGB15 expression upon induction by various abiotic stresses. **C**. Real time quantification of AtHMGB15 expression upon induction by cold stress at different time points. Bars represent the mean ± SD ($n = 3$). * and ** indicates a significant increase with respect to control ($P < 0.05$ and $P < 0.002$) by Students *t*-test. **D**. (i) Western blot using total cellular extract from wild type Arabidopsis seedling; showing specificity of AtHMGB15 antibody. (ii) Expression of AtHMGB15 protein under cold stress, where 150 ng of protein from cell lysates was evaluated by Western blot analysis. **E**. Immunoprecipitation of nuclear protein using anti-AtHMGB15 antibody from control and cold treated samples and analysed by western blotting using AtHMGB15 antibody.

2.10. Electrophoretic mobility shift assay

The DNA binding studies were done with PCR fragments obtained from the selected genes of qRT-PCR study. The fragments were end labelled with γP^{32} ATP (3500 Ci/mmol) using T4 polynucleotide kinase (Thermo scientific, #EK0031) and purified. 5×10^4 cpm γP^{32} labelled DNA (~7 fmol) was mixed with various concentrations of the full length AtHMGB15 or its individual domain ranging from 0.6 μM to 9 μM in presence of 1× EMSA buffer containing 10 mM Tris-HCl (pH 7.5), 5 mM NaCl, 0.1 mM EDTA, 0.5 mM MgCl2, 0.1 mM DTT, 5% glycerol and 1.25 μg/ml poly dI-dC. The DNA- protein mixture was incubated for 1 h on ice and were analysed by 5% native PAGE in 0.5× TBE at 4 °C. For binding assays with 23 bp synthetic oligonucleotide probes, the γP^{32} end labelled DNA (4×10^5 c.p.m., 50 fmol) was incubated with protein in 1× EMSA buffer on ice for 1 h and was resolved by 7% native PAGE gels supplemented with 5% glycerol.

2.11. DNase I footprinting

For DNase I footprinting of the promoter fragments of At1g28375, 1 μM of γP^{32} labelled primers were used to PCR amplify regions corresponding to 9959188 to 9959328 (141 bp) and 9959379 to 9959504 (126 bp). The 5′ labelled PCR fragments were then used for DNase I footprinting as described earlier by Roy et al. [31]. The primers used are listed in Supporting Table S5.

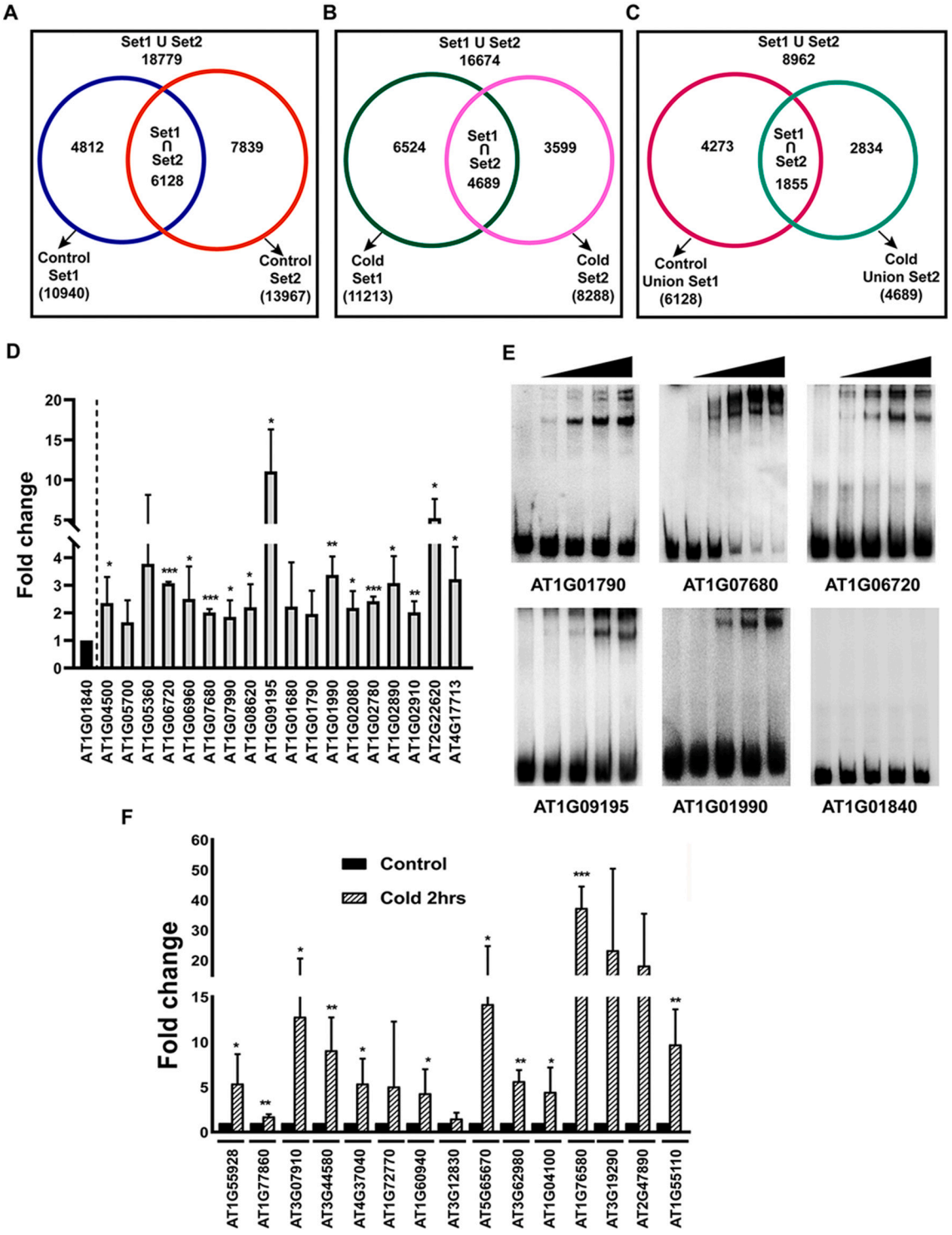

Fig. 2. Analysis of ChIP-chip data.
Venn diagram showing the number of genes associated with the binding of AtHMGB15 in replicate sets 1 and 2 under **A**. control condition, **B**. cold stressed condition (4 °C, 2 h). **C**. Venn diagram showing genes associated with AtHMGB15 under both control and cold conditions. **D**. ChIP-qPCR carried out for 18 genes associated with AtHMGB15 binding under control condition. The bars represent the mean ± SD (n = 3). * and ** indicates a significant increase (P < 0.05 and P < 0.002), with respect to a negative control region, calculated by Students t-test. **E**. EMSA performed with P^{32} labelled DNA fragments from selected genes using purified AtHMGB15 protein (0.6 μM–5 μM). **F**. ChIP-qPCR carried out for 15 genes associated with AtHMGB15 binding under cold condition. The bars represent the mean ± SD (n = 3). * and ** indicates a significant increase (P < 0.05 and P < 0.002) calculated by Students t-test with respect to binding under control condition.

2.12. SELEX

The oligo library contained 26 bp of random sequence flanked by TATTGACGATGACGGCAGCATCAA and GAATGGCCTCAGTAACGGGA CTAA. The first round of SELEX consisted of incubation of 10 pmol of full length AtHMGB15 protein (on bead) with 20 pmol library in binding buffer (10 mM Tris pH 7.5, 7.4 mM $MgCl_2$,50 mM Nacl, 100 ng/ml BSA,0.1% NP-40 and 5% glycerol) for 1 h. The beads were

washed extensively, and the bound oligo was subsequently eluted in the elution buffer (Binding buffer with 500 mM NaCl). The eluted oligo was then PCR amplified, and the SELEX enrichment procedure was repeated five times, with a total of 500 ng DNA for each round. After the final round of enrichment, the DNA fragments were cloned into TA vector (Thermo Scientific InsTAclone PCR cloning kit). DNA was isolated from individual colonies and sequenced. The sequences obtained were aligned, and the motif was generated using MEME.

3. Results

3.1. Expression of AtHMG15 increase during cold stress

AtHMGB15 is an ARID-HMG protein that belongs to the plant HMG-box family. Previous studies from our group have shown that ARID-HMG proteins can bind different DNA topologies through ARID-domain [21]. Expression analysis has indicated that *AtHMGB15* transcripts were highly enriched in flowering tissues, especially in pollen. The tissue specific expression was supported by the presence of multiple binding sites of homeobox transcription factors responsible for flower development at the promoter/upstream region of *AtHMGB15*. Further analysis of the *cis*-regulatory elements responsible for transcriptional regulations in the promoter of *AtHMGB15* revealed the presence of multiple transcription factor binding sites that are responsible for stress-induced gene expression (Fig. 1A). This led us to investigate whether the expression of AtHMGB15 is regulated by environmental cues. For this *Arabidopsis* seedlings (17–21 days old) were subjected to different environmental stresses and expression of *AtHMGB15* was compared with respect to that in control plants (Fig. 1B). Our result indicates that the expression of *AtHMGB15* increases with the induction of cold stress, peaking at 8–12 h, post cold stress application and then dropping dramatically by 24 h (Fig. 1C). Further, the protein levels of AtHMGB15 also showed a steady increase till 12 h as evident from western blot and immunoprecipitation data (Fig. 1D ii, E). The specificity of AtHMGB15 antibody was determined by western blot using total cellular extract that shows crossreactivity with only AtHMGB15 protein at ~50 kDa (Fig. 1D i, Fig. S1). The specificity of the antibody was further tested using total cellular extract of *athmgb15* mutant line. Western Blot result shows that AtHMGB15 antibody does not cross react with cellular extract of *athmgb15* mutant line (line 4.2), and this *athmgb15* line was further used for our study (Fig. S1). The significant upregulation of *AtHMGB15* at the mRNA and protein level suggests a new role of AtHMGB15 in cold stress response other than its role in flower development.

3.2. Identification of AtHMGB15 associated genomic regions in Arabidopsis seedlings

Previous studies have identified the role of HMGB-box architectural proteins in regulating various nuclear processes such as transcription, recombination, repair and replication [32]. Since AtHMGB15 belongs to the HMG-box domain containing protein, we investigated how AtHMGB15 aids in regulating the process of gene transcription during control and cold stress response. For this, we identified genome-wide AtHMGB15 targets in control and cold treated Arabidopsis seedlings using chromatin immunoprecipitation assay followed by custom oligonucleotide tiling array (see "Materials and methods"). To understand how AtHMGB15 regulates the onset of cold stress response, we have chosen 2 h cold stress treatment at 4 °C for our study. The reason for using 2 h stress point is to identify loci that were regulated by AtHMGB15 during early stress response. The ChIP assay was carried out from two independent biological replicates using anti-AtHMGB15 antibody where each replicate contains 60–70 Arabidopsis seedlings (22 days old) in both the control and cold treated samples. Genomic regions associated with AtHMGB15 occupancy were selected using Whitehead Per-Array Neighbourhood model (see "Materials and methods"). Using this method, we have identified 6128 significantly enriched ($pxbar_{min} < 0.05$) genes that were common among the two biological replicates in the control data set (Fig. 2A) and 4689 enriched ($pxbar_{min} < 0.05$) genes from the two cold replicates (Fig. 2B). In both control and cold, the two replicates shared a large number of target genes that covered more than 56% of the smaller set (Fig. 2A&B), indicating high quality. Therefore analysing the overlapping datasets is important as it would result in dealing with regions that have the most robust AtHMGB15 binding sites under different physiological conditions. A comparison between the control and cold data sets resulted in 1855 overlapping genes that accounted for ≈ 30% enriched gene from control and ≈ 40% from cold stressed samples (Fig. 2C). The ChIP-chip data was further tested by performing ChIP–qPCR and EMSA on randomly selected loci from overlapping sets (Fig. 2D,E&F). For Chip-qPCR, we randomly selected 18 candidate genes ($pxbar_{min} < 0.05$) from the common control data set and measured AtHMGB15 occupancy against a non-enriched gene ($pxbar_{min} > 0.7$) serving as the negative control. Pimers were designed flanking the enriched probe(s) such that it amplified a 250-300 bp DNA fragment. Our results indicated positive fold-change for all the selected genes, with 78% genes having a *p*-value < 0.05 (Fig. 2D). We further confirm the binding of AtHMGB15 to some of these loci by in vitro DNA binding assay using purified protein. The DNA binding assay was carried out with sequences encompassing AtHMGB15 binding probes that showed significant binding in the ChIP-chip assay (Fig. 2E). With increasing protein concentration, AtHMGB15 showed efficient binding with *At1g01790*, *At1g07680*, *At1g06720*, *At1g09195* and *At1g01990* loci whereas, *At1g01840*, which is a non-enriched locus, showed no binding with AtHMGB15. Similarly for cold data set, we randomly selected 15 candidate genes ($pxbar_{min} < 0.05$) from our ChIP-chip data that were enriched exclusively during cold stress and normalized it with respect to no binding under control conditions. Our results validated 79% of cold loci with p-value < 0.05 (Fig. 2F).

A circos plot was used to see the correlation between the genome-wide distribution of AtHMGB15 enriched DNA sequences, euchromatic regions and DNase1 hypersensitive sites (DHS) in *Arabidopsis* genome (Fig. 3A). On further zooming in our view to a 40 kb window from the circos plot for each chromosome, it showed that AtHMGB15 enriched DNA sequences overlap with the euchromatic regions of the chromosomes and DHS (Fig. 3B). The AtHMGB15 bound enriched probes ($p < 0.05$) were classified according to the position of the binding site relative to gene structure and the transcription start and end sites (TSSs &TESs). The data revealed that 42.64% and 52.24% of the total probes were bound to transcribed regions (exons and introns) in control and cold data sets respectively. Probes in the putative promoter region (1 kb upstream of TSS and 5′UTR) constituted 28.44% and 21.65% of total probes in control and cold treated samples respectively (Fig. 4A). The results, from the mapping of AtHMGB15 enriched probes with respect to transcription start& end sites, showed a wide distribution within a 2 kb window with a marked enrichment of AtHMGB15 binding within transcribed regions. Interestingly, higher AtHMGB15 binding was observed in the gene body compared to promoter/upstream region for cold treated sample compared to control (Fig. 4B).

3.3. Identification of AtHMGB15 binding motif

To investigate the binding motif of AtHMGB15, we first selected all enriched probes (pxbar < 0.05) from control and cold data sets. We next grouped these probes into three sub-groups: upstream; gene body that includes exons and introns and the intergenic region. The probes from these sets were analysed using the MEME-ChIP online tool (http://meme-suite.org/tools/meme-chip). The DREME analysis predicted one statistically significant "HWTATATA" motif that was common to all the three subgroups in both control and cold data sets. Another significant motif, CMAAAB, was found common to the upstream and intergenic group but not present in the gene body group (Fig. 5A). Interestingly,

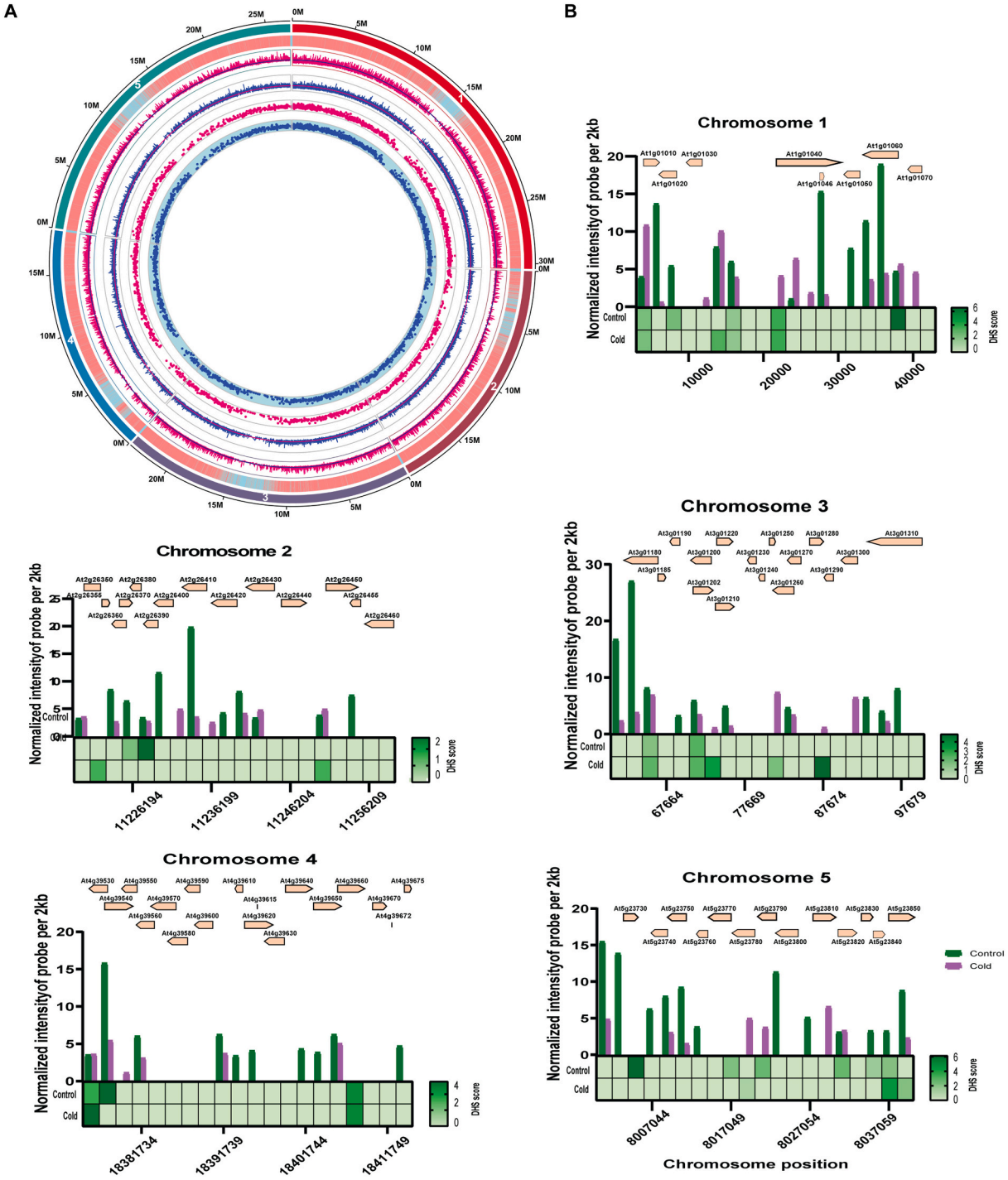

Fig. 3. Genome-wide AtHMGB15 occupancy during control and cold stressed conditions.
A. Circos plot representing the genome-wide occupancy of AtHMGB15. The outermost ring identifies the chromosome numbers. The other rings from outer to inner represent: Gene distribution; signal log ratio for AtHMGB15 binding under control condition; signal log ratio for AtHMGB15 binding under cold condition; DHS score under control condition; DHS score under cold condition. **B**. A 40 kb view of each chromosome showing AtHMGB15 binding, DHS score and gene distribution.

both the predicted motifs from the in silico analysis were primarily AT rich.

To validate the predicted binding site, we selected one of the enriched genes that showed maximum AtHMGB15 occupancy at the promoter and upstream region and tested its binding by EMSA. The 406 bp (−2056 to −1650) promoter region of At1g28375 shows three (P1,P2 and P3) enriched binding sites (pxbar < 0.05) of AtHMGB15 from ChIP-chip analysis. This region was divided into two regions RI and RII. The 298 bp RI region contained P1 and P2 probes whereas 198 bp RII region contained P2 and P3. EMSA results showed that both the regions (RI and RII) bound to purified AtHMGB15 protein (Fig. 5B). To narrow down the region of binding, RI was further divided into three parts RI^1(109 bp), RI^2(141 bp) and RI^3(90 bp) with respect to the two probes it contained. Similarly for the RII region, another smaller fragment RII^1 (126 bp) was designed around the P3 probe. Significant binding by AtHMGB15 was observed for the regions RI^2(141 bp) and RII^1 (126 bp) in a concentration dependent manner (Fig. 5B).

To precisely map the DNA binding site of AtHMGB15, we performed

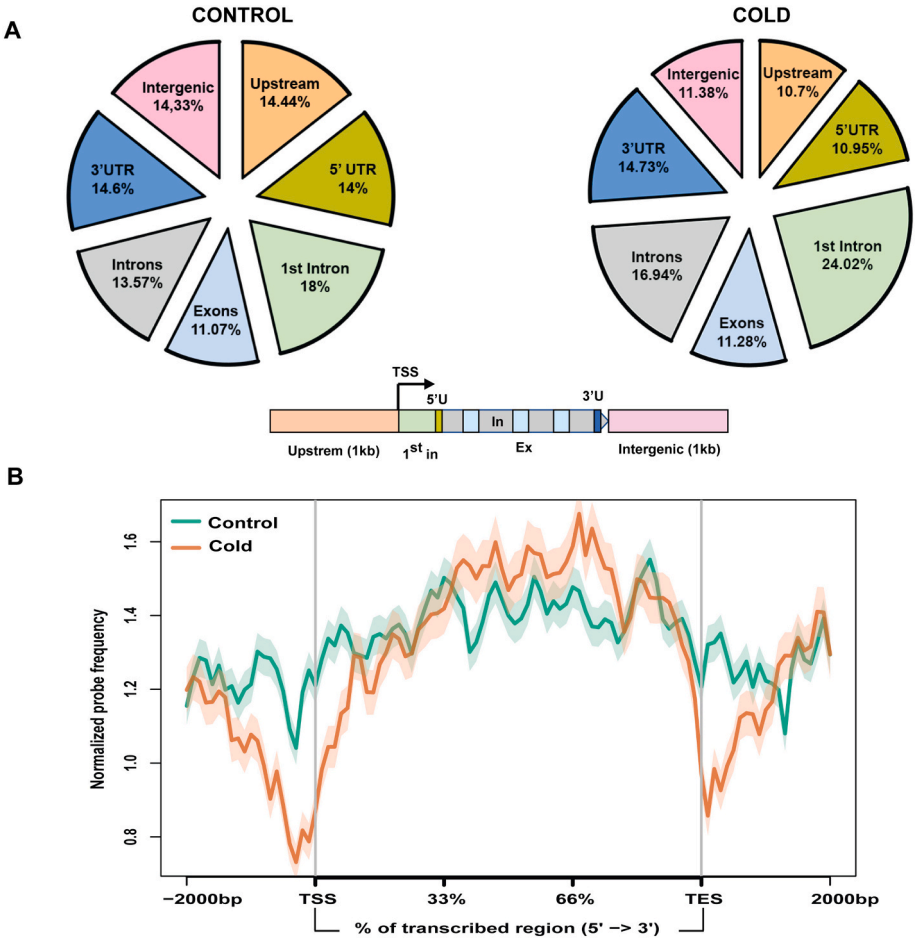

Fig. 4. Probe distribution of AtHMGB15.
A. Pie chart showing the probe distribution of AtHMGB15 binding with respect to gene structure (intragenic and intergenic regions) under control and cold conditions. **B**. A plot showing the normalized frequency of occurrence of binding sites of AtHMGB15 depicted across the promoter regions (shown in bp from 2000 to 0 relative to the presumed TSSs), transcribed regions (shown proportionally from 0 to 100% of total length), and 3′ regions (shown in bp from 0 to +2000 relative to the presumed TESs).

DNase I footprinting assay with RI^2(141 bp) and RII^1(126 bp). As shown in Fig. 6A, more than one protected sites were seen in both RI^2 and RII^1 fragments with increasing protein concentrations. The web logo constructed using the protected sites indicate the conserved motif "A(A/C)–ATA—(A/T)(A/T)" with conserved A and ATA residues. The motif obtained from DNase I assay shows significant homology alignment with the motif predicted from DREME viz. HWTATATA (Fig. 6B).

To validate the importance of the conserved residues in the binding sequence, mutation analysis was carried out with oligos containing the original sequence vs sequences with mutation in the conserved residues (Fig. 7A). It was observed that the mutation of the conserved A and ATA residues (Mut 4 oligo) completely abolished the binding of the AtHMGB15 protein. Moreover, mutation of ATA residue (Mut3 oligo) shows binding with AtHMGB15 only at higher protein concentrations. In a separate approach, the binding motif was also determined by Systematic Evolution of Ligands by Exponential Enrichment (SELEX) for the enrichment of AtHMGB15 binding sites using a 26 mer random oligo library. The motif obtained from the experiment also has a core ATA sequence consistent with DNase I footprinting assay (Fig. 7B).

Parallely, we performed a fluorescence anisotropy experiment with oligos containing both the predicted motifs: HWTATAT and CMAAAB, to check the binding affinity. We found that the AtHMGB15 binds to HWTATAT motif with higher affinity (K_d = 46 ± 2.29 nM) in comparison to CMAAAB motif (K_d = 130 ± 31.36 nM) (Fig. S2). The presence of the HWTATAT motif in the gene body and the higher binding affinity of AtHMGB15 to this motif is also in consonance with the enrichment of AtHMGB15 in the transcribed regions. Taken together, our footprinting and anisotropy data indicate that AtHMGB15 directly binds to the predicted AT stretch sequence motif, whereas, the CMAAAB motif that was also enriched in ChIP-chip analysis can be an indirect binding motif of AtHMGB15.

Previous studies have shown that ARID-domain containing protein binds to AT-rich DNA in a sequence specific manner [19]. Since AtHMGB15 prefers to bind to an AT rich sequence motif, we next investigated whether ARID or HMG-box domain of the protein was involved in DNA binding events. We thus carried out DNA binding studies with the full length protein and its truncated forms containing only the ARID and HMG-box domain using the RII^1 (126 bp) fragment. The result indicated that the DNA binding of the full length AtHMGB15 is mediated majorly through the ARID domain as no DNA-protein complexes were observed in case of the HMG domain (Fig. 7C).

3.4. Functional classification of enriched genes from ChIP-chip assay

We used our genome-wide binding data set to test, in an unbiased and thorough manner, the preferential binding of AtHMGB15 to different locus with specific biological functions. Therefore, we inquired all gene annotation categories using AgriGO (http://bioinfo.cau.edu.cn/agriGO/) for the enrichment of binding for three data sets: enriched in both control and cold (constant binding), enriched only in control (control only) and enriched only in cold (cold only). We found 47 Gene Ontology categories that displayed significantly enriched binding

A

CONTROL						COLD					
Upstream		Gene Body		Intergenic		Upstream		Gene Body		Intergenic	
Motif	E value	Motif	E value	Motif	E value	Motif	E value	Motif	E value	Motif	E value
CMAAAB	4.8E-66	TATATA	1.7E-29	CMAAAB	3.9E-54	CMAAAB	4.20E-48	TATRTATR	4.80E-33	CMAAAB	2.10E-31
HWTATATA	7.7E-23			TATATA	3.30E-07	ATATAWAB	1.30E-26			HTATATA	3.70E-12
CAAAB	2.10E-05			CAAAB	4.90E-04						

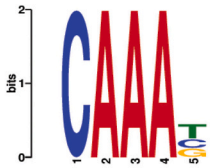

B

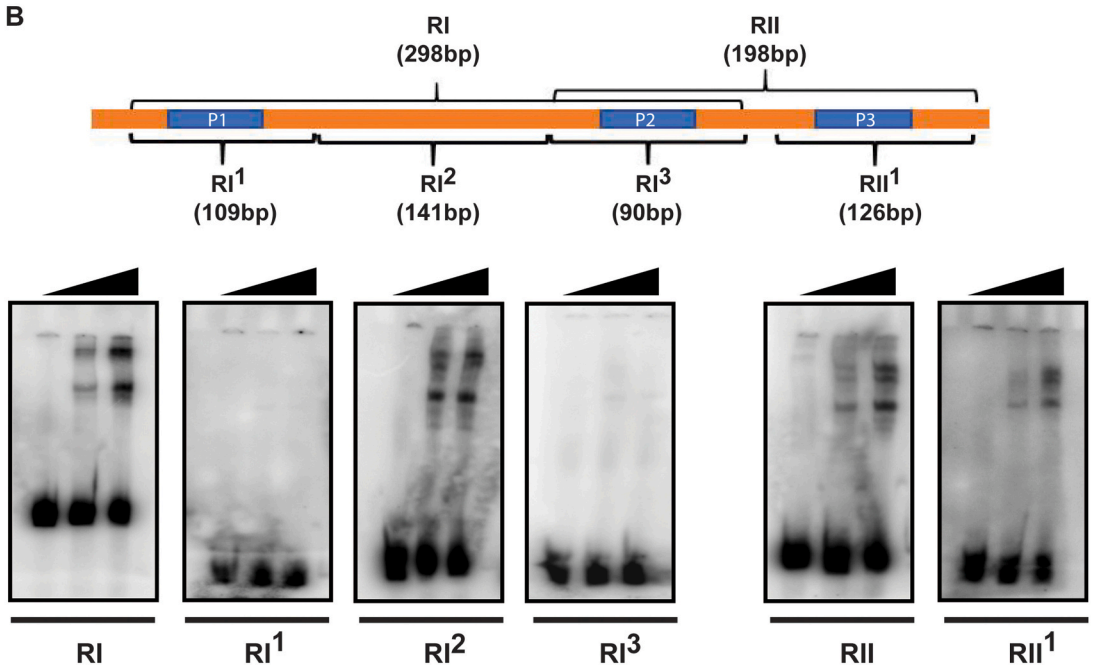

Fig. 5. Binding motifs identified from ChIP-chip data.
A. The two significant AtHMGB15 binding motifs identified from DREME analysis using control and cold data set. **B**. Schematic showing the *At1g28375* promoter region where P stands for the 60 bp probes obtained from ChIP-chip data and R stands for the regions used for EMSA. 0 to 7 μM of purified AtHMGB15 protein was used for DNA binding.

($p < 0.05$) in at least one of the three data sets. Some of the important GO categories of biological processes that were enriched in both control and cold data sets include transcription factor activity, pollen development and germination, abiotic stress response processes, hormone mediated signalling pathways, actin filament based movement, chromatin modification and circadian rhythm (Fig. 8). Response to ABA and gibberellic acid, ABA signalling, transcription factor activity, meiotic cell cycle and cellular component of CUL4 RING ubiquitin ligase complex were some of the important categories that were enriched in the control only set but excluded in the cold only set. Similarly, root development, helicase activity, chromatin modification and, mitochondria and plastids from cellular components were enriched in the cold only set but not in the control only set (Fig. 8). Some of the important transcription factor loci that show AtHMGB15 occupancy during control and cold stress are listed in Supporting Table S1.

3.5. Integration of ChIP-chip data with gene expression profiles during cold stress

In order to gain functional insights of AtHMGB15 target genes, we next integrated cold stress expression data obtained from Lee et al. [33] (GSE3326) with ChIP-chip data sets (Supporting Table S2). The expression data from Lee et al. had 939 significant (FDR < 1%) cold regulated genes, out of which 655 were cold upregulated, and 284 were down regulated. Integration of the transcriptome and ChIP-chip data (genes with pxbar < 0.05 and common to both replicates) showed 154 cold regulated genes (114 upregulated and 40 downregulated) that have AtHMGB15 occupancy under control only condition; 70 cold regulated loci (43 upregulated and 27 downregulated) that have AtHMGB15 occupancy only during cold stress condition and 67 cold regulated genes (45 upregulated and 22 downregulated) that showed AtHMGB15 enrichment under both control and cold condition (Supporting Table 2). Interestingly, genes involved in response to cold,

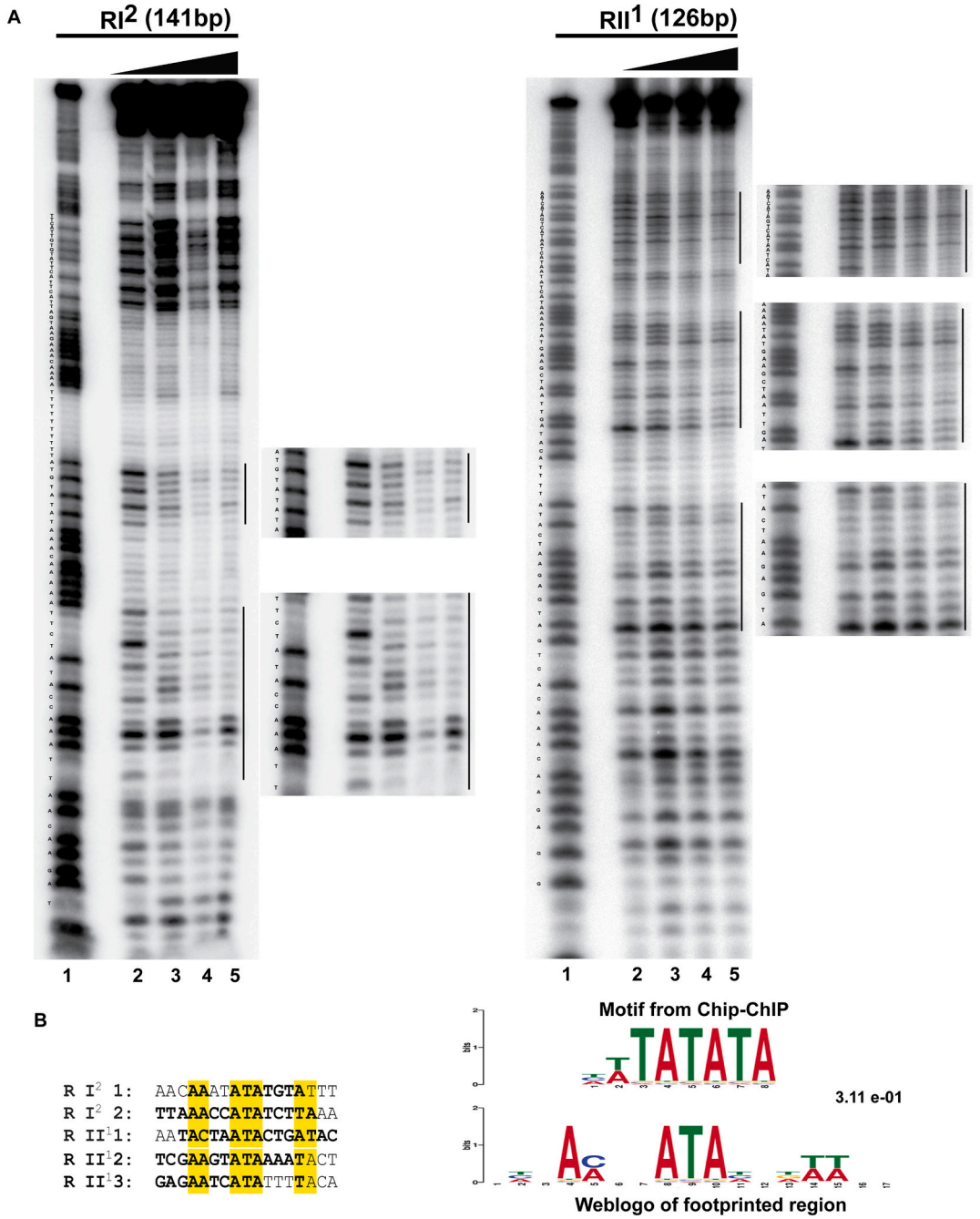

Fig. 6. DNase I footprinting assay to determine the binding site of AtHMGB15.
A. DNase I footprinting was done using 141 bp RI[2] and 126bpRII[1]. Lane 1: A/G ladder; lane 2–5: 0.01 U of DNase I in presence of 0-50 μM purified AtHMGB15 protein. **B**. Sequence alignment of footprint regions to determine the binding sequence of AtHMGB15 and subsequent alignment with motif obtained from DREME analysis.

response to abscisic acid stimulus, protein serine/threonine phosphatase activity were specifically present in control only data set. The cold only data set is enriched with genes involved in transcriptional regulation during abiotic stress response.

We next studied the gene regulatory network using all the cold responsive genes that showed AtHMGB15 occupancy, using Arabidopsis protein association network (STRING v11). The gene association networks of cold upregulated genes are significantly more clustered compared to cold downregulated genes, with high average node degree (up regulated: *P*-value < 1.0e-16; average node degree:2.98; downregulated P-value 0.000856; average node degree: 0.315). We, therefore, focused on the cold upregulated network for subsequent analysis. The main cold upregulated network consists of four clusters generated by the 'k means clustering' method (Fig. 9). The largest cluster (red color) consists of 156 gene count with very low average node degree (0.641) and thus omitted from further analysis. The other three cluster yellow, green and blue are smaller in size with a gene count of 25 (average node degree:10.3), 11 (average node degree:4.55) and 10 (average node degree:3.6) respectively. Downstream analysis reveals that these clusters are composed of groups of nodes that are more connected with each other and consist of enriched ontology and pathway components. The yellow cluster is enriched with nodes in response to organic substance (FDR: 4.11E-11) and plant MAPK signalling pathway (FDR:0.0429). The green cluster is enriched with nodes in

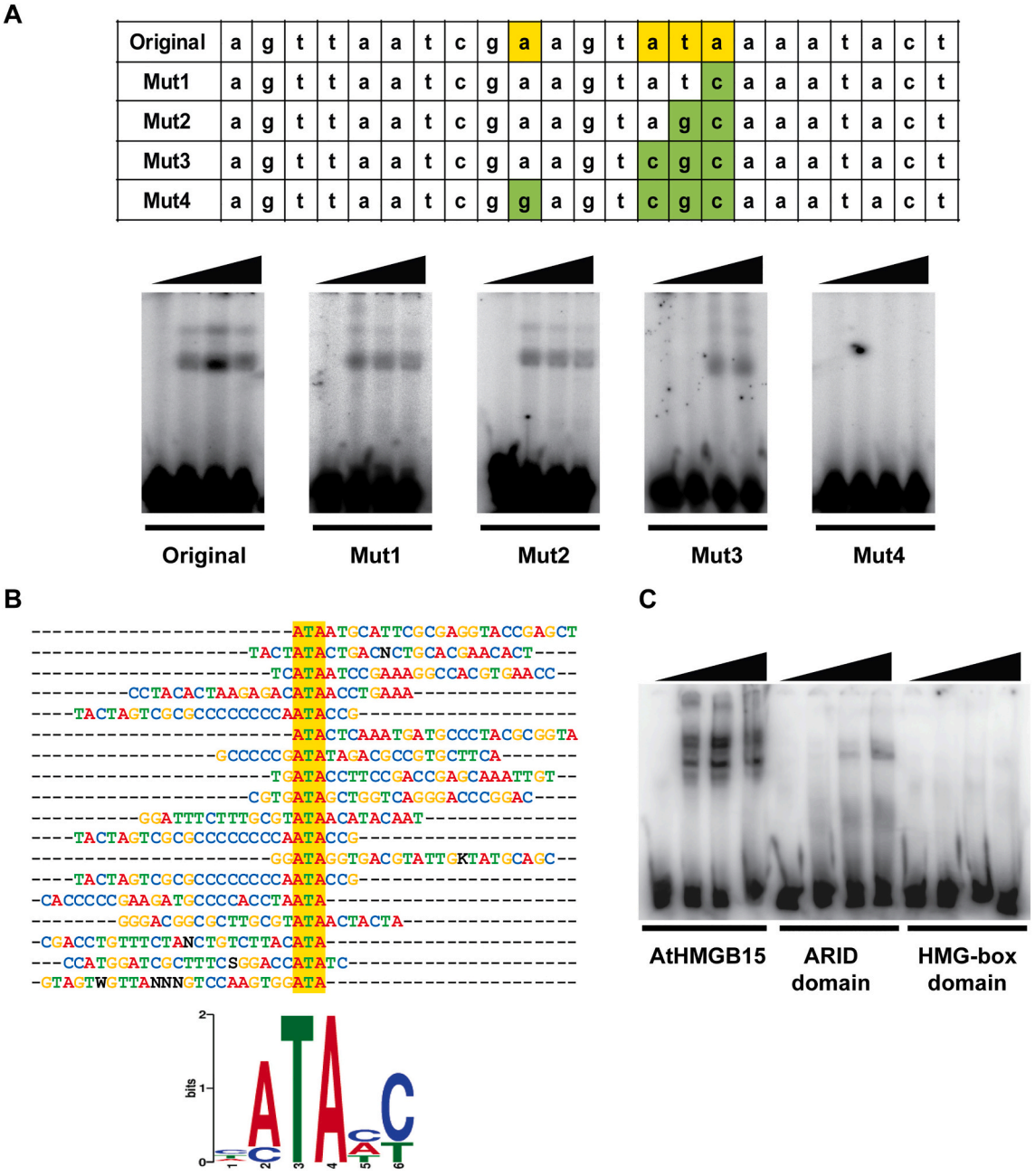

Fig. 7. Validation of AtHMGB15 binding site.
A. Original and mutated oligonucleotides used for validation of the sequence specificity of AtHMGB15 binding. EMSA result shows the binding of AtHMGB15 (0-9 μM) to mutated oligos. **B**. Sequences of 18 oligonucleotides used to determine the binding site of AtHMGB15 by SELEX approach. **C**. EMSA of 126bpRII[1] DNA fragment with full length AtHMGB15 and its truncated domains: ARID and HMG-box.

response to cold (FDR:5.59E-07) and plant hormone signal transduction pathway (FDR:2.86E-05) in addition to the MAPK signalling pathway (FDR:7.52E-05). The blue cluster is enriched with nodes playing a role in ion transport (FDR: 0.0345). Each of these three clusters is, however, interconnected through various nodes. Some other GO categories enriched in these clusters are: response to abscisic acid, transcription-DNA templated, response to abiotic stimulus, hormone mediated signalling pathway.

We next investigated whether binding of AtHMGB15 to these cold responsive loci has an effect on the transcription of these genes during cold stress response. To test this hypothesis, we have randomly selected 37 cold stress responsive genes that showed AtHMGB15 binding and studied the expression kinetics during cold stress in both wild type and *athmgb15* mutant lines (*athmgb15*, GABI_351D08). The result of expression study can be grouped into three clusters based on their cold induced expression patterns in wild type and *athmgb15* mutant lines. Genes belonging to group I includes transcription factors MYB1, NAC032, RAV1, DREB1a, protein kinases, phosphoesterase and cysteine proteases that showed cold induced gene expression in wild type plants whereas their expression is low or delayed in *athmgb*15 plants (Fig. 10A). Group II contains genes that showed similar expression at early time point but their expression at later stress time points diverged, with *athmgb*15 plants showing increase before wild-type plants (Fig. 10B). Group III contain genes that showed no change in expression profile between wild-type and mutant plants (Fig. 10C).

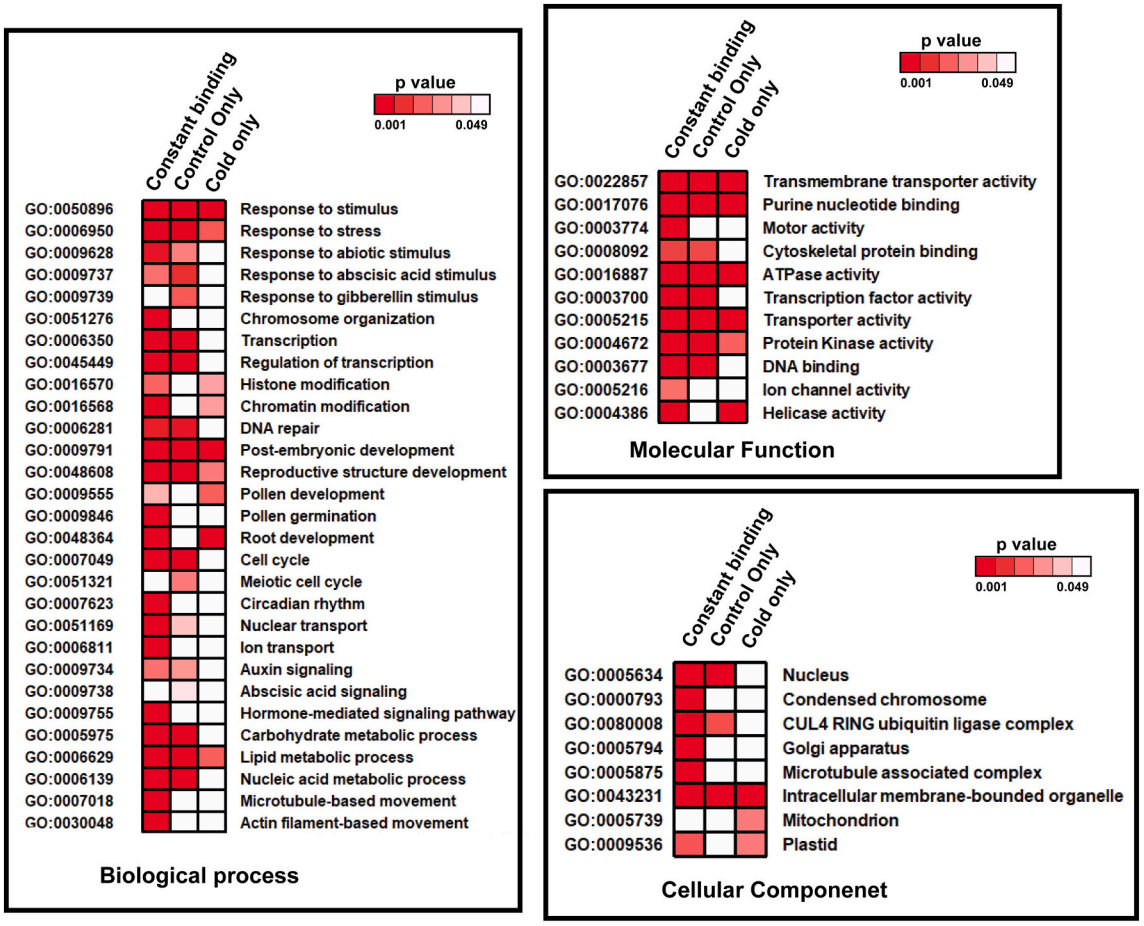

Fig. 8. Gene ontology analysis of AtHMGB15 ChIP-chip data.
Genes bound by AtHMGB15 were group into three categories; genes enriched in both control and cold stress (constant binding), genes enriched only in control (control only) and genes enriched only in cold (cold only). The enriched genes were then classified into major GO categories of Biological Process (BP), Molecular function (MF) and Cellular component [54]. Each category is shaded from white to red in increasing order of significance.

4. Discussion

AtHMGB15 is a novel plant specific protein containing two DNA binding domains, ARID domain and HMG domain, in a single polypeptide. Recent studies from Xia et al. have elucidated the biological role of AtHMGB15 in pollen biology [23]. The Ds mutant line of AtHMGB15 showed defective pollen morphology and retarded pollen tube growth, indicating a unique niche of the protein in the plant development. To delve deeper into the function of AtHMGB15 *in vivo* and to identify the spectrum of targets regulated by this protein, we carried out genome-wide studies with AtHMGB15. The presence of binding sites for various stress induced transcription factors at the promoter of AtHMGB15 and the cold induced induction of AtHMGB15 paved the way for identification of a novel role of AtHMGB15 in plant stress response. Exposure of plants to different adverse environmental conditions requires a switch in the gene expression program for immediate stress response and adaptability. The expression of arrays of stress responsive genes requires a change in chromatin structure to facilitate transcription. Architectural proteins have been shown to influence large chromatin structure to provide a proper platform for the formation of multiprotein complexes on the DNA backbone during transcription. Thus, it is assumed that an increase in the expression of AtHMGB15 during cold stress could be a pre-requisite for targeting structural constrains of chromatin structure to facilitate active transcription during stress response.

Previous studies have indicated the role of plant architectural protein HMGB in abiotic stress response in Arabidopsis [34]. Various isoforms of HMGB protein such as HMGB2, HMGB3 and HMGB4 were up-regulated during abiotic stress signals such as cold, salt and dehydration [35]. Moreover, transgenic Arabidopsis overexpressing HMGB2 or loss-of-function mutant of HMGB5 shows retarded germination and growth compared to wild-type plant during salt or drought stress conditions [35]. Although there has been no change in the transcript levels of stress responsive genes in HMGB2 overexpression lines; genes belonging to stress-responsive pathways were found to be down-regulated in *hmgb1* mutant [36]. Despite the documented role of ARID-HMGB group of proteins in plant development, the possible regulatory roles of this group in plant response to environmental stresses are largely unexplored. The ChIP-chip study carried out by us helped in identification of 6128 target genes of AtHMGB15 under control condition and 4689 target genes under cold stressed condition. Enrichment of the GO molecular function(MF) categories of pollen development and germination, and regulation of transcription seems as obvious outcomes. Some of the important genes in these categories belong to MICK_MADS transcription factors, pollen cell wall biosynthesis, actin binding proteins, calcium transporter, calcium dependent protein kinases, helicases and chromatin remodelers like SWI/SNF. Enrichment of chromatin modifications, helicase activity and actin filament further strengthen the predicted relationship, since chromatin remodelling complexes such as SWI/SNF or RSC have helicases and Actin related proteins as their functional components [37,38]. However, enrichment in categories of response to stress and abiotic stimulus is the unique highlight of the previously unknown role of AtHMGB15. Interestingly, some of the enriched loci that showed AtHMGB15 occupancy under control condition

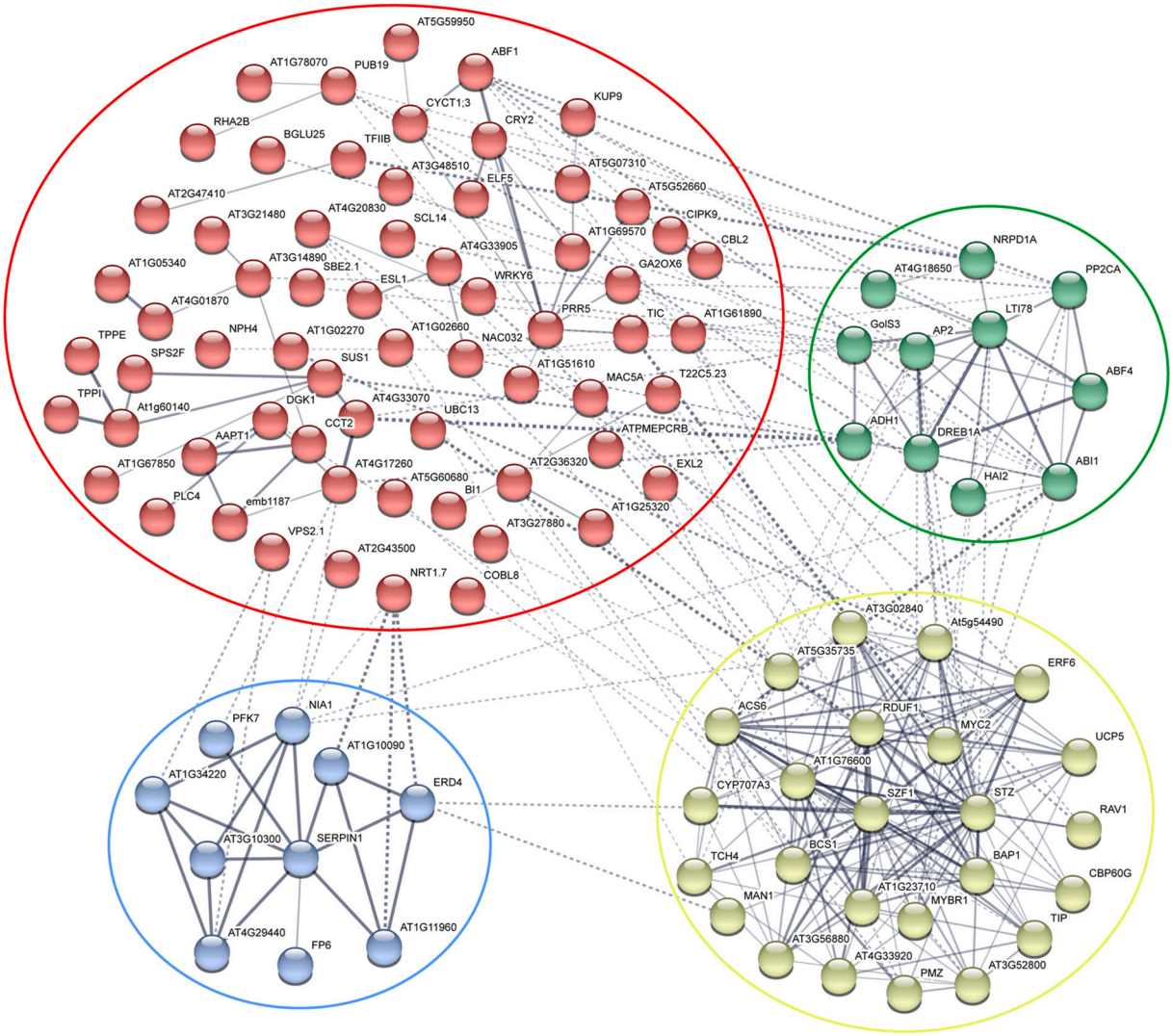

Fig. 9. Integration of AtHMGB15 ChIP-chip and cold transcriptome data.
A protein-protein interaction network of cold upregulated genes that have AtHMGB15 occupancy developed using STRING (v11). The network shows four major clusters of which green, yellow and blue have high confidence edges and high average node degree. To simplify the network visualization, all disconnected nodes were removed.

were found to be cold regulated genes. Moreover, network analysis of cold up-regulated genes that are enriched with AtHMGB15 binding revealed three significant clusters that have high connectivity and are involved in hormone signalling, stress response and ion transport. As mentioned earlier, HMG-box protein have the ability to induce changes in the chromatin structure that can aid as well as repress the process of transcription. The binding of AtHMGB15 to certain cold induced loci during control condition could lead to the formation of the pre-initiation complex to keep the promoters "primed" to facilitate rapid transcription. Our transcription data revealed that certain cold responsive loci showed decreased or delayed transcription in *athmgb15* plants than in wild type plants, while for some, transcription preceded in *athmgb15* plants than in wild type plants. Thus it is evident that AtHMGB15 protein can modulate the transcription process by inducing changes in chromatin structure of the target loci during cold stress response.

The role of plant hormone ABA in cold stress response is a debatable issue, even though enough genetic studies and molecular evidence have shown the role of ABA independent pathway in cold regulated gene expression [39–42]. Contrastingly many studies have also shown that genes involved in ABA biosynthesis and ABA signalling were transcriptionally regulated during cold stress [43]. We have also seen enrichment of AtHMGB15 occupancy in ABA biosynthesis as well as in ABA signalling genes; the latter is enriched in cold data set. CBF transcription factor plays the central role of cold signalling and is involved in the expression of an array of cold responsive genes [44–46]. Our data set shows enrichment of AtHMGB15 in CBF3 locus (DREB1A) and its positive regulator, ICE1 in control plants. Previous study by Vogel et al. has identified genes from Arabidopsis that are regulated by CBF protein in cold stress [47]. Interestingly, integration of our enriched data set with the transcriptome data of upregulated genes from CBF overexpression lines, obtained from Vogel et al., have revealed AtHMGB15 occupancy in 29% (44 out of 151) CBF regulons during control condition and 16% (24 out of 151) during cold stress. Out of these 44 genes, CBF regulated genes from control set, 31 were cold induced. Similarly, 16 CBF regulated genes from cold data set were found to be induced during cold stress response (Supporting Table S3). Moreover, the gene association network shows CBF as one the major node, which is highly interconnected with cold induced transcription factors and genes involved in cold signalling. Collectively, these observations suggest that AtHMGB15 plays a vital role in the transcription activation of CBF regulated genes during cold stress response.

Cold inducible genes can be grouped into two classes based on their kinetics of expression. The first group represent genes that are expressed rapid and transiently; and second group represent genes where expression

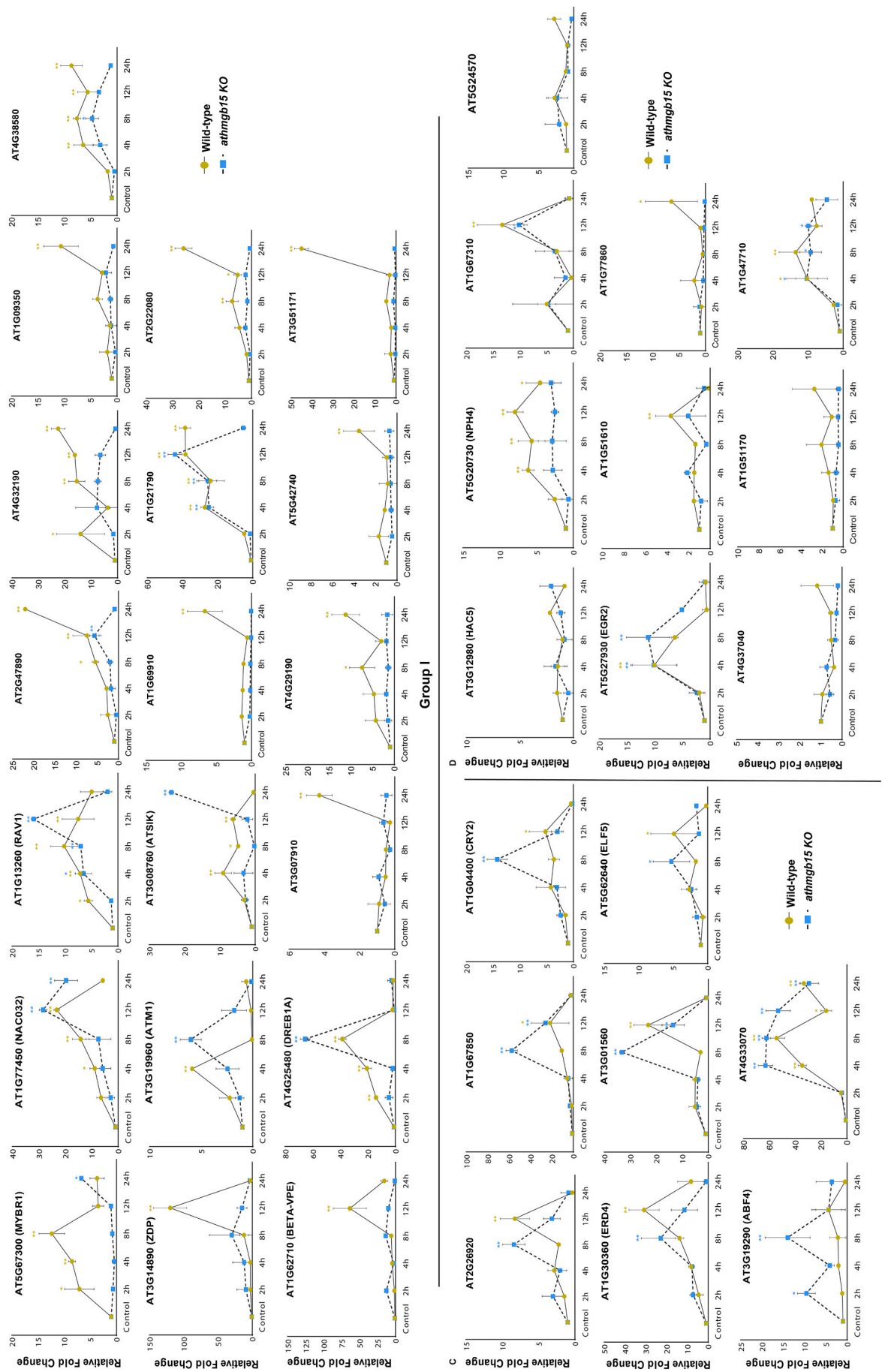

Fig. 10. Expression of cold induced genes in wild-type and *athmgb15* mutant plants.
A. Cold induced expression kinetics of Group I genes that showed increased in cold induced gene expression in wild type plants in comparison to *athmgb15* plants. **B.** Expression of Group II genes that showed cold induced gene expression earlier in *athmgb15* plants in comparison to wild type plants. **C.** Group III genes that showed no change in gene expression pattern in between *athmgb15* plants and wild type plants. The scatter plots represent the mean ± SD (n = 3). * and ** indicates a significant increase ($P < 0.05$ and $P < 0.005$). Two-way ANOVA with Dunnett's multiple comparison post-test was performed.

increases gradually with increasing time [48]. We have merged our 2 h ChIP-chip result with the transcriptome data of cold regulated genes from Lee et al. [33], and found 137 genes bound by AtHMGB15 of which 17 were upregulated early and 71 were upregulated late. Additionally, 3 genes were downregulated early and 46 were downregulated late. Similar results were obtained after merging the transcriptome data of abiotic stress regulated genes including cold from Seki et al. The result shows that AtHMGB15 bound to TFs belonging to *DREB*, *MYB*, *bHLH*, *WRKY* and *NAC* and signalling proteins like Ca^{2+} binding proteins. All of these genes were found to be upregulated early during cold stress response. Moreover, genes belonging to osmoprotectant like *AtGolS*, *AtP5CS*, *AtRafS1*; LEA protein family like *ERD10*, *RD17*; KIN proteins; hydrophilic protein like *RD29A*, *RD29B*; cellular metabolism proteins and other cold induced genes like *COR47*, being bound by AtHMGB15 at 2 h although their expression peaks at later time points. Thus, even though the expression of AtHMGB15 was found maximal at 12 h, performing ChIP-chip at 2 h could help us to identify AtHMGB15 binding loci that were rapidly expressed or repressed in early response to cold stress. For genes whose expression peaked or dropped at later time points, one could argue that AtHMGB15 was playing a role in priming these loci for transcriptional changes for a late response.

One of the essential aims of our study was to determine the sequence motif specific for AtHMGB15 binding. The EMSA results coupled with DNaseI protection analysis showed that AtHMGB15 preferred to bind AT rich sequences with a motif signature of "A(A/C)–ATA—(A/T)(A/T)". Further analysis shows increase in the distribution frequency of AT rich sequence motif at the gene body under cold stress response (Supporting Table S6) suggesting sequence specific enrichment of AtHMGB15 in the coding region to promote cold induced transcription. The in silico analysis also identified CMAAB motif as another enriched motif in the ChIP-chip study; however, we did not observe any footprinting at or near this sequence. It is possible that AtHMGB15 may be recruited to CMAAB sequence through protein-protein interactions with other factors (indirect binding). The CMAAB motif identified bears the best match with WLIM2A binding sequence, where WLIM2 belongs to the LIM family proteins of actin bundlers. Though WLIM2A is widely expressed, members of this family show pollen specific expression and the role of AtHMGB15 in pollen is already established [23,49].

Modulation of chromatin structure is a pre-requisite for the transcription of a gene. Chromatin landscape modification is achieved by concerted activities of histone modifiers, chromatin remodelers and architectural proteins. In order to initiate and progress the transcription process such actions are required throughout the locus that includes promoter and upstream regulatory regions as well as over the gene body. Previous genome-wide studies have shown distribution of chromatin remodellers not only in the proximity of the TSS but also in exons, introns and at the 3′-end of several genes, indicating more widespread distribution than typical transcription factors that have a major peak at TSS. Studies revealed that INO80 and ISW1 complexes occupancy entirely on the generic nucleosome array whereas RSC and SWI/SNF complexes were restricted to nucleosomes present at TSS proximity [50–52]. In consonance, recruitment of chromatin architectural proteins (CAPs) which aids in the process of modulating and stabilizing chromatin structure during transcription, may show a wide distribution pattern around the TSS, rather than exhibiting a narrow distribution spectrum or a specific peak. Genomewide studies have shown enrichment of chromatin architectural protein HMGD1 at upstream as well as downstream of TSS; suggesting its association with transcription initiation as well as elongation [53]. Our TSS/TES plot results also shows a wide distribution of AtHMGB15 biding with increment within transcribed regions which may be associated with a role played by it in transcriptional initiation (promoter clearance) and elongation. Moreover the increase in enrichment of AtHMGB15 in the transcribed region during cold in comparison to control condition indicates at the role played by the protein in transcriptional regulation during stress response.

In conclusion, this study provides a genome-wide binding profile of AtHMGB15 during both control, and early cold stressed conditions and identifies novel roles for this protein in stress response. Combination of the binding and expression data during cold stress allowed the identification of direct transcriptional targets of AtHMGB15 and indicated the involvement of the CBF dependent pathway during early cold response.

Supplementary data to this article can be found online at https://doi.org/10.1016/j.bbagrm.2020.194644.

Data availability

The microarray data sets are available from GEO (Gene Expression Omnibus) under accession number GSE140593.

CRediT authorship contribution statement

SC designed this research; RM performed the ChIP experiments. RM and AK performed DNA binding and footprinting experiments. PP, RM, AK, and SB analysed the ChIP-chip data. AD, RM, JM performed and analysed fluorescence anisotropy data. SC and RM wrote the manuscript. All the authors reviewed and approved the final version of this manuscript.

Declaration of competing interest

The authors have no conflict of interest to declare.

Acknowledgement

The authors would like to thank Dr. Pallob Kundu for showing his generosity by gifting the SELEX library and Dr. Supriyo Chowdhury for his academic inputs for SELEX experiment.

Funding

This work was supported by Council of Scientific & Industrial Research (CSIR), Government of India; Grant Numbers [38(1245)/10/EMR-II] and [38(1365)/13/EMR-II]; Science and Engineering Research Board (SERB), Government of India; Grant Numbers EMR/2017/000768 and Bose Institute, India.

References

[1] K. Luger, A.W. Mader, R.K. Richmond, D.F. Sargent, T.J. Richmond, Crystal structure of the nucleosome core particle at 2.8 A resolution, Nature 389 (1997) 251–260.
[2] K. Luger, M.L. Dechassa, D.J. Tremethick, New insights into nucleosome and chromatin structure: an ordered state or a disordered affair? Nat. Rev. Mol. Cell Biol. 13 (2012) 436–447.
[3] D.J. Tremethick, Higher-order structures of chromatin: the elusive 30 nm fiber, Cell 128 (2007) 651–654.
[4] M.S. Luijsterburg, M.F. White, R. van Driel, R.T. Dame, The major architects of chromatin: architectural proteins in bacteria, archaea and eukaryotes, Crit. Rev. Biochem. Mol. Biol. 43 (2008) 393–418.
[5] S.D. Taverna, H. Li, A.J. Ruthenburg, C.D. Allis, D.J. Patel, How chromatin-binding modules interpret histone modifications: lessons from professional pocket pickers, Nat. Struct. Mol. Biol. 14 (2007) 1025–1040.
[6] A.A. Travers, Priming the nucleosome: a role for HMGB proteins? EMBO Rep. 4 (2003) 131–136.
[7] D.T. Brown, T. Izard, T. Misteli, Mapping the interaction surface of linker histone H1 0 with the nucleosome of native chromatin in vivo, Nat. Struct. Mol. Biol. 13 (2006) 250.
[8] U. Gerstel, C. Park, U. Romling, Complex regulation of csgD promoter activity by global regulatory proteins, Mol. Microbiol. 49 (2003) 639–654.
[9] T. Bonaldi, G. Langst, R. Strohner, P.B. Becker, M.E. Bianchi, The DNA chaperone HMGB1 facilitates ACF/CHRAC-dependent nucleosome sliding, EMBO J. 21 (2002) 6865–6873.
[10] P.B. Becker, J.L. Workman, Nucleosome remodeling and epigenetics, Cold Spring Harb. Perspect. Biol. 5 (2013).
[11] M.E. Bianchi, A. Agresti, HMG proteins: dynamic players in gene regulation and differentiation, Curr. Opin. Genet. Dev. 15 (2005) 496–506.
[12] C.S. Malarkey, M.E. Churchill, The high mobility group box: the ultimate utility player of a cell, Trends Biochem. Sci. 37 (2012) 553–562.

[13] R. Mallik, A. Kundu, S. Chaudhuri, High mobility group proteins: the multifaceted regulators of chromatin dynamics, Nucleus 61 (2018) 213–226.
[14] R. Reeves, High mobility group (HMG) proteins: modulators of chromatin structure and DNA repair in mammalian cells, DNA Repair (Amst) 36 (2015) 122–136.
[15] M. Stros, D. Launholt, K.D. Grasser, The HMG-box: a versatile protein domain occurring in a wide variety of DNA-binding proteins, Cell. Mol. Life Sci. 64 (2007) 2590–2606.
[16] M. Antosch, S.A. Mortensen, K.D. Grasser, Plant proteins containing high mobility group box DNA-binding domains modulate different nuclear processes, Plant Physiol. 159 (2012) 875–883.
[17] R.F. Herrscher, M.H. Kaplan, D.L. Lelsz, C. Das, R. Scheuermann, P.W. Tucker, The immunoglobulin heavy-chain matrix-associating regions are bound by Bright: a B cell-specific trans-activator that describes a new DNA-binding protein family, Genes Dev. 9 (1995) 3067–3082.
[18] S.L. Gregory, R.D. Kortschak, B. Kalionis, R. Saint, Characterization of the dead ringer gene identifies a novel, highly conserved family of sequence-specific DNA-binding proteins, Mol. Cell. Biol. 16 (1996) 792–799.
[19] A. Patsialou, D. Wilsker, E. Moran, DNA-binding properties of ARID family proteins, Nucleic Acids Res. 33 (2005) 66–80.
[20] D. Wilsker, A. Patsialou, P.B. Dallas, E. Moran, ARID proteins: a diverse family of DNA binding proteins implicated in the control of cell growth, differentiation, and development, Cell Growth Differ. 13 (2002) 95–106.
[21] A. Roy, A. Dutta, D. Roy, P. Ganguly, R. Ghosh, R.K. Kar, A. Bhunia, J. Mukhopadhyay, S. Chaudhuri, Deciphering the role of the AT-rich interaction domain and the HMG-box domain of ARID-HMG proteins of Arabidopsis thaliana, Plant Mol. Biol. 92 (2016) 371–388.
[22] F.T. Hansen, C.K. Madsen, A.M. Nordland, M. Grasser, T. Merkle, K.D. Grasser, A novel family of plant DNA-binding proteins containing both HMG-box and AT-rich interaction domains, Biochemistry 47 (2008) 13207–13214.
[23] C. Xia, Y.J. Wang, Y. Liang, Q.K. Niu, X.Y. Tan, L.C. Chu, L.Q. Chen, X.Q. Zhang, D. Ye, The ARID-HMG DNA-binding protein AtHMGB15 is required for pollen tube growth in Arabidopsis thaliana, Plant J. 79 (2014) 741–756.
[24] K. Yamaguchi-Shinozaki, K. Shinozaki, A novel cis-acting element in an Arabidopsis gene is involved in responsiveness to drought, low-temperature, or high-salt stress, Plant Cell 6 (1994) 251–264.
[25] Y. Sakuma, K. Maruyama, F. Qin, Y. Osakabe, K. Shinozaki, K. Yamaguchi-Shinozaki, Dual function of an Arabidopsis transcription factor DREB2A in water-stress-responsive and heat-stress-responsive gene expression, Proc. Natl. Acad. Sci. U. S. A. 103 (2006) 18822–18827.
[26] N.A. AL-Quraan, GABA shunt deficiencies and accumulation of reactive oxygen species under UV treatments: insight from Arabidopsis thaliana calmodulin mutants, Acta Physiol. Plant. 37 (2015) 86.
[27] D. Roy, A. Paul, A. Roy, R. Ghosh, P. Ganguly, S. Chaudhuri, Differential acetylation of histone H3 at the regulatory region of OsDREB1b promoter facilitates chromatin remodelling and transcription activation during cold stress, PLoS One 9 (2014) e100343.
[28] G. Orphanides, W.-H. Wu, W.S. Lane, M. Hampsey, D. Reinberg, The chromatin-specific transcription elongation factor FACT comprises human SPT16 and SSRP1 proteins, Nature 400 (1999) 284.
[29] L. Shen, N. Shao, X. Liu, E. Nestler, ngs. plot: quick mining and visualization of next-generation sequencing data by integrating genomic databases, BMC Genomics 15 (2014) 284.
[30] T. Zhang, A.P. Marand, J. Jiang, PlantDHS: a database for DNase I hypersensitive sites in plants, Nucleic Acids Res. 44 (2016) D1148–D1153.
[31] D. Roy, J. Chakrabarty, R. Mallik, S. Chaudhuri, Rice Trithorax factor ULTRAPETALA 1 (OsULT1) specifically binds to “GAGAG” sequence motif present in Polycomb response elements, Biochim. Biophys. Acta Gene Regul. Mech. 1862 (2019) 582–597.
[32] R. Reeves, Nuclear functions of the HMG proteins, Biochim. Biophys. Acta 1799 (2010) 3–14.
[33] B.H. Lee, D.A. Henderson, J.K. Zhu, The Arabidopsis cold-responsive transcriptome and its regulation by ICE1, Plant Cell 17 (2005) 3155–3175.
[34] J.M. Kim, T.K. To, T. Nishioka, M. Seki, Chromatin regulation functions in plant abiotic stress responses, Plant Cell Environ. 33 (2010) 604–611.
[35] K.J. Kwak, J.Y. Kim, Y.O. Kim, H. Kang, Characterization of transgenic Arabidopsis plants overexpressing high mobility group B proteins under high salinity, drought or cold stress, Plant Cell Physiol. 48 (2007) 221–231.
[36] D.L. Lildballe, D.S. Pedersen, R. Kalamajka, J. Emmersen, A. Houben, K.D. Grasser, The expression level of the chromatin-associated HMGB1 protein influences growth, stress tolerance, and transcriptome in Arabidopsis, J. Mol. Biol. 384 (2008) 9–21.
[37] N.L. Klages-Mundt, A. Kumar, Y. Zhang, P. Kapoor, X. Shen, The nature of actin-family proteins in chromatin-modifying complexes, Front. Genet. 9 (2018) 398.
[38] H.L. Schubert, J. Wittmeyer, M.M. Kasten, K. Hinata, D.C. Rawling, A. Heroux, B.R. Cairns, C.P. Hill, Structure of an actin-related subcomplex of the SWI/SNF chromatin remodeler, Proc. Natl. Acad. Sci. U. S. A. 110 (2013) 3345–3350.
[39] M.R. Knight, H. Knight, Low-temperature perception leading to gene expression and cold tolerance in higher plants, New Phytol. 195 (2012) 737–751.
[40] J. Liu, Y. Shi, S. Yang, Insights into the regulation of C-repeat binding factors in plant cold signaling, J. Integr. Plant Biol. 60 (2018) 780–795.
[41] M.F. Thomashow, Role of cold-responsive genes in plant freezing tolerance, Plant Physiol. 118 (1998) 1–8.
[42] K. Yamaguchi-Shinozaki, K. Shinozaki, Transcriptional regulatory networks in cellular responses and tolerance to dehydration and cold stresses, Annu. Rev. Plant Biol. 57 (2006) 781–803.
[43] L. Xiong, K.S. Schumaker, J.K. Zhu, Cell signaling during cold, drought, and salt stress, Plant Cell 14 (Suppl) (2002) S165–S183.
[44] V. Chinnusamy, J.K. Zhu, R. Sunkar, Gene regulation during cold stress acclimation in plants, Methods Mol. Biol. 639 (2010) 39–55.
[45] Y. Liu, P. Dang, L. Liu, C. He, Cold acclimation by the CBF-COR pathway in a changing climate: lessons from Arabidopsis thaliana, Plant Cell Rep. 38 (2019) 511–519.
[46] J. Mizoi, K. Shinozaki, K. Yamaguchi-Shinozaki, AP2/ERF family transcription factors in plant abiotic stress responses, Biochim. Biophys. Acta 1819 (2012) 86–96.
[47] J.T. Vogel, D.G. Zarka, H.A. Van Buskirk, S.G. Fowler, M.F. Thomashow, Roles of the CBF2 and ZAT12 transcription factors in configuring the low temperature transcriptome of Arabidopsis, Plant J. 41 (2005) 195–211.
[48] M. Seki, M. Narusaka, J. Ishida, T. Nanjo, M. Fujita, Y. Oono, A. Kamiya, M. Nakajima, A. Enju, T. Sakurai, M. Satou, K. Akiyama, T. Taji, K. Yamaguchi-Shinozaki, P. Carninci, J. Kawai, Y. Hayashizaki, K. Shinozaki, Monitoring the expression profiles of 7000 Arabidopsis genes under drought, cold and high-salinity stresses using a full-length cDNA microarray, Plant J. 31 (2002) 279–292.
[49] J. Papuga, C. Hoffmann, M. Dieterle, D. Moes, F. Moreau, S. Tholl, A. Steinmetz, C. Thomas, Arabidopsis LIM proteins: a family of actin bundlers with distinct expression patterns and modes of regulation, Plant Cell 22 (2010) 3034–3052.
[50] K. Yen, V. Vinayachandran, K. Batta, R.T. Koerber, B.F. Pugh, Genome-wide nucleosome specificity and directionality of chromatin remodelers, Cell 149 (2012) 1461–1473.
[51] A. Sala, M. Toto, L. Pinello, A. Gabriele, V. Di Benedetto, A.M. Ingrassia, G. Lo Bosco, V. Di Gesu, R. Giancarlo, D.F. Corona, Genome-wide characterization of chromatin binding and nucleosome spacing activity of the nucleosome remodelling ATPase ISWI, EMBO J. 30 (2011) 1766–1777.
[52] M.Y. Tolstorukov, C.G. Sansam, P. Lu, E.C. Koellhoffer, K.C. Helming, B.H. Alver, E.J. Tillman, J.A. Evans, B.G. Wilson, P.J. Park, C.W. Roberts, Swi/Snf chromatin remodeling/tumor suppressor complex establishes nucleosome occupancy at target promoters, Proc. Natl. Acad. Sci. U. S. A. 110 (2013) 10165–10170.
[53] N. Nalabothula, G. McVicker, J. Maiorano, R. Martin, J.K. Pritchard, Y.N. Fondufe-Mittendorf, The chromatin architectural proteins HMGD1 and H1 bind reciprocally and have opposite effects on chromatin structure and gene regulation, BMC Genomics 15 (2014) 92.
[54] E. Malini, E. Maurizio, S. Bembich, R. Sgarra, P. Edomi, G. Manfioletti, HMGA Interactome: new insights from phage display technology, Biochemistry 50 (2011) 3462–3468.

Ecotoxicology and Environmental Safety 205 (2020) 111167

Contents lists available at ScienceDirect

Ecotoxicology and Environmental Safety

journal homepage: www.elsevier.com/locate/ecoenv

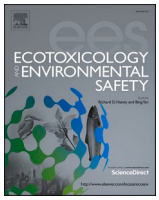

Salicylic acid mediated reduction in grain cadmium accumulation and amelioration of toxicity in *Oryza sativa* L. cv Bandana

Snehalata Majumdar [a], Sonal Sachdev [b], Rita Kundu [a,*]

[a] Department of Botany, Centre of Advanced Study, University of Calcutta, 35 Ballygunge Circular Road, Kolkata, 700019, West Bengal, India
[b] Division of Plant Biology, Bose Institute, P-1/12, CIT Road, Scheme VIIM, Kankurgachi, Kolkata, 700054, West Bengal, India

ARTICLE INFO

Keywords:
Rice
Salicylic acid
Cadmium
Yield
Grain
Cancer risk

ABSTRACT

Contamination of agricultural fields with Cadmium (Cd) due to several agricultural practices is increasing worldwide. The rice plants can easily take up Cd and accumulate it into different parts, including the grains, posing a threat to human health even at low concentration exposure. Several phytohormones, including Salicylic acid (SA) have been investigated since long for its alleviating properties under various biotic and abiotic stress conditions. In the present study, 100 μM SA application to ameliorate 25 μM Cd stress was studied for 72 h in hydroponics in *Oryza sativa* cv. Bandana seedlings. Pot experiments were done with same treatment condition and plants were grown till maturity. SA application to Cd exposed rice seedlings alleviated the stress condition, which was established by several physiological, biochemical, histochemical and gene expression analysis. SA treatment to Cd stressed seedlings showed elevated photosynthetic pigment content, on-protein thiol content and relieved the Cd induced growth inhibition considerably. It lowered the accumulation of ROS like, $O2^{-}$ and H_2O_2 with a regulated antioxidative enzymatic activity. SA application in Cd exposed rice seedlings had upregulated expression of *OsHMA3* and *OsPCS1* whereas*OsNRAMP2* gene was downregulated. Co-application of SA and Cd led to higher yield and improved agronomic traits in comparison to only Cd exposed plants under pot experimentation. Daily intake of Cd and Carcinogenic risk were also reduced by 99.75% and 99.99% respectively in the SA treated Cd stressed plants. SA positively affected the growth and tolerance of rice seedlings to Cd stress. Hence, SA addition to Cd contaminated soil can ensure rice cultivation without posing health risk to consumers.

1. Introduction

Cd pollution is one of the major environmental concerns of recent times. It is ranked 7th among the toxic substance priority list (Cotton et al., 1999; ATSDR, 2019). In most cases, increased amount of Cd in soil is anthropogenic and its concentration beyond threshold level is a serious threat. Application of excess phosphate fertilizers and contaminated irrigation water (Du et al., 2013; Kosolsaksakul et al., 2014), are instrumental in increasing Cd burden of the arable land. Cd is highly mobile and has a very high soil to plant transfer rate, which facilitates its accumulation in the grains and secure its niche in the food web (Irshad et al., 2020). Even at minute concentration it causes considerable impairment in plant growth and development, ultimately compromising crop yield and quality significantly (Zhang et al., 2015; Wang et al., 2018). Rice is one of the primary sources of calorie for Asian population (Gao et al., 2018) and intake of Cd contaminated grain has led to serious health hazards like skeletal damage, lung and prostate cancer and cardiovascular diseases (Jan et al., 2019). Our preliminary data showed a varied range of Cd status (BDL to 0.49 mg kg^{-1}) in grains and (1.76 mg $Kg^{-1}$to 13.8 mg kg^{-1}) in soil samples collected from agricultural fields located at different regions of West Bengal, much higher than the allowable limits (Unpublished data). According to CODEX, the maximum allowable limit of Cd in polished rice is 0.4 mg kg^{-1} whereas the same in other food crops is 0.10 mg kg^{-1} (Fu et al., 2008; Xue et al., 2014).

Heavy metals interfere with various essential cellular biomolecules through oxidative stress causing physiological, morphological and metabolic anomalies in plants, resulting in leaf chlorosis, membrane damage and protein degradation. Cd is also found to reduce the final plant height, number of panicles and tillers per plant significantly, thereby affecting the total yield of the crop plants (Huang et al., 2017). To combat the heavy metal induced toxicity, plants have evolved several mechanisms to defend (Singh and Shah, 2015; Khan et al., 2013) which include antioxidative enzymes, like, superoxide dismutase (SOD),

* Corresponding author.
E-mail address: kundu_rita@yahoo.co.in (R. Kundu).

https://doi.org/10.1016/j.ecoenv.2020.111167
Received 12 April 2020; Received in revised form 19 July 2020; Accepted 10 August 2020
Available online 19 August 2020

catalase (CAT), guaiacol peroxidase (POD) and non-enzymatic components (carotenoid, NP-SH, proline, etc.). Toxic metals and metalloids induce Phytochelatin synthase (*PCS*) to produce ligands called phytochelatins, that detoxify metalloids and non-essential toxic metals like Cd by sequestering it into vacuoles (Uraguchi et al., 2017). *Os*PCS played a crucial role in mitigation of Cd stress and down regulation of the gene decreased Cd uptake in rice seeds (Shri et al., 2014; Das et al., 2017). The family of natural resistance-associated macrophage proteins (*NRAMP*), another important group of transmembrane proteins involved in metal transport and homeostasis in both root and shoot, are considered 'general metal ion transporters' due to their ability to transport Mn^{2+}, Zn^{2+}, Cu^{2+}, Fe^{2+}, Cd^{2+},Ni^{2+} and Co^{2+} across plasma membrane into cytosol, or across tonoplast (Ullah et al., 2018; Mani et al., 2018). Xylem loading of Cd from symplasm takes place through the heavy metal transporting ATPases (*HMA*s) which belong to P1B-ATPases. *OsHMA3*, another ATPase coupled transporter, localized in the tonoplast play a significant role in vacuolar sequestration of heavy metals. Overexpression of *OsHMA3* is reported to decrease the Cd concentration in rice grains by 94–98% (Lu et al., 2019; Miyadate et al., 2011).

To reduce the Cd induced toxicity, amelioration of Cd stress is of paramount importance. Many plant molecules like Abscisic acid, Jasmonates and Salicylic Acid (SA) (Joseph et al., 2010) play a significant role in mitigating the heavy metal stress by modulating the gene expression of various transporters and altering the biochemical reactions (Emamverdian et al., 2020). Exogenous application of SA was reported to promote growth, increase photosynthetic efficiency, modify levels of osmoregulant, reduce ROS generation and up-regulate defense related genes (An and Mou, 2011; Zhang et al., 2013; Zengin et al., 2014; Anjum et al., 2018). Its anti-stress effects were studied in potato (Khan et al., 2015), wheat (Zengin et al., 2015) and tobacco (Abdul Halim &Phang, 2017) under aluminum, arsenic and lead stress respectively. Plants grown in soil treated with SA provided protection against heavy metal induced stress responses (Wani et al., 2017; Kohli et al., 2019), improved mineral status, reduced shoot and root Cd content in rice (Fatima et al., 2014). Other SA application methods (pre-treatment, foliar spray) were reported (Saruhan et al., 2012; Khan et al., 2014), where, pretreatment with SA was found to significantly reduce shoot Cd content (Cao et al., 2013). SA application under heavy metal stress and subsequent metal accumulation in grain has been studied across many crop species, but Cd accumulation pattern in different plant parts, especially in grains is nearly unexplored in rice. A recent study of SA application through foliar spray on leaves showed lowered Cd uptake in grains of brown rice (Wang et al., 2019). In Asian countries like India, pre-treatment or foliar spray application is laborious, time consuming and expensive, but application of SA can be done with irrigation water, saving cost and time.

We hypothesize that SA application in soil will be effective in minimizing grain Cd accumulation in *O. sativa* cv. Bandana. SA is believed to alleviate Cd toxicity, so, yield of the plants should remain unhampered upon SA application under Cd stress. Our initial field experiments have shown that Bandana, a high yielding variety, widely cultivated in West Bengal and different parts of India, is a moderate Cd accumulator. In the present study, various biochemical and physiological changes under Cd stress including plant growth, photosynthetic pigment content, lipid peroxidation, proline accumulation, non-protein thiol production, and ROS localization at the seedling stage were evaluated. To have an insight into the molecular mechanism behind it, expression of some selected Cd transport and sequestration related genes were also investigated. Pot experiment was conducted to assess the Cd status of different plant parts in the mature plants. Several agronomic traits including yield per plant, panicle length, panicle weight, tiller number, hollow seed percentage were studied to assess the ameliorating effect of SA. Health risk of Cd and SA treated rice was also assessed.

2. Materials and methods

2.1. Hydroponic experiment

2.1.1. Growth and treatment condition

Seeds of *Oryza sativa* cv. Bandana (procured from Bidhan Chandra Krishi Viswavidyalaya, West Bengal) were surface sterilized with 0.2% Dithane solution for 5–7 min, rinsed thoroughly with distilled water and soaked overnight (about 16 h), the soaked seeds were plated on 100mmX10mm borosilicate glass petri plates supplied with clean, moist filter paper, seeds were allowed to germinate in dark conditions at room temperature for 72 h. Upon germination (appearance of coleoptile), the plates were supplemented with 20 ml of half strength Hoagland's nutrient solution (Hoagland and Snyder, 1933) (pH 6.0) [1 mM KH_2PO_4, 5 mM KNO_3, 5 mM $Ca(NO_3)_2.4H_20$, 2 mM $MgSO_4.7H_2O$, micronutrients-11.8 μM $MnSO_4.7H_2O$, 0.7 μM $ZnSO_4.7H_2O$, 0.32 μM $CuSO_4.5H_2O$, 0.16 μM $(NH_4)_6Mo_7O_{24}.H_2O$, 6.3 μM H_3BO_3, 5 μM Fe-EDTA] and grown at 14/10 h photoperiod at 30±2 °C temperature and 70% relative humidity. Six days old seedlings with uniform size were subjected to treatment. Initial screening was done with different concentrations of Cd and SA, the following concentrations were chosen, based on half maximal inhibitory concentration (IC50) of Cd and the best growth enhancing concentration of SA. Four treatment sets were designed as follows, i) C (0 Cd + 0 SA), ii) T1 (25 μM or 4.52mgL^{-1} $CdCl_2$ + 100 μM or 13.81 mgL^{-1} SA), iii) T2 (25 μM $CdCl_2$ or 4.52mg$L^{-1}$$CdCl_2$+ 0 μM SA), iv) T3 (0 $CdCl_2$+100 μM or13.81 mgL^{-1} SA), with triplicates of each. Seedlings were treated for 72 h, shoots and roots from each set were harvested on the 9th day after plating.

2.1.2. Estimation of RWC, root and shoot length

Plantlets from each set were harvested and their fresh weight was taken. The shoot and root length of plantlets from each set were also recorded. RWC was calculated as [{(FW-DW)/(turgid weight-DW)} × 100] (Barr and Weatherley, 1962).

2.1.3. Analysis of oxidative damage related parameters

2.1.3.1. Estimation of chlorophyll. 100 mg of leaf samples from each set was chopped and extracted with 80% acetone. Absorbance was measured at 645 nm and 663 nm. The concentration of chlorophyll a, chlorophyll b were measured according to Arnon, 1949 and expressed as mg g^{-1} fresh weight.

2.1.3.2. Estimation of lipid peroxidation. Lipid peroxidation in shoot and root tissue was determined by the estimation of malondialdehyde (MDA) (Heath and Packer, 1968). 200 mg of fresh plant samples from each set was homogenized in 2 ml of 0.1% trichloroacetic acid (TCA) solution, the homogenate was centrifuged at 10,000×*g* for 5 min. For every 1 ml aliquot, 2 ml of 20% TCA containing 0.5% TBA was added, heated at 95 °C for 30 min and centrifuged at 10,000×*g* for 15 min. Absorbance of supernatant was taken at 532 nm and 600 nm. The concentration of MDA was calculated by using the molar extinction coefficient of 155.1 $mM^{-1}cm^{-1}$ and expressed as nmol g^{-1} fresh weight.

2.1.3.3. Estimation of hydrogen peroxide (H_2O_2). The concentration of endogenous H_2O_2 was determined (Sergiev et al., 1997). Briefly, 100 mg of tissue was homogenized in 1 ml of chilled 0.1% Trichloroacetic acid (TCA) and centrifuged at 12,000×*g* for 15 min. 0.5 ml of the supernatant was mixed with 0.5 ml of 10 mM Potassium Phosphate buffer (pH 7.0) and 1 ml 1 M Potassium Iodide, the final reaction mixture was read at 390 nm. The H_2O_2 content was calculated from standard curve of H_2O_2.

2.1.3.4. Localization of ROS accumulation in leaves. Localization of O_2^- and H_2O_2 radicals within the plant tissue was detected. Plant tissue was immersed in 50 mM phosphate buffer containing 0.2% Nitro blue

tetrazolium (NBT) (Jabs et al., 1996). H_2O_2 was detected by immersing the tissue in 3,3′-diaminobenzidine (DAB) (1 mg/ml) (Thordal-Christensen et al., 1997).

2.1.4. Analysis of tolerance related parameters

2.1.4.1. Estimation of non-protein thiol (NP-SH). The concentration of non-protein thiol (NPSH) was determined according to Cakmak and Marschner (1992). 100 mg of plant tissue was extracted with 1 ml of 5% orthophosphoric acid and centrifuged at 15,000×*g* for 15 mins at room temperature. To 0.5 ml of the aliquot, 2.4 ml of 150 mM phosphate buffer (pH 7.4) containing 5 mM EDTA and 0.5 ml of 6 mM 5,5-dithio-2, 2-dinitrobenzoic acid (Ellman's reagent) were added. The mixture was incubated for 15 min at room temperature and the end product was read at 412 nm.

2.1.4.2. Analysis of enzymatic antioxidant activity. 100 mg fresh tissue was homogenized in 600 µl of 50 mM Potassium Phosphate buffer (pH6.8) containing 0.1 mM EDTA and centrifuged at 13000 rpm for 15 min at 4 °C. The supernatant was used for the following assays:: The SOD activity was determined according to Beyer and Fridovich (1997). To 100 µl of the supernatant, 3 ml of solution containing 100 µM EDTA, 13 mM L-methionine, 75 µM NBT, 2 µM Riboflavin and 50 mM Potassium Phosphate buffer (pH7.8) were added. The reaction was illuminated under fluorescent lamp (Philips, 40 W) for 1.5 min, the light was turned off to stop the reaction. The absorbance was recorded at 630 nm. SOD activity was calculated by determining the amount of extract that led to 50% inhibition of NBT-reduction. The CAT activity as determined according to Havir and McHale (1987). To 100 µl of the extract, 3 ml solution containing 50 mM Potassium Phosphate buffer (pH7.0) and 20 mM H_2O_2were added. The decrease in absorbance was recorded at 240 nm.

2.1.4.3. Estimation of carotenoid content. 100 mg of leaf tissue from each set was chopped and extracted with 80% acetone. Absorbance was measured at 480 nm for presence of carotenoid according to (Arnon, 1949).

2.1.5. Analysis of molecular parameters

Total RNA was isolated from the samples using HiPurA Plant and Fungal RNA Miniprep Purification Kit according to manufacturer's instructions. The cDNA was synthesized from the RNA by First A synthesis kit (Thermo Scientific). This was followed by amplification using the designed primers. The primer sequences are *18SrRNA* (internal standard) (5′-TTC TAT GGG TGG TGG TGC AT-3′, 5′-GTG CGC CCA GAA CAT CTA AG-3′), *PCS1*(5′-AGG TCC TAC AGC AAA TCC GT-3′, 5′-ATT CCC ACT TAG CAA TGC GG-3′), *HMA3* (5′-GTT CAG CAT CGA CTC GTT CC-3′, 5′-CCA CAT TTT CCG GGT TTG GT-3′) and *NRAMP2*(5′-GCC CTC GTT GTT TCG TTC TT-3′, 5′-AAC AGC CCA ATA GCC CAG AT -3′).

2.2. Pot experiment

All the pot experiments were conducted at the Agricultural Experimental Farm, University of Calcutta, Baruipur, 24 paragana (South), West Bengal (22.35°N, 88.44°E) located in the Gangetic alluvial region, during June–September 2018–19 (with 14/10 h photoperiod, 30±2 °C temperature and 70% relative humidity). 100 germinated seedlings were placed in each pot with 2 kg of soil (16cm × 6cm × 10cm), then the seedlings were allowed to grow for 21days. 3–4 seedlings of uniform sizes were then transferred to separate pots (8cm × 10cm × 19cm) containing 3 kg of soil and grown till maturity. Plants were treated in the following concentrations and combinations, i) CP (0 $CdCl_2$+0 SA), ii) P1 (25 µM or 4.52 mg kg^{-1} $CdCl_2$ + 100 µM or 13.81 mg Kg^{-1}SA), iii) P2 (25 µM or 4.52 mg $Kg^{-1}CdCl_2$ + 0 µM SA),iv) P3 (0 $CdCl_2$+100 µM or13.81 mg kg^{-1} SA), the treatment was given by adding aqueous solution of $CdCl_2$ and SA in required amounts for 3 Kg of soil per pot, once during the growth period. Plant height was recorded during vegetative phase, at 45 days. Several agronomic traits were analyzed after complete maturation of the plants, including final height, total tiller number, effective tiller number, panicle length, panicle weight, total number of seed and hollow seed per panicle. The experiment was performed in triplicates. Data are represented as agronomic trait values per plant. Yield of the plants was calculated and expressed as g $plant^{-1}$.

2.2.1. Estimation of Cd content

The grain, shoot, root and soil samples were oven dried at 80 °C for 72 h 100 mg of each of the sub-sampled dried tissue was crushed individually and digested in HNO_3:HCl: $HClO_4$ (4:2:1), after complete digestion, the solution was made up to 25 ml volume with deionized distilled water (Barman et al., 2020), Cd content in the samples were determined by Inductively Coupled Plasma - Atomic Emission Spectrometry (ICP- AES) (SPECTRO Analytical Instruments GmbH, Germany).

2.2.2. Analysis of Cd content dependent quantitative factors

The extent of Cd transference from soil to crop and associated intake and risk factors were calculated as follows:

1. Bioconcentration factor (BCF) = $C_{root}/_{soil}$ (Kabata-Pendias and Mukherjee, 2007)
2. Translocation factor (TF) = C_{grain}/C_{shoot}orC_{grain}/C_{root} or C_{shoot}/C_{root} (Kalavrouziotis et al., 2012).
3. Daily intake of metal (DIM) in mg kg^{-1} day^{-1}= (C X IR)/BW (US EPA, 2004).
4. Cd exposure related cancer risk (CR) = DIM X SF (Rais et al., 2017).

Where C_{soil}, C_{root}, C_{shoot}, C_{grain} are Cd content in soil, root, shoot and grain respectively, C is metal content in grains in mg kg^{-1}, IR is ingestion rate in mg day^{-1} (an adult person of age range 20–40 years old consumes on an average 300 g rice per day, IR was calculated on this basis), SF is slope factor.

2.3. Statistical analysis: Levene's test was performed for homogeneity testing of variances, Shapiro wilk test was done for normality testing. One way analysis of variance (ANOVA) was performed with Tukey's honestly significant difference (hsd) test, using SPSS 17.0. Significant differences among the treatments were determined at 5% level of significance ($P < 0.05$). The experimental data was represented as mean ± standard deviation (SD), with triplicates for each set. Graphs were illustrated using Graphpad Prism 6 tool.

3. Results

3.1. SA escalated growth and RWC

The shoot and root growth of T2 set were reduced by 29.6% and 31.1% respectively, with regards to the untreated rice seedlings, while, the growth of T1 set increased by 0.4% and 2.3% with respect to shoot and root length of untreated rice seedlings (Fig. 1a). In comparison to control set, 6% and 21.4% reduction in shoot and root length of T3 set were observed. RWC was reduced by 35.5% in T2 set with respect to control, whereas a mere reduction of 1.6% was recorded in T1 set (Fig. 1b).

3.2. SA induced drop in oxidative damage related parameters

The total chlorophyll pigment content depleted in T2 set by 34.3% with respect to C set whereas, the simultaneous SA + Cd exposure elevated the amount of total chlorophyll content by 0.6% in T1 set (Fig. 2a). Accumulation of MDA in T2 shoot was 68.3% higher than C shoot, whereas MDA accumulation in T1 root increased by only 4.4% with respect to control, T3 shoot had lower accumulation of MDA,

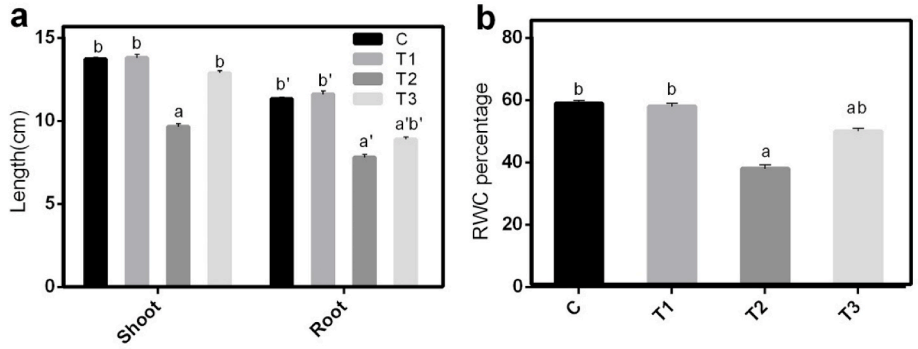

Fig. 1. Effect of Cd on physiological parameters a) shoot and root length b) Relative water content percentage. Values represent the mean of three replicates. Mean values represented by same letters are not significantly different, different letters represent statistical significance at $p < 0.05$, C (0 Cd + 0 SA), T1 (25 μM Cd + 100 μM SA), T2 (25 μM Cd + 0 μM SA), T3 (0 Cd + 100 μM SA).

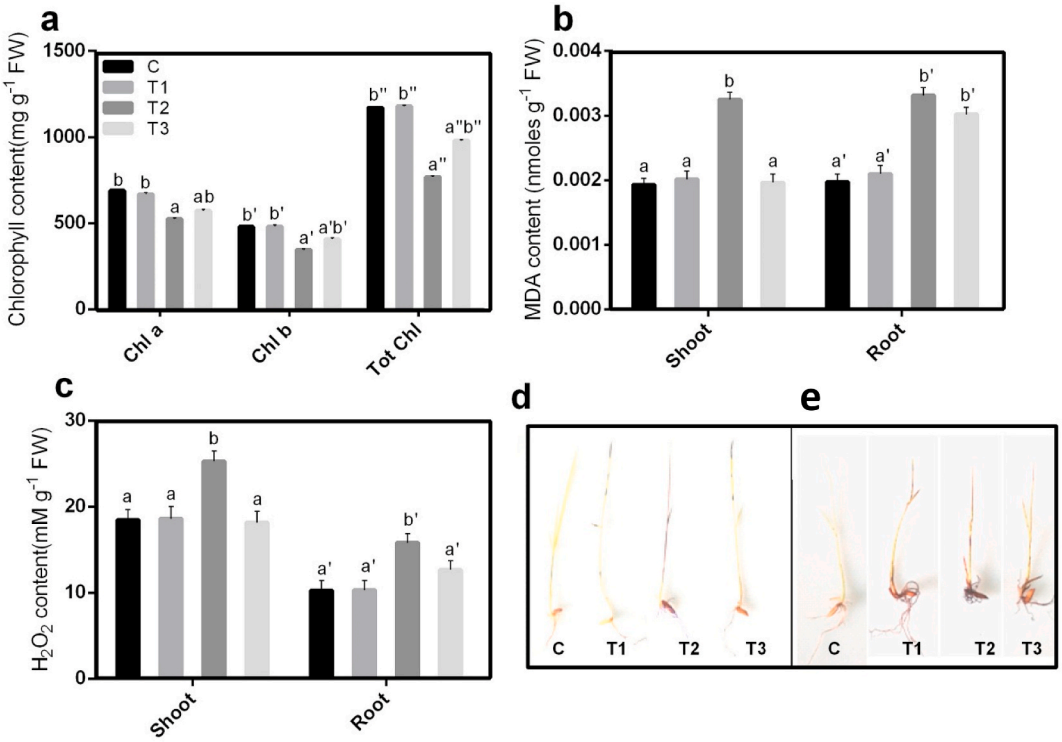

Fig. 2. Effect of Cd induced oxidative damage related parameters a) Chlorophyll content b)Malondialdehyde content c) Endogenous H_2O_2 content d) Localization of Superoxide anion e) Localization of H_2O_2. Values represent the mean of three replicates. Mean values represented by same letters are not significantly different, different letters represent statistical significance at $p < 0.05$, C (0 Cd + 0 SA), T1 (25 μM Cd + 100 μM SA), T2 (25 μM Cd + 0 μM SA), T3 (0 Cd + 100 μM SA).

accounting to 1.8% higher than c set (Fig. 2b). A similar trend was also observed in the accumulation of endogenous hydrogen peroxide. 0.38% higher accumulation of hydrogen peroxide with respect to control, was observed in T1 root, compared to a considerable increase of 53.7% in T2 root (Fig. 2c). Superoxide and hydrogen peroxide was detected by histochemical staining and it was observed that more Reactive Oxygen Species accumulated in T2 set in comparison to T1 set (Fig. 2d,2e).

3.3. SA altered stress scavengers

SA elevated the SOD activity in roots significantly by 62.3% in comparison to C set. It was found to be higher than theT2 seedlings which had 54.8% increase in root, T3 root exhibited a mere increase of 9% in the SOD activity (Fig. 3a). Root catalase activity increased by 85.3% and 157.8% in T1 and T2 sets respectively, in comparison to C set, however, a miniscule increase of 14.8% was observed in T3 set (Fig. 3b). SA application was able to modulate the antioxidant enzyme activities. T1 set showed 36.6% increase amount of non-protein thiol content in roots, with respect to C plants, whereas a slight increase of 14.4% was observed in T2 roots (Fig. 3c). No significant change was observed in carotenoid content (Fig. 3d).

3.4. Semi quantitative expression of *OsHMA3, OsPCS1 and OsNRAMP2* genes

According to densitometric analysis the *OsHMA3* and *OsPCS1* gene expression were found to be significantly upregulated in T1 set by 1.22 and 1.05 folds respectively, whereas the *OsNRAMP2* gene was found to be down regulated in T1 set by 0.85 folds. *OsHMA3* gene was down regulated by 0.85 folds, whereas *OsPCS1* and *OsNRAMP2* genes were up regulated by 1.015 and 1.028 folds in T2 set (Fig. 3e).

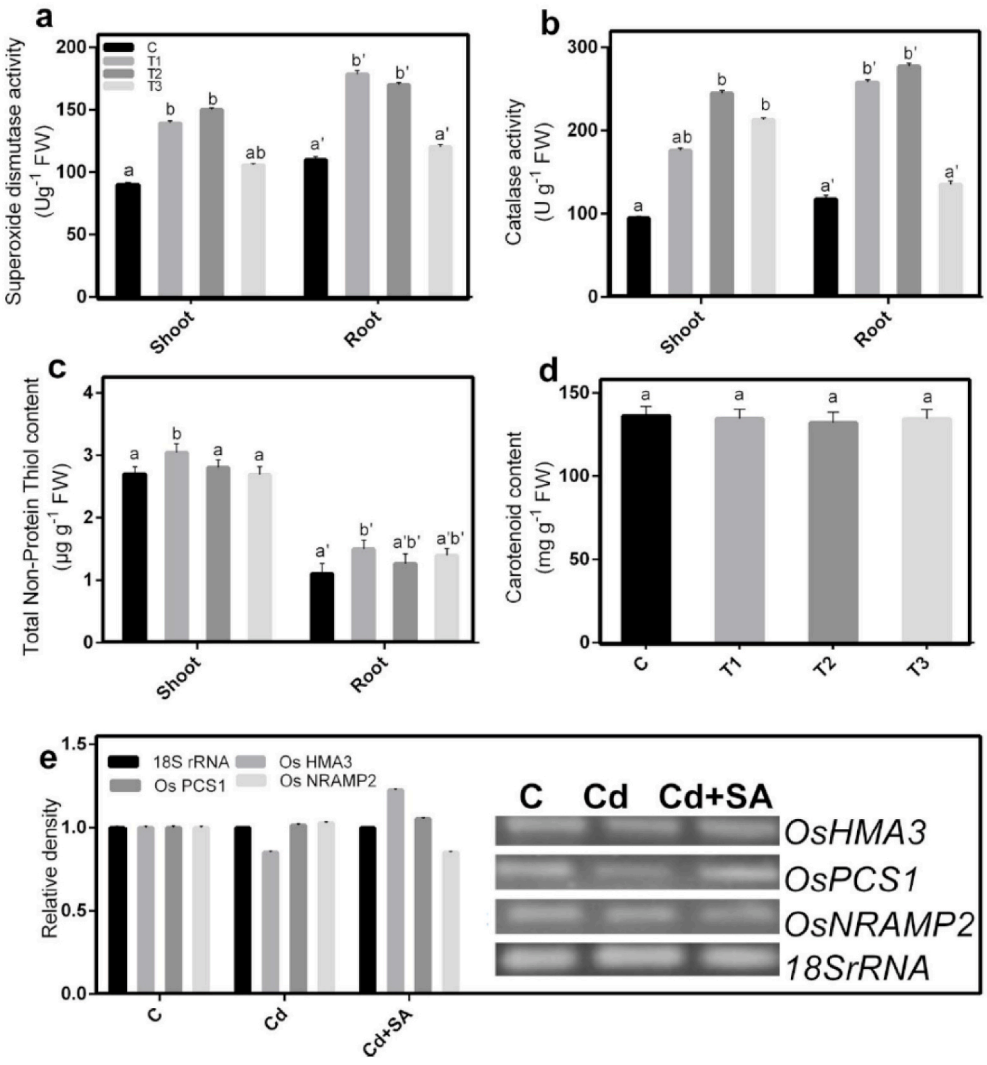

Fig. 3. SA induced alteration in stress scavengers and gene expression a)Superoxide dismutase activity b)Catalase activity c) Total non protein thiol content d)Carotenoid content in leaves e), i) Densitometric analysis using NIH ImageJ and Semi quantitative reverse transcriptase PCR amplification analysis documented by 1.8% Agarose gel analysis of amplicons. Values represent the mean of three replicates. Mean values represented by same letters are not significantly different, different letters represent statistical significance at $p < 0.05$, C (0 Cd + 0 SA), T1 (25 μM Cd + 100 μM SA), T2 (25 μM Cd + 0 μM SA), T3 (0 Cd + 100 μM SA).

3.5. Reduced Cd uptake and health risk potential

Cd concentration in grains of P2 set was 0.8 mg kg^{-1} rice, which was significantly reduced by 95% in grains of P1 set accounting to 0.004 mg kg^{-1} rice, the Cd concentration in shoot and root of P1 set was reduced by 82.6% and 54.1% respectively. Cd accumulation in P3 plants was not detected. The BCF of Cd was reduced by 54.16% in P1 plants in comparison to the P2 plants, in a similar way the TF (C_{grain}/C_{root}, C_{grain}/C_{shoot}, C_{shoot}/C_{root}) values were also reduced by 89.1%, 87.2% and 62.1% respectively in P1 plants with respect to the severely affected P2 plants. The DIM for P1 rice grains was reduced by 99.69% with respect to P2 rice. The lowered DIM for P1 rice also reduced the CR for P1 rice by 99.99% with respect to P2 rice grains (Table 1).

Table 1
Effect of SA application on Cd content and associated factors.

	CP	P1	P2	P3
Cd content (mg kg^{-1})				
Seed	ND	0.04 ± 0.0021	0.8 ± 0.0024	ND
Soil[a]	ND	2.68 ± 0.0022	2.68 ± 0.0021	ND
Shoot	ND	0.16 ± 0.0017	0.92 ± 0.0013	ND
Root	ND	0.44 ± 0.0020	0.96 ± 0.0019	ND
Associated factors				
BCF(g/s)	ND	0.164 ± 0.012	0.358 ± 0.0111	ND
TF (g/r)	ND	0.090 ± 0.021	0.833 ± 0.013	ND
TF (g/s)	ND	0.111 ± 0.031	0.869 ± 0.043	ND
TF (s/r)	ND	0.363 ± 0.01	0.958 ± 0.055	ND
DIM	ND	0.0008 ± 0.0009	0.32 ± 0.00046	ND
CR	ND	3.2×10^{-5}±0.00027	5.12 ± 0.00041	ND

[a] Residual Cd content.

3.6. Differential changes in agronomic traits and yield related components

Upon Cd exposure, all the studied agronomic parameters including plant height (both at 45 days and final), tiller number, grain attributes were hampered. Simultaneous application of SA and Cd were able to aid the recovery of the plants from the Cd induced toxicity. In P1 plants, yield attributes were significantly close to C and P3 plants. As the effective tillers in P1 plants increased by 81.48% with respect to P2 plants, total yield also considerably increased by 81.91% upon co-application of SA with Cd. The number of hollow seeds was decreased by 32.69% in P1 plants with respect to P2 plants. Traits like initial plant height, final plant height, total tiller number, total seed, and panicle weight changed trivially in P3 plants with respect to C plants (decrease percentage ranging from 0% to 7%). However, the yield was reduced by 23.6% in P3 plant with respect to C plants (Fig. 4a-i).

4. Discussion

The genotype Bandana used for the study, is one of the stable donor varieties, with high yield and productivity, widely used in breeding

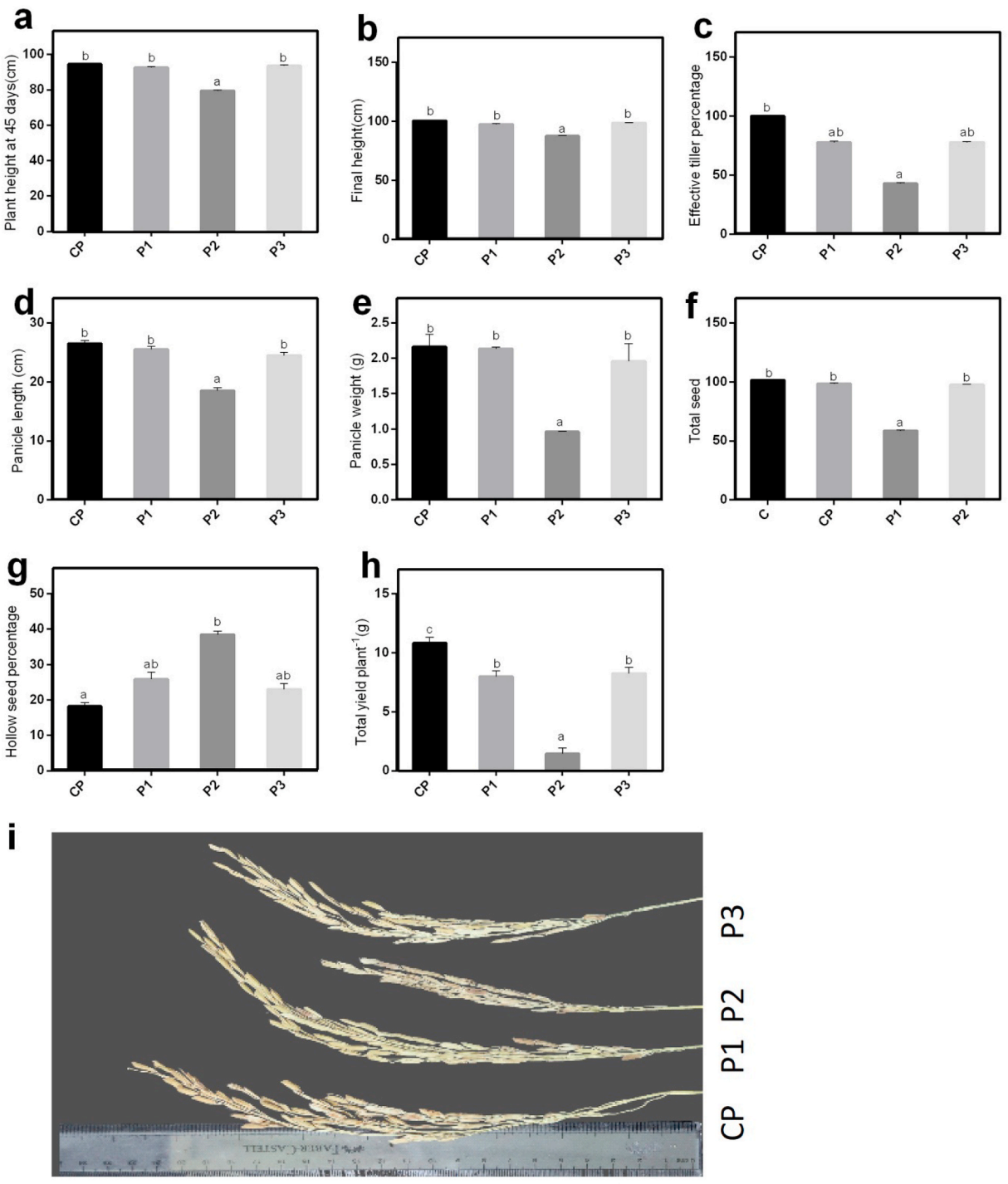

Fig. 4. Effect of SA application on various agronomic traits a) Plant height at 45 days b)Final plant height c) Effective tiller d) Panicle length e)Total seed f)Hollow seed percentage g)Panicle weight h)Total yield i) Pictographic representation of Panicles after maturity. Mean values represented by same letters are not significantly different, different letters represent statistical significance at $p < 0.05$, CP (0 Cd + 0 SA), P1 (25 μM Cd + 100 μM SA), P2 (25 μM Cd + 0 μM SA), P3 (0 Cd + 100 μM SA).

programs for its beneficial attributes (Jadhao et al., 2014; Poudel, 2018), but use of a Cd accumulating variety for breeding might lead to generation of Cd accumulating lines, posing threat to human health. Therefore, use of high yielding Cd accumulator varieties, as donors, can be accepted, provided Cd translocation to the grain is checked. In West Bengal, Cd contamination in agricultural soil may range from 1.76 mg kg^{-1} to 13.8 mg kg^{-1} (unpublished data), presenting high probability of Cd translocation and accumulation in grains. The Cd concentration selected for this study lies in the above mentioned limit and was found to cause moderate toxicity by significantly constraining normal growth and development of the plants. Simultaneous SA application in Cd stressed plants was found to ameliorate the stressed condition by enabling several defensive responses. It was observed that, application of only SA (at the present concentration) to plants was non-toxic.

SA application has been reported to alleviate several heavy metal toxicities including Cd (Hayat et al., 2010). Cd toxicity cause decreased uptake of water which leads to retarded growth of the root and shoot (Mondal et al., 2013), as well as biomass and may cause insufficient crop

yield (Ahmad et al., 2016). Hampered development is also reported in mungbean, and ground nut plants (Siddhu and Khan, 2012). Significant decrease in plant growth was seen in the present study under Cd stress, reduction in shoot and root length was observed in T2 set, in comparison to C set. In T1 set no reduction in shoot length was seen rather 2.3% increase in root length was observed. SA has been reported to alleviate Cd toxicity by several ways (Krantev et al., 2008; Guo et al., 2007; Belkhadi et al., 2010). Previously it was reported that, application of SA provided protection to arsenite exposed rice seedlings against stress and restored the plant growth parameters to a certain extent (Singh et al., 2017).

Chlorophyll metabolism and chloroplast ultrastructure are negatively affected due to the mineral stress induced by Cd (Djebali et al., 2005; Hakmaoui et al., 2007; Parmar et al., 2013; Arivazhagan and Sharavanan, 2015). We found that Cd negatively affected the chlorophyll synthesis in rice plants, plant growth and development were also compromised, only SA exposed plants had growth indices higher than Cd treated plants and close to T1 plants. Cd also hinders the uptake of nutrients like Fe, Mg which play significant role in chlorophyll synthesis, as reported in soybean (Xu et al., 2015), *Lemna minor* (Lu et al., 2018). Cd binds to essential Ca^{2+}sites and hinders the PSII photoactivation, by alteration of light harvesting complexes responsible for transfer of light to PSII reaction centre, the chlorophyll antenna complexes are responsible for conversion of light energy to electron transport from PSII, decreased oxygen evolution from PSII leads to modulated photochemical reactions, the energy storage process by synthesis of ATP and NADPH is impeded leading to impaired biochemical functions of the cell (Sytar et al., 2016; Rastogi et al., 2017; Dewez et al., 2018). We observed that SA application to Cd stressed plants improved the pigment content and growth, reports suggest that SA reduced Cd uptake and enhanced the uptake of Fe, Mg, Ca, thereby promoting chlorophyll synthesis (Lu et al., 2018). Hence SA application lowered Cd availability for Ca binding sites and leads to increased oxygen evolution by restoring PSII photoactivation. SA application improved the pigment content and growth as SA is reported to influence the RuBisCo activity, redox homeostasis and stomatal switch (Rivas-San Vicente and Plasencia, 2011). Similar effect was also seen in maize plants (Krantev et al., 2008).

Cd is known to induce production of hydrogen peroxide in many plants (Maksymiec and Krupa, 2006; Rodrı'guez-Serrano et al., 2009; Vestena et al., 2011; Zhao et al., 2012). Cd has the ability to compete and replace several important nutrients, like, Fe is replaced in several proteins leading to escalated free cellular Fe levels, which can directly induce ROS generation through Fenton and Haber-Weiss reactions (Cuypers et al., 2010). Cd induced increase in H_2O_2 is mainly synthesized by NADPH oxidase of plasma membrane or mitochondria or peroxisomes, which is subsequently transferred to other plant parts, this also induces accumulation of superoxide radicals and fatty acid hydroperoxides, ultimately leading to membrane damage (Garnier et al., 2006). T2 seedlings exhibited higher accumulation of ROS in the tissue, which was lowered significantly by SA application, this was congruent with previous reports. Our findings of histochemical detection of hydrogen peroxide and superoxide, indicated that application of SA to Cd treated seedlings could reduce the amount of endogenous ROS accumulation in the seedlings to considerable levels in comparison to T2 seedlings. Similar results were also reported in duckweed and perennial rye grass (Wang et al., 2013; Li et al., 2017). SA is reported to directly scavenge ROS by acting as an antioxidant (Popova et al., 2009), it jointly acts in a feed forward loop with glutathione and detoxifies ROS (Herrera-Vásquez et al., 2015). SA confers protection against heavy metal toxicity by detoxification of ROS thus reduces the degree of lipid peroxidation (Guo et al., 2007; Moussa and El-Gamal, 2010; Wang et al., 2013; Tamás et al., 2015; Khan et al., 2015). Cell membrane is prone to damage by redox active metals (Yılmaz and Parlak, 2011), higher the accumulation of MDA, higher is the level of oxidative stress (Hou et al., 2007). Cd induces oxidative stress, leading to enhanced MDA content, H_2O_2 content and electrolyte leakage (Schützendübel et al., 2002; Liu et al., 2003; Singh et al., 2006; Guo et al., 2007; Hsu and Kao, 2007; Xu et al., 2010; Srivastava et al., 2014). Our findings indicate lowered membrane damage with lowered amount of endogenous hydrogen peroxide accumulation in rice roots in T1 seedlings. Similar results were also reported in duckweed and perennial rye grass (Wang et al., 2013; Li et al., 2017, 2018). Damage indices were lower in T3 plant in comparison to T2 plants and were close to C plants, ensuring that SA alone had no toxicity in T3 plants.

NPT are one of the main components to detoxify ROS during heavy metal toxicity, they chelate with heavy metals facilitating their vacuolar sequestration and limiting their translocation to different plant tissues, they also act as signaling complexes and antioxidants (Li et al., 2011). We observed escalated levels of NPT in T1 as well as T2 set, however higher accumulation of NPT was observed in T1 set. The co-application of SA and Cd was reported to act synergistically resulting in increased synthesis of NPT, phytochelatin and glutathione (Gu et al., 2018).

The presence of antioxidant enzymes like SOD and CAT in different cellular organelles, protect the plants from oxidative damages. In the present study, SA application not only helped in alleviation of Cd induced growth impairment but also regulated the enzymatic activities. We observed that Cd stress significantly increased SOD and CAT activity in both shoot and root of T2 seedlings. Increased ROS generation due to Cd toxicity is counteracted by escalated activity of enzymatic antioxidants, higher SOD and CAT activity was observed under Cd stress in rice (Bari et al., 2019). However, SA application to Cd exposed plants enhanced the SOD activity whereas the CAT activity was reduced. SA applied Cd exposed kentucky blue grass was also found to have higher SOD activity than only Cd treated seedlings, (Guo et al., 2013), similar trend in SOD activity was observed in *Nymphaea tetragona* Georgi (Gu et al., 2018), *Lemna minor* (Lu et al., 2018), Chinese cabbage (Mba et al., 2007) and mustard plants (Ahmad et al., 2011). SA application has been reported to lower the CAT activity, a major H_2O_2 detoxifying enzyme in wheat and tomato (Sahu and Sabat, 2018; Yüzbaşıoğlu et al., 2019). SA is reported to donate electron for peroxidative cycle of catalase and lower its enzymatic activity by competitive inhibition (Ma et al., 2017). Hence, absence of such inhibitory role of SA on SOD activity might delineate the differential responses induced by SA on SOD and CAT activity. However, the enzymatic activity in T3 plants was similar to C plants, revealing that SA in absence of Cd exposure was unable to elicit anti-oxidative responses. The overall fold changes of biochemical, physiological and agronomic parameter analysis of SA and Cd exposed rice seedlings with respect to untreated ones is represented by color coded heat map (Fig. 5).

The chelation and sequestration of heavy metals are mainly carried out by metallothioneins and phytochelatins. The phytochelatins are synthesized as defense response, involving binding of sulphahydryl and carboxyl groups to a wide range of elements like Cd,Pb,Cu, Ni etc. (Cobbett, 2000; Emamverdian et al., 2015). *PCS* plays a significant role in the sequestration of Cd in *A. thaliana* (Chen et al., 2006; Liu et al., 2010; Kühnlenz et al., 2016). Function of *PCS* in Cd accumulation was established by *OsPCS* mutant studies, which showed lower accumulation. Constitutive expression of *PCS* occurs in plants, but they are upregulated in presence of metal/metalloid due to post transcriptional activation of the *PCS* gene (Cobbett, 2000; Vatamaniuk et al., 2000). Phytochelatins synthesized by *PCS* bind to Cd and form PC-Cd complexes which are sequestered in the vacuoles. Forming PC-Cd complexes and their subsequent sequestration into the vacuoles is crucial for Cd tolerance (Clemens et al., 1999; Ha et al., 1999; Vatamaniuk et al., 1999). Expression of *PCS1* slightly increased in T1 seedlings in comparison to the untreated ones, indicating higher PC synthesis, resulting in higher sequestration of Cd into the vacuoles. Cd sequestration is also mediated by Os*HMA3* (Morel et al., 2009). As observed in our study, the upregulated expression of *OsHMA3* in T1 set is statistically significant to the C and T2 set. There are no dedicated transporters for Cd transportation, so other ion transporters are used to transport Cd. *OsNRAMP2* is highly expressed in seedlings with high Cd accumulation properties.

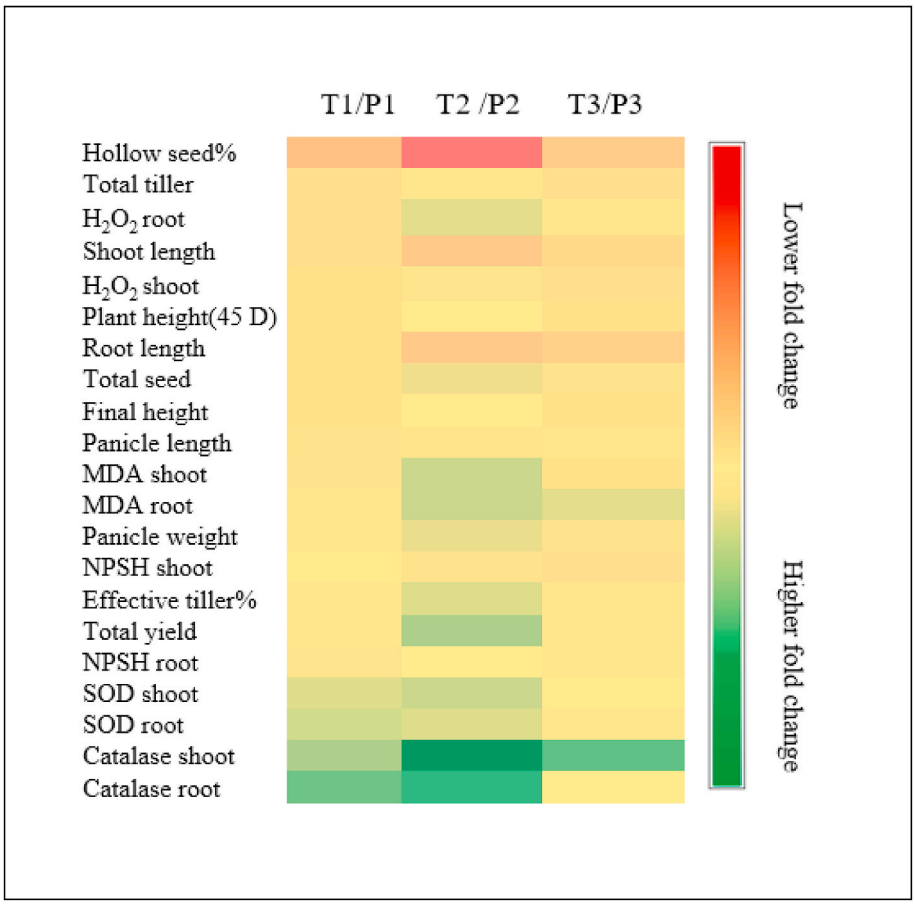

Fig. 5. Heat map analysis on the basis of fold change of treated rice seedlings with respect to untreated set, the assessed physiological, biochemical and agronomic are represented.. T1/P1 (25 μM Cd + 100 μM SA), T2/P2 (25 μM Cd + 0 μM SA), T3/P3 (0 Cd + 100 μM SA).

NRAMP2 allele from low Cd accumulating plants increased Cd sensitivity, SA application reduced *NRAMP2* expression suggesting lowered sensitivity of SA exposed plants (Zhao et al., 2018). The *OsNRAMP2* gene was downregulated in T1 seedlings. Increase of *OsNRAMP2* expression under Cd stress was observed which decreased on application of SA. The upregulation of the gene under Cd stress is similar to reports in ryegrass (Li et al., 2017). Application of SA to Cd exposed seedlings reduced the *NRAMP* expression owing to alleviating property of SA. The whole reaction cascade which follows after application of SA is represented schematically (Fig. 6).

The hydroponics is a well-balanced and controlled nutrient delivery system for lab-based experimentations, full term growth of rice plants in hydroponics require several infrastructural facilities and is expensive (Bado et al., 2016). In dearth of such prerequisites, the plants were grown in pot soil at the experimental farm, the soil used for pot experiments were Gangetic alluvial in nature with loamy clay consistency, the pH and organic carbon contents were reported to be 6.7 and 7.4 g kg^{-1} respectively (Mukherjee et al., 2019; Ghosh et al., 2020), providing favorable growth conditions for the plants. Additionally, owing to the near neutral pH and soil characters like high organic carbon content, loamy texture, the basal Cd uptake in Cd unexposed plants might be too low to be detected, as the Cd mobility is highly impaired in soil with clay loam texture (Hattori et al., 2006) with high organic carbon (Christensen et al., 1996) and near neutral pH (Xiaofang et al., 2019). Co-application of SA and Cd in rice plants have shown reduced accumulation of Cd in the root, shoot and grains of P1 plants. The influx of Cd is reported to reduce under Cd stress by SA application in peanuts and perennial ryegrass, the rearrangement of cell wall components might be a contributing factor here (Wang et al., 2013; Xu et al., 2015; Bai et al., 2015). Although the application of several organic acids (for eg. Citric, acetic, malic, succinic, oxalic) to soil (Sidhu et al., 2019) have exhibited increase in heavy metal bioavailability, yet, exogenous SA application has reduced elemental uptake by increasing citrate efflux from roots of treated seedlings, decreasing the Cd content in the root tips (Yang et al., 2003). Rhizospheric exudation of several secondary metabolites is reported to be a dynamic strategy to impede Cd uptake by roots (Bali et al., 2020). Unlike other low molecular weight organic acids, SA up to concentrations of 0.5 mM had no significant impact on soil anionic charges (Zhang et al., 2008). The TF(C_{shoot}/C_{root}) was greatly reduced in the P1 plants under influence of SA. The application of SA is reported to considerably reduce Cd uptake and toxicity in radish roots (Raza and Shafiq, 2013), Cd content reduced considerably in different parts of flax plant upon SA application (Belkhadi et al., 2010), wheat (Shakirova et al., 2016), oilseed rape (Ali et al., 2015), ryegrass (Wang et al., 2013; Bai et al., 2015), Kentucky bluegrass (Guo et al., 2013). Apart from cell wall rearrangement, SA is also reported to modify the functionality of various metal translocators resulting in reduced accumulation of the toxic metal in the aerial parts, due to its sequestration in the root vacuoles (Shi et al., 2009; Drazic et al., 2005), interaction between SA and Cd increased the synthesis of sulfhydryl groups (Metwally et al., 2003), promoting chelation of Cd ions, these cumulatively lowered the Cd translocation in the shoot, subsequently relieving the grains from Cd accumulation. The lowered *OsNRAMP*2, elevated *OsPCS*1 and *OsHMA*3 transcripts of the T1 seedlings contributed to hindered xylem loading, limiting the Cd deposition in shoot and grains. The reduced toxicity of Cd as a result of impaired Cd uptake by SA application, positively affected the yield related components in P1 plants in comparison to the P2 plants. SA application for amelioration of various stress have been

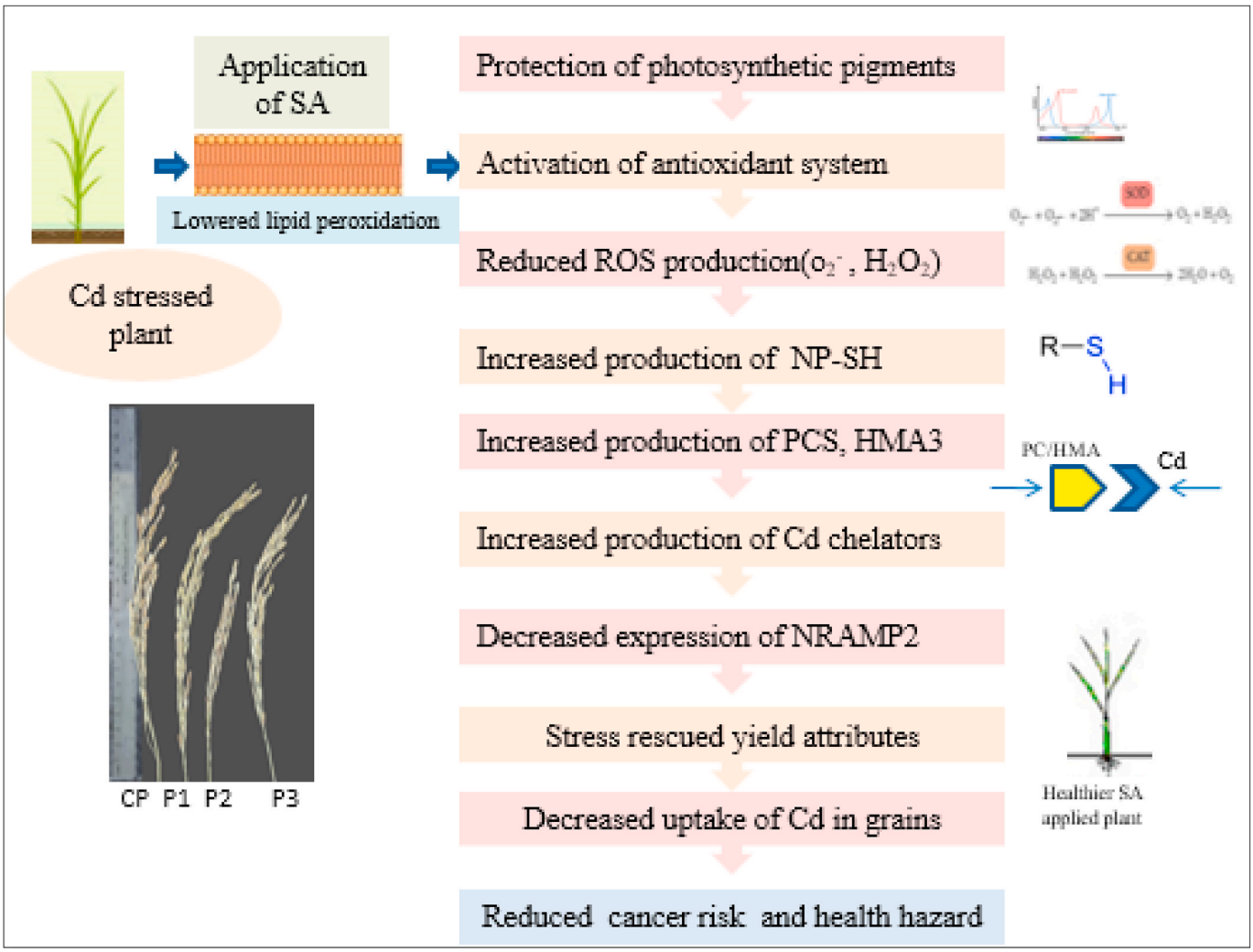

Fig. 6. Simplified schematic representing mechanism of SA providing Cd stress tolerance to rice plants, application of SA to Cd exposed rice seedling results in lowered membrane damage, enhanced photosynthetic pigment production, SA causes antioxidative burst, producing higher levels of ROS scavengers, minimizing free radicals from the plant cells, SA application increases production of NP-SH, required for production of thiol containing Cd chelators like phytochelatins. This causes chelation and sequestration of free divalent Cd ions, NRAMP2 expression is also reduced on SA application increasing tolerance of the seedlings towards Cd stress. Plants on reaching maturity exhibits better yield, lowered Cd uptake in P1 set, ultimately making the seeds of P1 set safe for consumption.

reported to enhance the yield related traits (like total panicle number, tiller number, total seed per panicle and total yield per plant). P1 plants had higher plant height in comparison to P2 plants, as, SA not only plays a major role in restricting Cd toxicity and uptake, but it also supports plant growth and development, by regulating photosynthetic efficiency, osmotic balance, ion homeostasis and anti-oxidative defense system (Khan et al., 2010, 2012a,b,c, 2013b, 2014; Nazar et al., 2011; Miura and Tada, 2014). These protective roles imparted by SA are highly congruent with our findings of hydroponic and pot experiments.

The bioavailable Cd is almost 40–50% lower than the total Cd content of soil, due to association of Cd with carbonates, oxides and other organic forms (Barman et al., 2020). The Cd contents of P2 seed (0.8 mg kg^{-1}) were much higher than the recommended limit (0.4 mg kg^{-1}) by CODEX, 2011, application of SA reduced 95% Cd accumulation in P1 with respect to P2. This is highly impactful, for further application in highly Cd contaminated areas or high Cd accumulating plants. 40.3% of total dietary intake of Cd is contributed by rice, which is reported to range between 0.021 and 0.022 mg kg^{-1} (Kim et al., 2019). The DIM for this cultivar is several folds higher than recent reports by Barman et al. (2020). The application of SA successfully reduced the Cd content in the grains of P1 plants, which resulted in 99.69% lower DIM. The higher the DIM higher will be the occurrence rates of Cd induced disease manifestations ranging from acute bone problems to fatal conditions like cancer. In non-smokers, dietary Cd is strongly associated with gastric cancer (Kim et al., 2019), breast cancer (Grioni et al., 2019). The CR was also reduced on application of SA in P1 plants in comparison to P2 plants. People who are more exposed to heavy metals through grains, vegetables and water are at a higher risk for the development of cancer in future (Zhang et al., 2018; Rezapour et al., 2018).

5. Conclusion

SA application to soil was found to be highly promising in reducing grain Cd content, increasing crop yield in comparison to Cd stressed SA unapplied plants, the cancer risk was also significantly reduced making it safe for consumption. In the present scenario, the rising exposure of the mankind to hazardous materials, is allowing elevated occurrence of diseases and fatalities. The unrestricted use of phosphate fertilizers in agricultural field is subjecting the cereals and crops to uptake Cd substantially, ultimately entering the food chain. So, finding mitigation strategies to reduce Cd deposition in grains, is of utmost importance. SA was found to ensure restricted Cd entry into the rice grains, making it a cost effective and easy way to combat the serious Cd threat.

Author contributions

Snehalata Majumdar: Conceptualization, Data curation, Formal analysis, Investigation, Methodology, Validation, Writing - original draft, Writing-review & editing, Sonal Sachdev: Methodology, Validation, Rita Kundu: Conceptualization, Investigation, Formal analysis, Visualization, Supervision, Writing - review & editing.

Funding

This study was funded by Department of Biotechnology (West Bengal) [76(Sanc.)-BT/P/Budget/RD-14/2017; March 27, 2018].

Ethical approval

This article does not contain any studies with human participants or animals performed by any of the authors.

Declaration of competing interest

The authors declare that they have no known competing financialinterestsor personal relationships that could have appeared to influence the work reported in this paper.

Acknowledgements

S M acknowledges Department of Biotechnology, Government of India, for her fellowship. S S acknowledges UGC for her fellowship. Authors would like to acknowledge CAS, Dept. of Botany, University of Calcutta, DST-FIST for infrastructural and instrumentation facilities. Authors are grateful to Dr. S Tripathy for providing the experimental field facility in University's Agricultural farm, Baruipur. Authors also acknowledge I.I.T Bombay for ICP/AES analysis. Financial assistance from WBDBT is also gratefully acknowledged. The authors are also thankful to Prof. S. Bhattacharya, Bidhan Chandra Krishi VishwaVidyalaya for providing the rice seed.

Appendix A. Supplementary data

Supplementary data to this article can be found online at https://doi.org/10.1016/j.ecoenv.2020.111167.

References

Agency for Toxic Substance and Disease Registry, 2019. https://www.atsdr.cdc.gov/spl/index.html.

Ahmad, P., Allah, E.A., Hashem, A., Sarwat, M., Gucel, S., 2016. Exogenous application of selenium mitigates cadmium toxicity in Brassica juncea L.(Czern& Cross) by up-regulating antioxidative system and secondary metabolites. J. Plant. Growth. Regul. 35 (4), 936–950. https://doi.org/10.1007/s00344-016-9592-3.

Ahmad, P., Nabi, G., Ashraf, M., 2011. Cadmium-induced oxidative damage in mustard [Brassica juncea (L.) Czern. &Coss.] plants can be alleviated by salicylic acid. South Afr. J. Bot. 77 (1), 36–44. https://doi.org/10.1016/j.sajb.2010.05.003.

Ali, E., Maodzeka, A., Hussain, N., Shamsi, I.H., Jiang, L., 2015. The alleviation of cadmium toxicity in oilseed rape (Brassica napus) by the application of salicylic acid. Plant Growth Regul. 75 (3), 641–655. https://doi.org/10.1007/s10725-014-9966-0.

An, C., Mou, Z., 2011. Salicylic acid and its function in plant immunity F. J. Integr. Plant Biol. 53 (6), 412–428. https://doi.org/10.1111/j.1744-7909.2011.01043.x.

Arivazhagan, V., Sharavanan, P.S., 2015. Effect of cadmium on photosynthetic responses and biochemical contents of maize plants. Am. J. Environ. Eng. Sci. 2 (3), 32.

Arnon, D.I., 1949. Copper enzymes in isolated chloroplasts. Polyphenoloxidase in Beta vulgaris. Plant Physiol. 24 (1), 1. https://doi.org/10.1104/pp.24.1.

Bado, S., Forster, B.P., Ghanim, A.M., Jankowicz-Cieslak, J., Berthold, G., Luxiang, L., 2016. Protocol for screening for salt tolerance in rice. In: Protocols for Pre-field Screening of Mutants for Salt Tolerance in Rice, Wheat and Barley. Springer, Cham, pp. 21–31. https://doi.org/10.1007/978-3-319-26590-2_1.

Bai, X., Dong, Y., Kong, J., Xu, L., Liu, S., 2015. Effects of application of salicylic acid alleviates cadmium toxicity in perennial ryegrass. Plant Growth Regul. 75 (3), 695–706. https://doi.org/10.1007/s10725-014-9971-3.

Bali, A.S., Sidhu, G.P.S., Kumar, V., 2020. Root exudates ameliorate cadmium tolerance in plants: a review. Environ. Chem. Lett. https://doi.org/10.1007/s10311-020-01012-x.

Bari, M.A., Akther, M.S., Reza, M.A., Kabir, A.H., 2019. Cadmium tolerance is associated with the root-driven coordination of cadmium sequestration, iron regulation, and ROS scavenging in rice. Plant Physiol. Biochem. 136, 22–33. https://doi.org/10.1016/j.plaphy.2019.01.007.

Barman, F., Majumdar, S., Arzoo, S.H., Kundu, R., 2020. Genotypic variation among 20 rice cultivars/landraces in response to cadmium stress grown locally in West Bengal, India. Plant Physiol. Biochem. https://doi.org/10.1016/j.plaphy.2020.01.019.

Barr, H.D., Weatherley, P.E., 1962. A re-examination of the relative turgidity technique for estimating water deficit in leaves. Aust. J. Biol. Sci. 15 (3), 413–428. https://doi.org/10.1071/bi9620413.

Belkhadi, A., Hediji, H., Abbes, Z., Nouairi, I., Barhoumi, Z., Zarrouk, M., Chaïbi, W., Djebali, W., 2010. Effects of exogenous salicylic acid pre-treatment on cadmium toxicity and leaf lipid content in Linumusitatissimum L. Ecotoxicol. Environ. Saf. 73 (5), 1004–1011. https://doi.org/10.1016/j.ecoenv.2010.03.009.

Cakmak, I., Marschner, H., 1992. Magnesium deficiency and high light intensity enhance activities of superoxide dismutase, ascorbate peroxidase, and glutathione reductase in bean leaves. Plant Physiol. 98 (4), 1222–1227. https://doi.org/10.1104/pp.98.4.1222.

Cao, F., Liu, L., Ibrahim, W., Cai, Y., Wu, F., 2013. Alleviating effects of exogenous glutathione, glycinebetaine, brassinosteroids and salicylic acid on cadmium toxicity in rice seedlings (Oryza sativa). Agrotechnology 2 (1), 107–112.

Chen, A., Komives, E.A., Schroeder, J.I., 2006. An improved grafting technique for mature Arabidopsis plants demonstrates long-distance shoot-to-root transport of phytochelatins in Arabidopsis. Plant Physiol. 141 (1), 108–120. https://doi.org/10.1104/pp.105.072637.

Christensen, J.B., Jensen, D.L., Christensen, T.H., 1996. Effect of dissolved organic carbon on the mobility of cadmium, nickel and zinc in leachate polluted groundwater. Water Res. 30 (12), 3037–3049. https://doi.org/10.1016/s0043-1354(96)00091-7.

Clemens, S., Kim, E.J., Neumann, D., Schroeder, J.I., 1999. Tolerance to toxic metals by a gene family of phytochelatin synthases from plants and yeast. EMBO J. 18 (12), 3325–3333. https://doi.org/10.1093/emboj/18.12.3325.

Cobbett, C.S., 2000. Phytochelatins and their roles in heavy metal detoxification. Plant Physiol. 123 (3), 825–832. https://doi.org/10.1104/pp.123.3.825.

Codex Alimentarius Commission, 2011. Joint FAO/WHO food standards programme codex committee on contaminants in foods. fifth session. In: Working Document for Information and Use in Discussions Related to Contaminants and Toxins in the GSCTFF, CF/5 INF/1. FAO/WHO, The Hague.

Cotton, F.A., 1999. Survey of transition-metal chemistry. In: Advanced Inorganic Chemistry, sixth ed. John Wiley and Sons, ISBN 0-471-19957-5, p. 633. https://doi.org/10.1016/s0039-9140(99)00269-6.

Cuypers, A., Plusquin, M., Remans, T., Jozefczak, M., Keunen, E., Gielen, H., Opdenakker, K., Nair, A.R., Munters, E., Artois, T.J., Nawrot, T., 2010. Cadmium stress: an oxidative challenge. Biometals 23 (5), 927–940. https://doi.org/10.1007/s10534-010-9329-x.

Das, N., Bhattacharya, S., Bhattacharyya, S., Maiti, M.K., 2017. Identification of alternatively spliced transcripts of rice phytochelatin synthase 2 gene OsPCS2 involved in mitigation of cadmium and arsenic stresses. Plant Mol. Biol. 94 (1–2), 167–183. https://doi.org/10.1007/s11103-017-0600-1.

Dewez, D., Goltsev, V., Kalaji, H.M., Oukarroum, A., 2018. Inhibitory effects of silver nanoparticles on photosystem II performance in Lemna gibba probed by chlorophyll fluorescence. Curr. Plant Biol. 16, 15–21. https://doi.org/10.1016/j.cpb.2018.11.006.

Djebali, W., Zarrouk, M., Brouquisse, R., El Kahoui, S., Limam, F., Ghorbel, M.H., Chaïbi, W., 2005. Ultrastructure and lipid alterations induced by cadmium in tomato (Lycopersiconesculentum) chloroplast membranes. Plant Biol. 7 (4), 358–368. https://doi.org/10.1055/s-2005-837696.

Drazic, G., Mihailovic, N., 2005. Modification of cadmium toxicity in soybean seedlings by salicylic acid. Plant Sci. 168 (2), 511–517. https://doi.org/10.1016/j.plantsci.2004.09.019.

Du, Y., Hu, X.F., Wu, X.H., Shu, Y., Jiang, Y., Yan, X.J., 2013. Affects of mining activities on Cd pollution to the paddy soils and rice grain in Hunan province, Central South China. Environ. Monit. Assess. 185 (12), 9843–9856. https://doi.org/10.1007/s10661-013-3296-y.

Emamverdian, A., Ding, Y., Xie, Y., 2020. The role of new members of phytohormones in plant amelioration under abiotic stress with an emphasis on heavy metals. Pol. J. Environ. Stud. 29 (2) https://doi.org/10.15244/pjoes/108687.

Emamverdian, A., Ding, Y., Mokhberdoran, F., Xie, Y., 2015. Heavy metal stress and some mechanisms of plant defense response. Sci. World J. 2015, 1–18. https://doi.org/10.1155/2015/756120.

EPA, A., 2004. Risk assessment guidance for superfund. In: Volume I: Human Health Evaluation Manual (Part E, Supplemental Guidance for Dermal Risk Assessment), vol. 5. EPA/540/R/99.

Fatima, R.N., Javed, F., Wahid, A., 2014. Salicylic acid modifies growth performance and nutrient status of rice (Oryza sativa) under cadmium stress. Int. J. Agric. Biol. 16 (6) https://doi.org/10.12692/ijb/6.4.177-183.

Fu, J., Zhou, Q., Liu, J., Liu, W., Wang, T., Zhang, Q., Jiang, G., 2008. High levels of heavy metals in rice (Oryzasativa L.) from a typical E-waste recycling area in southeast China and its potential risk to human health. Chemosphere 71 (7), 1269–1275. https://doi.org/10.1016/j.chemosphere.2007.11.065.

Gao, M., Zhou, J., Liu, H., Zhang, W., Hu, Y., Liang, J., Zhou, J., 2018. Foliar spraying with silicon and selenium reduces cadmium uptake and mitigates cadmium toxicity in rice. Sci. Total Environ. 631, 1100–1108. https://doi.org/10.1016/j.scitotenv.2018.03.047.

Ghosh, S., Chakrabarti, K., Mukherjee, A.K., Tripathi, S., 2020. Different rice based cropping systems can influence various soil organic carbon pools in a clay loam soil

of West Bengal. Int. J. Curr. Microbiol. App. Sci 9 (3), 1884–1897. https://doi.org/10.20546/ijcmas.2020.903.219.
Grioni, S., Agnoli, C., Krogh, V., Pala, V., Rinaldi, S., Vinceti, M., Contiero, P., Vescovi, L., Malavolti, M., Sieri, S., 2019. Dietary cadmium and risk of breast cancer subtypes defined by hormone receptor status: a prospective cohort study. Int. J. Canc. 144 (9), 2153–2160. https://doi.org/10.1002/ijc.32039.
Gu, C.S., Yang, Y.H., Shao, Y.F., Wu, K.W., Liu, Z.L., 2018. The effects of exogenous salicylic acid on alleviating cadmium toxicity in Nymphaea tetragona. Georgi. S. Afr. J. Bot. 114, 267–271. https://doi.org/10.1016/j.sajb.2017.11.012.
Guo, B., Liang, Y.C., Zhu, Y.G., Zhao, F.J., 2007. Role of salicylic acid in alleviating oxidative damage in rice roots (Oryza sativa) subjected to cadmium stress. Environ. Pollut. 147 (3), 743–749. https://doi.org/10.1016/j.envpol.2006.09.007.
Guo, Q., Meng, L., Mao, P.C., Jia, Y.Q., Shi, Y.J., 2013. Role of exogenous salicylic acid in alleviating cadmium-induced toxicity in Kentucky bluegrass. Biochem. Systemat. Ecol. 50, 269–276. https://doi.org/10.1016/j.bse.2013.05.002.
Ha, S.B., Smith, A.P., Howden, R., Dietrich, W.M., Bugg, S., O'Connell, M.J., Goldsbrough, P.B., Cobbett, C.S., 1999. Phytochelatin synthase genes from Arabidopsis and the yeast Schizosaccharomyces pombe. Plant Cell 11 (6), 1153–1163. https://doi.org/10.1105/tpc.11.6.1153.
Hakmaoui, A., Ater, M., Boka, K., Baron, M., 2007. Copper and cadmium tolerance, uptake and effect on chloroplast ultrastructure. Studies on Salix purpurea and Phragmitesaustralis. ZeitschriftfürNaturforschung C 62 (5–6), 417–426. https://doi.org/10.1515/znc-2007-5-616.
Hattori, H., Kuniyasu, K., Chiba, K., Chino, M., 2006. Effect of chloride application and low soil pH on cadmium uptake from soil by plants. Soil Sci. Plant Nutr. 52 (1), 89–94. https://doi.org/10.1111/j.1747-0765.2006.00007.x.
Havir, E.A., McHale, N.A., 1987. Biochemical and developmental characterization of multiple forms of catalase in tobacco leaves. Plant Physiol. 84 (2), 450–455. https://doi.org/10.1104/pp.84.2.450.
Hayat, Q., Hayat, S., Irfan, M., Ahmad, A., 2010. Effect of exogenous salicylic acid under changing environment: a review. Environ. Exp. Bot. 68 (1), 14–25. https://doi.org/10.1016/j.envexpbot.2009.08.005.
Heath, R.L., Packer, L., 1968. Photoperoxidation in isolated chloroplasts: I. Kinetics and stoichiometry of fatty acid peroxidation. Arch. Biochem. Biophys. 125 (1), 189–198. https://doi.org/10.1016/0003-9861(68)90654-1.
Herrera-Vásquez, A., Salinas, P., Holuigue, L., 2015. Salicylic acid and reactive oxygen species interplay in the transcriptional control of defense genes expression. Front. Plant Sci. 6, 171. https://doi.org/10.3389/fpls.2015.00171.
Hoagland, D.R., Snyder, W.C., 1933. Effects of deficiencies of boron and certain 16 other elements: (b) Susceptibility to injury from sodium salts. In: Proc Am SocHort 17 Sci, vol. 30, pp. 288–294.
Hou, W., Chen, X., Song, G., Wang, Q., Chang, C.C., 2007. Effects of copper and cadmium on heavy metal polluted waterbody restoration by duckweed (Lemna minor). Plant Physiol. Biochem. 45 (1), 62–69. https://doi.org/10.1016/j.plaphy.2006.12.005.
Hsu, Y.T., Kao, C.H., 2007. Toxicity in leaves of rice exposed to cadmium is due to hydrogen peroxide accumulation. Plant Soil 298 (1–2), 231–241. https://doi.org/10.1007/s11104-007-9357-7.
Huang, Y., Liao, M., Ye, Z., Li, T., 2017. Cd concentrations in two low Cd accumulating varieties of rice and their relationships with soil Cd content and their relation under field conditions. J. Ecol. Rural Environ. 33 (8), 748–754.
Irshad, M.K., Chen, C., Noman, A., Ibrahim, M., Adeel, M., Shang, J., 2020. Goethite-modified biochar restricts the mobility and transfer of cadmium in soil-rice system. Chemosphere 242, 125152. https://doi.org/10.1016/j.chemosphere.2019.125152.
Jabs, T., Dietrich, R.A., Dangl, J.L., 1996. Initiation of runaway cell death in an Arabidopsis mutant by extracellular superoxide. Science 273 (5283), 1853–1856. https://doi.org/10.1126/science.273.5283.1853.
Jadhao, K.R., Samal, K.C., Pradhan, S.K., Rout, G.R., 2014. Studies on molecular characterization of DREB gene in Indica rice (Oryza sativa L.). Hered. Genet. 3 (3) https://doi.org/10.4172/2161-1041.1000133, 2161-1041.
Jan, M., Shah, G., Masood, S., Iqbal Shinwari, K., Hameed, R., Rha, E.S., Jamil, M., 2019. Bacillus cereus enhanced phytoremediation ability of rice seedlings under cadmium toxicity. BioMed Res. Int. https://doi.org/10.1155/2019/8134651, 2019.
Joseph, B., Jini, D., Sujatha, S., 2010. Insight into the role of exogenous salicylic acid on plants grown under salt environment. Asian J. Crop Sci. 2 (4), 226–235. https://doi.org/10.3923/ajcs.2010.226.235.
Kabata-Pendias, A., Mukherjee, A.B., 2007. Trace Elements from Soil to Human. Springer Science & Business Media. https://doi.org/10.1007/978-3-540-32714-1.
Kalavrouziotis, I.K., Koukoulakis, P., Kostakioti, E., 2012. Assessment of metal transfer factor under irrigation with treated municipal wastewater. Agric. Water Manag. 103, 114–119. https://doi.org/10.1016/j.agwat.2011.11.002.
Khan, A.L., Waqas, M., Hussain, J., Al-Harrasi, A., Hamayun, M., Lee, I.J., 2015. Phytohormones enabled endophytic fungal symbiosis improve aluminum phytoextraction in tolerant Solanum lycopersicum: an examples of Penicillium janthinellum LK5 and comparison with exogenous GA3. J. Hazard Mater. 295, 70–78. https://doi.org/10.1016/j.jhazmat.2015.04.008.
Khan, M.I.R., Asgher, M., Khan, N.A., 2014. Alleviation of salt-induced photosynthesis and growth inhibition by salicylic acid involves glycinebetaine and ethylene in mungbean (Vigna radiata L.). Plant Physiol. Biochem. 80, 67–74. https://doi.org/10.1016/j.plaphy.2014.03.026.
Khan, N., Syeed, S., Masood, A., Nazar, R., Iqbal, N., 2010. Application of salicylic acid increases contents of nutrients and antioxidative metabolism in mungbean and alleviates adverse effects of salinity stress. Int. J. Plant Biol. 1 (1) https://doi.org/10.4081/pb.2010.e1 e1-e1.
Kim, H., Lee, J., Woo, H.D., Kim, D.W., Choi, I.J., Kim, Y.I., Kim, J., 2019. Association between dietary cadmium intake and early gastric cancer risk in a Korean population: a case–control study. Eur. J. Nutr. 58 (8), 3255–3266. https://doi.org/10.1007/s00394-018-1868-x.
Kohli, S.K., Bali, S., Tejpal, R., Bhalla, V., Verma, V., Bhardwaj, R., Alqarawi, A.A., Abd_Allah, E.F., Ahmad, P., 2019. In-situ localization and biochemical analysis of biomolecules reveals Pb-stress amelioration in Brassica juncea L. by co-application of 24-Epibrassinolide and Salicylic Acid. Sci. Rep. 9 (1), 1–15. https://doi.org/10.1038/s41598-019-39712-2.
Kosolsaksakul, P., Farmer, J.G., Oliver, I.W., Graham, M.C., 2014. Geochemical associations and availability of cadmium (Cd) in a paddy field system, northwestern Thailand. Environ. Pollut. 187, 153–161. https://doi.org/10.1016/j.envpol.2014.01.006.
Krantev, A., Yordanova, R., Janda, T., Szalai, G., Popova, L., 2008. Treatment with salicylic acid decreases the effect of cadmium on photosynthesis in maize plants. J. Plant Physiol. 165 (9), 920–931. https://doi.org/10.1016/j.jplph.2006.11.014.
Kühnlenz, T., Hofmann, C., Uraguchi, S., Schmidt, H., Schempp, S., Weber, M., Lahner, B., Salt, D.E., Clemens, S., 2016. Phytochelatin synthesis promotes leaf Zn accumulation of Arabidopsis thaliana plants grown in soil with adequate Zn supply and is essential for survival on Zn-contaminated soil. Plant Cell Physiol. 57 (11), 2342–2352. https://doi.org/10.1093/pcp/pcw148.
Li, T., Di, Z., Islam, E., Jiang, H., Yang, X., 2011. Rhizosphere characteristics of zinc hyperaccumulator Sedum alfredii involved in zinc accumulation. J. Hazard Mater. 185 (2–3), 818–823. https://doi.org/10.1016/j.jhazmat.2010.09.093.
Li, T., Xu, W.H., Chai, Y.R., Wang, Z.Y., Xie, D.T., 2017. Differences of Cd uptake and expression of Cd-tolerance related genes in two varieties of ryegrasses. Bulg. Chem. Commun. 49 (3), 697–705.
Liu, J.G., Liang, J.S., Li, K.Q., Zhang, Z.J., Yu, B.Y., Lu, X.L., Yang, J.C., Zhu, Q.S., 2003. Correlations between cadmium and mineral nutrients in absorption and accumulation in various genotypes of rice under cadmium stress. Chemosphere 52 (9), 1467–1473. https://doi.org/10.1016/s0045-6535(03)00484-3.
Liu, W.J., Wood, B.A., Raab, A., McGrath, S.P., Zhao, F.J., Feldmann, J., 2010. Complexation of arsenite with phytochelatins reduces arsenite efflux and translocation from roots to shoots in Arabidopsis. Plant Physiol. 152 (4), 2211–2221. https://doi.org/10.1104/pp.109.150862.
Lu, C., Zhang, L., Tang, Z., Huang, X.Y., Ma, J.F., Zhao, F.J., 2019. Producing cadmium-free Indica rice by overexpressing OsHMA3. Environ. Int. 126, 619–626. https://doi.org/10.1016/j.envint.2019.03.004.
Lu, Q., Zhang, T., Zhang, W., Su, C., Yang, Y., Hu, D., Xu, Q., 2018. Alleviation of cadmium toxicity in Lemna minor by exogenous salicylic acid. Ecotoxicol. Environ. Saf. 147, 500–508. https://doi.org/10.1016/j.ecoenv.2017.09.015.
Ma, X., Deng, D., Chen, W., 2017. Inhibitors and activators of SOD, GSH-px, and CAT. Enzyme inhibitors and activators 29, 207. https://doi.org/10.5772/65936.
Maksymiec, W., Krupa, Z., 2006. The effects of short-term exposition to Cd, excess Cu ions and jasmonate on oxidative stress appearing in Arabidopsis thaliana. Environ. Exp. Bot. 57 (1–2), 187–194. https://doi.org/10.1016/j.envexpbot.2005.05.006.
Mani, A., Sankaranarayanan, K., 2018. In silico analysis of natural resistance-associated macrophage protein (NRAMP) family of transporters in rice. Protein J. 37 (3), 237–247. https://doi.org/10.1007/s10930-018-9773-y.
Mba, F.O., Zhi-Ting, X., Hai-Jie, Q., 2007. Salicylic acid alleviates the cadmium toxicity in Chinese cabbages (Brassica chinensis). Pakistan J. Biol. Sci. 10, 3065–3071. https://doi.org/10.3923/pjbs.2007.3065.3071.
Metwally, A., Finkemeier, I., Georgi, M., Dietz, K.J., 2003. Salicylic acid alleviates the cadmium toxicity in barley seedlings. Plant Physiol. 132 (1), 272–281. https://doi.org/10.1104/pp.102.018457.
Miura, K., Tada, Y., 2014. Regulation of water, salinity, and cold stress responses by salicylic acid. Front. Plant Sci. 5, 4. https://doi.org/10.3389/fpls.2014.00004.
Miyadate, H., Adachi, S., Hiraizumi, A., Tezuka, K., Nakazawa, N., Kawamoto, T., Katou, K., Kodama, I., Sakurai, K., Takahashi, H., Satoh-Nagasawa, N., 2011. OsHMA3, a P1B-type of ATPase affects root-to-shoot cadmium translocation in rice by mediating efflux into vacuoles. New Phytol. 189 (1), 190–199. https://doi.org/10.1111/j.1469-8137.2010.03459.x.
Mondal, N.K., Das, C., Roy, S., Banerjee, A., 2013. Effect of varying cadmium stress on chickpea (Cicer arietinum L) seedlings: an ultrastructural study. Ann. Environ. Sci. 7 (1), 5.
Morel, M., Crouzet, J., Gravot, A., Auroy, P., Leonhardt, N., Vavasseur, A., Richaud, P., 2009. AtHMA3, a P1B-ATPase allowing cd/Zn/co/Pb vacuolar storage in Arabidopsis. Plant Physiol. 149 (2), 894–904. https://doi.org/10.1104/pp.108.130294.
Mukherjee, A.K., Tripathi, S., Mukherjee, S., Mallick, R.B., Banerjee, A., 2019. Effect of integrated nutrient management in sunflower (Helianthus annuus L.) on alluvial soil. Curr. Sci. 117 (8), 1364. https://doi.org/10.18520/cs/v117/i8/1364-1368.
Nazar, R., Iqbal, N., Syeed, S., Khan, N.A., 2011. Salicylic acid alleviates decreases in photosynthesis under salt stress by enhancing nitrogen and sulfur assimilation and antioxidant metabolism differentially in two mungbean cultivars. J. Plant Physiol. 168 (8), 807–815. https://doi.org/10.1016/j.jplph.2010.11.001.
Parmar, P., Kumari, N., Sharma, V., 2013. Structural and functional alterations in photosynthetic apparatus of plants under cadmium stress. Bot. Stud. 54 (1), 45. https://doi.org/10.1186/1999-3110-54-45.
Popova, L.P., Maslenkova, L.T., Yordanova, R.Y., Ivanova, A.P., Krantev, A.P., Szalai, G., Janda, T., 2009. Exogenous treatment with salicylic acid attenuates cadmium toxicity in pea seedlings. Plant Physiol. Biochem. 47 (3), 224–231. https://doi.org/10.1016/j.plaphy.2008.11.007.
Poudel, A.P., 2018. Analysis of growth and yield attributing characteristic of direct seeded upland rice genotypes in western hills of Nepal. Acta sci. agric.(ISSN: 2581-365X) Acta sci. agric 2 (7), 117–122.

Rastogi, A., Zivcak, M., Sytar, O., Kalaji, H.M., He, X., Mbarki, S., Brestic, M., 2017. Impact of metal and metal oxide nanoparticles on plant: a critical review. Front. Chem. https://doi.org/10.3389/fchem.2017.00078, 2017.

Raza, S.H., Shafiq, F., 2013. Exploring the role of salicylic acid to attenuate cadmium accumulation in radish (Raphanussativus). Int. J. Agric. Biol. 15 (3).

Rezapour, S., Kouhinezhad, P., Samadi, A., 2018. The potential ecological risk of soil trace metals following over five decades of agronomical practices in a semi-arid environment. Chem. Ecol. 34 (1), 70–85. https://doi.org/10.1080/02757540.2017.1404585.

Rivas-San Vicente, M., Plasencia, J., 2011. Salicylic acid beyond defence: its role in plant growth and development. J. Exp. Bot. 62 (10), 3321–3338. https://doi.org/10.1093/jxb/err031.

Rodríguez-Serrano, M., Romero-Puertas, M.C., Sparkes, I., Hawes, C., Luis, A., Sandalio, L.M., 2009. Peroxisome dynamics in Arabidopsis plants under oxidative stress induced by cadmium. Free FreeRadic. Biol. Med. 47 (11), 1632–1639. https://doi.org/10.1016/j.freeradbiomed.2009.09.012.

S Schützendübel, A., Nikolova, P., Rudolf, C., Polle, A., 2002. Cadmium and H2O2-induced oxidative stress in Populus× canescens roots. Plant Physiol. Biochem. 40 (6–8), 577–584. https://doi.org/10.1016/s0981-9428(02)01411-0.

Sahu, G.K., Sabat, S.C., 2018. Salicylic acid modulates isoenzyme pattern of enzymatic antioxidants in wheat. Indian J. Plant Physiol. 23 (3), 486–493. https://doi.org/10.1007/s40502-018-0384-6.

Saruhan, N., Saglam, A., Kadioglu, A., 2012. Salicylic acid pretreatment induces drought tolerance and delays leaf rolling by inducing antioxidant systems in maize genotypes. Acta Physiol. Plant. 34 (1), 97–106. https://doi.org/10.1007/s11738-011-0808-7.

Sergiev, I., Alexieva, V., Karanov, E.V., SERGIEV, I., Karanov, E., Sergiev, L., Karanova, E., ALEXIEVA, V., Alexieva, V.V., 1997. Effect of spermine, atrazine and combination between them on some endogenous protective systems and stress markers in plants. Comp. Ren. Del. Academie Bul. des Sci. 51, 121–124.

Shakirova, F.M., Allagulova, C.R., Maslennikova, D.R., Klyuchnikova, E.O., Avalbaev, A. M., Bezrukova, M.V., 2016. Salicylic acid-induced protection against cadmium toxicity in wheat plants. Environ. Exp. Bot. 122, 19–28. https://doi.org/10.1016/j.envexpbot.2015.08.002.

Shri, M., Dave, R., Diwedi, S., Shukla, D., Kesari, R., Tripathi, R.D., Trivedi, P.K., Chakrabarty, D., 2014. Heterologous expression of Ceratophyllumdemersumphytochelatin synthase, CdPCS1, in rice leads to lower arsenic accumulation in grain. Sci. Rep. 4, 5784. https://doi.org/10.1038/srep05784.

Siddhu, G., Khan, M.A., 2012. Effects of cadmium on growth and metabolism of Phaseolus mungo. J. Environ. Biol. 33 (2), 173.

Sidhu, G.P.S., Bali, A.S., Bhardwaj, R., 2019. Role of organic acids in mitigating cadmium toxicity in plants. In: Cadmium Tolerance in Plants. Academic Press, pp. 255–279. https://doi.org/10.1016/b978-0-12-815794-7.00010-2.

Singh, A.P., Dixit, G., Kumar, A., Mishra, S., Kumar, N., Dixit, S., Singh, P.K., Dwivedi, S., Trivedi, P.K., Pandey, V., Dhankher, O.P., 2017. A protective role for nitric oxide and salicylic acid for arsenite phytotoxicity in rice (Oryza sativa L.). Plant Physiol. Biochem. 115, 163–173. https://doi.org/10.1016/j.plaphy.2017.02.019.

Singh, I., Shah, K., 2015. Evidences for suppression of cadmium induced oxidative stress in presence of sulphosalicylic acid in rice seedlings. Plant Growth Regul. 76 (1), 99–110. https://doi.org/10.1007/s10725-015-0023-4.

Sytar, O., Brestic, M., Taran, N., Zivcak, M., 2016. Plants used for biomonitoring and phytoremediation of trace elements in soil and water. In: Ahmad, Parvaiz (Ed.), Plant Metal Interaction: Emerging Remediation Techniques. Elsevier, ISBN 978-0-12-803158-2, pp. 361–384. https://doi.org/10.1016/b978-0-12-803158-2.00014-x, 2016.

Tamás, L., Mistrík, I., Alemayehu, A., Zelinová, V., Bočová, B., Huttová, J., 2015. Salicylic acid alleviates cadmium-induced stress responses through the inhibition of Cd-induced auxin-mediated reactive oxygen species production in barley root tips. J. Plant Physiol. 173, 1–8. https://doi.org/10.1016/j.jplph.2014.08.018.

Thordal-Christensen, H., Zhang, Z., Wei, Y., Collinge, D.B., 1997. Subcellular localization of H2O2 in plants. H2O2 accumulation in papillae and hypersensitive response during the barley—powdery mildew interaction. Plant J. 11 (6), 1187–1194. https://doi.org/10.1046/j.1365-313x.1997.11061187.x.

Ullah, I., Wang, Y., Eide, D.J., Dunwell, J.M., 2018. Evolution, and functional analysis of Natural Resistance-Associated Macrophage Proteins (NRAMPs) from Theobroma cacao and their role in cadmium accumulation. Sci. Rep. 8 (1), 1–15. https://doi.org/10.1038/s41598-018-32819-y.

Uraguchi, S., Tanaka, N., Hofmann, C., Abiko, K., Ohkama-Ohtsu, N., Weber, M., Kamiya, T., Sone, Y., Nakamura, R., Takanezawa, Y., Kiyono, M., 2017. Phytochelatin synthase has contrasting effects on cadmium and arsenic accumulation in rice grains. Plant Cell Physiol. 58 (10), 1730–1742. https://doi.org/10.1093/pcp/pcx114.

Vatamaniuk, O.K., Mari, S., Lu, Y.P., Rea, P.A., 1999. AtPCS1, a phytochelatin synthase from Arabidopsis: isolation and in vitro reconstitution. Proc. Natl. Acad. Sci. Unit. States Am. 96 (12), 7110–7115. https://doi.org/10.1073/pnas.96.12.7110.

Vatamaniuk, O.K., Mari, S., Lu, Y.P., Rea, P.A., 2000. Mechanism of heavy metal ion activation of phytochelatin (PC) synthase blocked thiols are sufficient for PC synthase-catalyzed transpeptidation of glutathione and related thiol peptides. J. Biol. Chem. 275 (40), 31451–31459. https://doi.org/10.1074/jbc.m002997200.

Vestena, S., Cambraia, J., Ribeiro, C., Oliveira, J.A., Oliva, M.A., 2011. Cadmium-induced oxidative stress and antioxidative enzyme response in water hyacinth and salvinia. Braz. J. Plant Physiol. 23 (2), 131–139. https://doi.org/10.1590/s1677-04202011000200005.

Wang, F., Tan, H., Zhang, Y., Huang, L., Ding, Y., Chen, Z., Zhu, C., 2019. Salicylic Acid Application Alleviates Cadmium Accumulation in Brown Rice by Modulating its Shoot to Grain Translocation in Rice, 31 December 2019. PREPRINT (Version 1) available at Research Square. https://doi.org/10.21203/rs.2.19653/v1.

Wang, J., Fang, Y., Tian, B., Zhang, X., Zeng, D., Guo, L., Hu, J., Xue, D., 2018. New QTLs identified for leaf correlative traits in rice seedlings under cadmium stress. Plant Growth Regul. 85 (2), 329–335. https://doi.org/10.1007/s10725-018-0393-5.

Wang, Q., Liang, X., Dong, Y., Xu, L., Zhang, X., Kong, J., Liu, S., 2013. Effects of exogenous salicylic acid and nitric oxide on physiological characteristics of perennial ryegrass under cadmium stress. J. Plant Growth Regul. 32 (4), 721–731. https://doi.org/10.1007/s00344-013-9339-3.

Wani, A.B., Chadar, H., Wani, A.H., Singh, S., Upadhyay, N., 2017. Salicylic acid to decrease plant stress. Environ. Chem. Lett. 15 (1), 101–123. https://doi.org/10.1007/s10311-016-0584-0.

Xiaofang, L.I., Dongmei, Z.H.O.U., 2019. A meta-analysis on phenotypic variation in cadmium accumulation of rice and wheat: implications for food cadmium risk control. Pedosphere 29 (5), 545–553. https://doi.org/10.1016/s1002-0160(19)60828-3.

Xu, J., Wang, W., Yin, H., Liu, X., Sun, H., Mi, Q., 2010. Exogenous nitric oxide improves antioxidative capacity and reduces auxin degradation in roots of Medicagotruncatula seedlings under cadmium stress. Plant Soil 326 (1–2), 321. https://doi.org/10.1007/s11104-009-0011-4.

Xu, L.L., Fan, Z.Y., Dong, Y.J., Kong, J., Bai, X.Y., 2015. Effects of exogenous salicylic acid and nitric oxide on physiological characteristics of two peanut cultivars under cadmium stress. Biol. Plant. (Prague) 59 (1), 171–182. https://doi.org/10.1007/s10535-014-0475-9.

Xue, D., Jiang, H., Deng, X., Zhang, X., Wang, H., Xu, X., Hu, J., Zeng, D., Guo, L., Qian, Q., 2014. Comparative proteomic analysis provides new insights into cadmium accumulation in rice grain under cadmium stress. J. Hazard Mater. 280, 269–278. https://doi.org/10.1016/j.jhazmat.2014.08.010.

Yang, Z.M., Wang, J., Wang, S.H., Xu, L.L., 2003. Salicylic acid-induced aluminum tolerance by modulation of citrate efflux from roots of Cassia tora L. Planta 217 (1), 168–174. https://doi.org/10.1007/s00425-003-0980-0.

Yılmaz, D.D., Parlak, K.U., 2011. Changes in proline accumulation and antioxidative enzyme activities in Groenlandiadensa under cadmium stress. Ecol. Indicat. 11 (2), 417–423. https://doi.org/10.1016/j.ecolind.2010.06.012.

Yüzbaşıoğlu, Elif, Dalyan, Eda, 2019. Salicylic acid alleviates thiram toxicity by modulating antioxidant enzyme capacity and pesticide detoxification systems in the tomato (Solanum lycopersicum Mill.). Plant Physiol. Biochem. 135, 322–330. https://doi.org/10.1016/j.plaphy.2018.12.023.

Zengin, F., 2014. Exogenous treatment with salicylic acid alleviating copper toxicity in bean seedlings. Proc. Natl. Acad. Sci. India B Biol. Sci. 84 (3), 749–755. https://doi.org/10.1007/s40011-013-0285-4.

Zengin, F., 2015. Effects of exogenous salicylic acid on growth characteristics and biochemical content of wheat seeds under arsenic stress. J. Environ. Biol. 36 (1), 249.

Zhang, J.Q., Dong, Y.H., 2008. Effect of low-molecular-weight organic acids on the adsorption of norfloxacin in typical variable charge soils of China. J. Hazard Mater. 151 (2–3), 833–839. https://doi.org/10.1016/j.jhazmat.2007.11.046.

Zhang, P.-J., et al., 2013. Feeding by whiteflies suppresses downstream jasmonic acid signaling by eliciting salicylic acid signaling. J. Chem. Ecol. 39, 612–619. https://doi.org/10.1007/s10886-013-0283-2.

Zhang, X., Chen, H., Jiang, H., Lu, W., Pan, J., Qian, Q., Xue, D., 2015. Measuring the damage of heavy metal cadmium in rice seedlings by SRAP analysis combined with physiological and biochemical parameters. J. Sci. Food Agric. 95, 2292–2298. https://doi.org/10.1002/jsfa.6949.

Zhang, Y., Yin, C., Cao, S., Cheng, L., Wu, G., Guo, J., 2018. Heavy metal accumulation and health risk assessment in soil-wheat system under different nitrogen levels. Sci. Total Environ. 622, 1499–1508. https://doi.org/10.1016/j.scitotenv.2017.09.317.

Zhao, F.Y., Han, M.M., Zhang, S.Y., Wang, K., Zhang, C.R., Liu, T., Liu, W., 2012. Hydrogen peroxide-mediated growth of the root system occurs via auxin signaling modification and variations in the expression of cell-cycle genes in rice seedlings exposed to cadmium stress. J. Integr. Plant Biol. 54 (12), 991–1006. https://doi.org/10.1111/j.1744-7909.2012.01170.x.

Zhao, J., Yang, W., Zhang, S., Yang, T., Liu, Q., Dong, J., Fu, H., Mao, X., Liu, B., 2018. Genome-wide association study and candidate gene analysis of rice cadmium accumulation in grain in a diverse rice collection. Rice 11 (1), 61. https://doi.org/10.1186/s12284-018-0254-x.